12-2009

Wind Energy Assessment Study for Nevada -- Tall Tower Deployment (Stone Cabin)

Darko Koracin
Desert Research Institute, Darko.Koracin@dri.edu

R. Reinhardt
Desert Research Institute

Gregory D. McCurdy
Desert Research Institute, Greg.McCurdy@dri.edu

Marshall Liddle
Desert Research Institute, marshall.liddle@dri.edu

Travis E. McCord
Desert Research Institute, Travis.McCord@dri.edu

National Renewable Energy Laboratory
A national laboratory of the U.S. Department of Energy
Office of Energy Efficiency & Renewable Energy
Innovation for Our Energy Future

Wind Energy Assessment Study for Nevada – Tall Tower Deployment (Stone Cabin)

26 June 2005 – 31 December 2007

D. Koracin, R. Reinhardt, G. McCurdy,
M. Liddle, T. McCord, R. Vellore, T. Minor,
B. Lyles, D. Miller, and L. Ronchetti
Desert Research Institute
Reno, Nevada

Subcontract Report
NREL/SR-550-47085
December 2009

NREL is operated for DOE by the Alliance for Sustainable Energy, LLC Contract No. DE-AC36-08-GO28308

Wind Energy Assessment Study for Nevada – Tall Tower Deployment (Stone Cabin)

26 June 2005 – 31 December 2007

D. Koracin, R. Reinhardt, G. McCurdy,
M. Liddle, T. McCord, R. Vellore, T. Minor,
B. Lyles, D. Miller, and L. Ronchetti
Desert Research Institute
Reno, Nevada

NREL Technical Monitor: H. Thomas and M. Schwartz
Prepared under Subcontract No. NDO-5-44431-01

Subcontract Report
NREL/SR-550-47085
December 2009

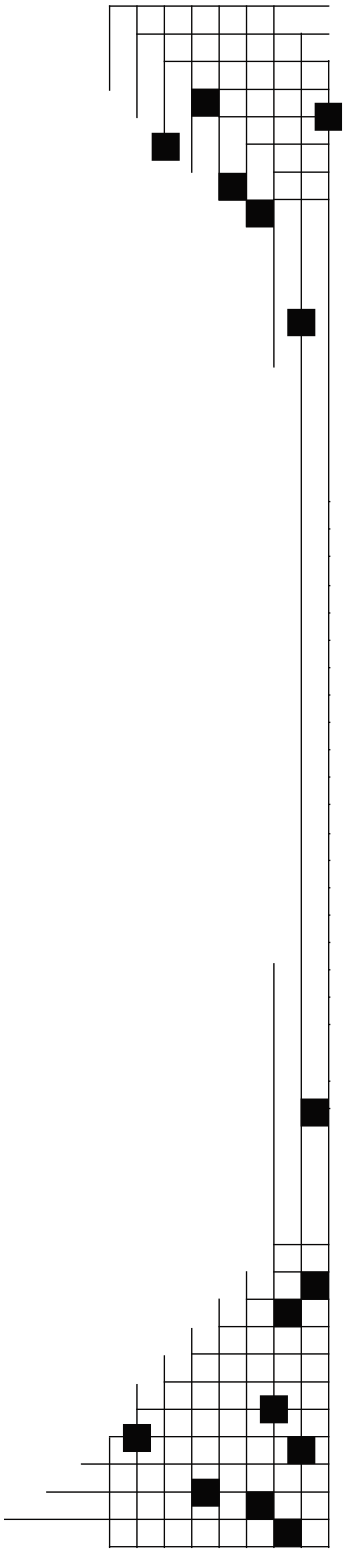

National Renewable Energy Laboratory
1617 Cole Boulevard, Golden, Colorado 80401-3393
303-275-3000 • www.nrel.gov

NREL is a national laboratory of the U.S. Department of Energy
Office of Energy Efficiency and Renewable Energy
Operated by the Alliance for Sustainable Energy, LLC

Contract No. DE-AC36-08-GO28308

Available electronically at http://www.osti.gov/bridge

Available for a processing fee to U.S. Department of Energy
and its contractors, in paper, from:
U.S. Department of Energy
Office of Scientific and Technical Information
P.O. Box 62
Oak Ridge, TN 37831-0062
phone: 865.576.8401
fax: 865.576.5728
email: mailto:reports@adonis.osti.gov

Available for sale to the public, in paper, from:
U.S. Department of Commerce
National Technical Information Service
5285 Port Royal Road
Springfield, VA 22161
phone: 800.553.6847
fax: 703.605.6900
email: orders@ntis.fedworld.gov
online ordering: http://www.ntis.gov/ordering.htm

This publication received minimal editorial review at NREL

Printed on paper containing at least 50% wastepaper, including 20% postconsumer waste

Acknowledgements

This work was funded by the U.S. Department of Energy. The authors are grateful to Marc Schwartz for guidance and helpful advice. Connie Komomua of NREL and Travis McCord of DRI are acknowledged for editing the manuscript.

List of Acronyms and Abbreviations

ATC	American Tower Corporation
NaN	not a number
NREL	National Renewable Energy Laboratory
RDP	relative difference product
SD	squared difference
sodar	solar detection and ranging
TKE	turbulence kinetic energy

Table of Contents

List of Figures

List of Tables

1 Introduction

The objective of this work effort was to characterize wind shear and turbulence for representative wind-developable areas in Nevada. This information and the models that provide it will be useful in specifying the appropriate technology and helping the developer choose the optimum orientation and spacing for a particular landscape. A key element in this study is the measurement of turbulence at three levels above the ground (40, 60, and 80 m) at the existing tower near Tonopah (Stone Cabin). Most previous wind power density estimates are based on surface wind measurements and various extrapolation formulas, which are rarely verified, to provide estimates at hub heights. In addition, the study will provide new insight into long-term statistics of turbulence at multiple levels that can be used to estimate its effects on turbine operation and maintenance.

2 Site Selection

Task

Locate and secure site location for the project. Suitable site characteristics for this project include tall towers with heights of approximately 80 meters (m) located within 25 miles of existing or planned power lines and situated near developable landscapes. Additionally, the towers must be providing two-way, real-time communication to the Desert Research Institute.

Results and Status

Initial communications with Cellular One that were terminated due to newly initiated merger negotiations with another telecommunications company. Subsequent searches for a viable alternative resulted in contact being made to American Tower Corporation (ATC) in October 2005. Discussions with Jeffrey Deal at ATC began shortly thereafter and the Stone Cabin site in Nevada was chosen as a possible site location. The tower, owned by ATC, on the Stone Cabin site is the tallest tower in Nevada (80 meters tall). It is located approximately 31 miles east by northeast of Tonopah, Nevada along U.S. Route 6. **Figure 1** shows its location with respect to the four 50 meter metrological towers, used by DRI, the environmental research arm of the Nevada System of Higher Education, in the Wind energy assessment study for Nevada (Phases I and II). Approval to investigate the site further was given by Marc Schwartz via email on 15 Dec. 2005.

The site was again discussed with Marc Schwartz and Mary Jane Hale at a meeting held at NREL's National Wind Technology Center on 14 and 15 March 2006. The tower's drawbacks, its large structural members and communication horns at the top, were also discussed. However, the benefits of its location, with respect to local terrain and its ability to support anemometer booms, became clearer after the analysis of the wind measurements by both standard and sonic anemometers were performed, and outweighed the drawbacks. Consequently, site selection of the American Tower Corporation tower at Stone Cabin, Nevada, was approved and a fully executable lease agreement was delivered to DRI on 2 Dec. 2006.

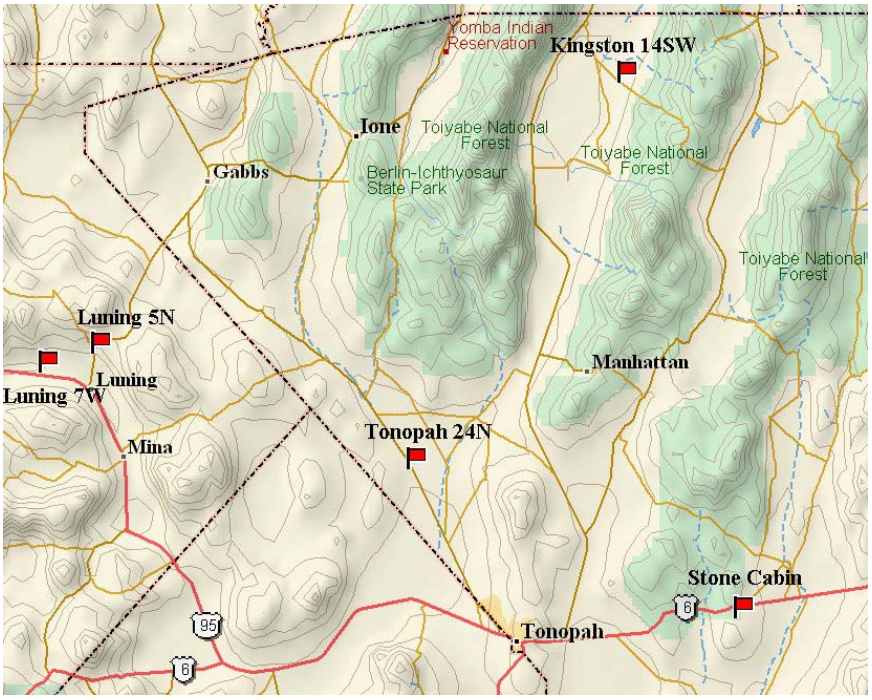

Figure 1. Location of the ATC tower at Stone Cabin

3 Deployment and Testing of Equipment

Task

Purchase the necessary meteorological equipment and install and test it on site.

Results and Status

The tower was equipped in February 2007. As proposed, the instrumentation was deployed and tested.

3.1 Stone Cabin Tower Anemometer Mounting Details

Wind measurement sensors were installed on the Stone Cabin tower on two tower legs at three elevations (40, 60 and 80 m above the land surface, respectively), totaling six instruments. At each elevation, cup anemometers were installed off the northern tower leg and 3-D sonic anemometers were installed off the southern tower leg. Sensor mounts were designed to insure the least amount of tower influence on the wind measurements as possible.

3.1.1 Cup Anemometer Mount

Cup anemometers were mounted on rigid (non-guyed) booms, consisting of an aluminum pipe (1.32" OD x 10' long), an “off-the-shelf” pipe bracket and a fabricated clamp. The clamp was designed to attach to the tower’s double angle iron cross brace, and is not guyed to the tower (**Figure 2**).

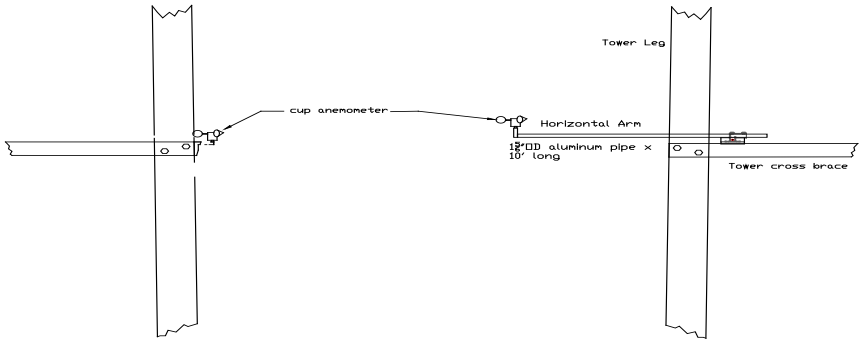

Figure 2. Cup anemometer generalized mount configuration

The angle iron clamp was designed to grip the double 2 ½" angle iron tower cross member (**Figure 3**). "Off-the-shelf" pipe brackets were modified to allow the boom to be retracted, for sensor installation and maintenance. The boom is a 10' long, 1" aluminum pipe (1.32" OD); however, a second clamp was used to insure a secure and stiff attachment to the tower cross member, so the sensor is only be 8' or so from the tower leg.

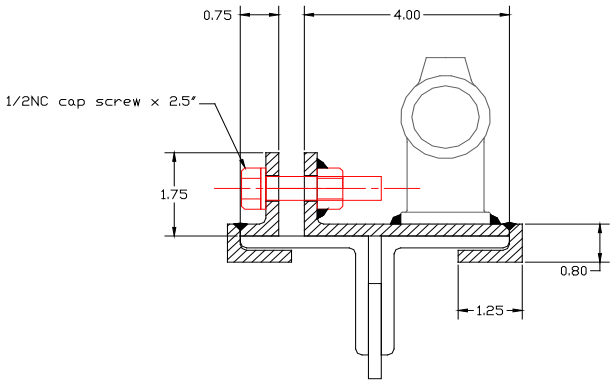

Figure 3. Cup anemometer angle iron clamp detail

3.1.2 3-D Sonic Anemometer Mount

The sonic anemometer measures wind speed in all three directions and, due to its short sampling path, is very sensitive to vertical sensor movement; therefore, these booms were designed to minimize sensor movement. This boom consisted of a 2"x 2"x10' aluminum tube mounted to the tower using the same fixture as the cup anemometers (**Figure 4**). This allowed the sensor arm to be extended to a length where the solid stabilizer arms could then be attached to the tower. The stabilizer arms were attached on solid pivots near the sensor mount. The pivots allowed the stabilizer to be adjustable to the pitch of the tower leg. The tower leg clamps (**Figures 5 and 6**) were designed to grip the tower leg without the clamp bolt being directly on the leg surface, through the use of the clamp plate. The use of the clamp plate allowed attachment at almost any point along the tower leg. This configuration allowed the instrumentation to be mounted without having specific engineering details about each tower mount point. Examples for the need of this flexibility can be seen in the photos of Section 3.3 where one of the 80 meter height struts was mounted to a support platform rather than the tower leg.

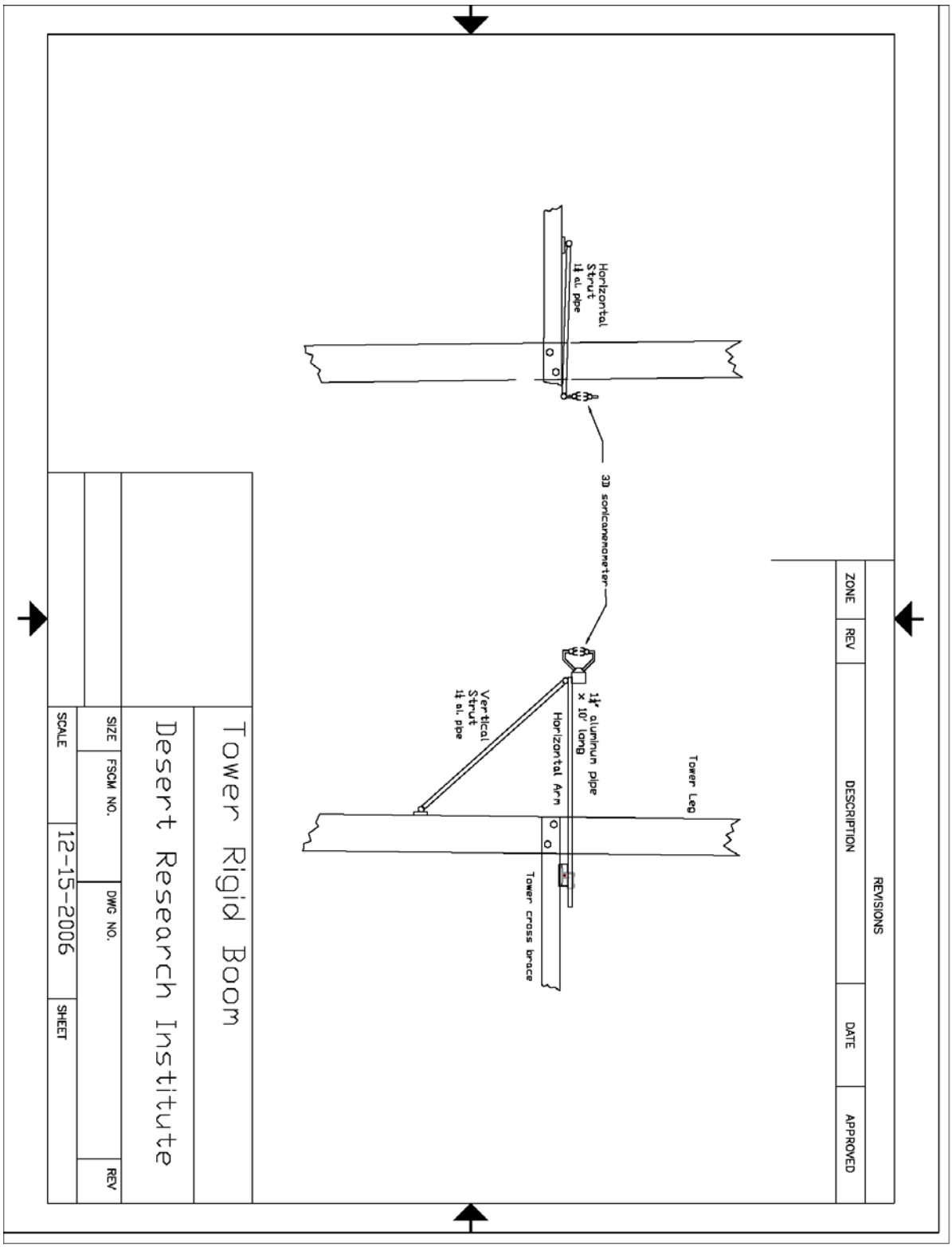

Figure 4. 3-D sonic generalized tower boom mount

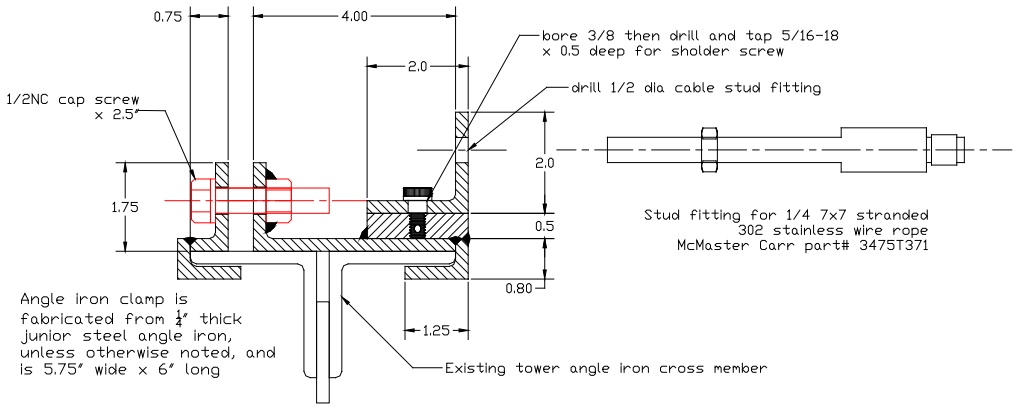

Figure 5. Guy cable angle iron clamp detail

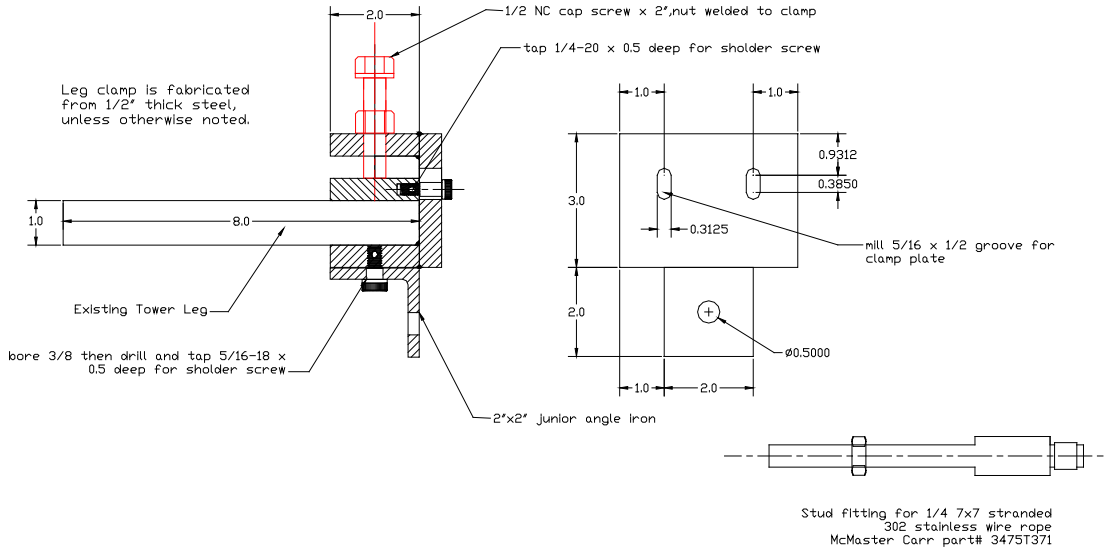

Figure 6. Guy cable leg clamp detail

3.2 Instrument Specifications

3.2.1 Specifications of Sonic Anemometer CSAT3 (from www.campbellsci.com)

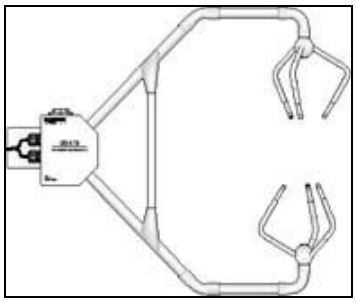

Figure 7. Campbell Scientific CSAT3 sonic anemometer

Specifications

Measurements

Outputs: u_x, u_y, u_z, c (u_x, u_y, u_z are wind components referenced to the anemometer axes; c is speed of sound)

Speed of Sound: Determined from three acoustic paths; corrected for cross-wind effects

Measurement Rate: programmable from 1 to 60 Hz, instantaneous measurements; two over-sampled modes are block averaged to either 20 Hz or 10 Hz

Measurement Resolution: u_x, u_y is 1 mm s^{-1} rms; u_z is 0.5 mm s^{-1} rms; c is 15 mm s^{-1} (0.025°C) rms; values are for instantaneous measurements made on a constant signal; noise is not affected by sample rate

Accuracy*

Offset error: <±4.0 cm s^{-1} (u_x, u_y)
<±2.0 cm s^{-1} (u_z)

Gain error: <±2% of reading (wind vector within ±5° of horizontal)
<±3% of reading (wind vector within ±10° of horizontal)
<±6% of reading (wind vector within ±20° of horizontal)

Rain: Innovative ultrasonic signal processing and user-installable wicks considerably improve the performance of the anemometer under all rain events

Output Signals

Digital SDM: CSI 33.3 k baud serial interface for datalogger/sensor communication. Data type is 2-byte integer per output plus 2-byte diagnostic

Digital RS-232

Baud rate: 9600, 19200 bps

Data type: 2-byte integer per output plus 2-byte diagnostic

Analog

Number of outputs: 4

Voltage range: ±5 V

Number of bits: 12

Reporting Range

SDM and RS-232 Digital Outputs

Full scale wind: ±65.535 m s^{-1} autoranging between four ranges; least significant bit is 0.25 to 2 mm s^{-1}

Speed of sound: 300 to 366 m s^{-1} (-50° to +60°C); least significant bit is 1 mm s^{-1} (0.002°C)

Analog Outputs:

Output	Range	LSB
u_x, u_y	±30 m s^{-1}, ±60 m s^{-1}	15 mm s^{-1}, 30 mm s^{-1}
u_z	±8 m s^{-1}	4 mm s^{-1}
c	300 to 366 m s^{-1} (-50° to +60°C)	16 mm s^{-1} (0.026°C)

**Accuracy specifications assume -30° to +50°C operating range; wind speeds < 30 m s^{-1}; wind angles between ±170°.*

3.2.2 *Specifications of NRG #200P Wind Direction Vane and #40C Cup Anemometer (from www.nrgsystems.com)*

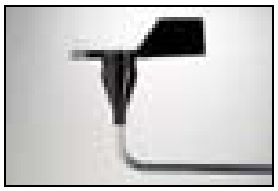

Figure 8. The NRG Systems #200P wind direction vane

SPECIFICATIONS

Description	Sensor type	continuous rotation potentiometric wind direction vane
	Applications	• wind resource assessment • meteorological studies • environmental monitoring
	Sensor range	360° mechanical, continuous rotation
	Instrument compatibility	all NRG loggers
Output signal	Signal type	Analog DC voltage from conductive plastic potentiometer, 10K ohms
	Transfer function	Output signal is a ratiometric voltage
	Accuracy	potentiometer linearity within 1%
	Dead band	8° Maximum, 4° Typical
	Output signal range	0 V to excitation voltage (excluding deadband)
Power requirements	Supply voltage	Regulated potentiometer excitation of 1 V to 15 V DC
Response characteristics	Threshold	1 m/s (2.2 miles per hour)
Installation	Mounting	onto a 13 mm (0.5 inch) diameter mast with cotter pin and set screw
	Tools required	0.25 inch nut driver, petroleum jelly, electrical tape
Environmental	Operating temperature range	-55 °C to 60 °C (-67 °F to 140 °F)
	Operating humidity range	0 to 100% RH
	Lifespan	50 million revolutions (2-6 years normal operation)
Physical	Connections	4-40 brass hex nut/post terminals
	Weight	0.14 kg (0.3 pounds)
	Dimensions	• 21 cm (8.3 inches) length x 12 cm (4.3 inches) height • 27 cm (10.5 inches) swept diameter
Materials	Body	black UV stabilized static-dissipating plastic
	Shaft	stainless steel
	Bearing	stainless steel
	Wing	black UV stabilized injection molded plastic
	Boot	protective PVC sensor terminal boot included
	Terminals	brass

Figure 9. The #40C cup anemometer

SPECIFICATIONS

Description	Sensor type	3-cup anemometer
	Applications	• wind resource assessment • meteorological studies • environmental monitoring
	Sensor range	1 m/s to 96 m/s (2.2 mph to 214 mph) (highest recorded)
	Instrument compatibility	all NRG loggers
Output signal	Signal type	low level AC sine wave, frequency linearly proportional to windspeed
	Transfer function	m/s = (Hz x 0.765) + 0.35 [miles per hour = (Hz x 1.711) + 0.78]
	Accuracy	within 0.1 m/s (0.2 mph) for the range 5 m/s to 25 m/s (11 mph to 55 mph)
	Calibration	each anemometer individually calibrated, calibration reports provided via electronic download
	Output signal range	0 Hz to 125 Hz (highest recorded)
Response characteristics	Threshold	0.78 m/s (1.75 miles per hour)
	Distance constant (63% recovery)	3.0 m (10 feet)
	Moment of inertia	68 x 10^{-6} S-ft^2
	Swept diameter of rotor	190 mm (7.5 inches)
Installation	Mounting	onto a 13 mm (0.5 inch) diameter mast with cotter pin and set screw
	Tools required	0.25 inch nut driver, petroleum jelly, electrical tape
Environmental	Operating temperature range	-55 °C to 60 °C (-67 °F to 140 °F)
	Operating humidity range	0 to 100% RH
Physical	Connections	4-40 brass hex nut/post terminals
	Weight	0.14 kg (0.3 pounds)
	Dimensions	• 3 cups of conical cross-section, 51 mm (2 inches) dia. • 81 mm (3.2 inches) overall assembly height
Materials	Cups	one piece injection-molded black polycarbonate
	Body	housing is black ABS plastic
	Shaft	beryllium copper, fully hardened
	Bearing	modified Teflon, self-lubricating
	Magnet	Indox 1, 25 mm (1 inch) diameter, 13 mm (0.5 inch) long, 4 poles
	Coil	single coil, bobbin wound, 4100 turns of #40 wire, shielded for ESD protection
	Boot	protective PVC sensor terminal boot included
	Terminals	brass

3.3 Photos of Mounted Instrumentation

Figure 10 shows the mounted instrumentation on the Stone Cabin tower.

Figure 10. Photos of the mounted standard and sonic anemometers at 40, 60, and 80 m on the Stone Cabin tower

4 Data Acquisition

Task

Connect the on-site data logger to the communications equipment and ensure that all data can be consistently communicated and stored on-line.

Results and Status

Data collection started on February 8, 2007. The data was stored onsite and manually downloaded approximately once a month and recorded on DVD. **Table 1** shows the current structure of the stored files for the standard (**Table 1**) and sonic (**Table 2**) data sets.

Table 1. List of Archived Standard Anemometer Wind Data for the Stone Cabin Tower

Currently Archived Standard Anemometer Data for Stone Cabin (40, 60, and 80 m)					
File number	Size	Start date	Start time	End date	End time
40	572.0 kb	02/08/07	05:22:00 PM	02/10/07	11:00:00 AM
41	188.7 kb	02/10/07	11:01:00 AM	02/11/07	12:00:00 AM
63	7.6 Mb	02/11/07	12:01:00 AM	03/05/07	12:59:00 PM
64	164.4 kb	03/05/07	01:01:00 PM	03/06/07	12:00:00 AM
92	6.3 Mb	03/06/07	12:01:00 AM	04/02/07	11:59:00 PM
95	1.3 Mb	04/03/07	12:00:00 AM	04/06/07	05:54:00 PM
120	8.1 Mb	04/06/07	05:55:00 PM	04/30/07	02:15:00 PM
156	12.4 Mb	04/30/07	02:16:00 PM	06/05/07	06:35:00 PM
203	15.8 Mb	06/05/07	06:36:00 PM	07/22/07	10:00:00 AM
234	10.6 Mb	07/22/07	10:01:00 AM	08/22/07	04:25:00 PM
262	9.8 Mb	08/22/07	04:26:00 PM	09/20/07	06:25:00 PM

Table 2. List of Archived Sonic Anemometer Wind Data for the Stone Cabin Tower

Currently Archived Sonic Anemometer Data for Stone Cabin		
Measurement Height	Start date	End date
40 m:	02/08/07	02/24/07
	02/26/07	03/09/07
	04/02/07	04/29/07
	06/05/07	09/19/07
60 m:	02/08/07	03/09/07
	04/02/07	04/29/07
	06/05/07	09/19/07
80 m:	02/08/07	03/09/07
	04/02/07	04/29/07
	06/05/07	09/19/07

5 Database Development and Programming

Task

Create links from Internet to database. Use existing, previously developed algorithms and develop new ones as needed to provide the required statistical analyses.

Results and Status

The 20 Hz sonic anemometer data reside on our process computers. The standard anemometer data were archived at 1-minute intervals for all three levels and publicly accessible on the Internet at:

http://www.wrcc.dri.edu/cgi-bin/rawMAIN.pl?nvwnd6

We have also processed and posted 10 minute standard anemometer data from the 50 m towers at five levels in western Nevada (near Tonopah), and they are also publicly available on the Internet at:

http://www.wrcc.dri.edu/cgi-bin/rawMAIN.pl?nvwnd1
http://www.wrcc.dri.edu/cgi-bin/rawMAIN.pl?nvwnd2
http://www.wrcc.dri.edu/cgi-bin/rawMAIN.pl?nvwnd3
http://www.wrcc.dri.edu/cgi-bin/rawMAIN.pl?nvwnd4

Details on the 50 meter towers and their data can be found in Belu and Koracin (2009).

6 Maintenance

Task

Monitor the data received in real-time for evidence of a system malfunction. Generate a work order to the equipment subcontractor or visit the site as soon as possible to resolve sensor problems. Otherwise, the site will be visited quarterly for general inspection and testing.

Results and Status

A detailed list of all installation and maintenance events is as follows:

Feb. 5-9, 2007	Site installation. (Greg McCurdy, Brad Lyles, Mike Betke and crew)
Feb. 10, 2007	Site visit for equipment check and data retrieval. (Greg McCurdy)
Mar. 5, 2007	Site visit for equipment check and data retrieval. Minor programming adjustments to data collection computer. (Greg McCurdy)
Apr. 3, 2007	Site visit for equipment check and data retrieval. Found data collection computer locked up. Operating system adjustments of virus protection software (seemed to be the cause of the problem). (Greg McCurdy)
Apr. 6, 2007	Site visit to check on previous changes, verification of operation and data collection processes. Operation normal. (Greg McCurdy)
Apr. 30, 2007	Site visit for equipment check and data retrieval. Operation normal. (Greg McCurdy)

Jun. 5, 2007	Site visit for equipment check and data retrieval. Operation normal. (Greg McCurdy)
Jul. 22, 2007	Site visit for equipment check and data retrieval. Operation normal. (Greg McCurdy)
Aug. 22, 2007	Site visit for equipment check and data retrieval. Operation normal. (Greg McCurdy)
Sep. 20, 2007	Site visit for equipment check and data retrieval. Operation normal. (Greg McCurdy)
Dec. 5, 2007	Site visit for equipment check and data retrieval. Operation normal. (Greg McCurdy)

Operation normal - all sensors functioning, data collection routines checked, all data retrieved from collection computer, collection computer file system maintenance done, power systems check, and visual inspection of sensor physical condition (orientation and mounting).

7 Turbulence, Statistics, and Analysis

Task

The main objective is to determine the structure and temporal variability of turbulence using sonic anemometers at vertical levels relevant to hub heights. This section will also address the extent to which turbulence transfer can be inferred from profile measurements of winds and temperature. The study will include a time series analysis of winds and turbulence and estimation of their parametric and non-parametric statistical distributions; spectral analysis of winds and turbulence fluxes that determine expected peak energy; and determination of the strength of diurnal effects at high elevations. Statistics of the winds and turbulence will be performed for each season as well as analysis of the properties of the turbulence for various wind speed regimes.

We also will examine the validity of using acoustic sounder measurements to infer turbulence transfer through measurements of wind velocity fluctuations and the temperature-structure function. Seasonal and annual statistics of acoustic sounder vs. tall tower data will be compared and the impact on the computation of wind power density will be assessed. This assessment will provide insight into the feasibility and usefulness of using acoustic sounders for wind energy studies.

Results and Status

7.1 Comparison Between Sonic and Standard Anemometer Measurements

Sonic and standard anemometers use entirely different principles in order to measure wind speed and direction. Standard anemometers, such as cup and vane or propeller and vane designs, rely on the momentum in the wind to determine their angular momentum (or angular orientation, in the case of wind vanes); that is, to spin the cups or propeller. Because of this reliance on the angular momentum of the cups or propeller (which have angular inertia, however light they have been built), there is an inherent time lag for these designs to detect a change in wind speed. They are not generally sensitive enough to detect the wind variances that determine the turbulence flux quantities.

Sonic anemometers do not rely on direct measurement of the wind's momentum. Their operating principle is to measure the change in the speed of sound of the air across several different paths. By measuring the Doppler signal, a sonic anemometer can measure turbulence fluxes. This aspect of sonic anemometers is illustrated in Section 4. In theory, this design should allow sonic anemometers to be very sensitive to changes in wind speeds.

In this section, we have assembled plots illustrating various comparisons of the sonic and standard anemometer data from Stone Cabin, NV. These plots are arranged by time domains in 2007, which are as follows: 9-27 February, 2-29 April, 5-30 June, 1-31 July, 1-31 August, 1-20 September, and the complete time domain of 9 February-20 September. In each time domain, there are time series, scatter plots, and histograms comparing the sonic and standard anemometer results at the three measurement heights: 40, 60, and 80 m AGL.

The frequency of sampling of the sonic anemometers was 20 measurements per second. For the standard anemometers, it was one measurement per second. For the purpose of better comparison with our simulated data sets, which give hourly results, we have created and used three different averaging schemes for the anemometer data, which average over different subsets of each hour to give one value to represent the entire hour. The three subsets were averaged over the whole hour, averaging over the last ten minutes in each hour, and averaging over the last one minute in each hour. These three averaging schemes are shown in the plots of the first time domain (9-27 February).

Over the time scales involved here (roughly monthly), it is hard to see any significant differences between these averaging schemes when we look at the plots. The scatter plots of **Figures 13, 15, and 16** show very close agreement between the different averaging schemes, with somewhat weaker agreement at 80 m. So, for the purpose of comparing sonic and standard anemometers, we have relied on the ten minute averages.

The scatter plots over all time domains show strong agreement between the sonic and standard anemometers, with correlations ranging from .78 to almost unity (.99). The time series and histograms show an interesting difference between these anemometer types—a difference we would suspect from the design differences mentioned above. In the time series, we often notice that the sonic data seems like a green fringe above the standard data at higher wind values (for example, see **Figure 11**, top plot, on 21-23 February). Although they track each other closely, the sonic data seems to register slightly higher wind values during periods of strong winds. In addition, the standard anemometer histograms show much larger counts of observations in the lowest bin (0-1 m/s), see **Figures 13, 18, and 21**. These findings are consistent with the view that standard anemometers are not as sensitive as sonics at very low wind speeds, nor do they react quickly enough at higher wind speed to register some changes. Both of these contentions are supported by the fact that the mean wind speeds are consistently higher from the sonic data. Notice that the bias for the entire period is greatest at 80 m (0.7 m/s) and decreases to 0.5 and 0.4 m/s at 60 and 40 m, respectively.

In some cases (**Figures 19 and 34**), there are sharp wind speed peaks over 20 m/s at 80 m that are not recorded by the sonic anemometer. This should be examined further in the future. **Figure 34** also shows that there are peaks over 15 m/s that were recorded at all levels.

Figure 35 shows that the agreement between the sonic and the standard anemometer decreases with increasing height, possibly due to differences in measurement techniques and also due to tower structure and flow shadowing.

The scatter plots, and associated correlation coefficient and bias, comparing wind speed at 80 m with each of the other heights (40 and 60 m) indicate that there is a certain noise in measuring wind speed at 80 m. This is possibly due to the large antennas at 80 m (see **Figure 10**). Consequently, the time series plots show much better agreement between the sonic and standard anemometer measurements at 40 m and 60 m, compared to 80 m.

Because of this better sensitivity, and since sonic anemometers also provide turbulence flux information, we conclude that they might be more appropriate for measuring long term wind patterns than the conventional anemometers. However, we should also consider an issue of possible need for more frequent calibration and maintenance.

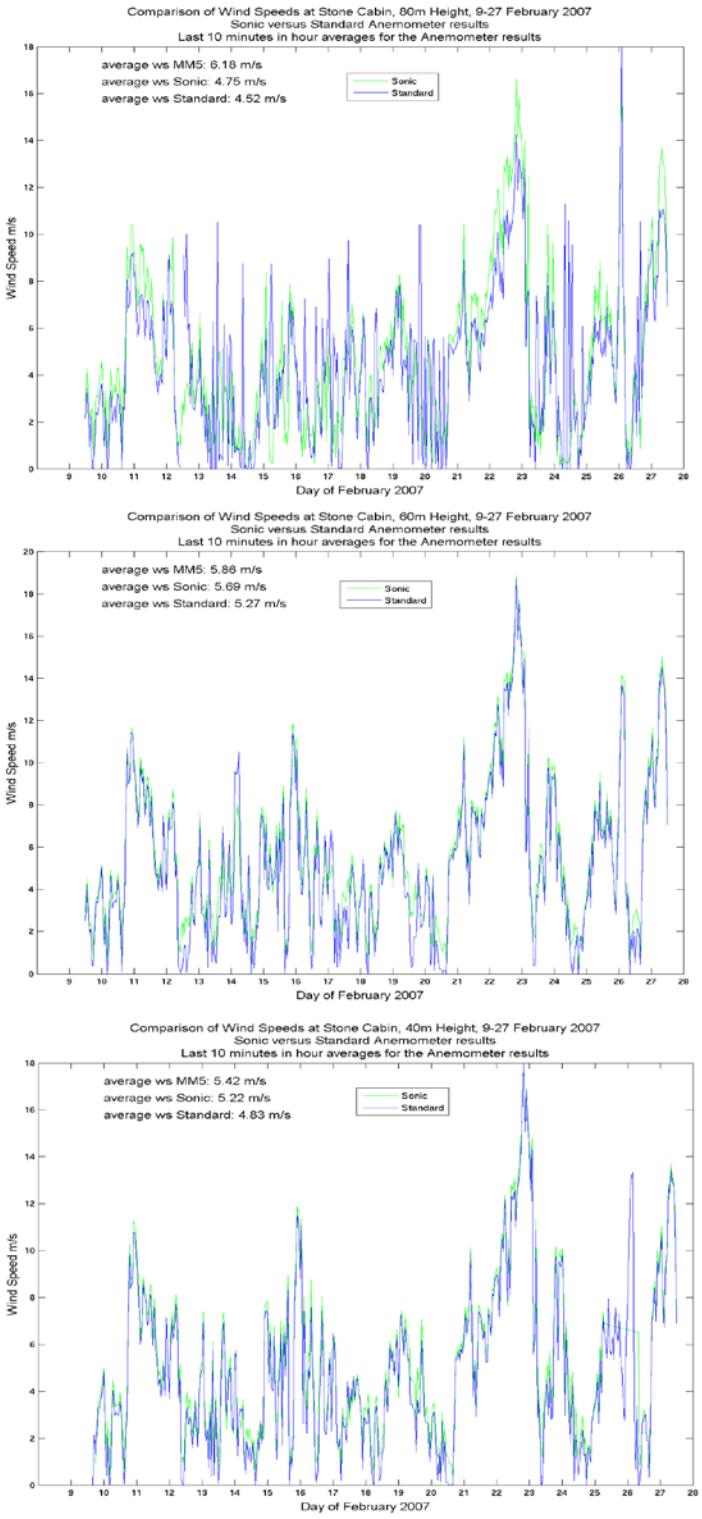

Figure 11. 10-minute averaged sonic (green) and standard (blue) anemometer measurements of wind speeds for the period 9-27 February 2007 at (top) 80 m, (center) 60 m, and (bottom) 40 m.

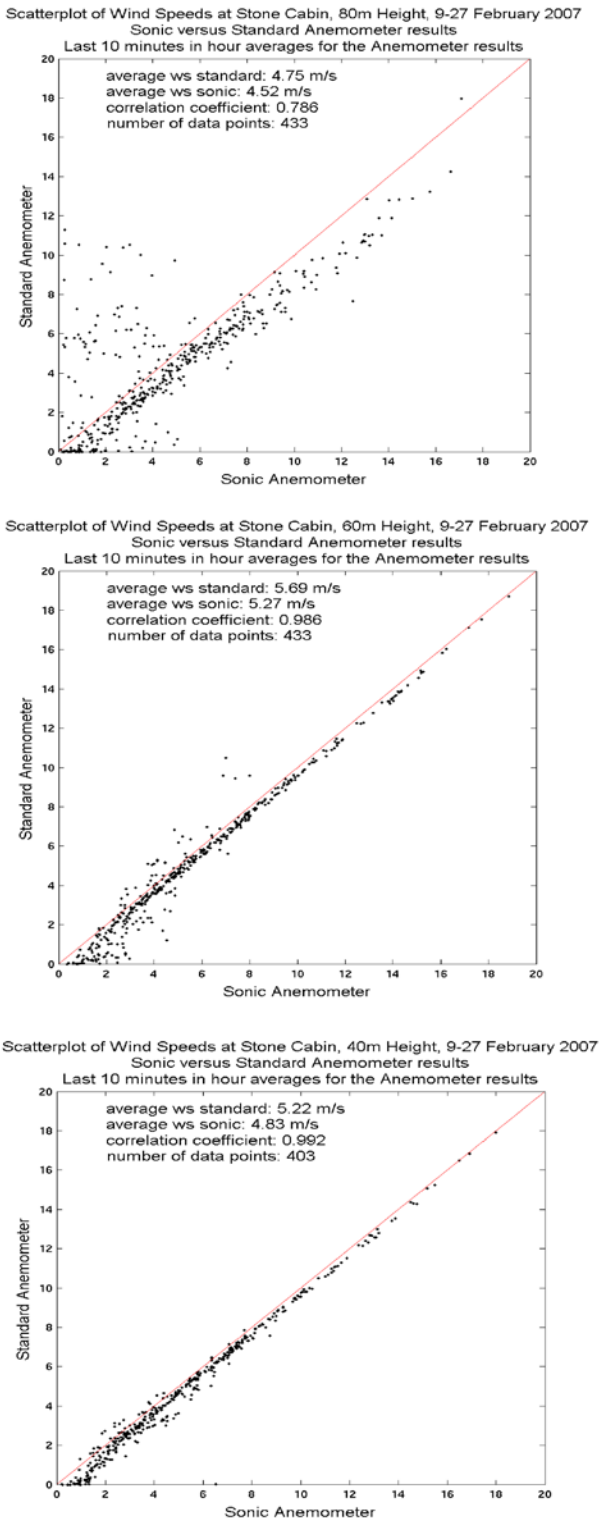

Figure 12. Scatterplots of 10-minute averaged sonic vs. standard anemometer measurements of wind speeds for the period 9-27 February 2007 at (top) 80 m, (center) 60 m, and (bottom) 40 m.

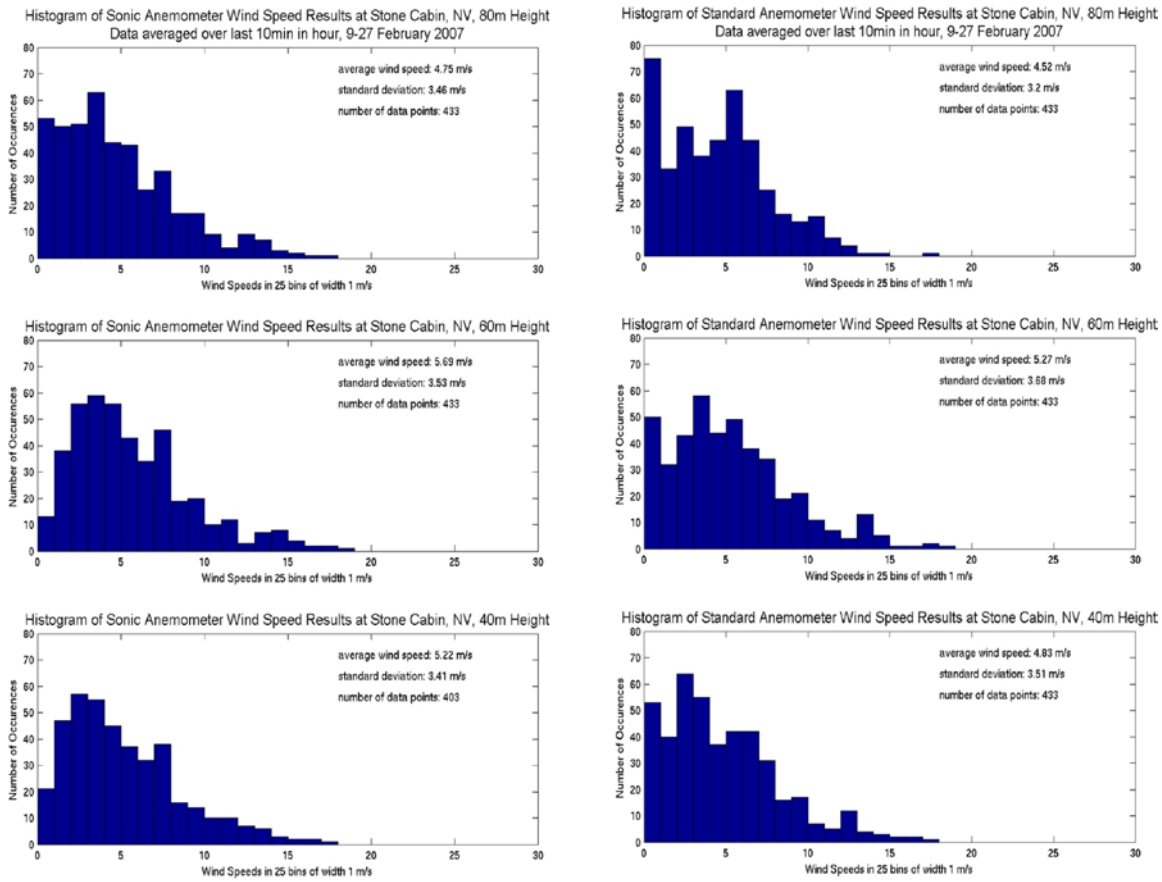

Figure 13. Histograms of 10-minute averaged sonic (left) and standard (right) anemometer measurements of wind speeds for the period 9-27 February 2007 at (top) 80 m, (center) 60 m, and (bottom) 40 m.

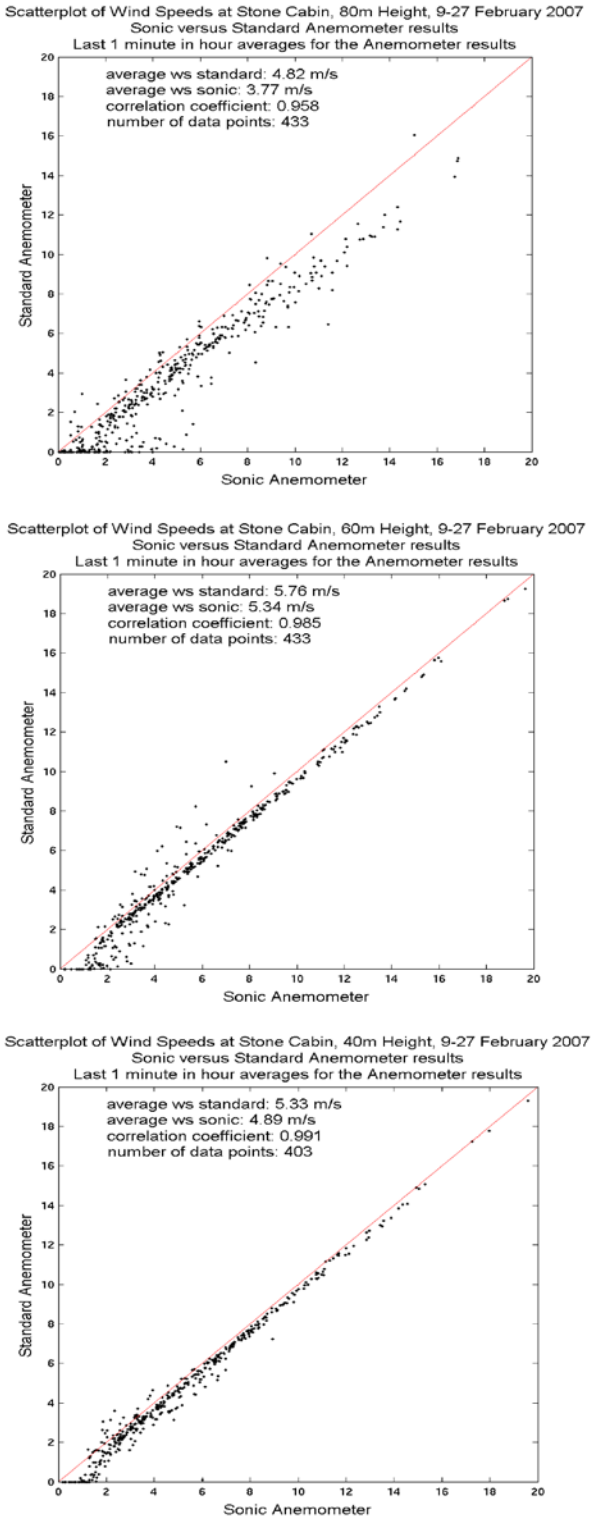

Figure 14. Scatterplots of 1-minute averaged sonic vs. standard anemometer measurements of wind speeds for the period 9-27 February 2007 at (top) 80 m, (center) 60 m, and (bottom) 40 m.

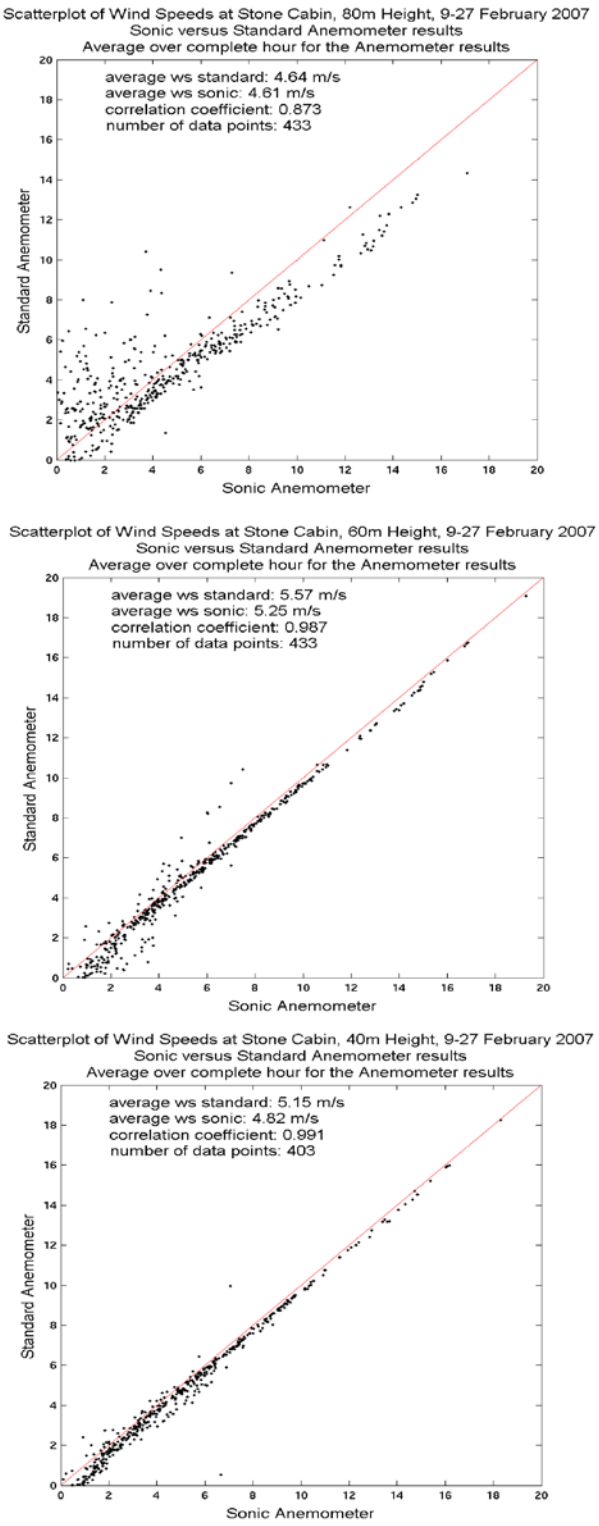

Figure 15. Scatterplots of hourly averaged sonic vs. standard anemometer measurements of wind speeds for the period 9-27 February 2007 at (top) 80 m, (center) 60m, and (bottom) 40 m.

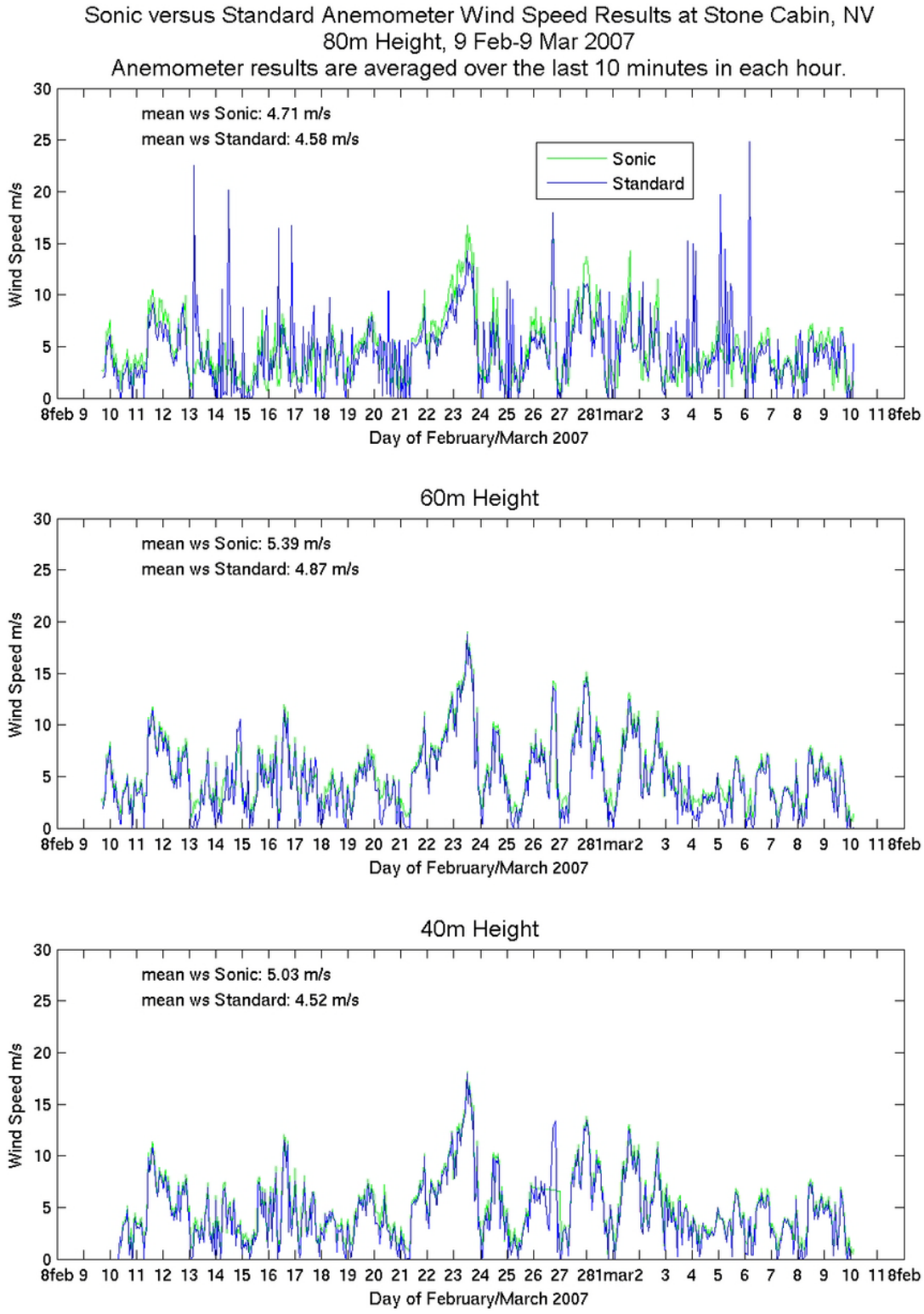

Figure 16. 10-minute averaged sonic (green) and standard (blue) anemometer measurements of wind speeds for the period 9 February-9 March 2007 at (top) 80 m, (center) 60 m, and (bottom) 40 m.

(The package MATLAB is used to estimate the mean values.)

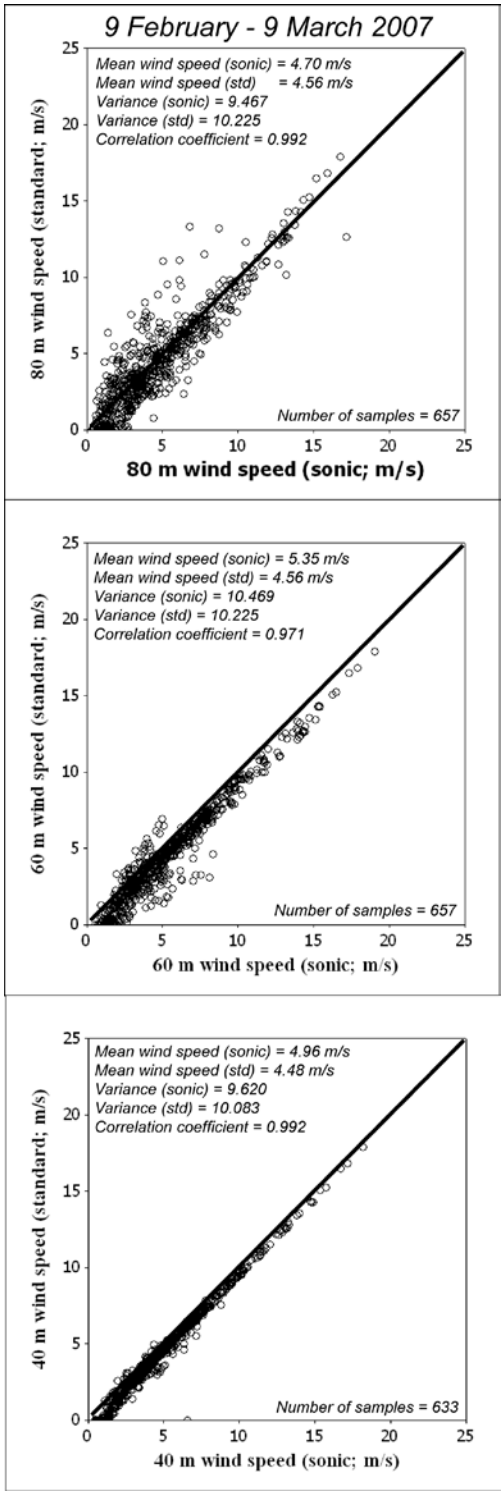

Figure 17. Scatterplots of 10-minute averaged sonic vs. standard anemometer measurements of wind speeds for the period 9 February-9 March 2007 at (top) 80 m, (center) 60 m, and (bottom) 40 m.

The package MINITAB was used to estimate the statistical parameters. Wind speeds greater than 25 m s^{-1} were not included. The number of sample pairs is indicated in each box.

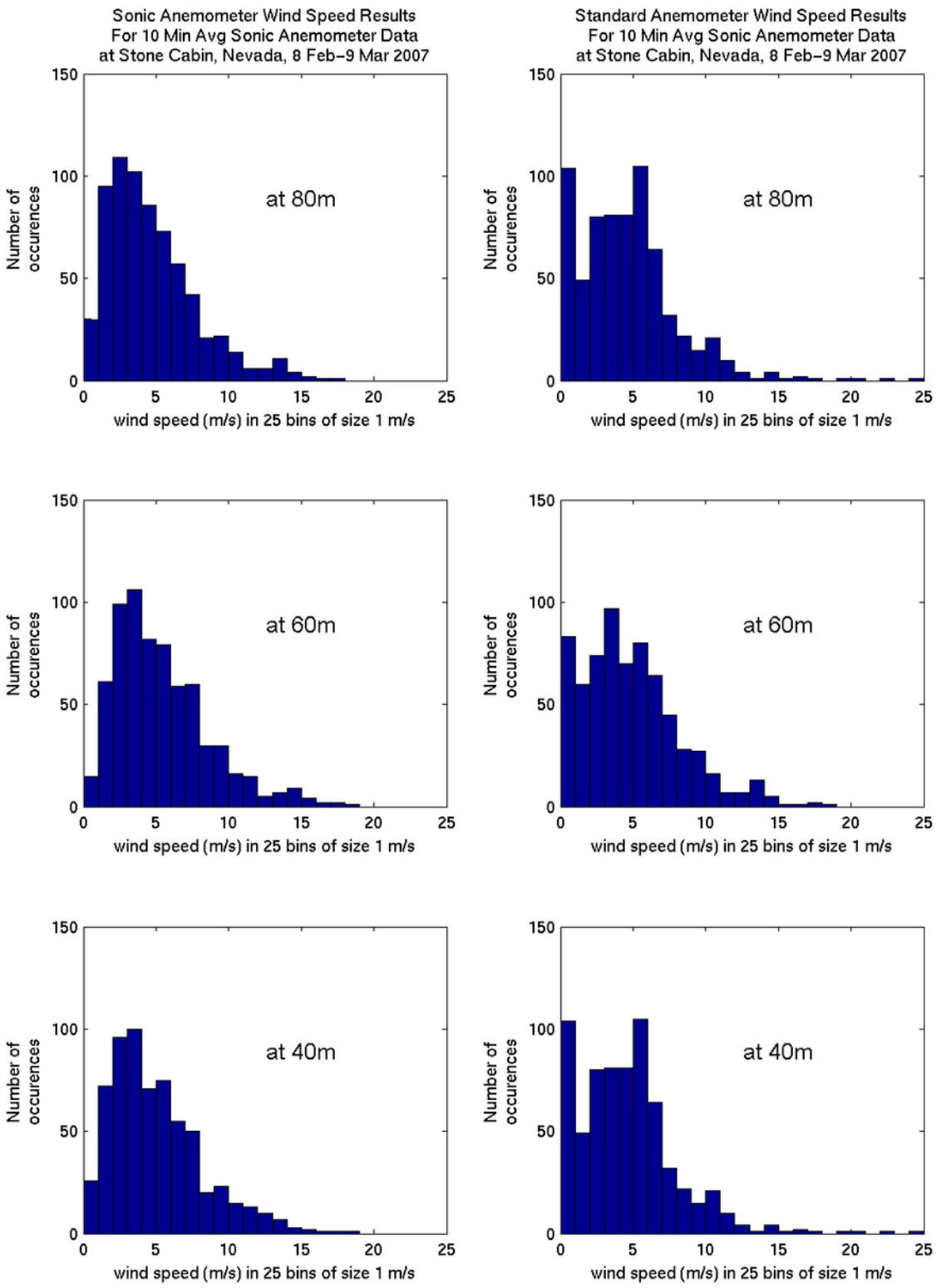

Figure 18. Histograms of 10-minute averaged sonic (left) and standard (right) anemometer measurements of wind speeds for the period 9 February-9 March 2007 at (top) 80 m, (center) 60 m, and (bottom) 40 m.

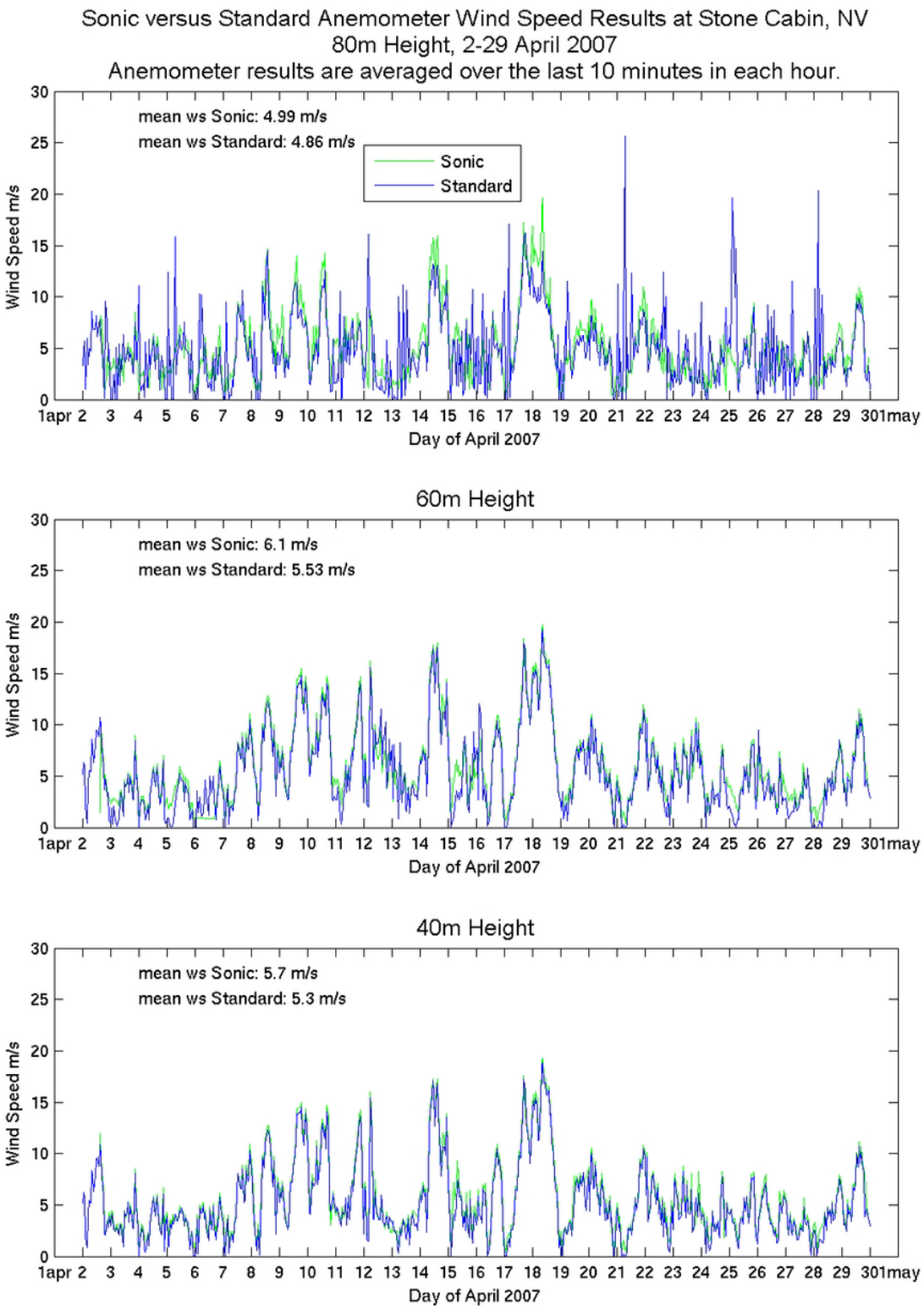

Figure 19. 10-minute averaged sonic (green) and standard (blue) anemometer measurements of wind speeds for the period 2-29 April 2007 at (top) 80 m, (center) 60 m, and (bottom) 40 m.

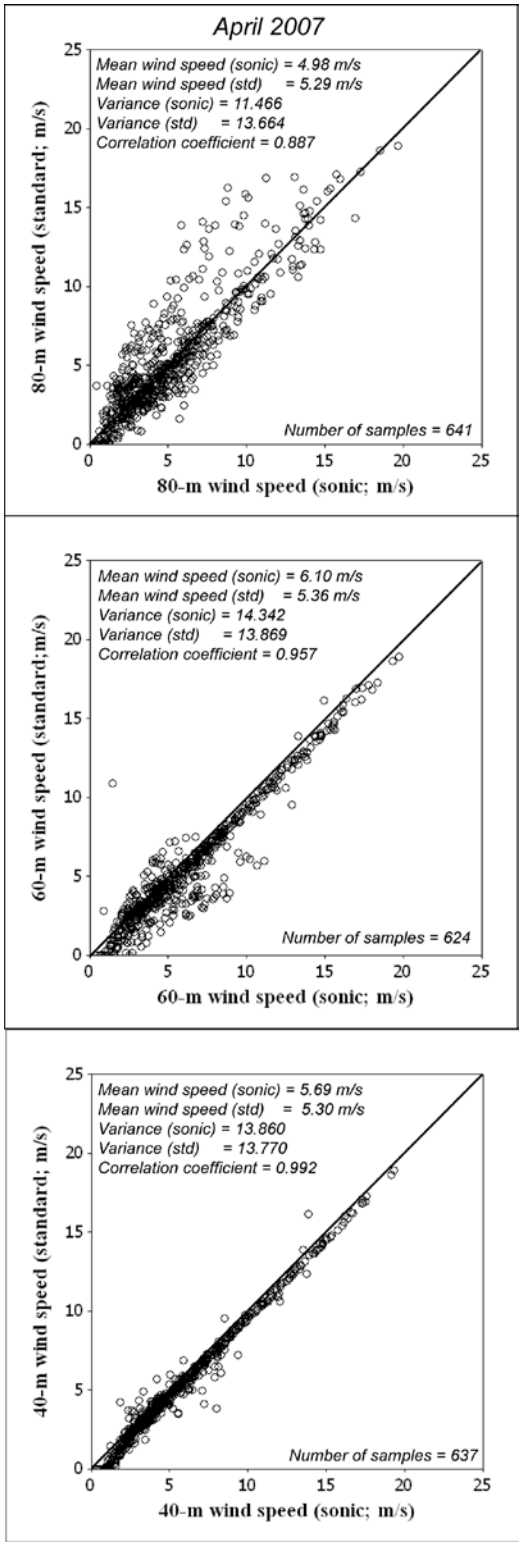

Figure 20. Scatterplots of 10-minute averaged sonic vs. standard anemometer measurements of wind speeds for the period 2-29 April 2007 at (top) 80 m, (center) 60 m, and (bottom) 40 m.

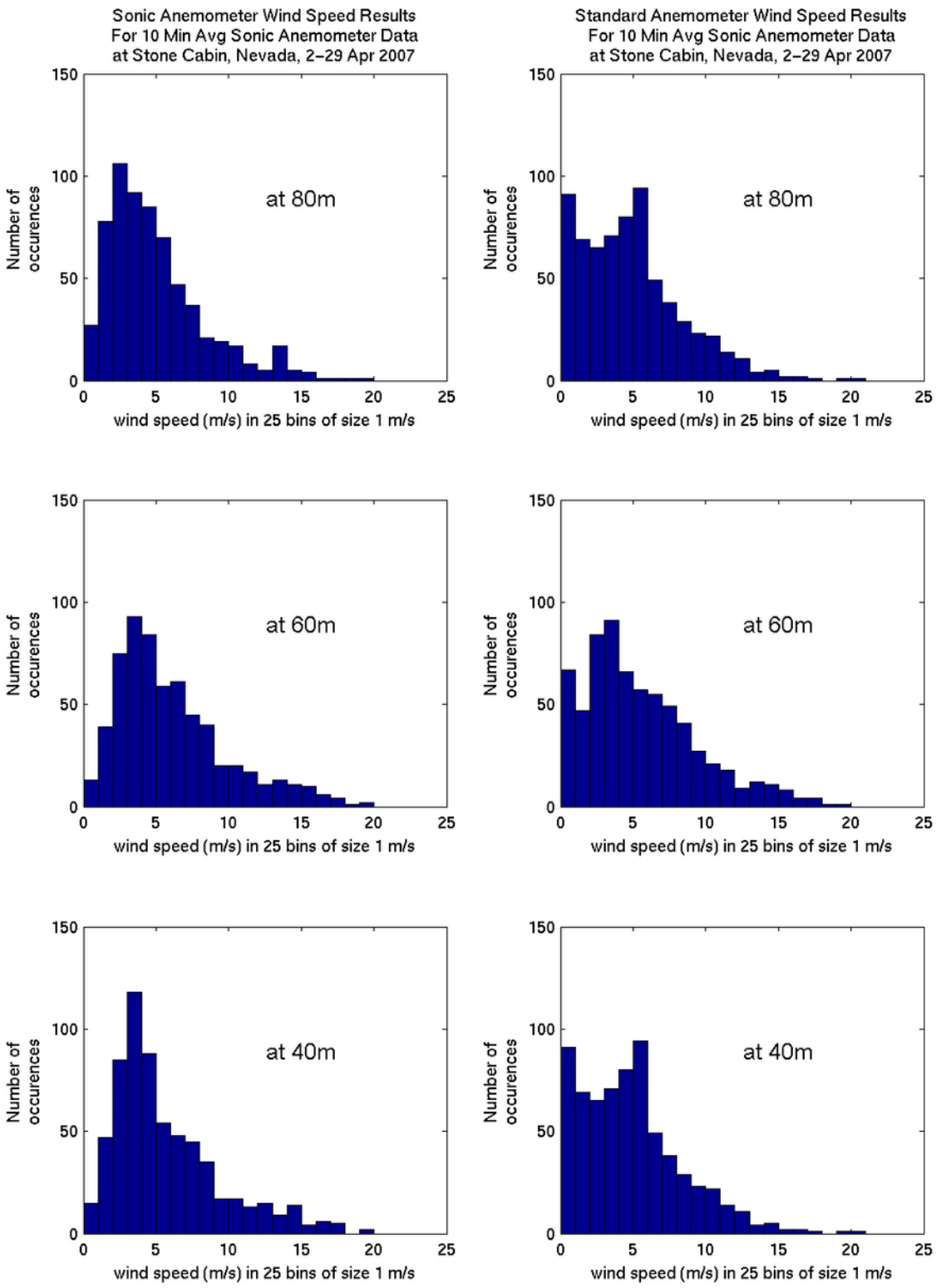

Figure 21. Histograms of 10-minute averaged sonic (left) and standard (right) anemometer measurements of wind speeds for the period 2-29 April 2007 at (top) 80 m, (center) 60 m, and (bottom) 40 m.

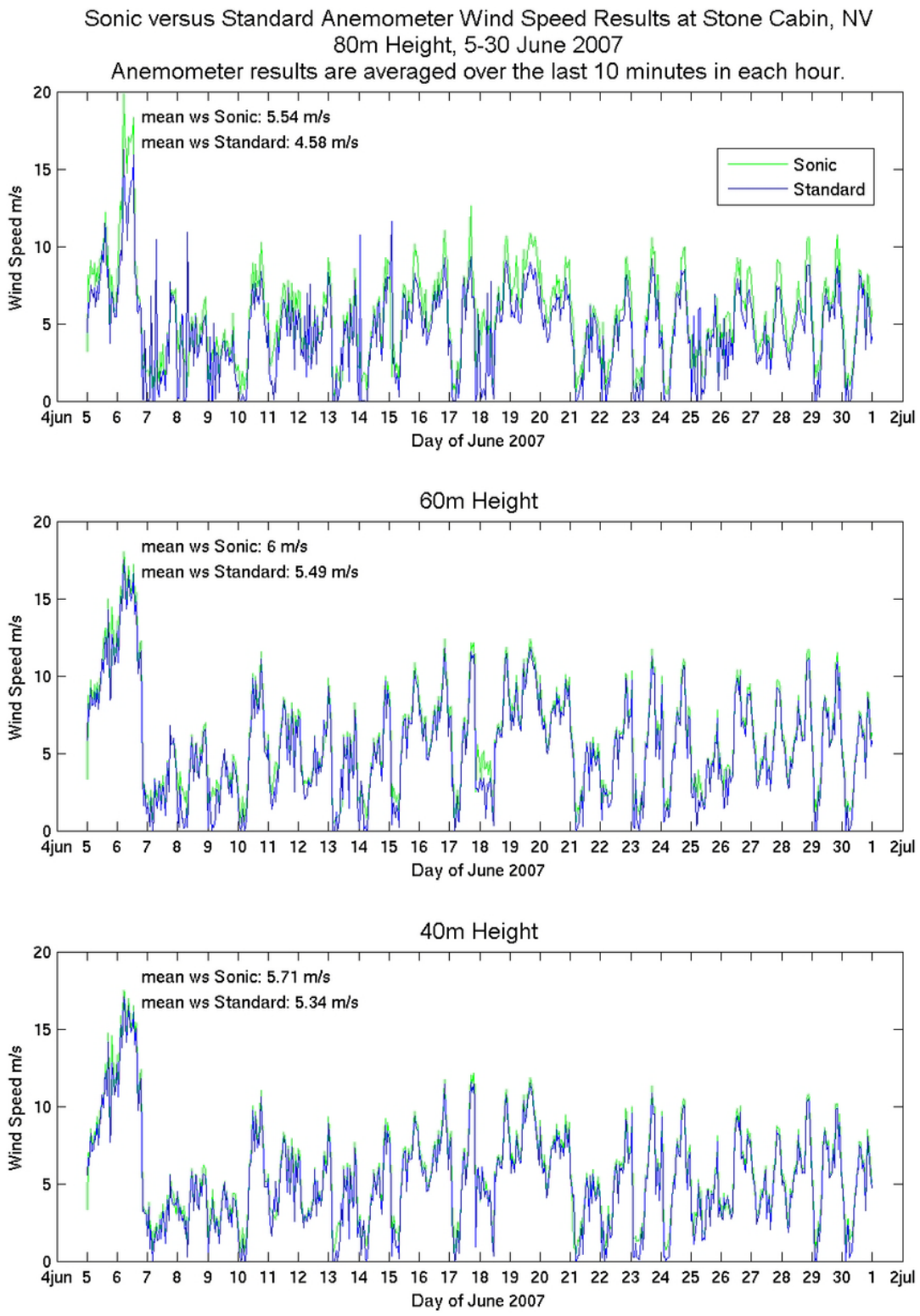

Figure 22. 10-minute averaged sonic (green) and standard (blue) anemometer measurements of wind speeds for the period 5-30 June 2007 at (top) 80 m, (center) 60 m, and (bottom) 40 m.

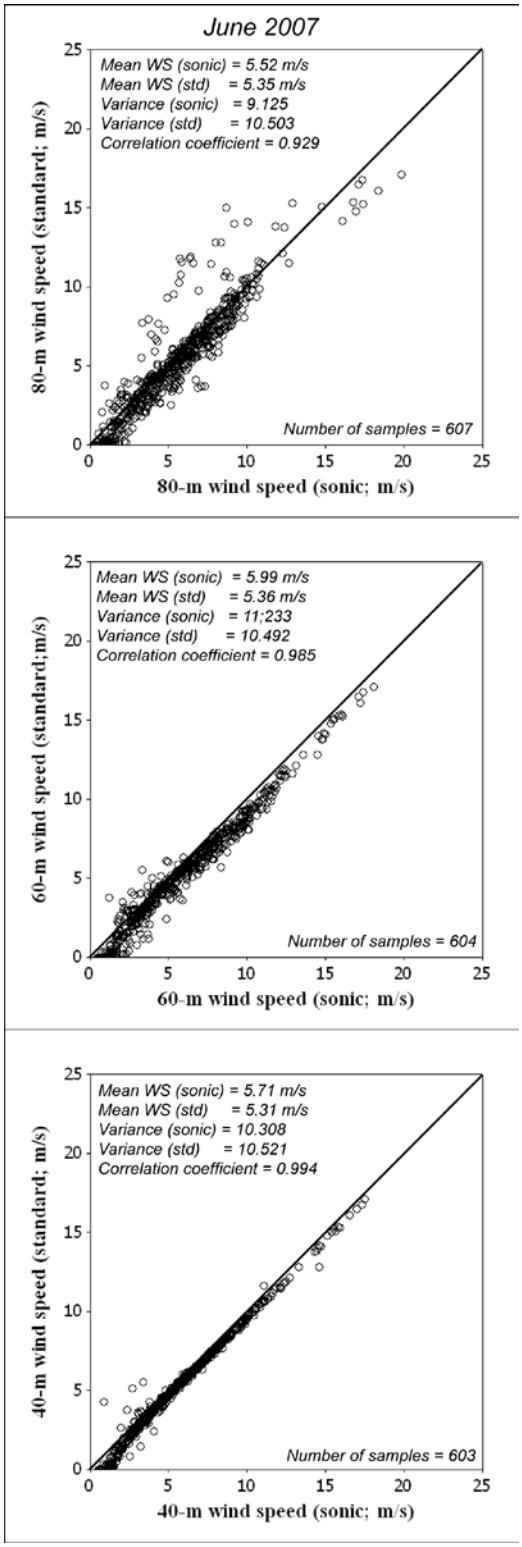

Figure 23. Scatterplots of 10-minute averaged sonic vs. standard anemometer measurements of wind speeds for the period 5-30 June 2007 at (top) 80 m, (center) 60 m, and (bottom) 40 m.

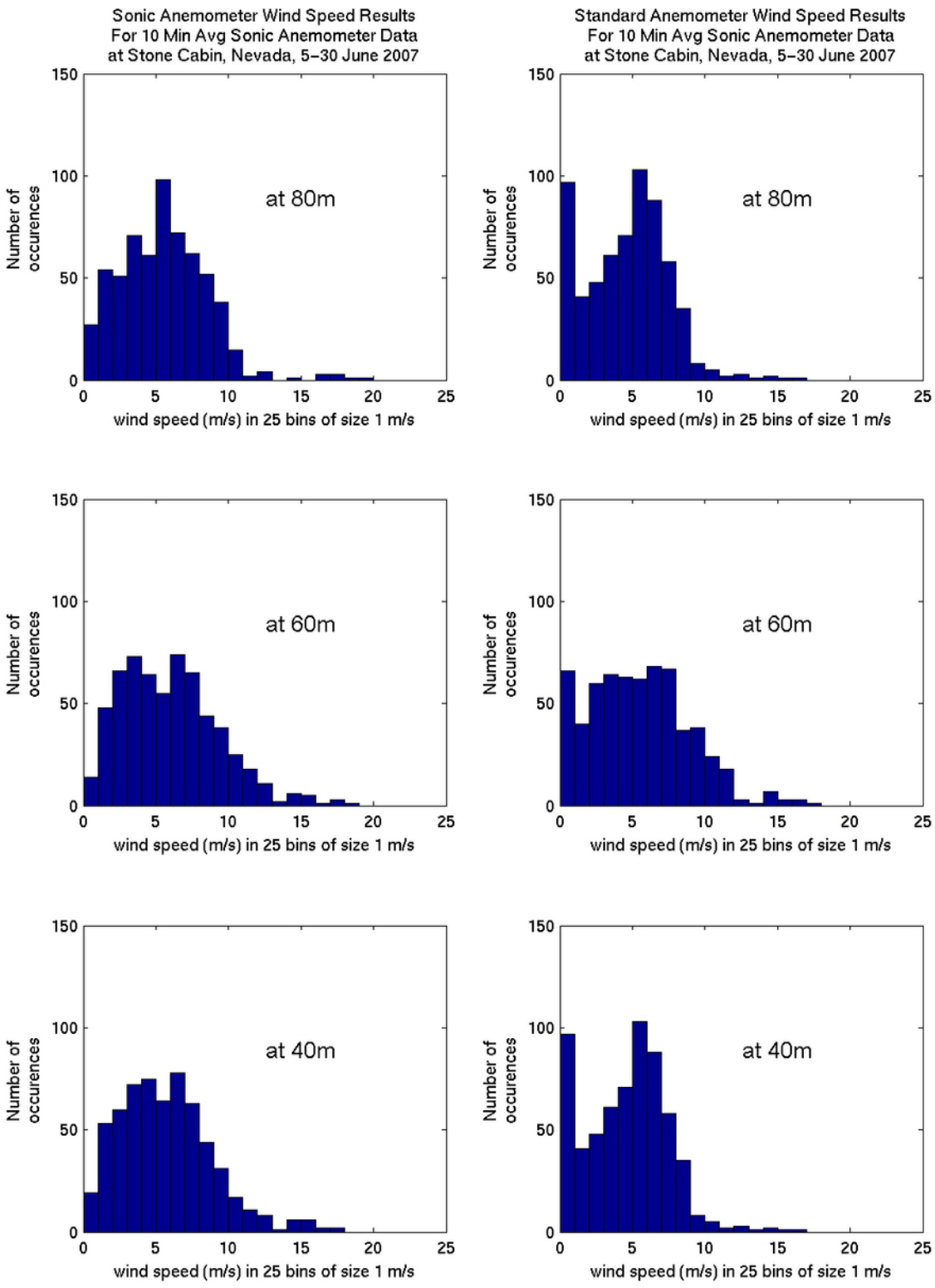

Figure 24. Histograms of 10-minute averaged sonic (left) and standard (right) anemometer measurements of wind speeds for the period 5-30 June 2007 at (top) 80 m, (center) 60 m, and (bottom) 40 m.

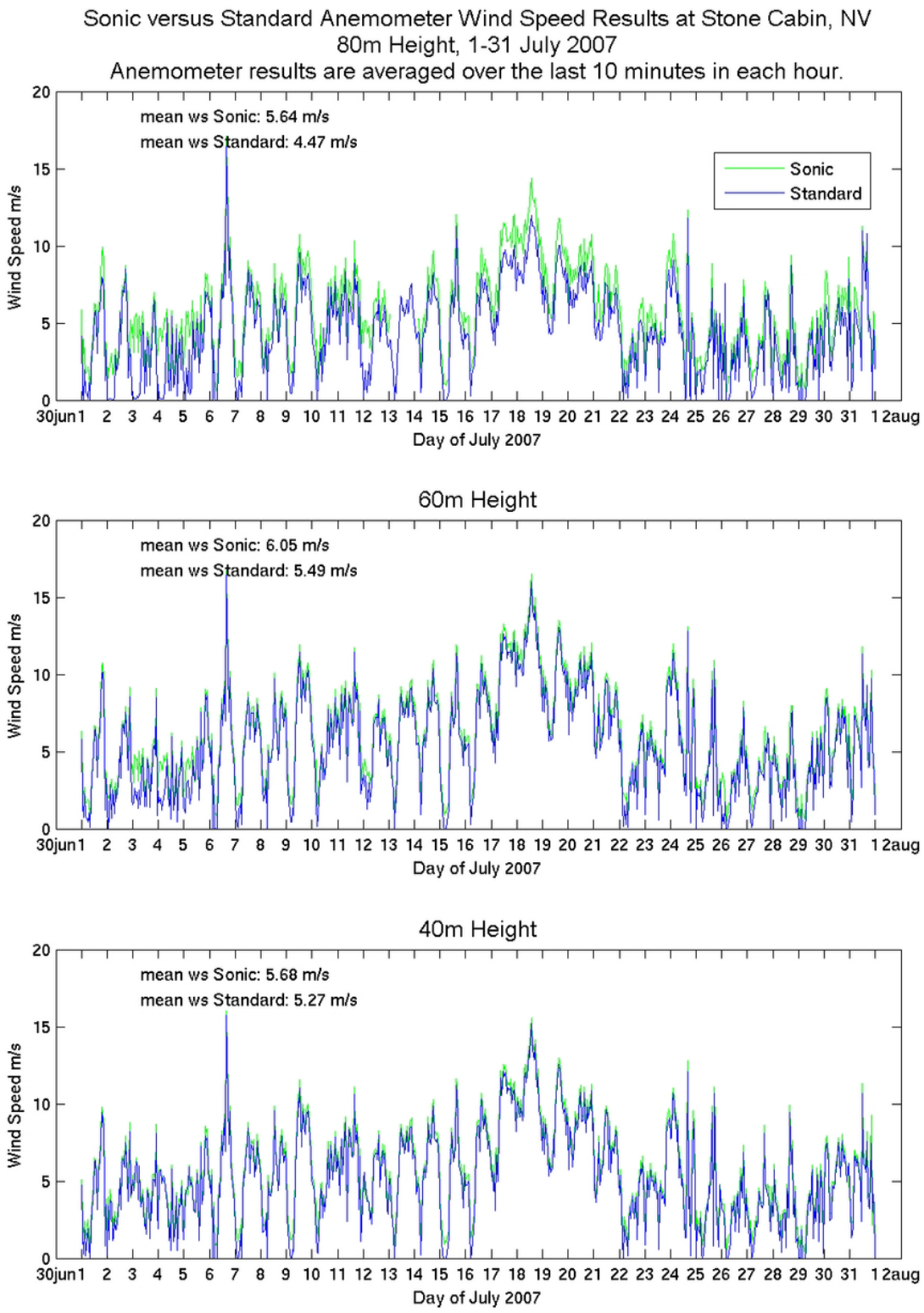

Figure 25. 10-minute averaged sonic (green) and standard (blue) anemometer measurements of wind speeds for the period July 2007 at (top) 80 m, (center) 60 m, and (bottom) 40 m.

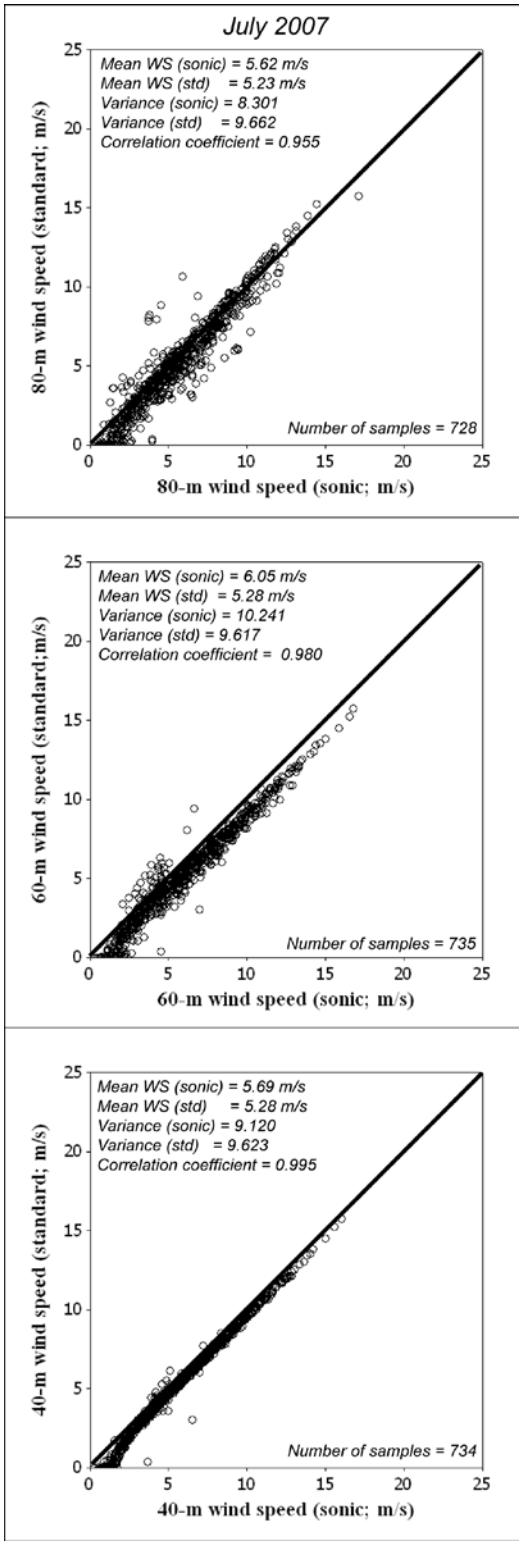

Figure 26. Scatterplots of 10-minute averaged sonic vs. standard anemometer measurements of wind speeds for the period July 2007 at (top) 80 m, (center) 60 m, and (bottom) 40 m.

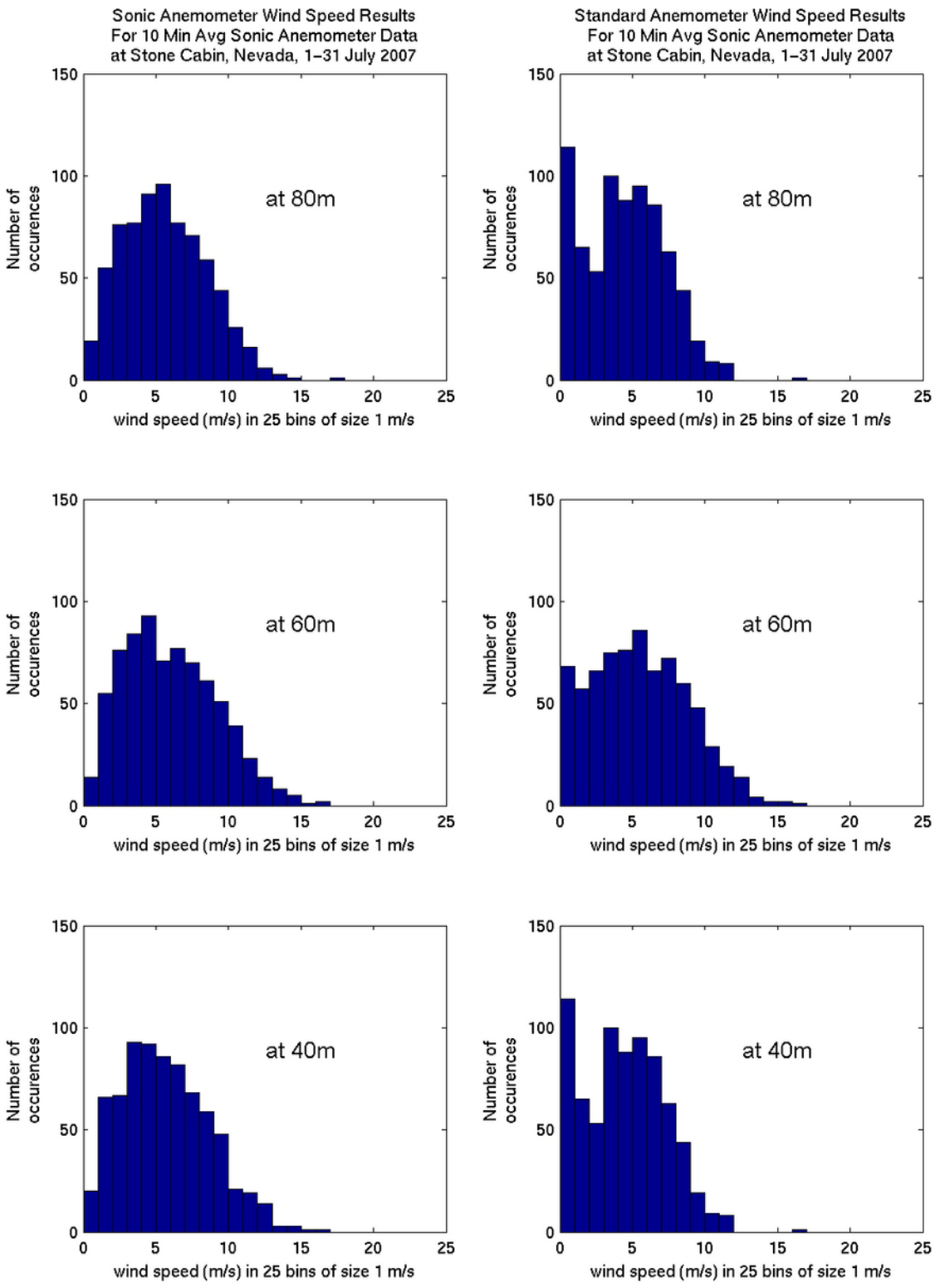

Figure 27. Histograms of 10-minute averaged sonic (left) and standard (right) anemometer measurements of wind speeds for the period July 2007 at (top) 80 m, (center) 60 m, and (bottom) 40 m.

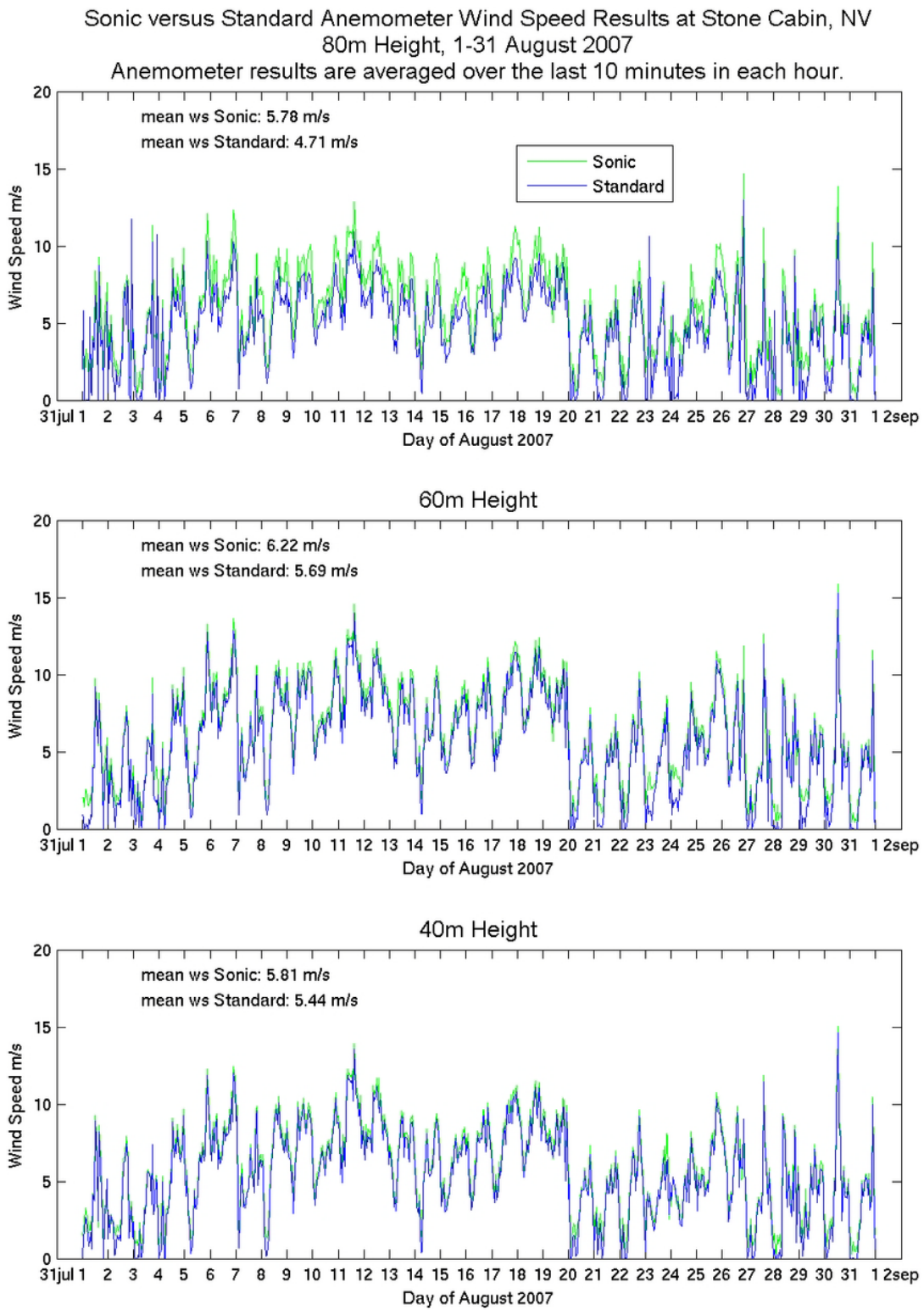

Figure 28. 10-minute averaged sonic (green) and standard (blue) anemometer measurements of wind speeds for the period August 2007 at (top) 80 m, (center) 60 m, and (bottom) 40 m.

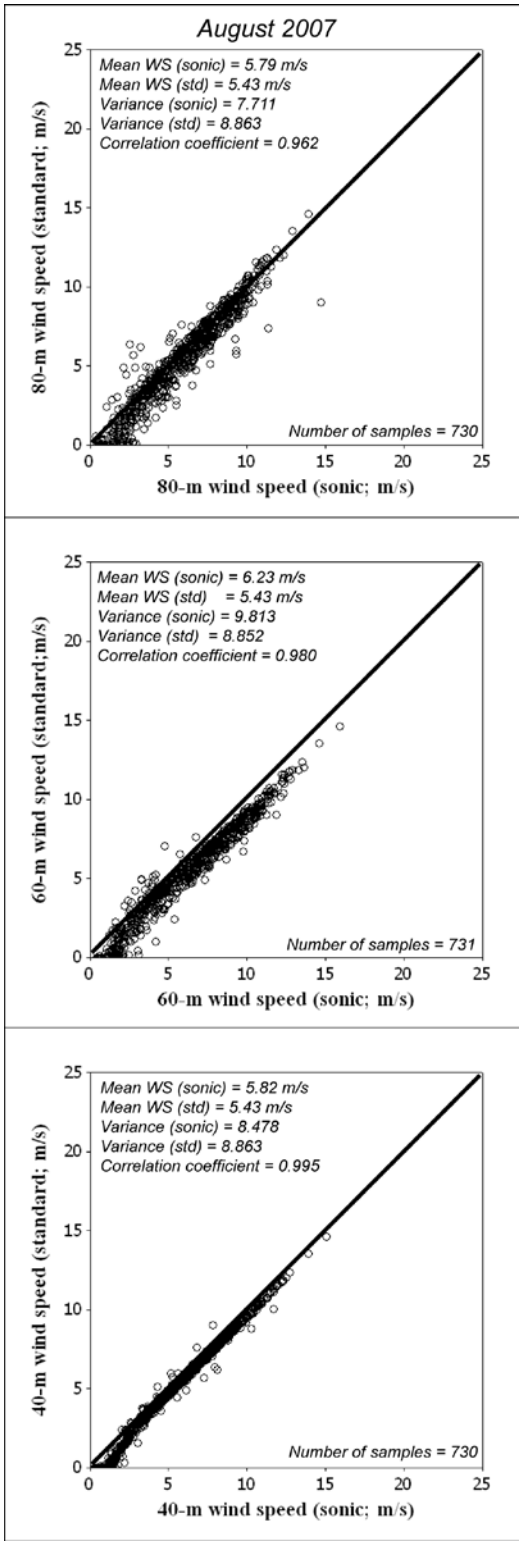

Figure 29. Scatterplots of 10-minute averaged sonic vs. standard anemometer measurements of wind speeds for the period August 2007 at (top) 80 m, (center) 60 m, and (bottom) 40 m.

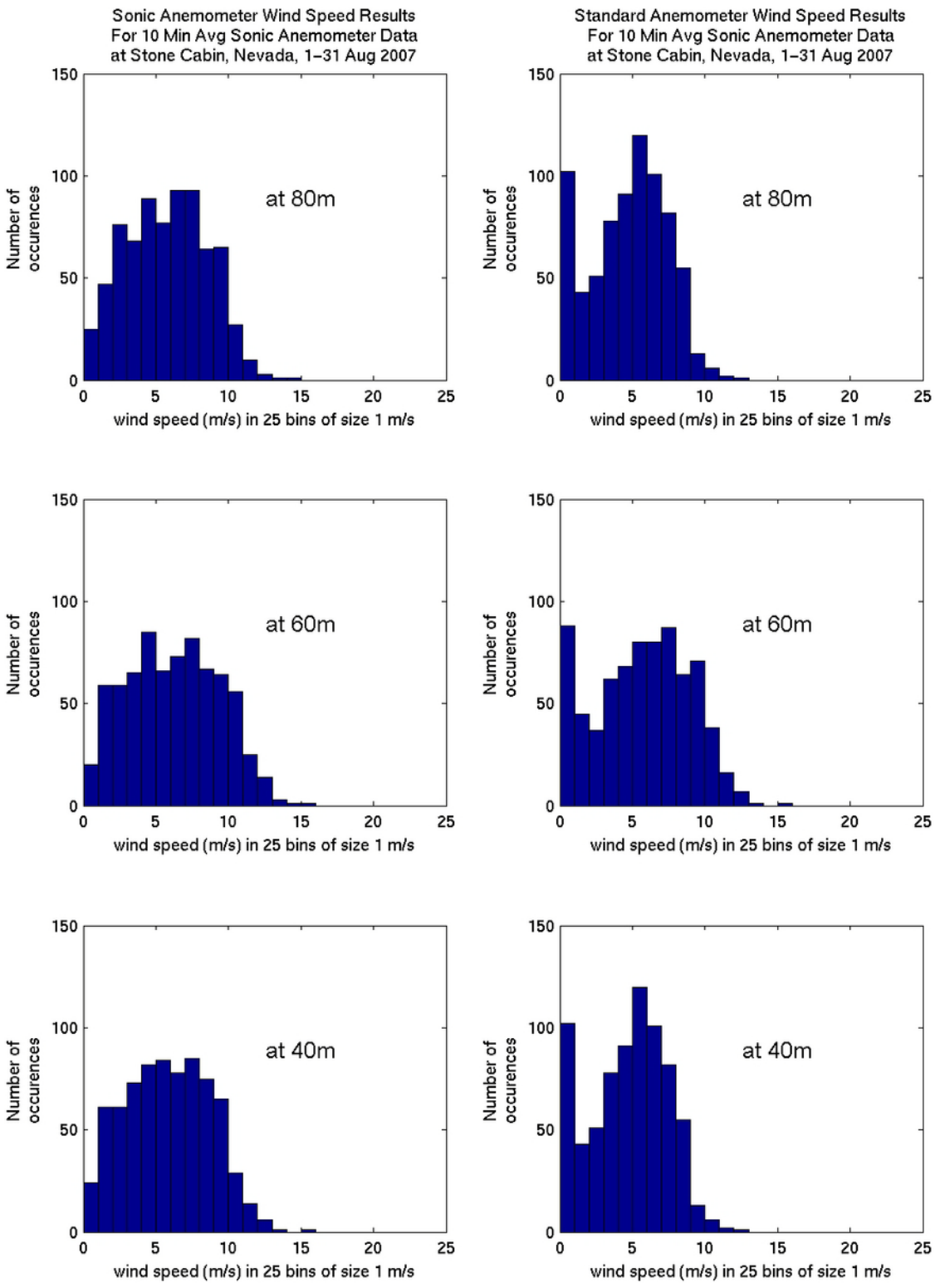

Figure 30. Histograms of 10-minute averaged sonic (left) and standard (right) anemometer measurements of wind speeds for the period August 2007 at (top) 80 m, (center) 60 m, and (bottom) 40 m.

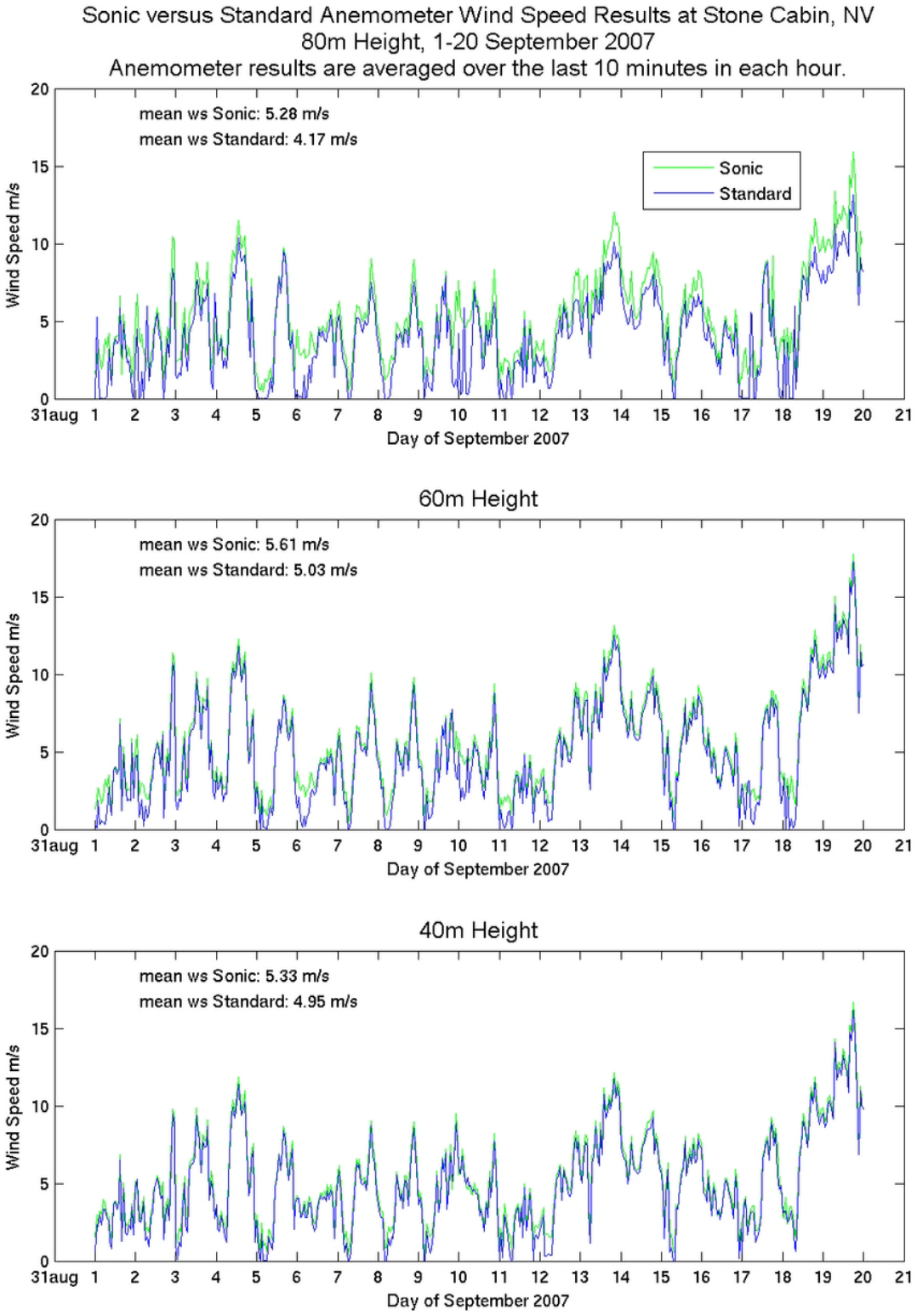

Figure 31. 10-minute averaged sonic (green) and standard (blue) anemometer measurements of wind speeds for the period 1-20 September 2007 at (top) 80 m, (center) 60 m, and (bottom) 40 m.

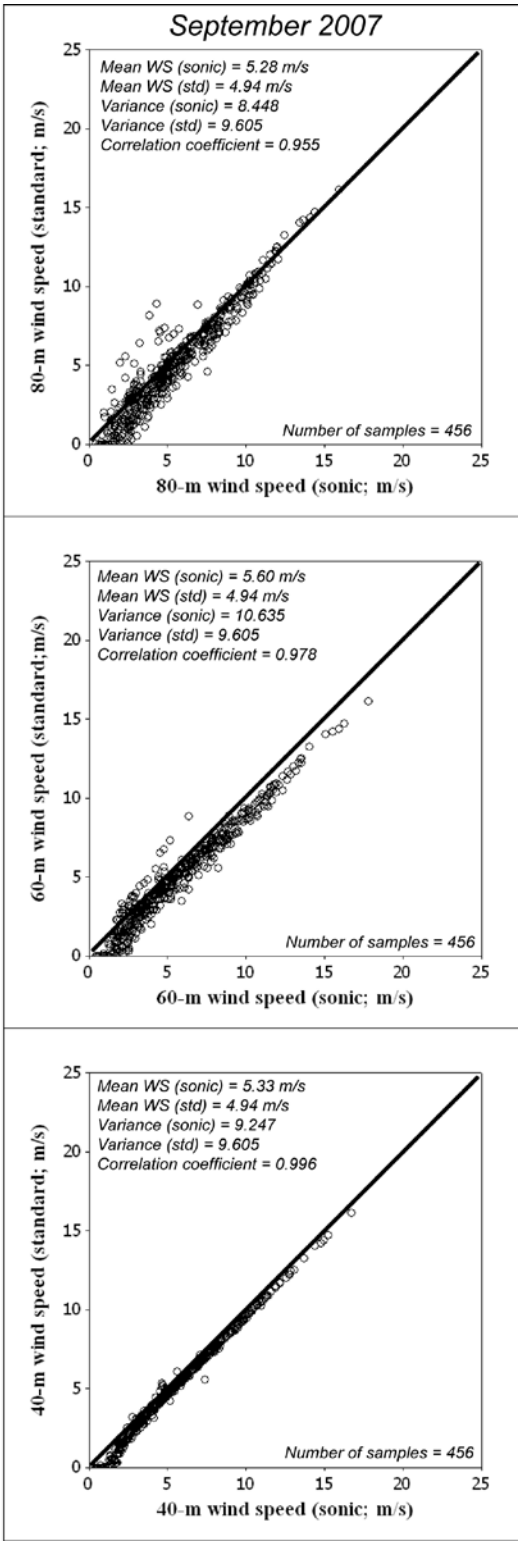

Figure 32. Scatterplots of 10-minute averaged sonic vs. standard anemometer measurements of wind speeds for the period 1-20 September 2007 at (top) 80 m, (center) 60 m, and (bottom) 40 m.

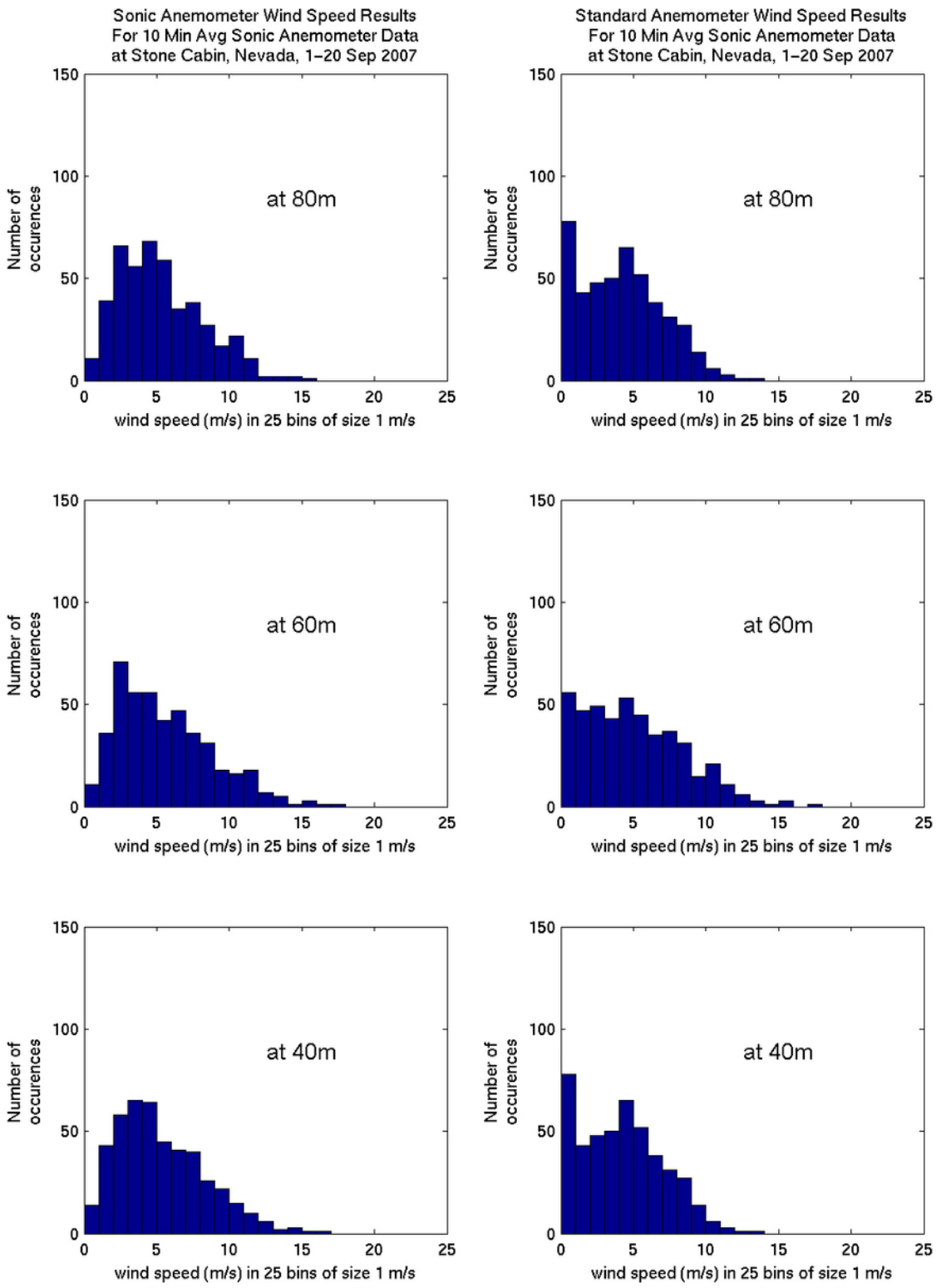

Figure 33. Histograms of 10-minute averaged sonic (left) and standard (right) anemometer measurements of wind speeds for the period 1-20 September 2007 at (top) 80 m, (center) 60 m, and (bottom) 40 m.

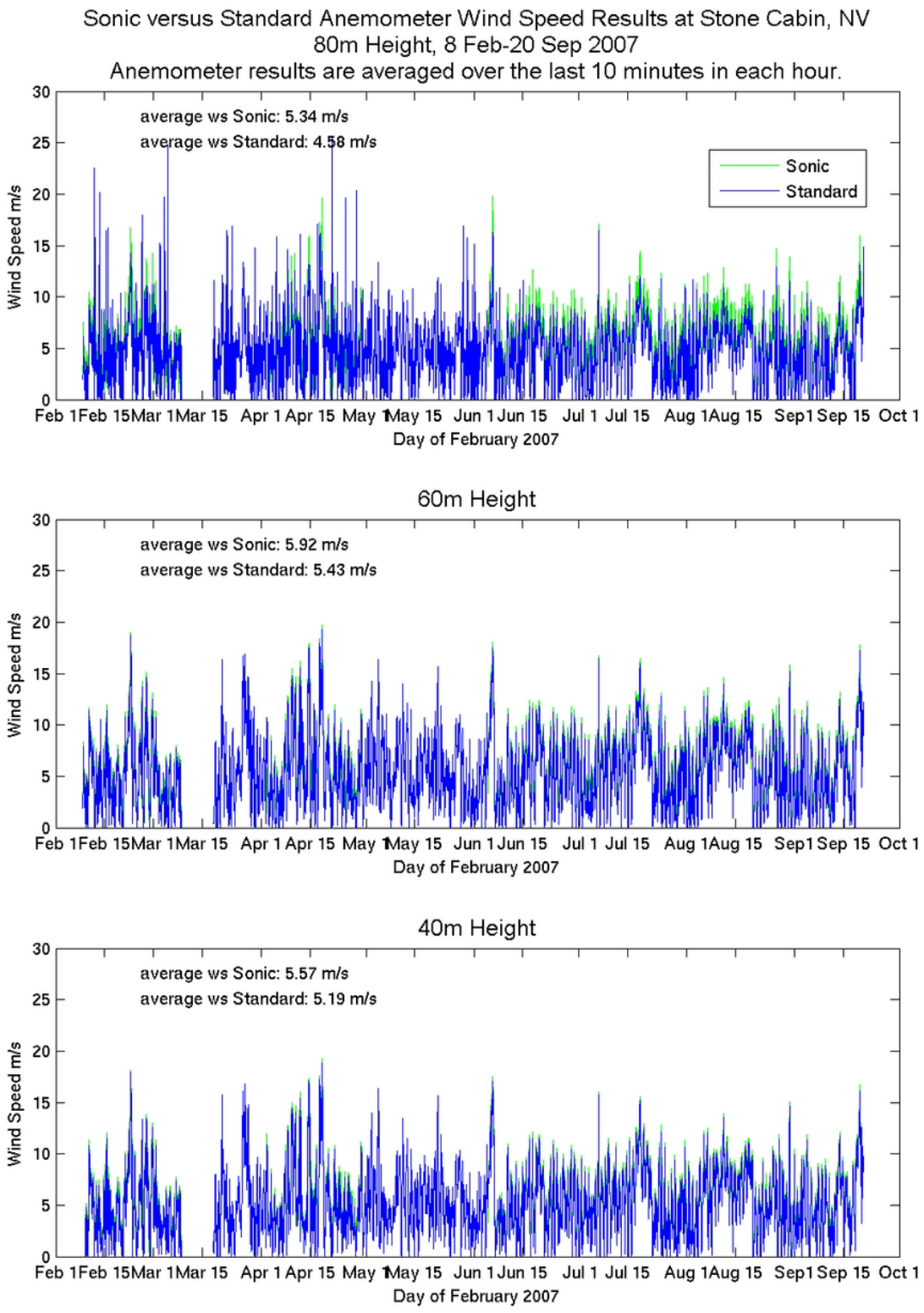

Figure 34. 10-minute averaged sonic (green) and standard (blue) anemometer measurements of wind speeds for the period February-September 2007 at (top) 80 m, (center) 60 m, and (bottom) 40 m.

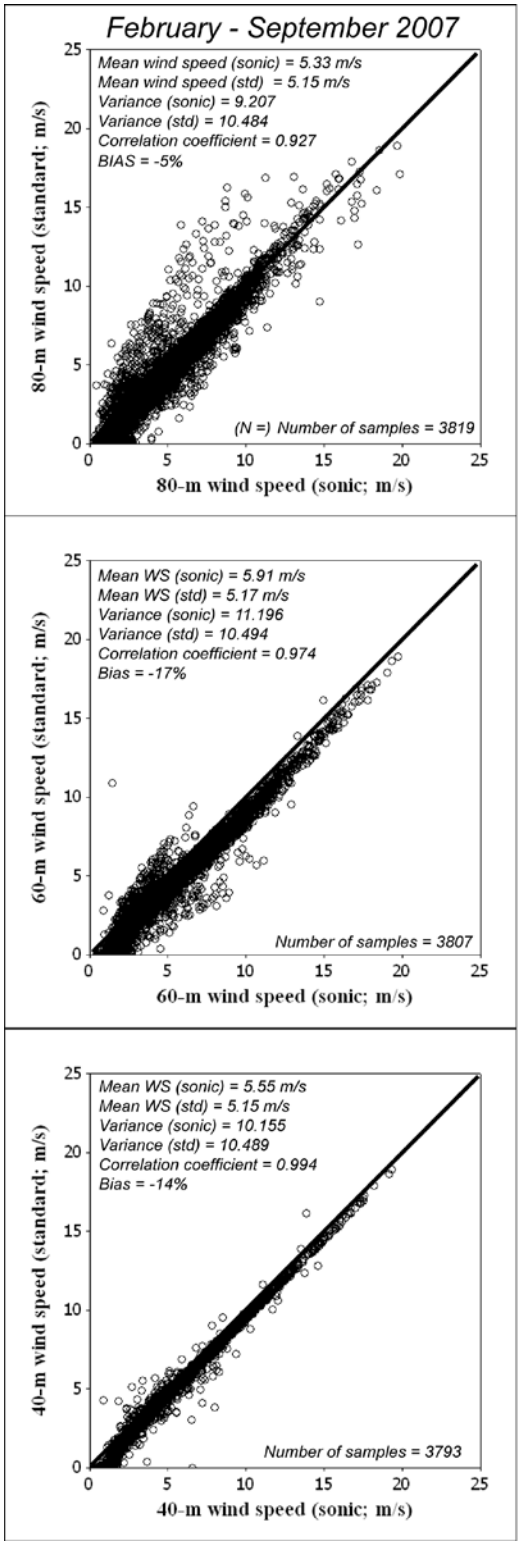

$$BIAS = (1/N) \sum_{i=1}^{N} \frac{Std(i) - Sonic(i)}{Sonic(i)} \times 100\ \%$$

Figure 35. Scatterplots of 10-minute averaged sonic vs. standard anemometer measurements of wind speeds for the period February-September 2007 at (top) 80 m, (center) 60 m, and (bottom) 40 m.

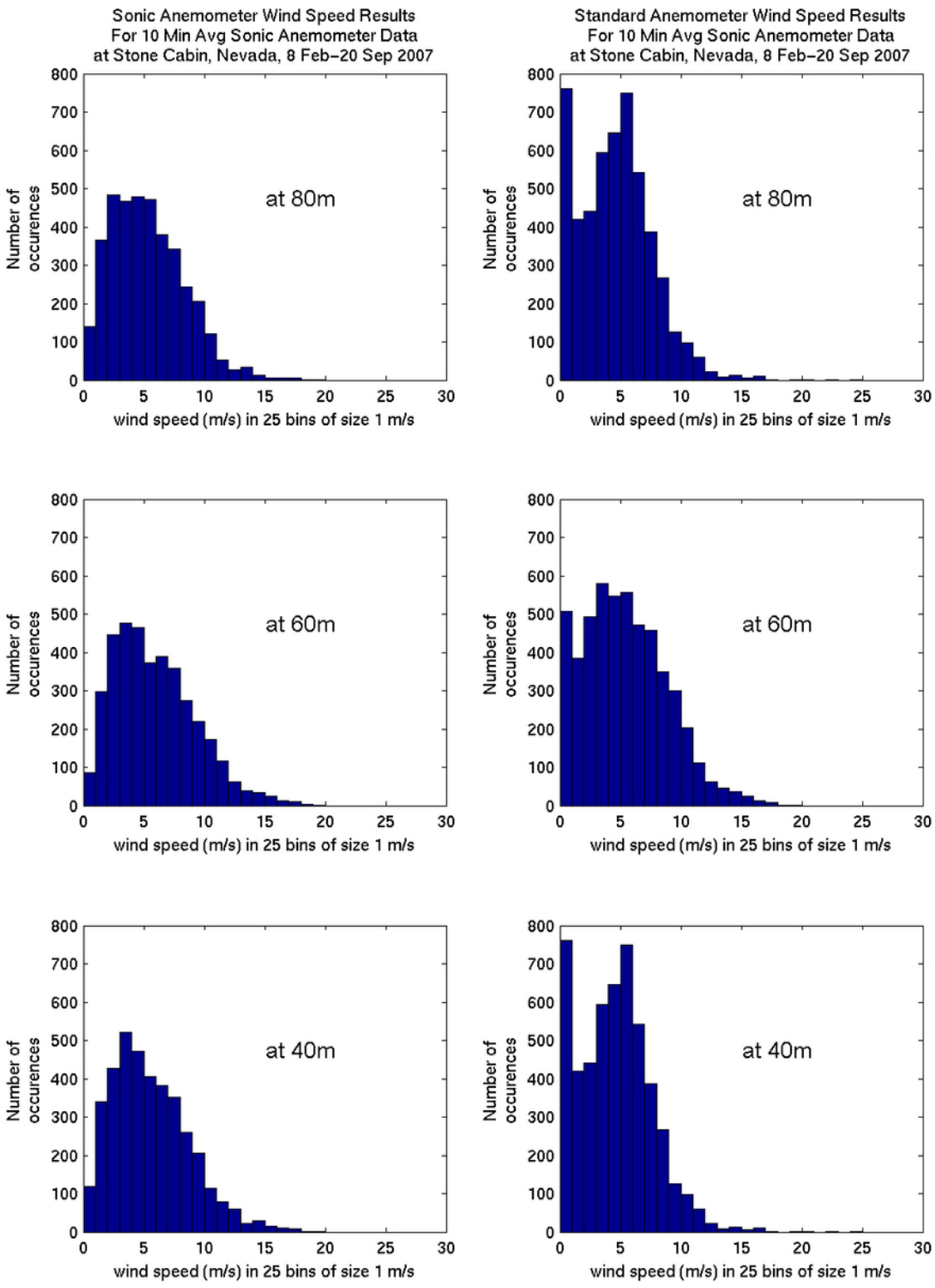

Figure 36. Histograms of 10-minute averaged sonic (left) and standard (right) anemometer measurements of wind speeds for the period February-September 2007 at (top) 80 m, (center) 60 m, and (bottom) 40 m.

7.1.1 Sodar at Kingston and Tonopah, 2005

Introduction to Sodar

Figure 37. Minisodar 4000

Image from ASC's website: http://minisodar.org

Sonic **D**etection **A**nd **R**anging (sodar) is an emerging technology for measuring the wind profile in the bottom of the boundary layer. It operates by sending a sonic pulse directly upwards and measuring the fine characteristics—especially the Doppler shift—of the return signals. Unlike a conventional or sonic anemometer, sodar is able to measure wind speed, direction, and turbulence fluxes not just at one point but upwards along a vertical line extending (depending on the sodar array used) from 15-20 m above the surface to 50 m or up to over 200 m above the surface.

Since sodar has the potential for measuring winds at the hub height of large modern wind rotors, it may become a feasible tool to assess the usefulness of a particular site for the production of wind energy, without needing to erect an expensive tall tower and mount conventional anemometers on. Powered by a solar array and small enough to fit into a large van, it is also relatively mobile.

In the data acquisition for this report, we used a Minisodar 4000 made by the Atmospheric Systems Corporation of Santa Clarita, California (Figure 37). The basic specifications of this instrument are quoted below, from the company Web site, http://minisodar.org.

Sodar Manufacturer:	Atmospheric Systems Corp.
Sodar Model:	Minisodar 4000
Maximum Height:	200 meters
Minimum Height:	20 meters
Height Resolution:	5 meters
Frequency:	4500 Hz
Averaging & Reporting Interval:	User Selectable
Wind Speed Range:	0 to 45 m/s
Wind Speed Accuracy:	< 0.50 m/s (WS > 2 m/s)
Wind Direction Accuracy:	± 5 degrees (WS > 2 m/s)

This sodar unit was set up and operated remotely in two locations in Nevada where DRI-Western Regional Climate Center also had tall (50 m) wind measurement towers that recorded wind measurements at 10-50 m in 10 m increments. The measurements took place at Kingston, Nevada, from 15 June through 13 July, 2005, and then at Tonopah, Nevada, from 11 November through 31 December, 2005. See **Figure 1** for the geographical setup of these locations.

In this section, we assess the accuracy of the sodar by comparing it to the conventional anemometer measurements from the nearby tall towers. We also look at the quality of the sodar data as it changes with measurement height. These aspects of the sodar's performance are important in light of its potential use in assessing the wind energy generating capacity at perhaps remote sites.

Data Quality

Description of the data used (locations/coordinates, elevation, etc.)

Station 17 Tonopah 24NW (Wind Tower) Nevada:
Data begin date: 11 November 2005
Wind data (good wind speed and direction)
Begin date: 11 November 2005
End date: 31 December 2005
Data time increment: 5 minutes for sodar; 10 minutes for tower

Ongoing data collection? No.
Latitude 38° 22' 20"
Longitude 117° 28' 18"
Elevation 5035 ft.

Station 18 Kingston 14SW (Wind Tower) Nevada:
Data begin date: 15 June 2005
Wind data (good wind speed and direction)
Begin date: 15 June 2005
End date: 13 July 2005
Data time increment: 5 minutes for sodar; 10 minutes for tower
Significant omitted data blocks? no

Ongoing data collection? No.
Latitude 39° 02' 44"
Longitude 117° 00' 03"
Elevation 5839 ft.

Exact number of sodar data points: Kingston 8352
Tonopah 13938

Generally, the sodar data at 20 m, 30 m, 40 m, and 50 m is sound at both sites, with a slight but progressive decrease in the quality of data with height—more and more NaNs (NaN: Not a Number). The NaN density plots in **Figures 38 through 51** show this progression clearly. Outliers were not a significant problem at any height.

The data at 10 m was quite bad (mostly NaN) at both sites. This was evidently because this sodar did not work well at distances very close to the system. The best data was at 20 m (as judged by its scarcity of NaNs and outliers), and it gradually and consistently decreases in quality with increasing height. The data at 60 m was marginal at both sites, with NaNs over 10% of total entries, and the data was comprised of almost 25% NaNs at 70 m.

As mentioned in the description of the data section above for Tonopah, there was some data missing from the last third of the time period, which show in the NaN density plots as thin white lines.

The time series (only the 20 m time series are shown here; the other heights show similarly) in **Figures 52 and 53** show that at a gross level the sodar data tracked the tower data well.

See the data check summaries below for details of the data quality per height level.

Kingston Sodar Data Check Summary:

Date	File	Completed?	Status
7/13/2007	Kingston_sodar_DC_10 m.mat	Yes	bad data, 5571 NaNs, 8352 total entries
			5571/8352*100 = 66.7% NaNs > 10% limit
7/13/2007	Kingston_sodar_DC_20 m.mat	Yes	good data, 4 NaNs, 8352 total entries
			4/8352*100 = 0.05% NaNs
7/18/2007	Kingston_sodar_DC_30 m.mat	Yes	good data, 22 NaNs, 8352 total entries
			22/8352*100 = 0.3% NaNs
7/18/2007	Kingston_sodar_DC_40 m.mat	Yes	good data, 70 NaNs, 8352 total entries
			70/8352*100 = 0.8% NaNs
7/18/2007	Kingston_sodar_DC_50 m.mat	Yes	good data, 309 NaNs, 8352 total entries
			309/8352*100 = 3.7% NaNs
7/18/2007	Kingston_sodar_DC_60 m.mat	Yes	bad data, 909 NaNs, 8352 total entries
			909/8352*100 = 10.9% NaNs > 10% limit
7/18/2007	Kingston_sodar_DC_70 m.mat	Yes	bad data, 1998 NaNs, 8352 total entries
			1998/8352*100 = 23.9% NaNs > 10% limit

Tonopah Sodar Data Check Summary:

Date	File	Completed?	Status
7/25/2007	Tonopah_sodar_DC_10 m.mat	yes	bad data, 12875 NaNs, 13931 total entries
			12875/13931*100 = 92.4% NaNs
7/25/2007	Tonopah_sodar_DC_20 m.mat	yes	good data, 98 NaNs, 13938 total entries
			98/13938*100 = 0.7% NaNs
7/26/2007	Tonopah_sodar_DC_30 m.mat	yes	good data, 257 NaNs, 13939 total entries
			257/13939*100 = 1.8% NaNs
7/26/2007	Tonopah_sodar_DC_40 m.mat	yes	good data, 736 NaNs, 13938 total entries
			736/13938*100 = 5.3% NaNs
7/26/2007	Tonopah_sodar_DC_50 m.mat	yes	good data, but at limit:
			1398 NaNs, 13938 total entries
			1398/13938*100 = 10.0% NaNs
7/26/2007	Tonopah_sodar_DC_60 m.mat	yes	bad data, NaNs > 10% of total entries
			2355 NaNs, 13937 total entries
			2355/13937*100 = 16.9% NaNs
7/26/2007	Tonopah_sodar_DC_70 m.mat	yes	bad data, NaNs > 10% of total entries
			3699 NaNs, 13937 total entries
			3699/13937*100 = 26.5% NaNs

NaN Density Plots—Tonopah

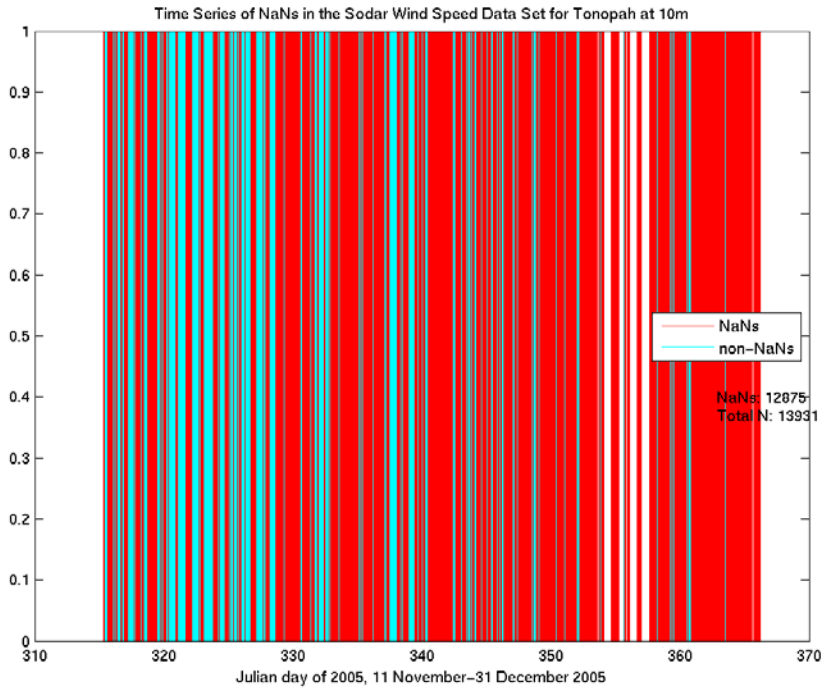

Figure 38. Graphic showing the positions and frequency of 'good' vs. NaN (bad data) results from the sodar at Tonopah at 10m AGL. Cyan bars indicate good data; red indicates NaN; white indicates missing data.

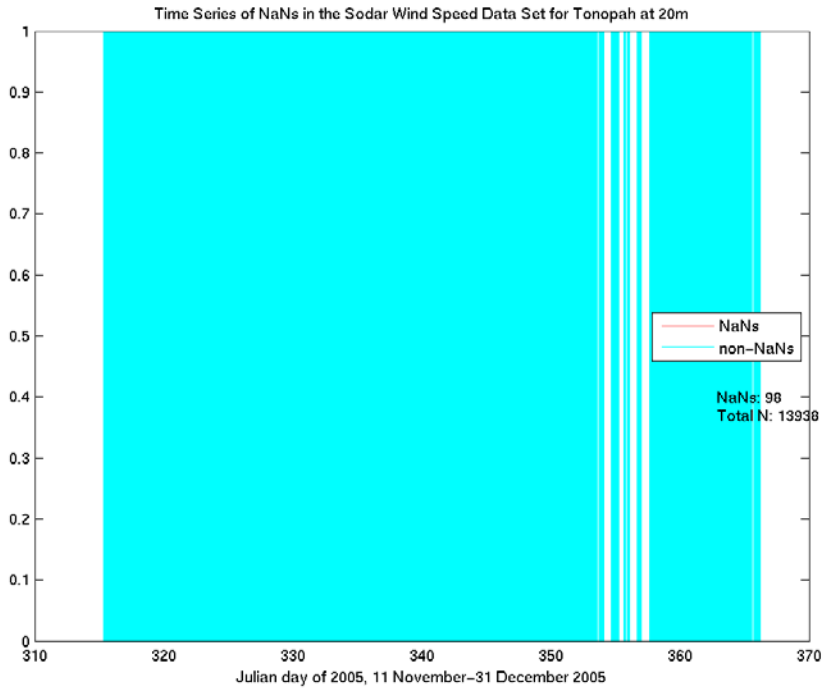

Figure 39. Same as Figure 38, but for 20 m AGL

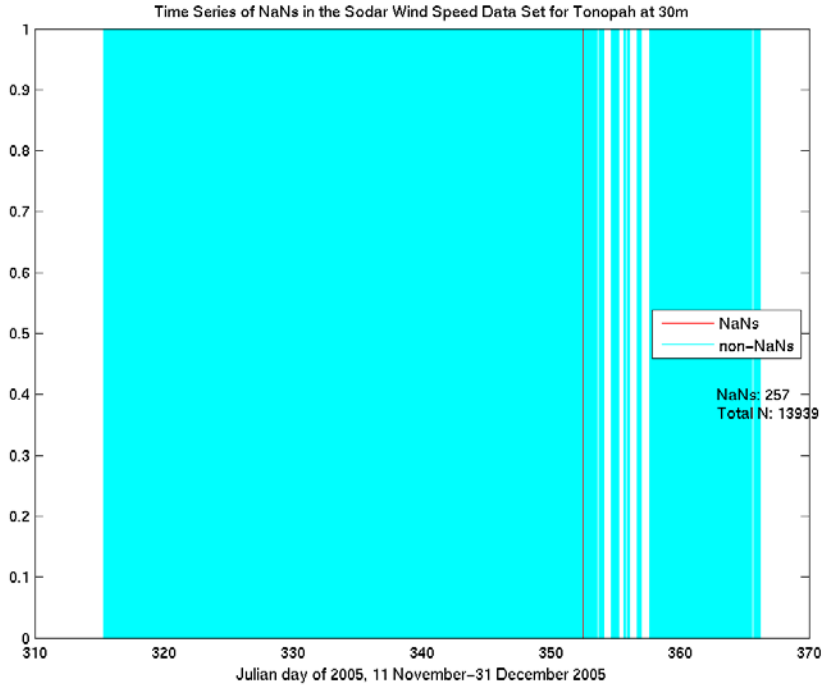

Figure 40. Same as Figure 38, but for 30 m AGL

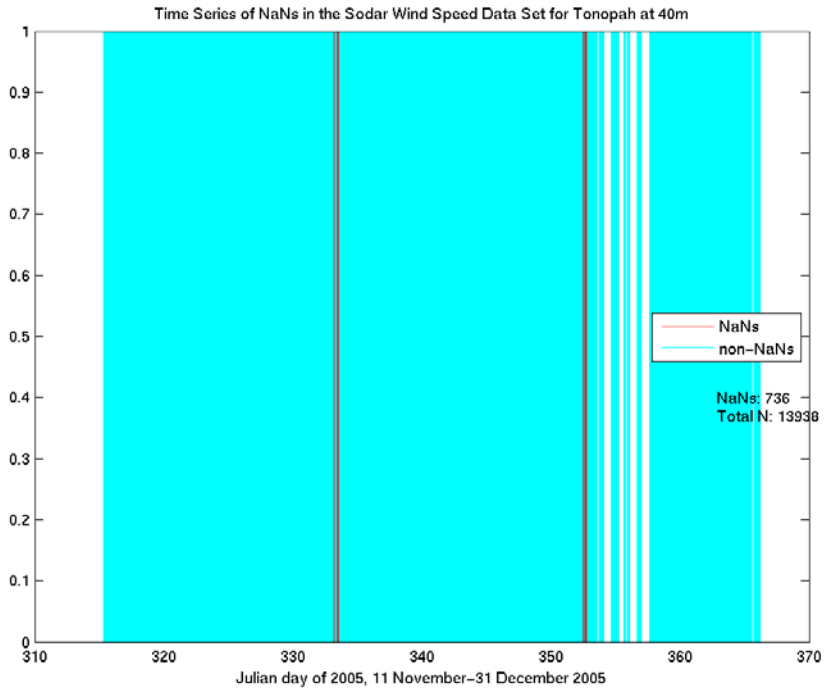

Figure 41. Same as Figure 5-38, but for 40 m AGL

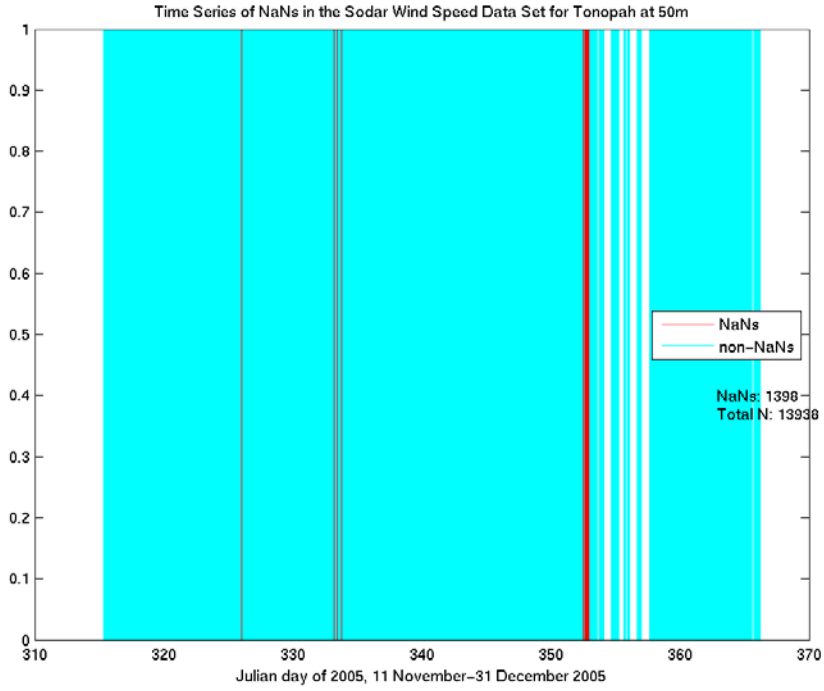

Figure 42. Same as Figure 38, but for 50 m AGL

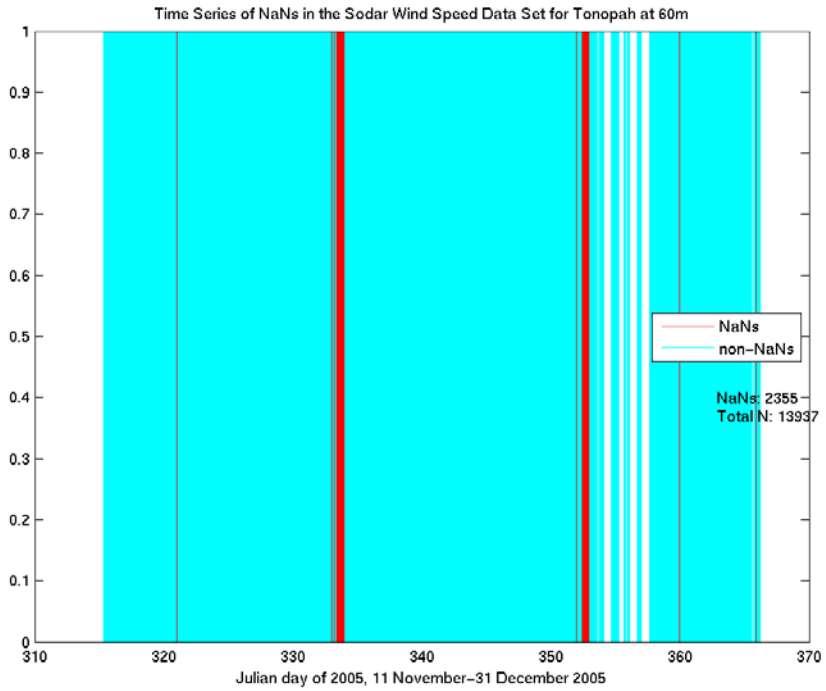

Figure 43. Same as Figure 38, but for 60 m AGL

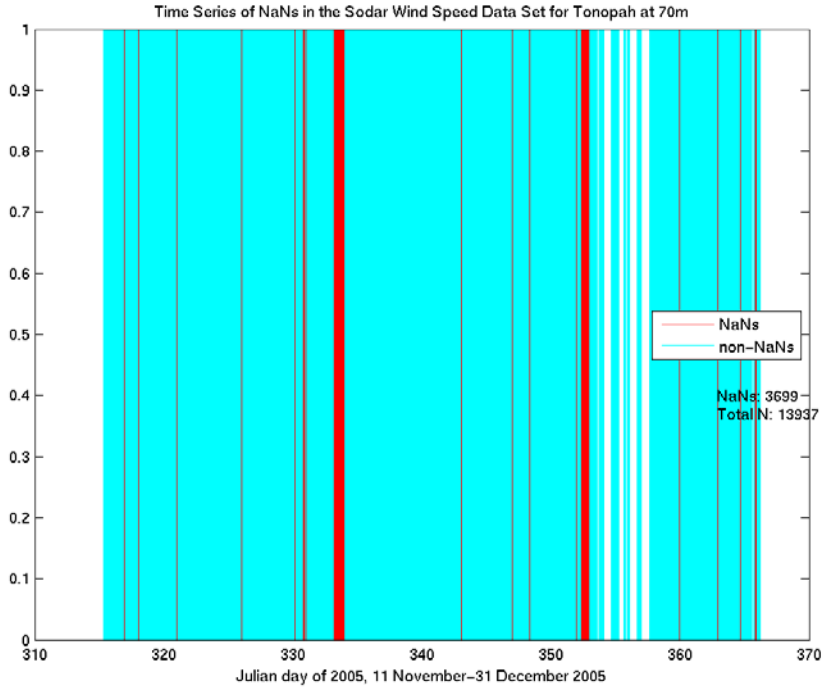

Figure 44. Same as Figure 38, but for 70 m AGL

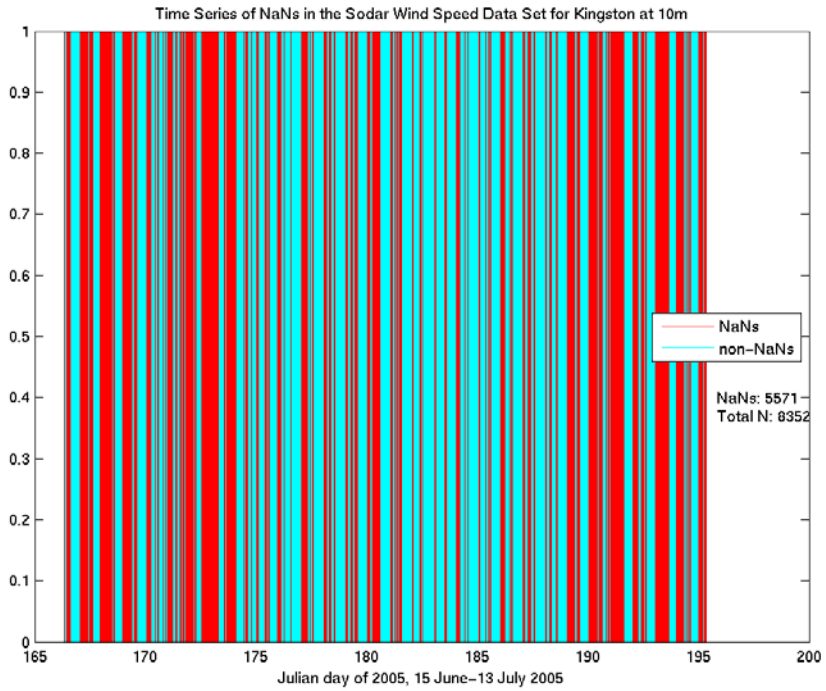

Figure 45. Graphic of data quality (similar to Figure 38) for the Kingston location for 10 m AGL

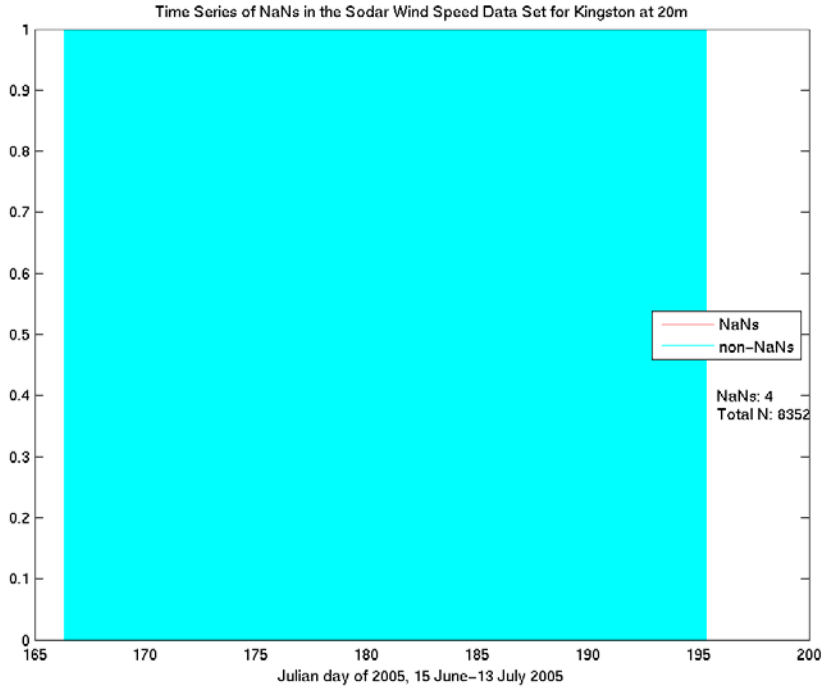

Figure 46. Same as Figure 45, but for 20 m AGL

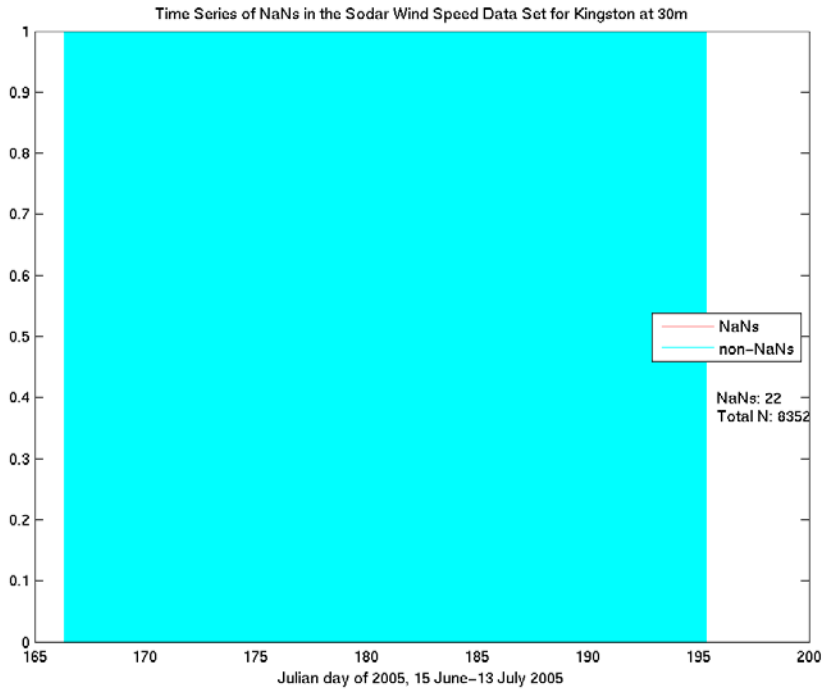

Figure 47. Same as Figure 45, but for 30 m AGL

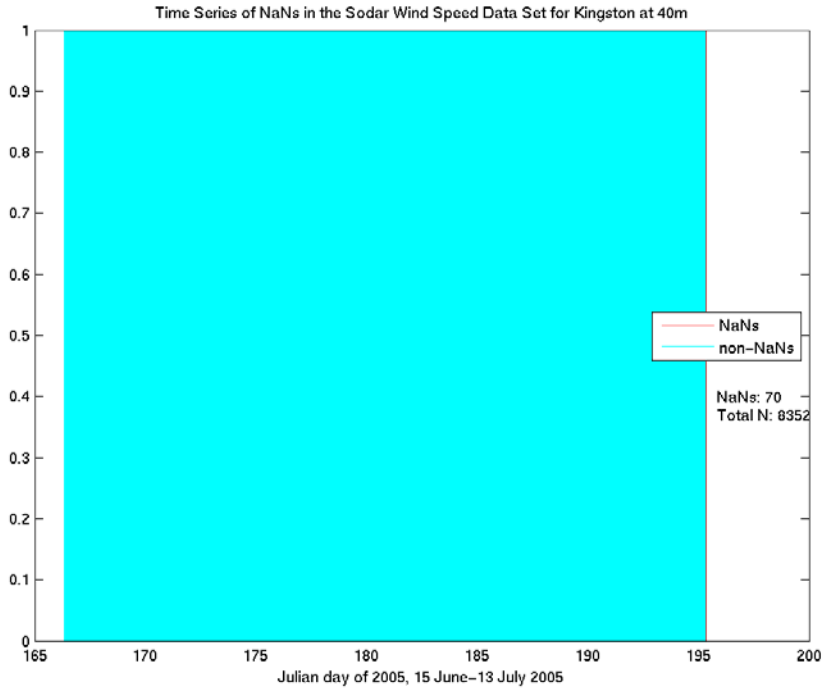

Figure 48. Same as Figure 45, but for 40 m AGL

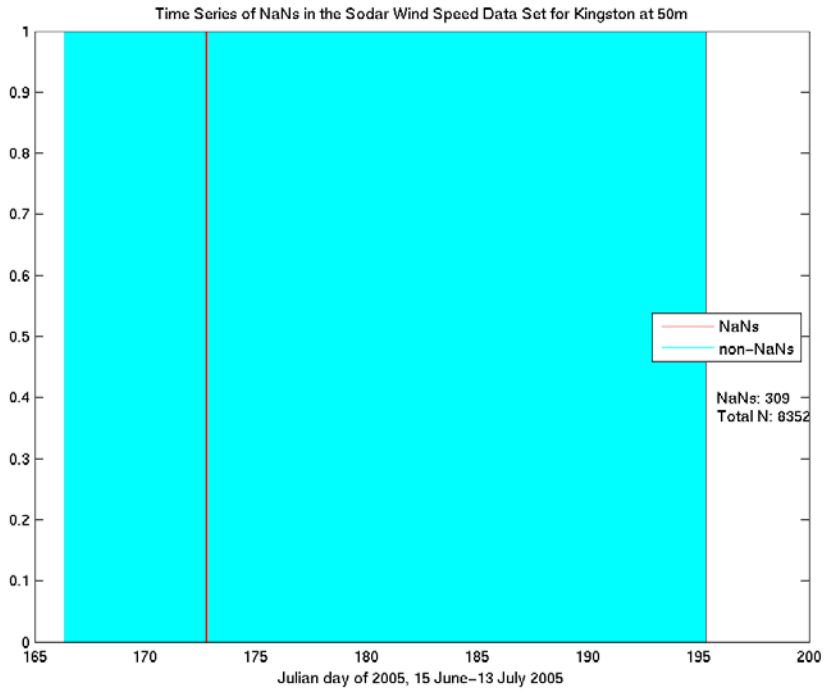

Figure 49. Same as Figure 45, but for 50 m AGL

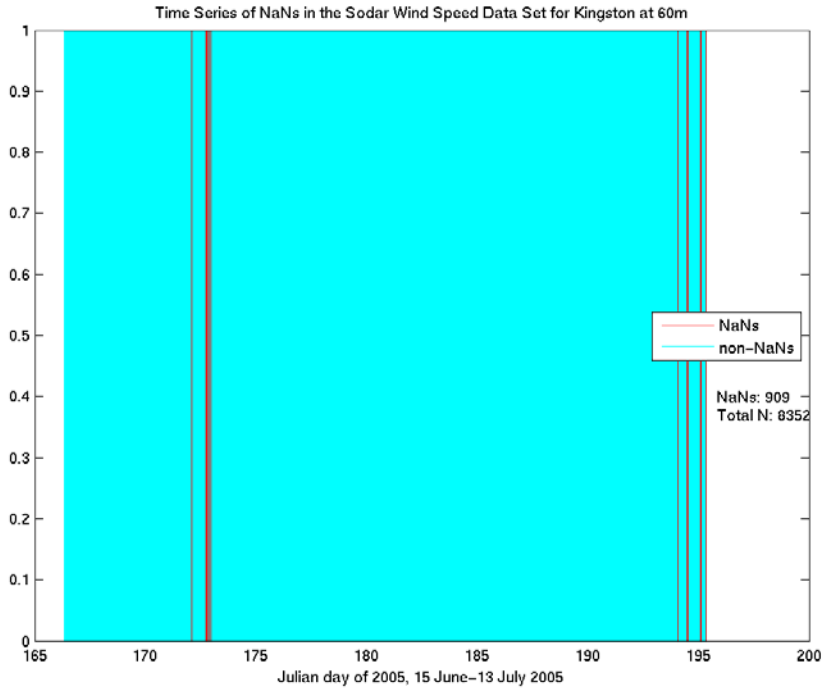

Figure 50. Same as Figure 45, but for 60 m AGL

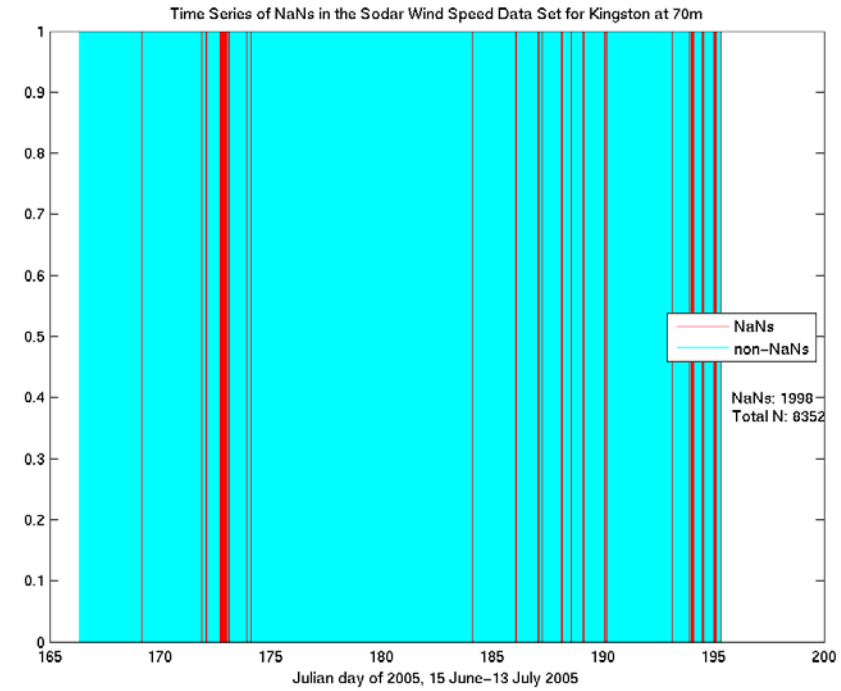

Figure 51. Same as Figure 45, but for 70 m AGL

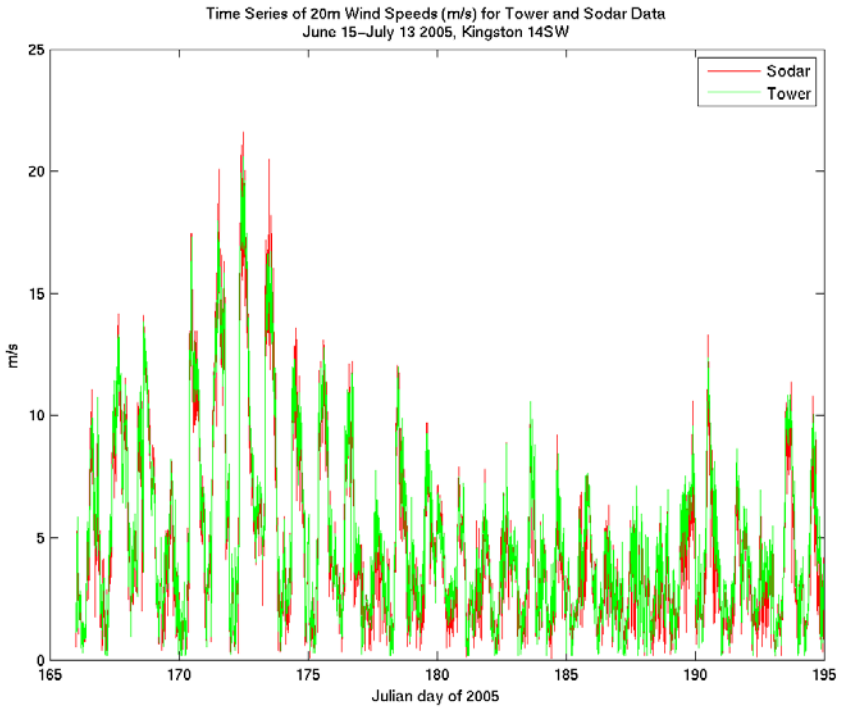

Figure 52. Comparison of sodar- and tower-measured wind speed at Kingston at 40 m AGL for Julian days 166-195 (May 15-June 14, 2005)

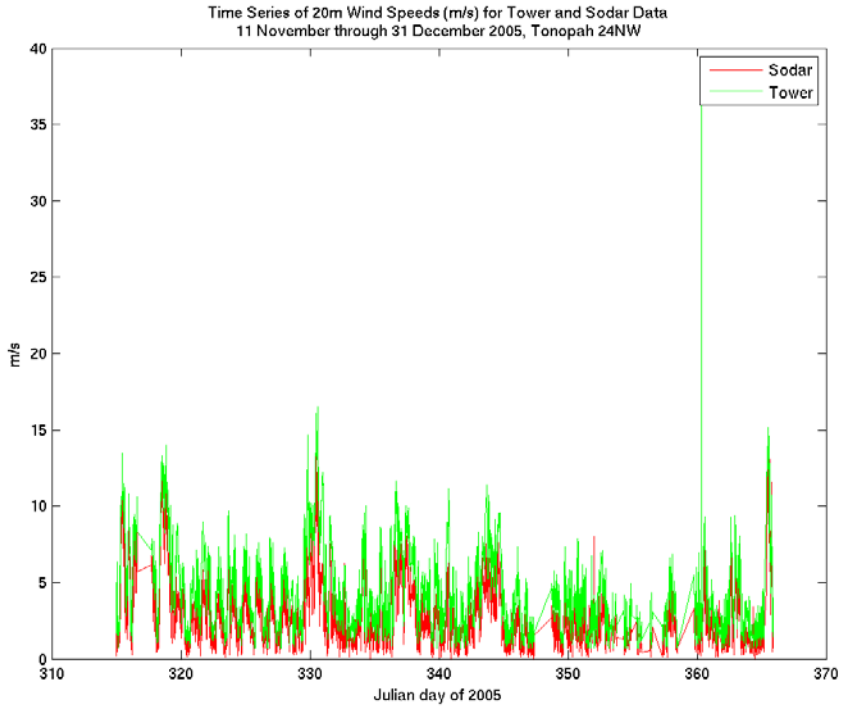

Figure 53. Same as Figure 52, but for 11 November-31 December 2005

Description of the Analysis

In MATLAB and Excel, we assembled tables of the basic statistics governing the sodar and tower wind speed data (**Tables 3 through 8**), starting with summaries like that below, then progressing to the tables and figures in the next section.

Kingston 10 m Daily Wind Speed summary—example 15 June-13 July 2005

	SODAR			TOWER		
Day	avg	max	min	avg	max	min
1	3.33	7.54	0.51	4.15	9.60	0.27
2	3.80	8.73	0.90	6.36	12.00	0.18
3	5.61	10.67	1.41	6.72	12.70	1.08
4	3.04	5.74	0.35	3.68	7.57	0.23
5	4.45	9.88	0.99	6.28	15.61	0.18
6	4.16	6.13	2.28	8.04	16.32	0.57
7	1.90	3.49	0.80	8.35	18.57	0.29
8	3.44	5.43	1.32	7.83	15.17	0.34
9	4.38	10.83	0.83	5.59	11.41	0.72
10	4.46	9.39	0.87	5.44	11.70	0.21
11	4.36	8.86	0.54	4.98	10.92	0.90
12	2.59	5.40	0.28	3.19	7.23	0.21
13	4.65	10.14	0.71	4.43	11.03	0.18
14	2.92	7.42	0.37	4.14	8.70	0.94
15	2.20	5.69	0.08	3.66	6.85	1.47
16	2.45	5.03	0.28	3.05	5.93	0.18
17	2.53	4.87	0.37	3.14	8.26	0.22
18	2.92	6.84	0.53	3.60	10.00	0.18
19	2.64	6.89	0.13	3.46	7.98	0.24
20	2.59	5.11	0.65	3.41	6.71	0.18
21	2.20	4.30	0.16	2.85	5.21	0.30
22	2.26	5.77	0.39	2.79	6.60	0.19
23	1.70	5.29	0.20	2.76	5.90	0.18
24	2.70	5.05	0.59	4.11	8.14	0.27
25	3.95	6.79	2.00	4.65	11.46	0.51
26	3.15	6.75	0.30	3.31	8.08	0.18
27	1.61	4.93	0.05	2.94	6.56	0.18
28	2.29	5.87	0.48	4.43	10.08	0.18
29	2.26	4.96	0.70	3.77	9.37	0.22

Table 3. Summary of Wind Speed Data as Measured by the Sodar and the Tower Anemometer at Kingston for 15 June-13 July 2005

Kingston Sodar and Tower Data Summary Wind Speed (m/s) for 15 June-13 July 2005							
Height	Data	avg	std	avgmax	N	NaNs	corrcoef
10 m	Sodar:	3.04	1.9	6.68	4031	2677	0.546
10 m	Tower:	4.55	3.23	9.85	4031	0	0.546
20 m	Sodar:	4.59	3.62	11.21	4031	1	0.997
20 m	Tower:	4.94	3.61	10.78	4031	0	0.997
30 m	Sodar:	4.8	3.81	11.95	4031	10	0.995
30 m	Tower:	5.15	3.76	11.23	4031	0	0.995
40 m	Sodar:	4.98	3.8	12.17	4031	32	0.984
40 m	Tower:	5.27	3.88	11.47	4031	0	0.984
50 m	Sodar:	5.08	3.66	12.06	4031	130	0.96
50 m	Tower:	5.42	3.97	11.81	4031	0	0.96

Table 4. Summary of Wind Speed Data as Measured by the Sodar and the Tower Anemometer at Tonopah for 11 November-31 December 2005

Tonopah Sodar Data Summary Wind Speed (m/s) for 11 November-31 December 2005							
Height	Data	avg	std	avgmax	N	NaNs	corrcoef
10 m	Sodar:	5.64	2.82	NaN	480	5764	0.446
10 m	Tower:	4.05	2.5	8.43	6244	0	0.446
20 m	Sodar:	2.8	2.07	6.58	6196	46	0.977
20 m	Tower:	4.36	2.66	8.82	6242	0	0.977
30 m	Sodar:	3.21	2.43	7.27	6129	112	0.989
30 m	Tower:	4.42	2.71	8.67	6241	0	0.989
40 m	Sodar:	3.55	2.71	7.91	5917	325	0.99
40 m	Tower:	4.65	2.85	9.09	6242	0	0.99
50 m	Sodar:	3.78	2.88	8.67	5649	593	0.988
50 m	Tower:	4.84	2.96	9.49	6242	0	0.988

Table 5. Differences in the Daily Average Wind Speeds as Measured by the Tower Anemometer and as Measured by the Sodar at Kingston for 15 June-13 July 2005

Kingston Tower minus Sodar difference of daily averages Wind Speed (m/s) for 15 June-13 July 2005					
day	10 m	20 m	30 m	40 m	50 m
1	0.82	0.31	0.27	0.12	0.03
2	2.56	0.2	0.14	-0.02	-0.05
3	1.11	0.17	0.05	-0.11	-0.05
4	0.64	0.25	0.23	0.05	0.16
5	1.83	0.24	0.12	0.09	0.1
6	3.88	0.2	0.13	0.35	1.05
7	6.45	0.46	0.95	2.05	3.34
8	4.39	0.36	0.28	0.33	0.81
9	1.21	0.27	0.21	0.02	-0.05
10	0.98	0.35	0.21	0.02	0.08
11	0.62	0.27	0.27	0.16	0.19
12	0.6	0.46	0.47	0.28	0.12
13	-0.22	0.21	0.13	0.06	-0.14
14	1.22	0.32	0.34	0.26	0.17
15	1.46	0.19	0.23	0.08	0.31
16	0.6	0.33	0.34	0.24	0.35
17	0.61	0.18	0.23	0.12	0.07
18	0.68	0.35	0.42	0.32	0.25
19	0.82	0.37	0.46	0.3	0.22
20	0.82	0.31	0.3	0.17	0.27
21	0.65	0.25	0.3	0.2	0.22
22	0.53	0.24	0.24	0.11	-0.05
23	1.06	0.5	0.52	0.31	0.08
24	1.41	0.58	0.54	0.23	-0.02
25	0.7	0.76	0.65	0.48	0.4
26	0.16	0.49	0.51	0.44	0.32
27	1.33	0.59	0.59	0.44	0.36
28	2.14	0.6	0.5	0.42	0.46
29	1.51	0.5	0.52	0.32	0.25
averages:	1.40	0.36	0.35	0.27	0.32

Table 6. Same as Table 5, but for Daily Wind Speed Maxima

Kingston Tower minus Sodar difference of daily maxima Wind Speed (m/s) for 15 June-13 July 2005					
day	10 m	20 m	30 m	40 m	50 m
1	2.06	-0.31	-0.06	-0.5	0.05
2	3.27	-0.91	-1.41	-0.73	-0.91
3	2.03	-0.28	-0.24	-0.97	-1.04
4	1.83	-0.48	-1.61	-1.48	0.62
5	5.73	-0.12	-1.81	-2.2	-0.04
6	10.19	-2.12	-2.69	-2.42	0.95
7	15.08	-1.02	-1.73	-0.44	5.13
8	9.74	-3.77	-2.91	-1.87	-2.6
9	0.58	-1.31	-2.05	-2.07	-2.54
10	2.31	-0.29	-2.65	-2.67	-3.61
11	2.06	-0.46	-0.53	-0.74	-0.26
12	1.83	1.59	0.72	0.43	-0.19
13	0.89	-0.08	-0.48	-0.34	-0.88
14	1.28	-0.44	0.08	-0.23	-0.53
15	1.16	-0.4	-0.86	-1.35	0.99
16	0.9	-0.53	0.03	-0.72	0.24
17	3.39	-0.01	0.07	-0.1	-0.42
18	3.16	0.93	1.05	0.89	1.03
19	1.09	-0.75	-0.9	-0.65	-0.32
20	1.6	0.07	0.05	-0.45	0.31
21	0.91	-0.83	-0.77	-0.54	-0.69
22	0.83	0.1	-0.22	-0.76	-0.52
23	0.61	0.93	0.31	-0.4	-0.58
24	3.09	-1.01	0.08	0.25	-0.41
25	4.67	-0.9	-1.4	-0.6	0.26
26	1.33	0.55	0.37	0.72	0.46
27	1.63	0.79	1.27	0.94	0.51
28	4.21	-0.51	-1.33	-0.56	-0.73
29	4.41	-0.74	-1.29	-0.66	-1.56
averages:	3.17	-0.42	-0.72	-0.70	-0.25

Table 7. Differences in the Daily Average Wind Speeds as Measured by the Tower Anemometer and as Measured by the Sodar at Tonopah for 11 November-31 December 2005

Tonopah Tower minus Sodar difference of daily averages Wind Speed (m/s) for 11 November-31 December 2005					
day	10 m	20 m	30 m	40 m	50 m
1	-1.49	1.46	1.1	1.04	1.02
2	1.17	1.61	1.16	0.99	0.99
3	4.33	1.6	1.08	0.99	0.83
4	0.46	1.81	1.16	1.16	1.21
5	-3.23	2.42	1.79	1.47	1.32
6	-3.52	1.18	1.11	1.01	0.88
7	-0.05	2	1.55	1.48	1.54
8	-1.47	1.44	1.24	1.16	1
9	0.95	1.39	1.27	1.14	1.16
10	-3.92	1.41	1.22	0.97	0.99
11	-0.33	1.36	1.13	0.97	0.9
12	-1.3	1.15	1.01	0.9	0.94
13	-2.27	1.29	1.22	1.07	1.01
14	-2.21	1.35	1.19	1.14	1.03
15		2.31	1.21	1.01	1.26
16	1.12	3.44	2.22	1.92	1.75
17	0.34	2.43	1.76	1.63	1.3
18	-0.94	1.45	1.27	1.38	1.5
19		0.99	0.68	0.54	0.29
20	0.38	1.29	0.79	0.75	0.77
21	-1.8	1.26	0.93	0.96	1.03
22	-2.77	2.03	1.38	1.26	1.34
23	-0.95	2.13	1.62	1.28	1.18
24	-2.88	1.76	1.42	1.24	1.22
25	-0.19	1.79	1.53	1.36	1.38
26	2.03	2.04	1.72	1.41	1.21
27		1.06	1.03	1.16	1.03
28	-2.02	1.64	1.23	1.33	1.27
29	-0.83	2.52	1.79	1.33	1.37
30	-2.28	2.33	1.68	1.32	1.28
31	-1.29	1.07	1.16	1.04	1.06
32	-4.72	1.3	1.14	1.18	1.15
33		1.02	1.12	1.04	0.97
34	-5.12	1.98	1.58	1.71	1.54
35		1.56	1.27	1.23	1.13
36	-3.32	1.69	1.35	1.32	1.24
37	-3.99	0.88	0.71	0.75	0.72
38		1.21	0.63	0.49	0.95
39		0.61	0.74	0.93	0.91
40		0.91	0.83	0.91	0.97
41	-0.26	0.72	0.8	0.94	1
42		0.99	1.08	1.07	1.08
43	-2.78	1.05	0.98	0.98	1.04
44		1.36	1.12	1.1	1.11
45		1.35	1.37	1.2	1.33
46	-0.87	1.59	1.19	1.2	1.36
47		0.85	0.97	0.97	1.03
48		1.37	0.94	0.91	0.99
49	-2.94	1.45	1.13	1.04	1.03
50		0.79	0.71	0.82	0.93
51		1.63	1.62	2.28	2.83
average:	-1.36	1.52	1.21	1.15	1.14

Table 8. Differences in the Daily Maximum Wind Speeds as Measured by the Tower Anemometer and as Measured by the Sodar at Kingston for 11 November-31 December 2005

Kingston Tower minus Sodar difference of daily maxima Wind Speed (m/s) for 11 November-31 December 2005					
day	10 m	20 m	30 m	40 m	50 m
1	3.01	1.16	1.79	1.72	1.91
2	1.57	1.74	2.16	1.62	1.45
3	5.32	1.16	0.12	0.31	0.13
4	4.8	1.59	0.95	1.19	0.8
5	0.3	3.16	2.02	1.22	1.02
6	-4.05	1.56	1.6	1.63	1.06
7	-0.34	3.15	1.88	1.46	0.79
8	-2.69	1.07	0.92	1.06	-6.9
9	-1.46	2.05	2.4	-0.27	-0.08
10	-2.02	2.07	1.15	-1.31	1.35
11	-2.99	1.46	1.46	1.06	0.54
12	-1.64	1.03	1.1	0.45	1.09
13	-2.13	1.53	1	0.85	1.32
14	-2.01	1.65	1.61	1.24	1.3
15		3.97	3.37	2.6	2.5
16	7.98	2.91	1.94	2.01	3.55
17	2.66	4.23	0.91	0.78	0.08
18	-2.84	-0.11	-1.18	1.38	1.88
19		0.93	0.43	0.5	0.77
20	5.69	1.82	1.07	0.8	0.72
21	2.53	0.64	0.38	0.4	-0.91
22	0.99	3.17	2.13	1.13	1.34
23	-0.86	1.87	1.21	0.81	-6.58
24	-2.43	1.98	1.16	0.55	0.46
25	0.79	2.95	1.82	1.83	0.75
26	6.84	4.83	3.47	1.13	-0.88
27		2.52	2.31	2.03	1.5
28	0.5	1.77	0.99	0.41	0.48
29	1.89	3.82	2.78	1.53	0.6
30	0.51	1.97	2.2	0.92	0.51
31	-2.78	2.11	2.26	1.66	1.94
32	-1.05	1.62	0.62	1.25	1.2
33		0.97	0.99	1.48	1.32
34	-3.75	2.31	2.12	1.17	0.59
35		2.27	2.02	1.69	1.02
36	0.56	2.12	1.85	1.09	0.09
37	-0.98	1.89	1.62	0.09	0.55
38		-0.95	-1.59	-1.92	-2.78
39		1.14	-2.17	0.86	0.93
40		1.29	1.03	1.01	1.13
41	1.07	1.03	0.6	0.97	1.17
42		2.06	1.3	1.5	1.46
43	-0.37	1.25	0.74	0.96	0.84
44		1.84	1.21	1.22	1.55
45		1.53	1.58	1.4	1.62
46		20.78	7.13	9.03	10.51
47		1.4	1.68	1.11	0.91
48		1.34	0.93	0.47	0.21
49	1.1	1.94	1.17	0.8	0.56
50		0.72	-0.45	0.62	1.17
51		2.04	1.51	2.72	3.35
average:	1.44	2.24	1.40	1.18	0.82

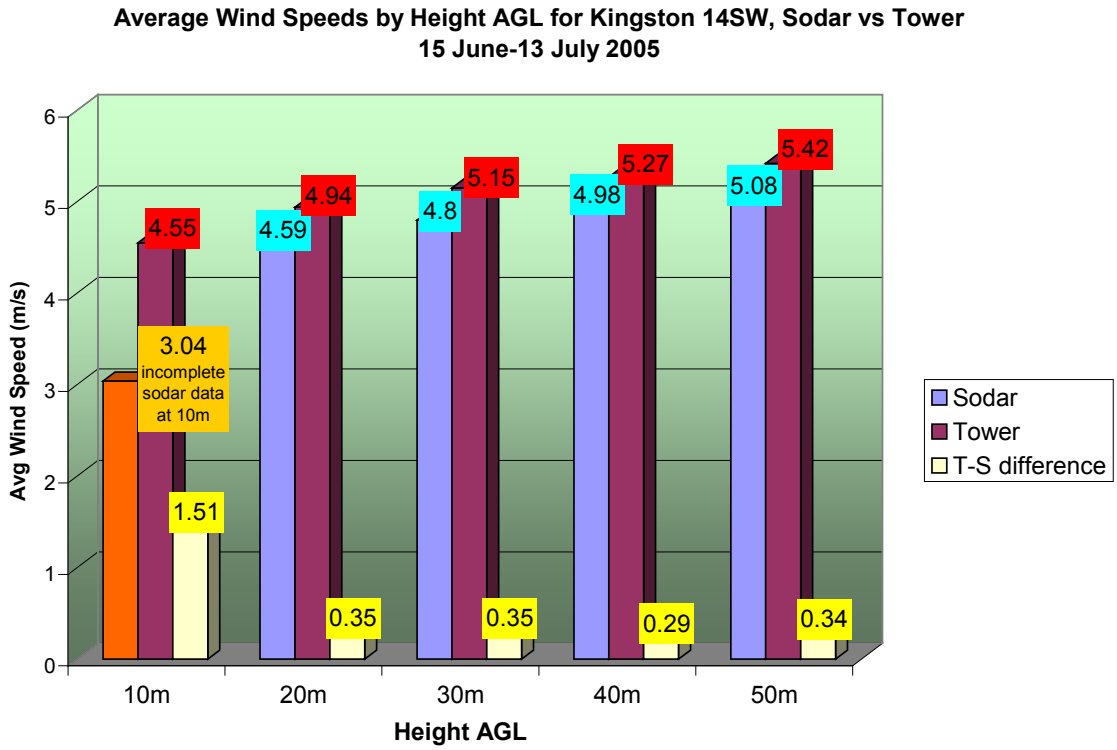

Figure 54. Comparison of average wind speeds by height as measured by the sodar and the tower anemometer, and differences, for the period 15 June-13 July 2005 at Kingston

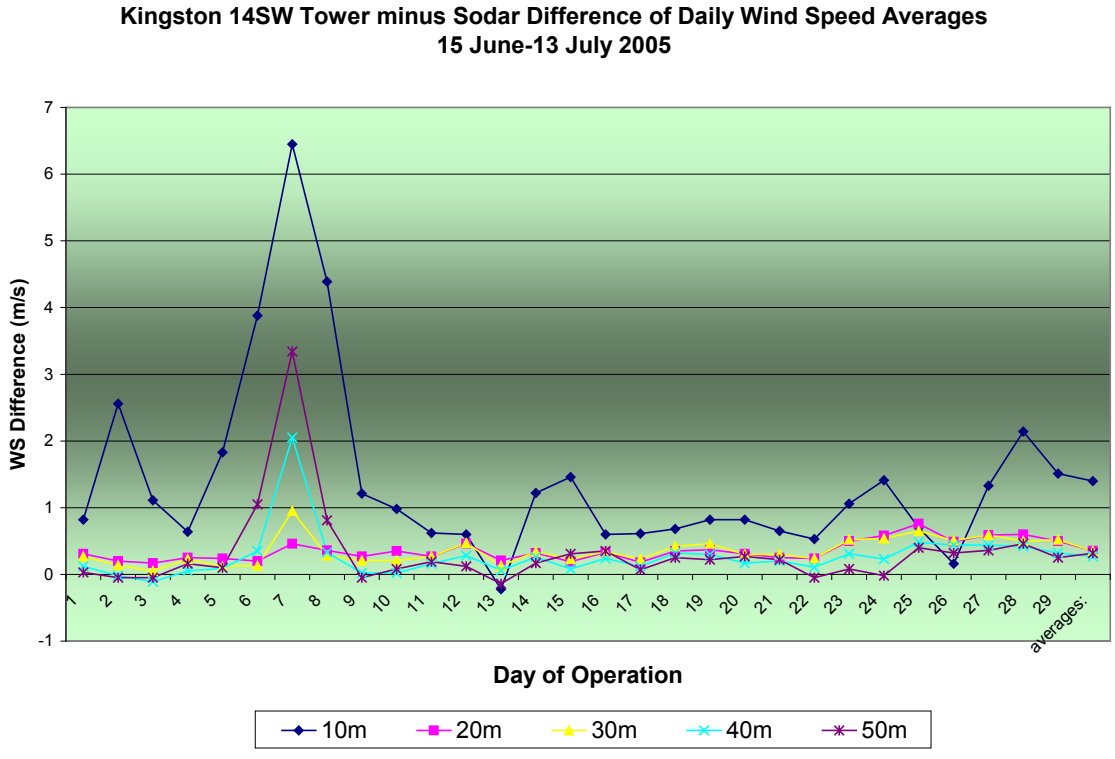

Figure 55. Time series of differences between daily average tower and sodar measured wind speeds by height at Kingston for the period 15 June-13 July 2005

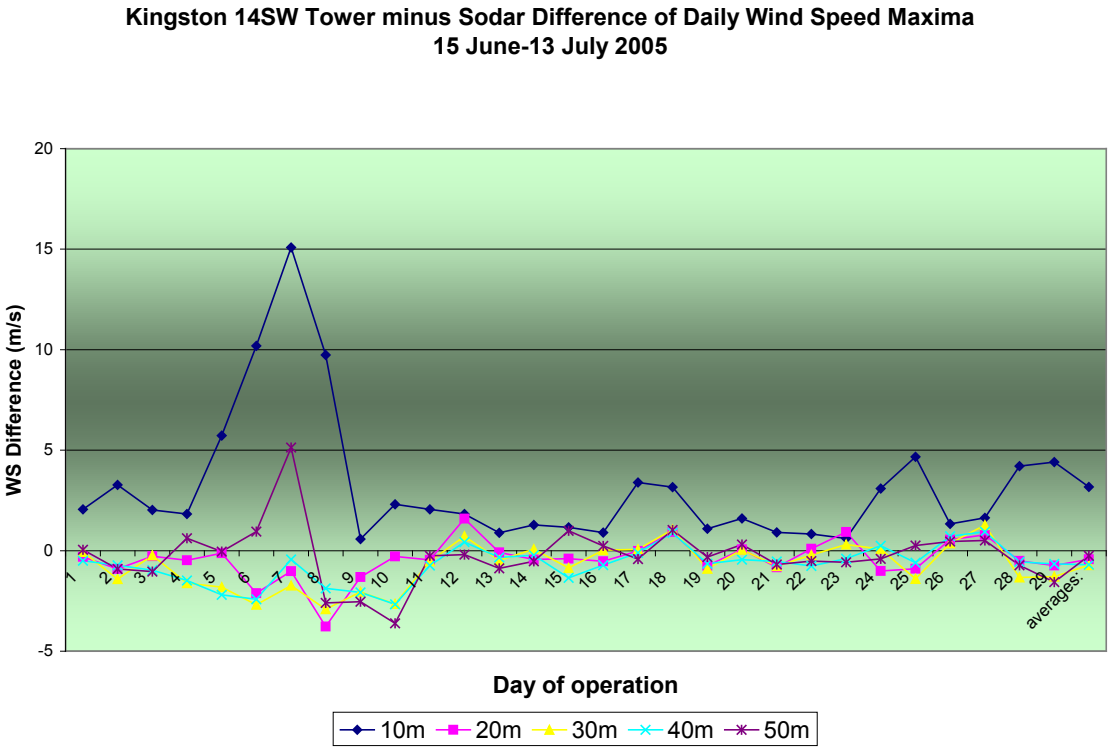

Figure 56. Same as Figure 55, but for daily wind speed maxima

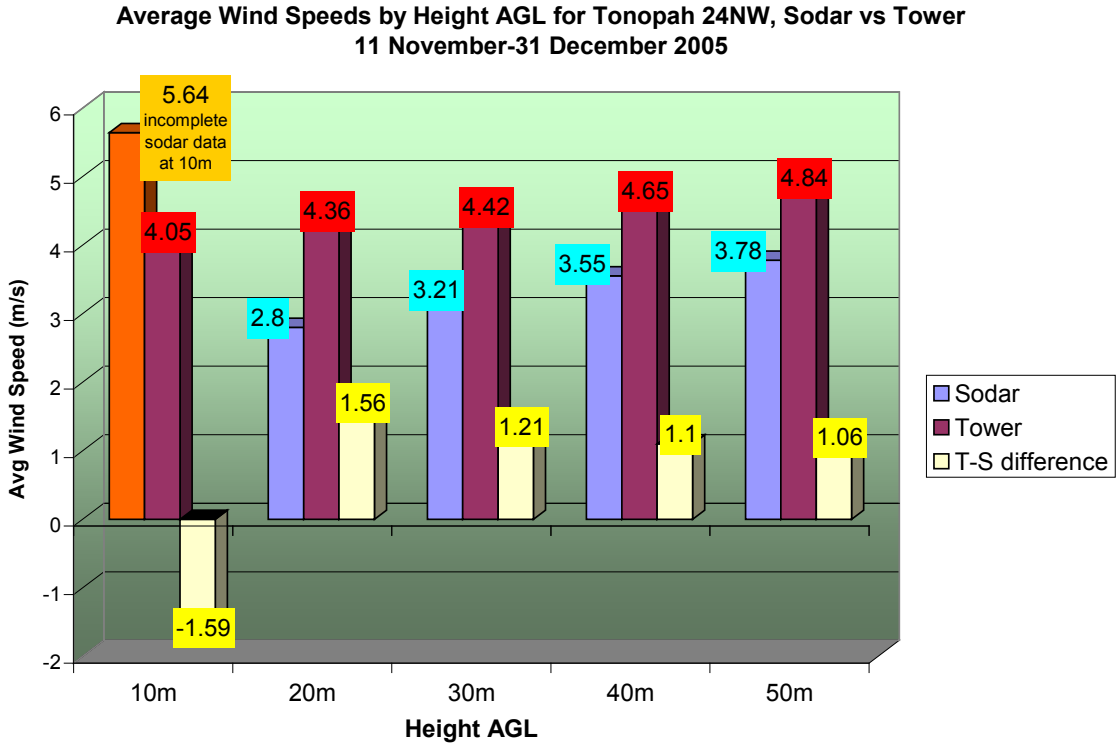

Figure 57. Comparison of average wind speeds by height as measured by the sodar and the tower anemometer, and differences, for the period 11 November-31 December 2005 at Tonopah

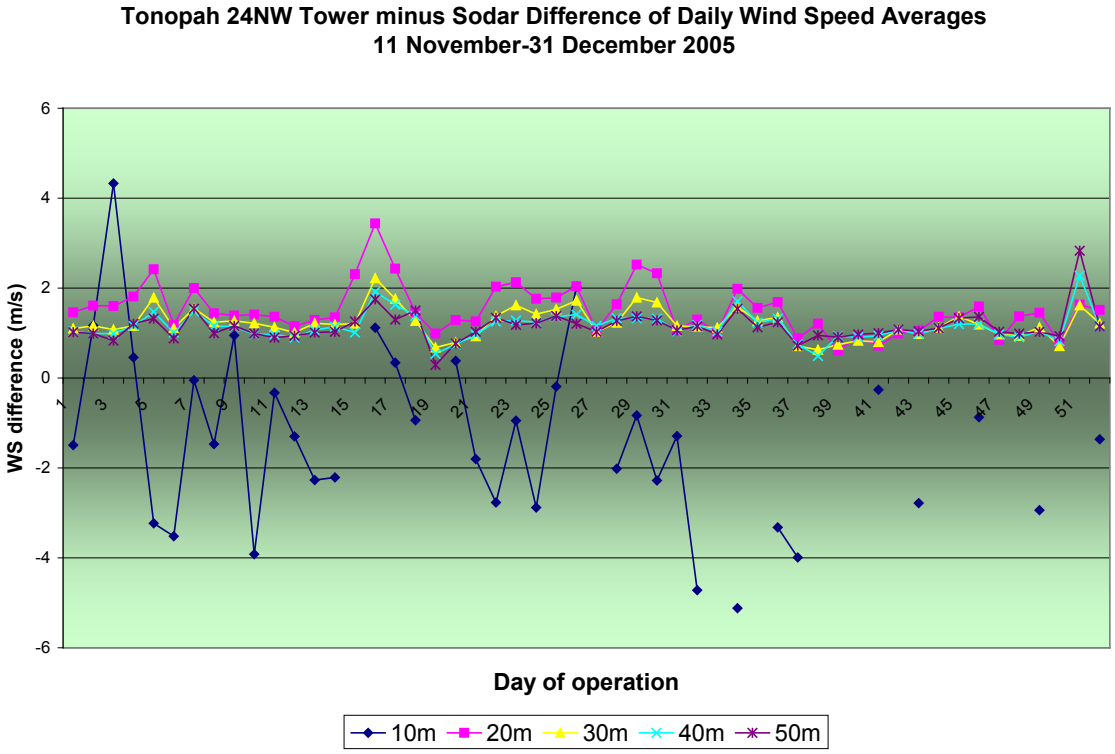

Figure 58. Time series of differences between daily average tower and sodar measured wind speeds by height at Tonopah for the period 11 November-31 December 2005

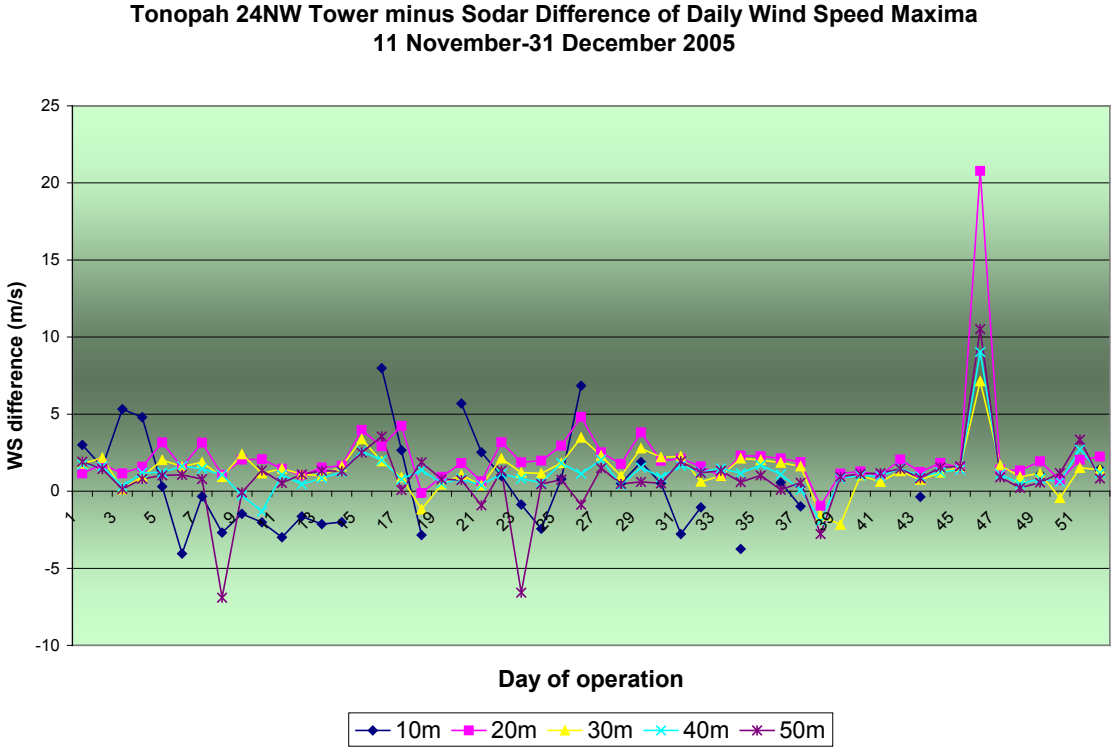

Figure 59. Same as Figure 58, but for daily wind speed maxima

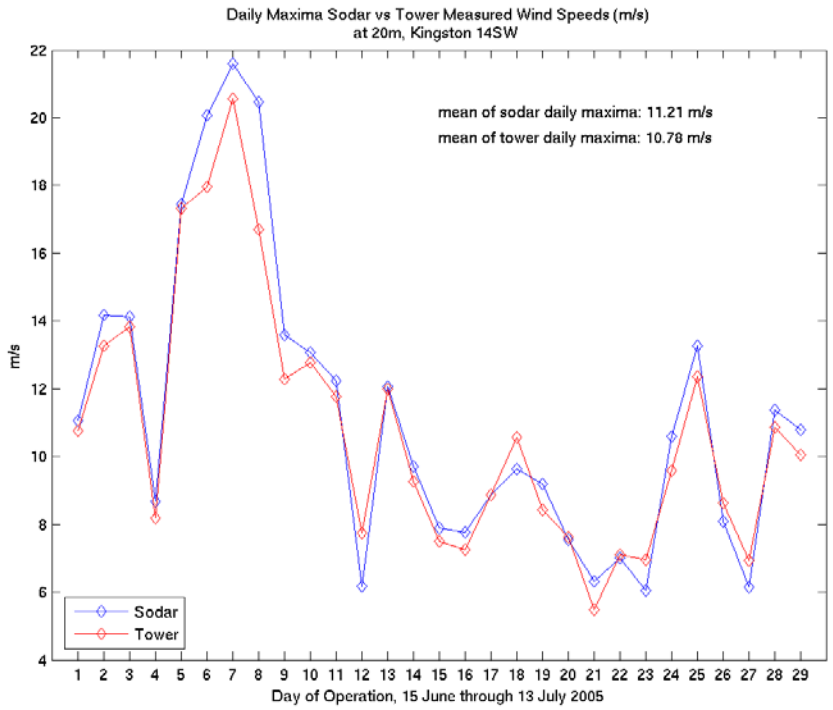

Figure 60. Time series of sodar- and tower-measured daily maximum wind speeds at Kingston for the period 15 June-13 July 2005

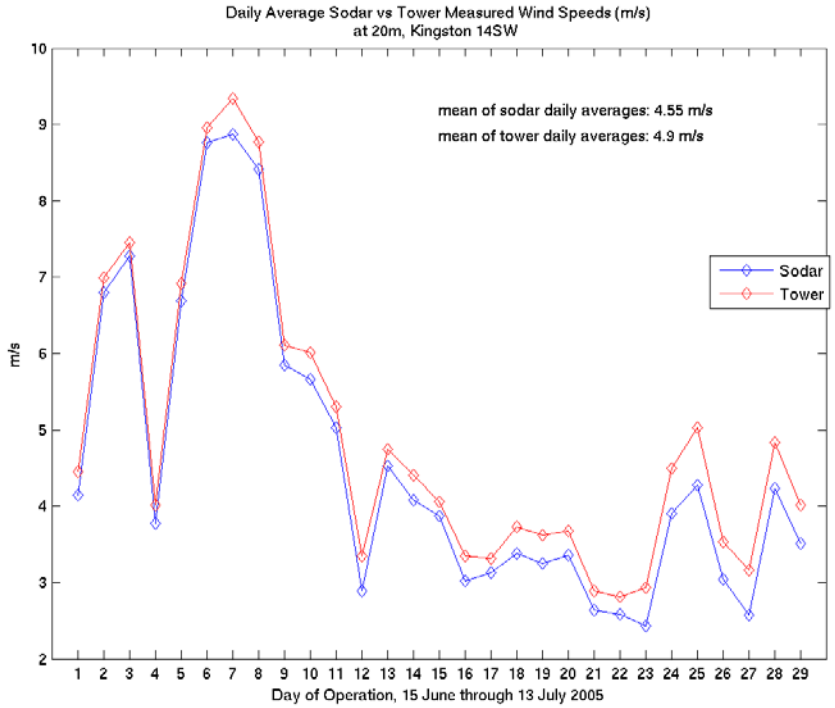

Figure 61. Same as Figure 60, but for daily average wind speeds

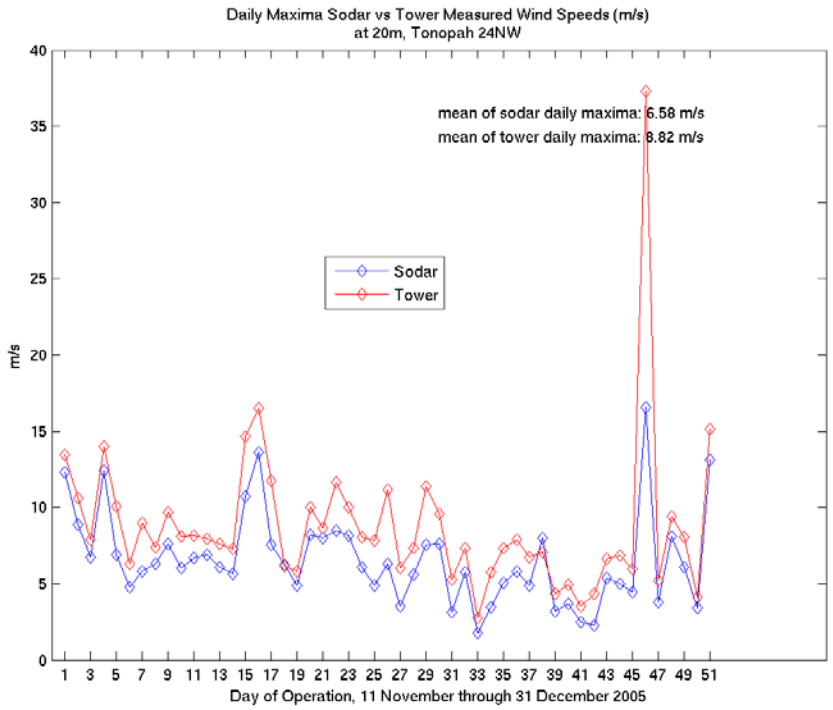

Figure 62. Time series of sodar- and tower-measured daily maximum wind speeds at Tonopah for the period 11 November-31 December 2005

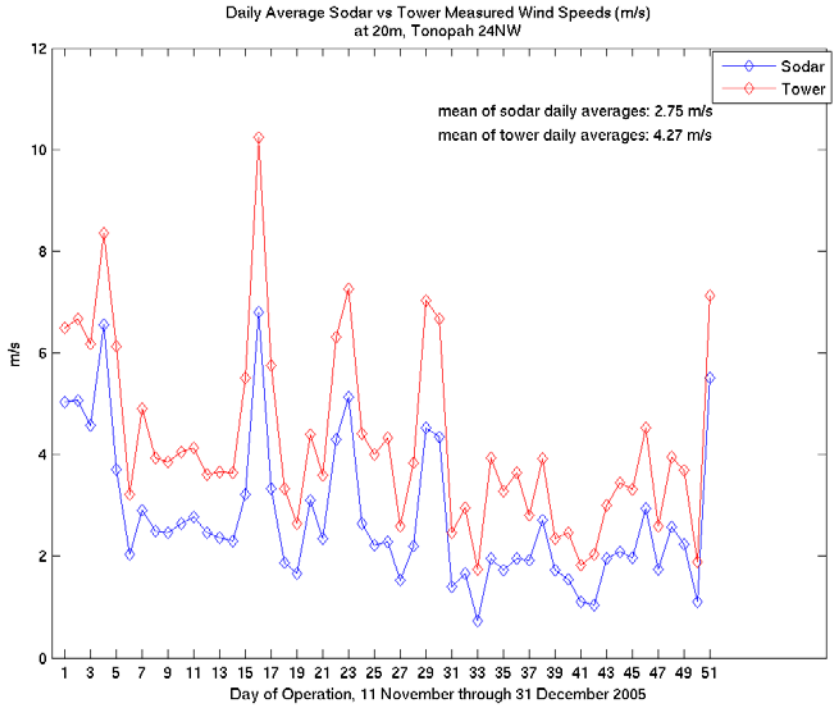

Figure 63. Same as Figure 62, but for daily average wind speeds

Conclusions

We have been looking for patterns in the differences between the sodar data and the tower data, both spatially and temporally, in order to assess the accuracy and sensitivity of the sodar wind speed measurements relative to the towers' anemometers. In doing this, we have assumed the conventional anemometer data to be the standard for wind speed measurement—in effect, to be "truth."

The data check summaries show the quick decrease in sodar data quality above 50 m, by the rapid increase in NaNs. The good data (i.e., mean data with NaNs and outliers numbering less than 10% of the total number of data entries) is confined for both locations to the 20, 30, 40, and 50 m heights above ground level.

Looking at **Figures 54 and 57**, one can notice that there is no strong correlation between height above the ground and the tower minus sodar average wind speed differences. (Throughout this analysis we are neglecting the 10 m sodar data as being too incomplete to tell us anything other than that this sodar system doesn't work well at 10 meters. For our purposes—that is, our interest in what is happening at rotor hub height—this is not a problem. However, the 10 m data were included for completeness.). In **Figure 54** (Kingston), the differences stay pretty close to constant. In **Figure 57** (Tonopah), these differences show a small decreasing trend with height. In both figures it is not completely clear that the sodar becomes significantly more or less accurate with height when compared to the tower data.

Figures 55, 56, 58, and 59 are plots of the tower minus sodar differences for the daily wind speed averages and maxima. These are included because they show that there is no increase or decrease in the accuracy of the sodar over the time periods considered. From this, we can infer that the calibration of the sodar does not get worse with time.

Figures 60 and 61 show the daily wind speed maxima and averages at 20 m for Kingston, while **Figures 62 and 63** show the same for Tonopah. These plots are representative of the results at the different heights. If the sodar were resolving higher wind speeds differently than low wind speeds when compared to the towers, we might see a different pattern in the maxima plots versus how the daily sodar wind speed averages track the tower daily wind speed data. For instance, since the sodar was taking measurements every five minutes to the towers' ten, there is a greater chance for the sodar to catch a short-lived high wind speed result that the tower might miss, and the results should therefore trend slightly higher than the daily averages. In fact the plots suggest this may be the case. Although the daily averages are lower for the sodar results, the daily maxima are relatively greater (in the case of the Kingston 20 m maxima, they are absolutely greater). This is, however, only a slight trend. Otherwise the maxima track quite similarly to the daily averages, suggesting a similar level of measurement sensitivity toward the higher winds.

Regarding the statistical analysis of the comparison between the sodar and tower data (**Figures 54 to 59**) and neglecting the 10 m level, daily average differences between the wind speeds measured by the tower and sodar are less than 0.4 m/s (and positive) at the Kingston location and less than 1.6 ms^{-1}(negative) at the Tonopah location. Average differences between the maximum daily wind speeds measured by the tower and sodar are less than 0.8 ms^{-1} (and negative) at the Kingston location and less than 2.3 ms^{-1} (and positive) at the Tonopah location

These results, when taken together, make a good case that the primary problems with this sodar usage were two: the initial calibration of the unit and its inability to extend its measurement reach much above 50 m. Some of the differences could be also related to calibration of the anemometers. We have seen that the sodar was sensitive to wind changes between 20 and 50 m and tracked well with the tower data. From these results, it seems likely that if the sodar were well calibrated it would yield measurements coming close to the accuracy and reliability of the tower anemometers over that range of measurement heights.

Nor do we see any basis in these results for distinguishing between the sodar performances at Kingston and Tonopah. Both sites show similar average wind speeds on the period of action (Kingston slightly larger), and both are at similar elevations. Considering how the sodar works, it is a pertinent question whether the amount of particulate matter in the air affects the sodar's accuracy, and whether there was a difference in the air quality in this respect between the two sites. However, the data collected for these sites does not include any data types useful for investigating this question.

Because this particular sodar was a small portable unit, we should not expect its measuring reach to extend very high into the boundary layer. It is hoped that a larger and more powerful unit should be able to resolve wind speeds up to the hub height of modern large rotors—80, 90, or over 100 m height. However, powering such a unit in a remote location may become a challenge.

7.2 Sonic Anemometer Measurements of Turbulence Fluxes

We have obtained Stone Cabin 20-Hz sonic anemometer data stored on DVDs for the period from 8 February to 20 September 2007 for 40, 60, and 80m levels. Programs to read in data and compute turbulence fluxes were completed. For 10-min periods, the following turbulence fluxes were computed:

$$\overline{u'^2},\ \overline{v'^2},\ \overline{w'^2}$$

$$\overline{u'v'},\ \overline{u'w'},\ \overline{v'w'}$$

$$TKE = 0.5\left[\overline{u'^2} + \overline{v'^2} + \overline{w'^2}\right]$$

Time series plots (**Figures 64 through 121**) of turbulence kinetic energy (TKE; m^2s^{-2}), momentum fluxes (u'w', v'w'; m^2s^{-2}) and heat fluxes (w'T'; K m s^{-1}) for the complete domain time domain (8 February 2007 – 20 September 2007) obtained from the high frequency (20 Hz) sonic anemometer measurements. For clarity, the plots are further arranged by the month (8 February – 9 March, 2-29 April, 5-30 June, 1-31 July, 1-31 August, and 1-20 September 2007).

While examining the time series (**Figures 64 through 70**) and statistics (**Table 9**) of the TKE, it is apparent that there are many sharp peaks of TKE at all levels. Some of them are greater than 60 m^2s^{-2} (**Figure 71**). Some of the large peaks that occurred generally at only one level were excluded from the statistic analysis (**Table 9**). Since these are 10-min averages each including 12000 samples, these values need to be considered in this first report. Some of these large values could be associated with the system malfunctions. Average values for the entire period are relatively reasonable (below 2 m^2s^{-2}) and indicate increase of the TKE with height. Scatter plots of the TKE (**Figures 120 through 130**) indicate that there is a possible problem with

measurements at 80 m since the scatter plots of the TKE between 40 and 60 m show pretty close agreement, while any combination with 80 m worsens the comparison. Similarly as in the case with the wind speed analysis, this could be related to the obstruction antennas at 80 m (see **Figure 10**).

A time series of the u'u' variance (**Figure 70**) shows large peaks (especially at 40 m) that contribute to the large values of observed TKE. Some of the peaks coincide at all levels, but many of them (especially at the beginning of the period) could be related to problems with the measurement technique.

A time series of v'v' variance (**Figure 78**) indicates more uniform behavior (especially at 40 m) compared to the u'u' plot.

Since the plot of w'w' variance (**Figure 85**) shows much smaller values compared to u'u' and v'v' plots, one can conclude that the most contribution to large TKE peaks are coming from u'u' component. This could be related to the mounting orientation and the tower's flow shadowing effects.

Although a time series of u'v' (**Figure 92**) indicates sharp peaks, notice that most of them are coinciding at all levels. The values of this parameter appear to be similar at all levels.

Statistics of the u'w' kinematic momentum flux component shows that the average values are negative (as expected) (**Table 9**); however, time series of the same parameter is quite noisy at 40 m with a significant number of sharp peaks.

In contrast to u'w' behavior, a time evolution of v'w' (**Figure 106**) is more uniform at all levels with more noise (or realistic variability) at higher levels.

Plots of w'T' have sharp isolated peaks of several order of magnitude larger than most of the values, especially at 40 m. Since the peaks generally do not coincide at various levels, there might be some problems with detecting this parameter. These peaks could be removed in further analysis.

Table 9. Summary Statistics of the TKE, Momentum and Heat Fluxes Results for the Seven Different Time Domains[a]

8 feb-20 sep	N	mean	std	max	min
TKE80m	22672	1.99	2.69	28.69	0.01
TKE60m	22732	1.53	1.65	27.23	0
TKE40m	22550	1.56	1.74	35.01	0.01
u'w'80m	22672	-0.07	0.38	3.53	-10.83
u'w'60m	22732	-0.02	0.23	2.58	-9.69
u'w'40m	22550	-0.01	0.4	5.05	-19.99
v'w'80m	22672	-0.03	0.37	3.1	-5.05
v'w'60m	22732	-0.01	0.23	2.21	-2.26
v'w'40m	22550	-0.02	0.21	8.44	-2.3
u'v'80m	22672	0.06	0.89	18.24	-19.94
u'v'60m	22732	0.06	0.67	19.05	-9.03
u'v'40m	22550	0.07	0.67	15.32	-10.31
w'T'80m	22672	0.08	0.16	10.28	-2.02
w'T'60m	22732	0.08	0.15	8.41	-0.39
w'T'40m	22550	0.07	0.33	1.22	-20.27

8 feb-9 mar	N	mean	std	max	min
TKE80m	4078	1.65	2.12	25.36	0.01
TKE60m	4082	1.01	1.15	27.23	0.01
TKE40m	3840	1.12	1.71	35.01	0.01
u'w'80m	4078	-0.08	0.37	1.85	-10.83
u'w'60m	4082	-0.02	0.22	1.14	-9.69
u'w'40m	3840	-0.05	0.74	1.18	-19.99
v'w'80m	4078	-0.07	0.33	1.65	-3.19
v'w'60m	4082	0	0.15	1.19	-1.47
v'w'40m	3840	-0.02	0.13	0.81	-1.48
u'v'80m	4078	0.13	0.76	18.24	-3.9
u'v'60m	4082	0.05	0.5	19.05	-4.17
u'v'40m	3840	0.05	0.48	15.32	-4.64
w'T'80m	4078	0.03	0.18	10.28	-1.45
w'T'60m	4082	0.03	0.16	8.41	-0.15
w'T'40m	3840	-0.01	0.65	0.44	-20.27

2-29 apr	N	mean	std	max	min
TKE80m	3709	3.19	4.13	28.69	0.01
TKE60m	3607	1.81	1.78	18.98	0
TKE40m	3718	1.79	1.87	20.73	0.01
u'w'80m	3709	-0.09	0.52	2.31	-3.87
u'w'60m	3607	0	0.22	1.17	-1.87
u'w'40m	3718	0.03	0.44	5.05	-10.8
v'w'80m	3709	-0.07	0.51	3.1	-5.05
v'w'60m	3607	0.04	0.25	1.92	-1.97
v'w'40m	3718	0.01	0.27	8.44	-2.06
u'v'80m	3709	0.25	1.37	11.29	-19.94
u'v'60m	3607	0.12	0.83	12.71	-9.03
u'v'40m	3718	0.09	0.84	14.21	-10.31
w'T'80m	3709	0.06	0.13	1.63	-2.02
w'T'60m	3607	0.07	0.12	0.79	-0.39
w'T'40m	3718	0.05	0.34	1.06	-11.01

5-30 june	N	mean	std	max	min
TKE80m	3736	2.4	3.35	26.63	0.02
TKE60m	3716	1.79	1.76	15.33	0.01
TKE40m	3688	1.83	1.83	19.94	0.02
u'w'80m	3736	-0.06	0.45	3.53	-3.57
u'w'60m	3716	0	0.24	1.41	-2.6
u'w'40m	3688	0	0.27	1.26	-7.55
v'w'80m	3736	-0.03	0.41	2.63	-4.6
v'w'60m	3716	0.01	0.26	2.21	-1.45
v'w'40m	3688	-0.01	0.23	1.72	-1.51
u'v'80m	3736	0.11	1.05	10.09	-5.01
u'v'60m	3716	0.08	0.71	7.01	-4.39
u'v'40m	3688	0.11	0.72	6.63	-4.52
w'T'80m	3736	0.12	0.17	1.6	-0.31
w'T'60m	3716	0.12	0.17	1.56	-0.38
w'T'40m	3688	0.12	0.22	1.22	-6.46

Table 9, Continued

1-31 july	N	mean	std	max	min
TKE80m	4342	1.69	1.8	16.22	0.01
TKE60m	4522	1.65	1.77	16.61	0.01
TKE40m	4498	1.63	1.73	15.57	0.01
u'w'80m	4342	-0.07	0.3	2.23	-3.19
u'w'60m	4522	-0.03	0.24	2.58	-2.53
u'w'40m	4498	-0.02	0.21	2.01	-1.45
v'w'80m	4342	-0.02	0.32	1.94	-3.82
v'w'60m	4522	-0.04	0.23	1.29	-1.61
v'w'40m	4498	-0.05	0.21	1.06	-1.66
u'v'80m	4342	-0.06	0.68	7.33	-5.82
u'v'60m	4522	0.04	0.71	11.39	-5.19
u'v'40m	4498	0.06	0.7	11.15	-5.08
w'T'80m	4342	0.1	0.16	1.1	-0.46
w'T'60m	4522	0.1	0.16	1.23	-0.37
w'T'40m	4498	0.1	0.16	0.92	-0.34

1-31 aug	N	mean	std	max	min
TKE80m	4498	1.48	1.64	11.44	0.01
TKE60m	4497	1.49	1.64	11.55	0
TKE40m	4498	1.5	1.6	11.14	0.01
u'w'80m	4498	-0.06	0.25	2.4	-2.48
u'w'60m	4497	-0.03	0.22	1.11	-2.06
u'w'40m	4498	-0.02	0.21	1.45	-2.52
v'w'80m	4498	0	0.28	2.23	-2.64
v'w'60m	4497	-0.03	0.23	1.56	-2.26
v'w'40m	4498	-0.04	0.2	1.22	-1.97
u'v'80m	4498	-0.04	0.58	6.17	-5.85
u'v'60m	4497	0.05	0.63	9.18	-8.56
u'v'40m	4498	0.06	0.62	6.93	-4.07
w'T'80m	4498	0.09	0.15	0.92	-0.39
w'T'60m	4497	0.1	0.16	0.95	-0.26
w'T'40m	4498	0.1	0.16	0.76	-1.22

1-20 sep	N	mean	std	max	min
TKE80m	2736	1.56	1.64	16.25	0.01
TKE60m	2736	1.43	1.49	13.41	0.01
TKE40m	2736	1.43	1.48	14.23	0.01
u'w'80m	2736	-0.06	0.28	1.6	-1.98
u'w'60m	2736	-0.03	0.22	1.24	-1.5
u'w'40m	2736	-0.02	0.22	1.11	-3.35
v'w'80m	2736	0.01	0.3	1.91	-2.68
v'w'60m	2736	-0.02	0.22	1.13	-2.26
v'w'40m	2736	-0.03	0.19	1.04	-2.3
u'v'80m	2736	-0.04	0.6	6.28	-4.59
u'v'60m	2736	0.02	0.59	5.03	-4.32
u'v'40m	2736	0.05	0.58	4.16	-4.07
w'T'80m	2736	0.08	0.14	1.12	-0.32
w'T'60m	2736	0.08	0.14	1.12	-0.39
w'T'40m	2736	0.08	0.15	1.08	-1.25

[a] Time domains include the complete time domain for this project—8 Feb-20 Sept 2007—as well as the monthly results: 8 Feb-9 Mar, 2-29 Apr, 5-30 June, 1-31 July, 1-31 Aug, and 1-20 Sept. (N = number of samples; std = standard deviation, max, min = maximum and minimum values in the time series.)

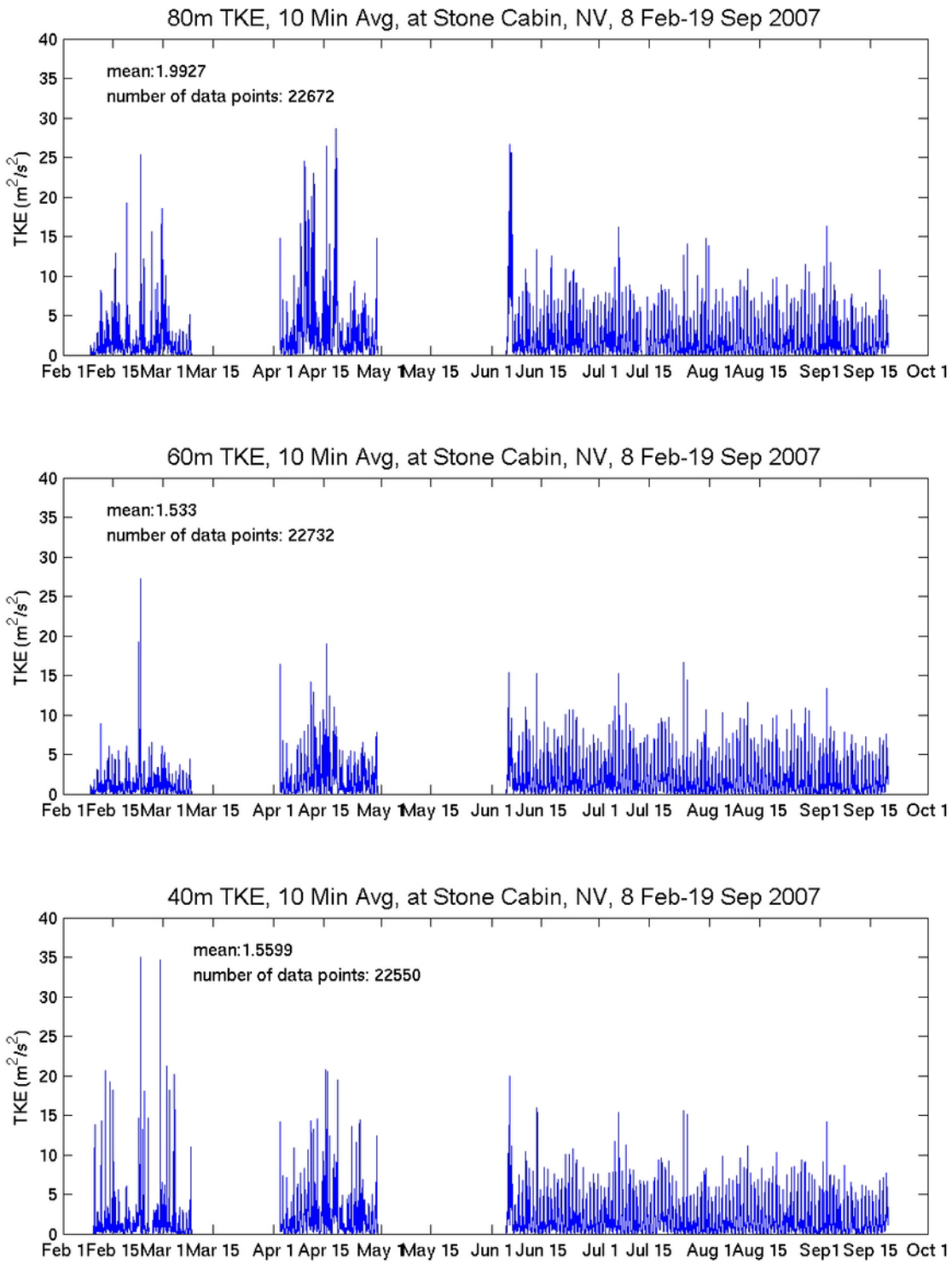

Figure 64. Sonic-measured turbulence kinetic energy (TKE; units in $m^2 s^{-2}$) at different height levels (averaged over 10 minute period) at Stone Cabin for the period 8 Feb 2007-19 Sept 2007. The mean and population of the dataset are indicated (top) at 80 m, (center) at 60 m, and (bottom) at 40 m heights.

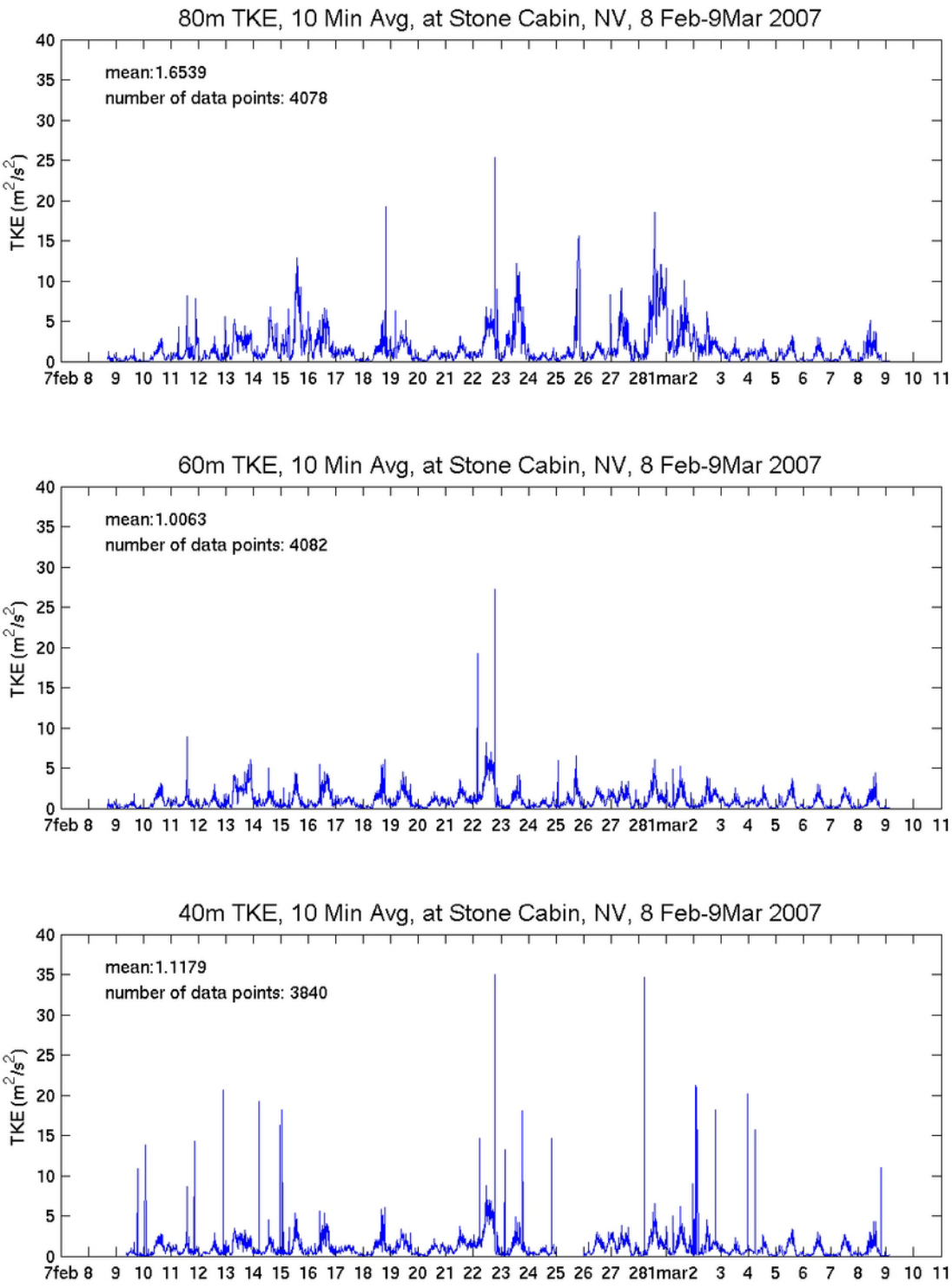

Figure 65. Same as Figure 64, but for a subset period 8 Feb-9 Mar 2007

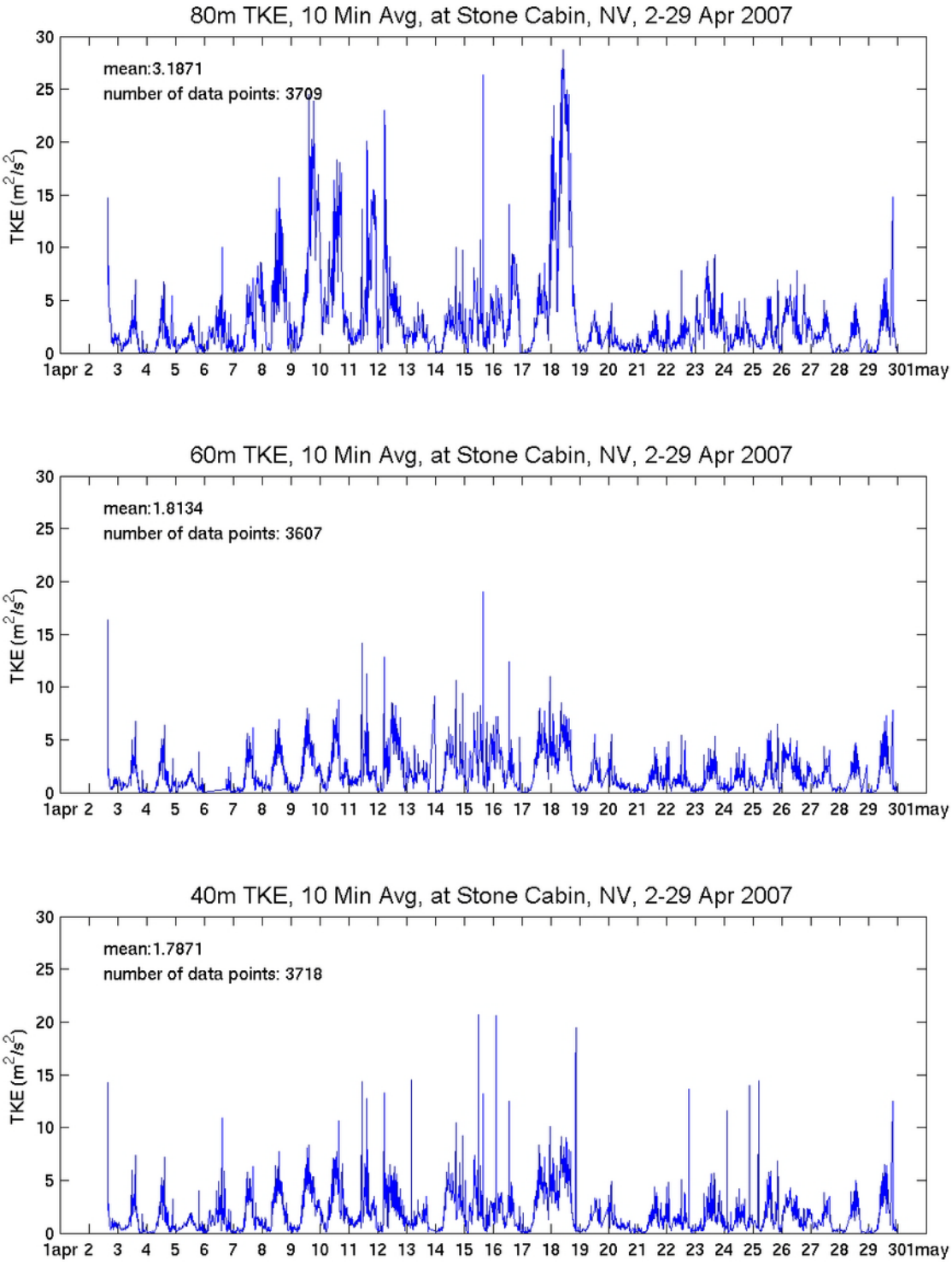

Figure 66. Same as Figure 64, but for a subset period 2-29 April 2007

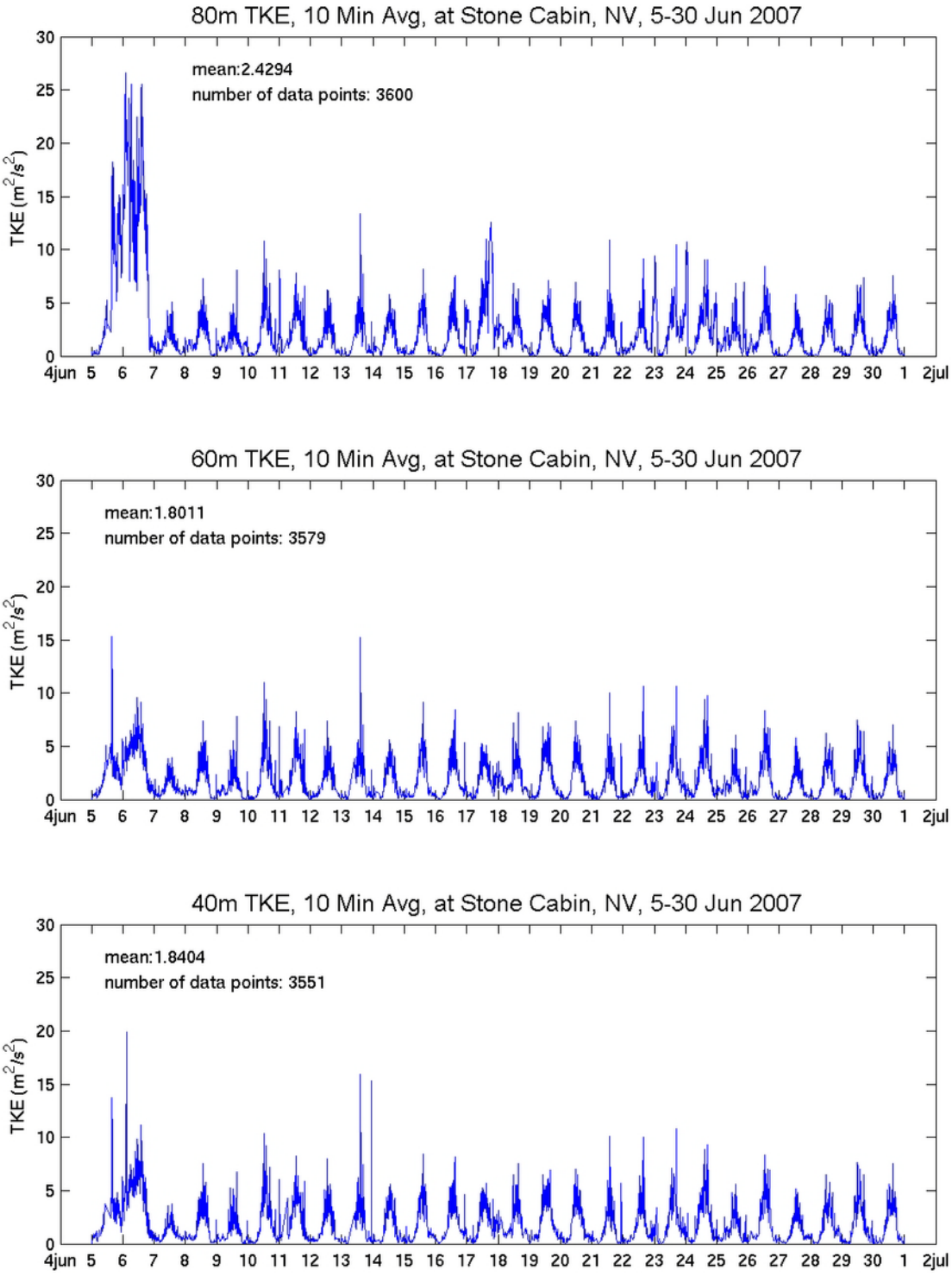

Figure 67. Same as Figure 64, but for a subset period 5-30 June 2007

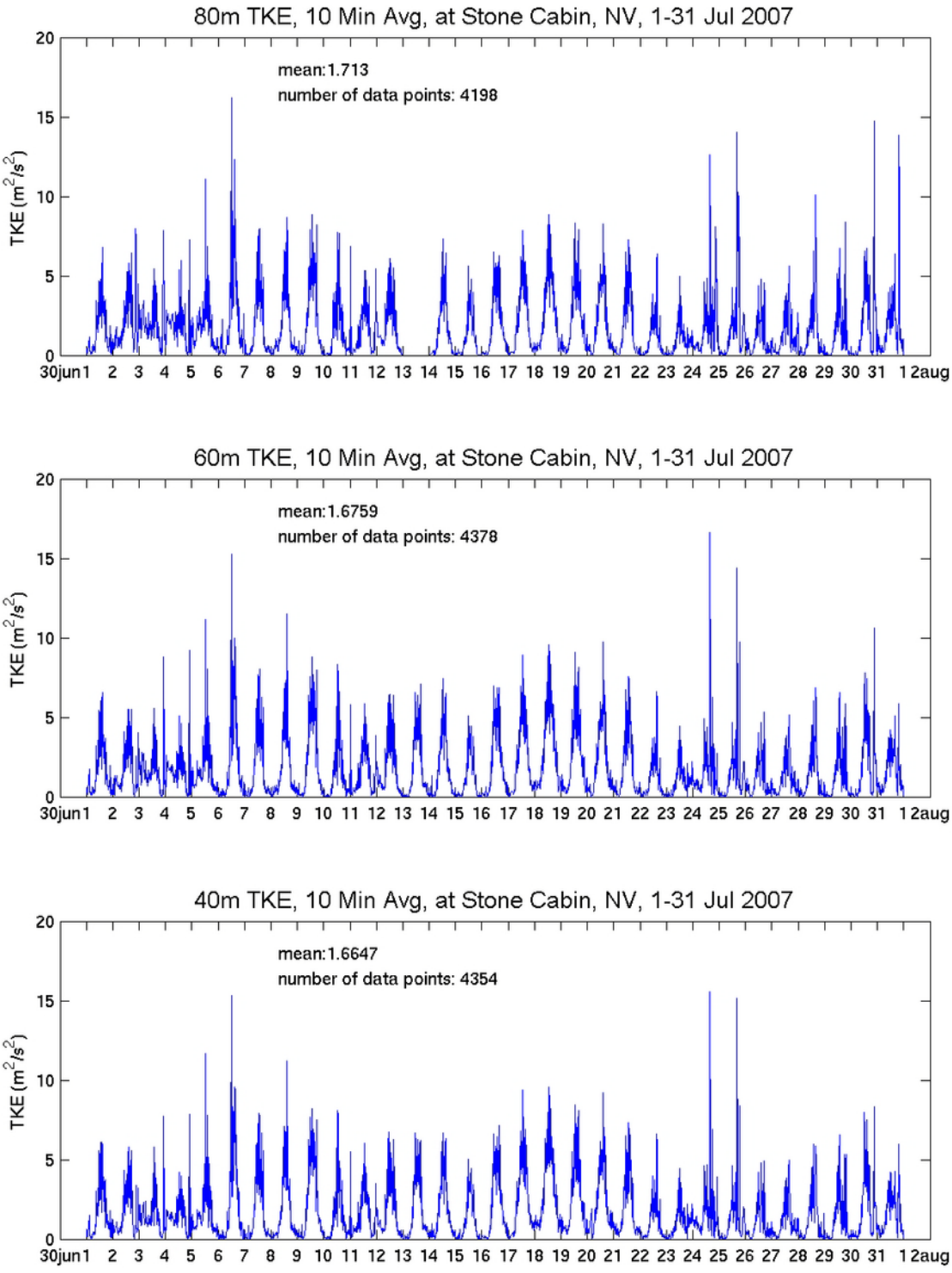

Figure 68. Same as Figure 64, but for a subset period 1-31 July 2007

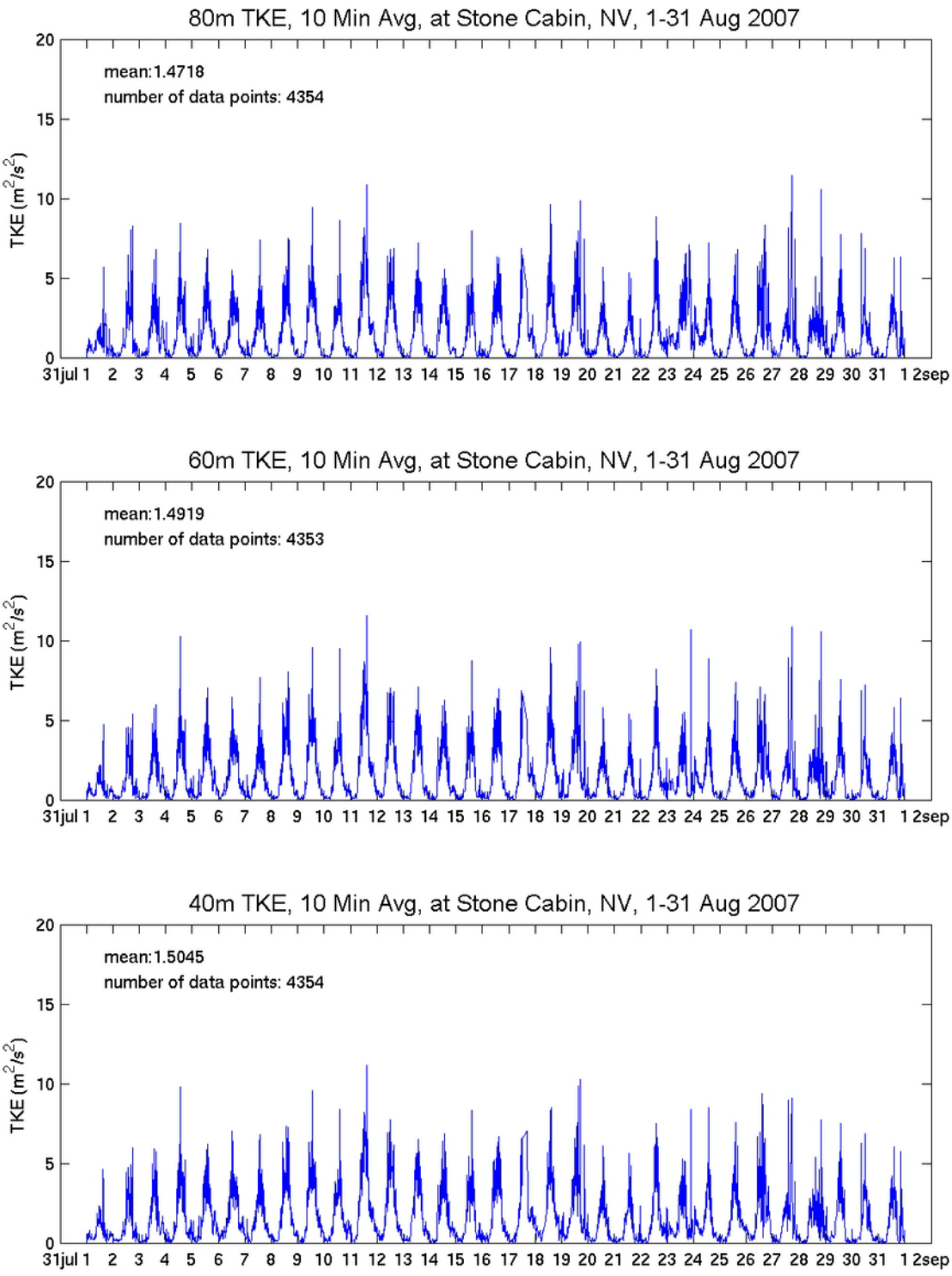

Figure 69. Same as Figure 64, but for a subset period 1-31 August 2007

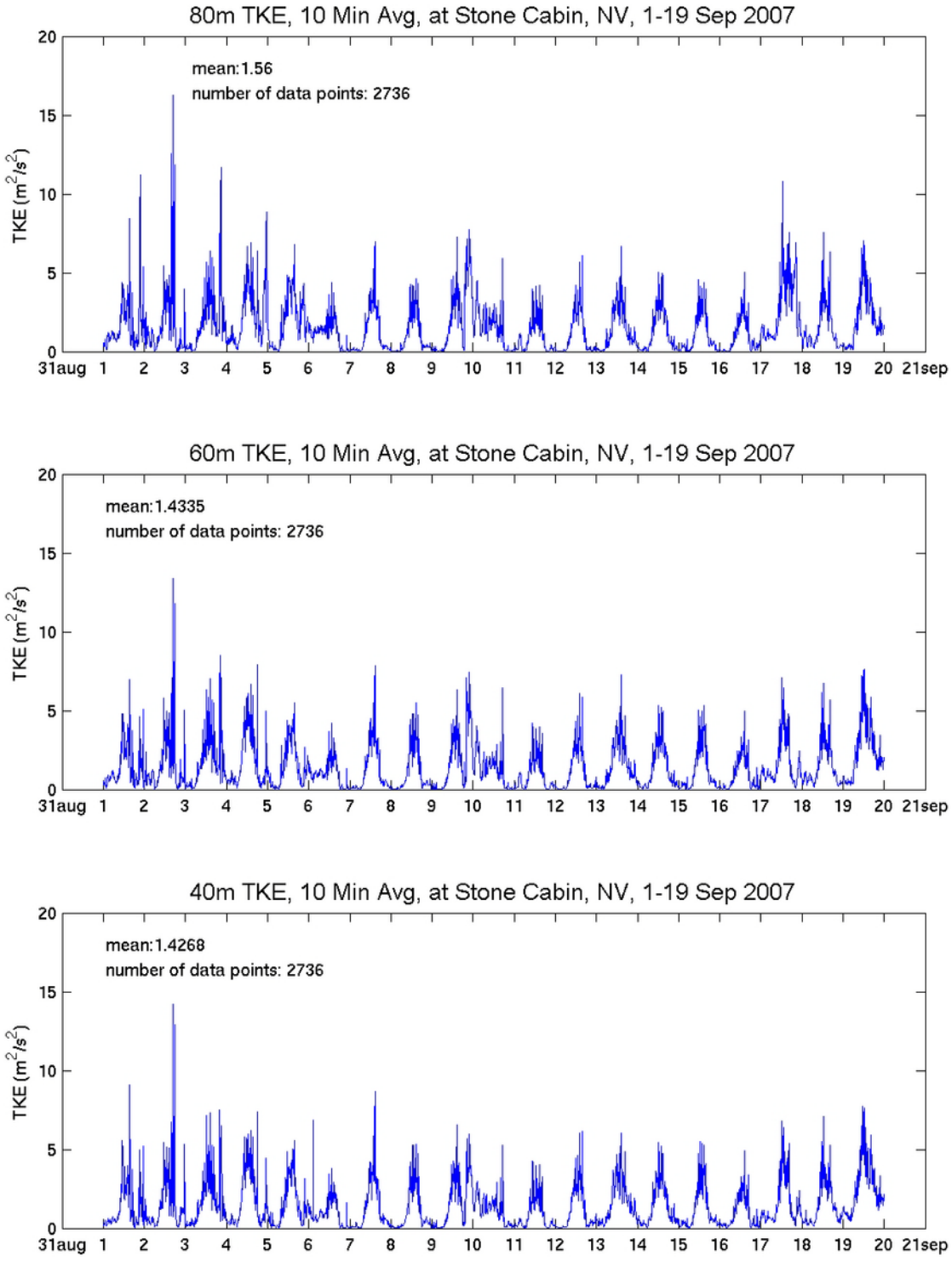

Figure 70. Same as Figure 64, but for a subset period 1-19 September 2007

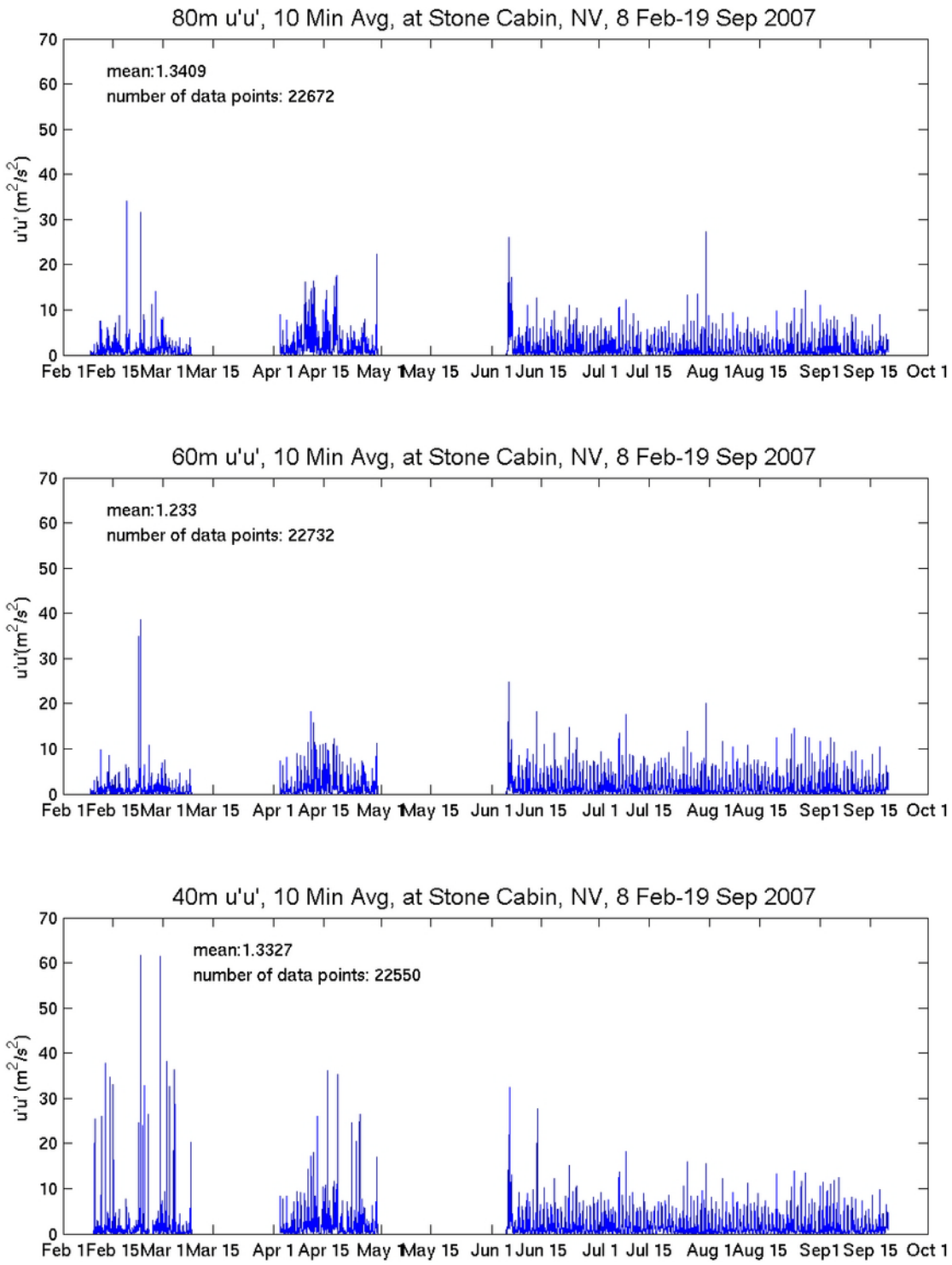

Figure 71. Sonic-measured turbulence momentum flux component u' u' (units in m^2 s^{-2}) at different height levels (averaged over 10-minute period) at Stone Cabin for the period 8 Feb 2007-19 Sept 2007. The mean and population of the dataset are indicated (top) at 80 m, (center) at 60 m, and (bottom) at 40 m heights.

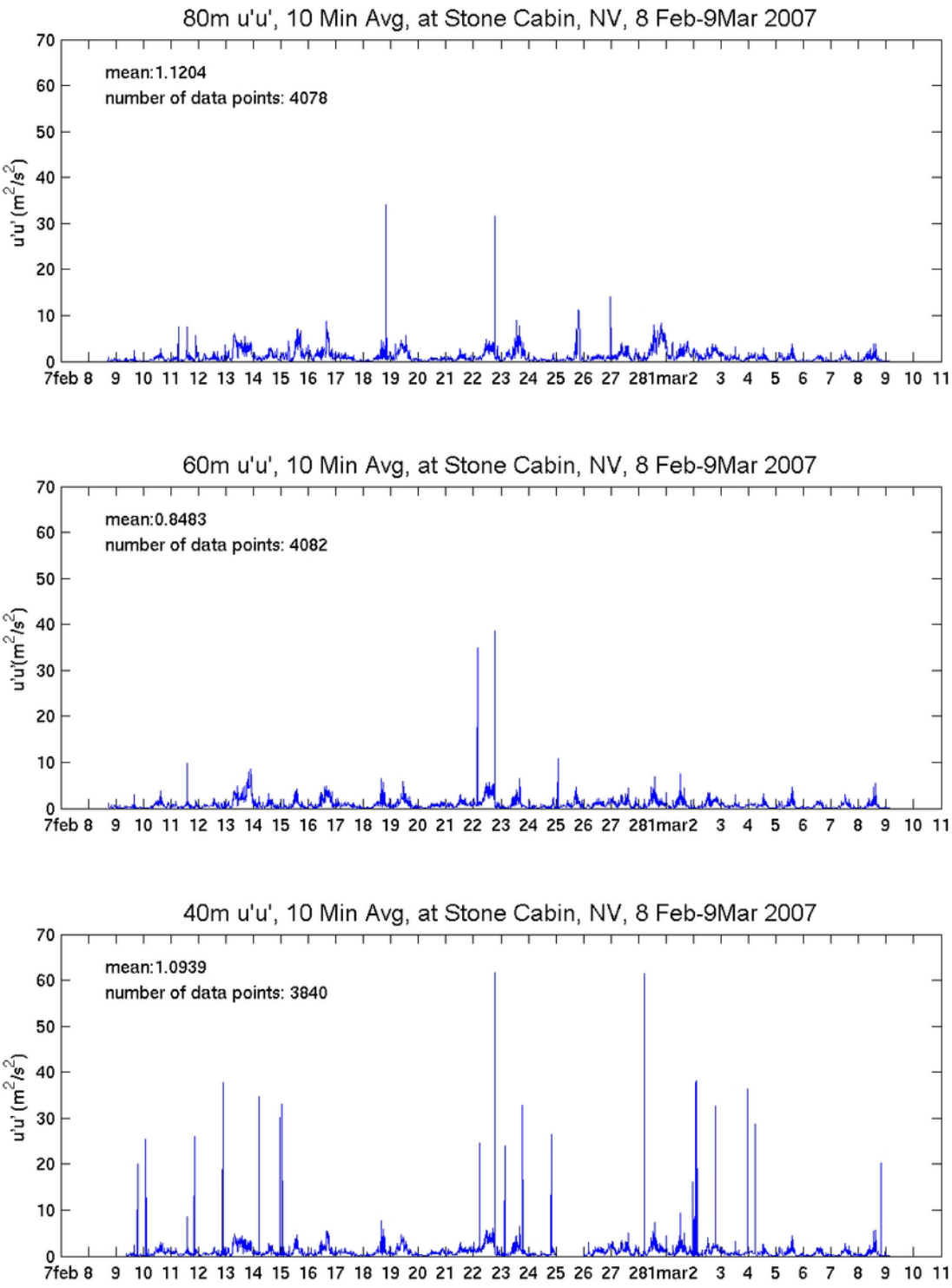

Figure 72. Same as Figure 71, but for a subset period 8 Feb-9 Mar 2007

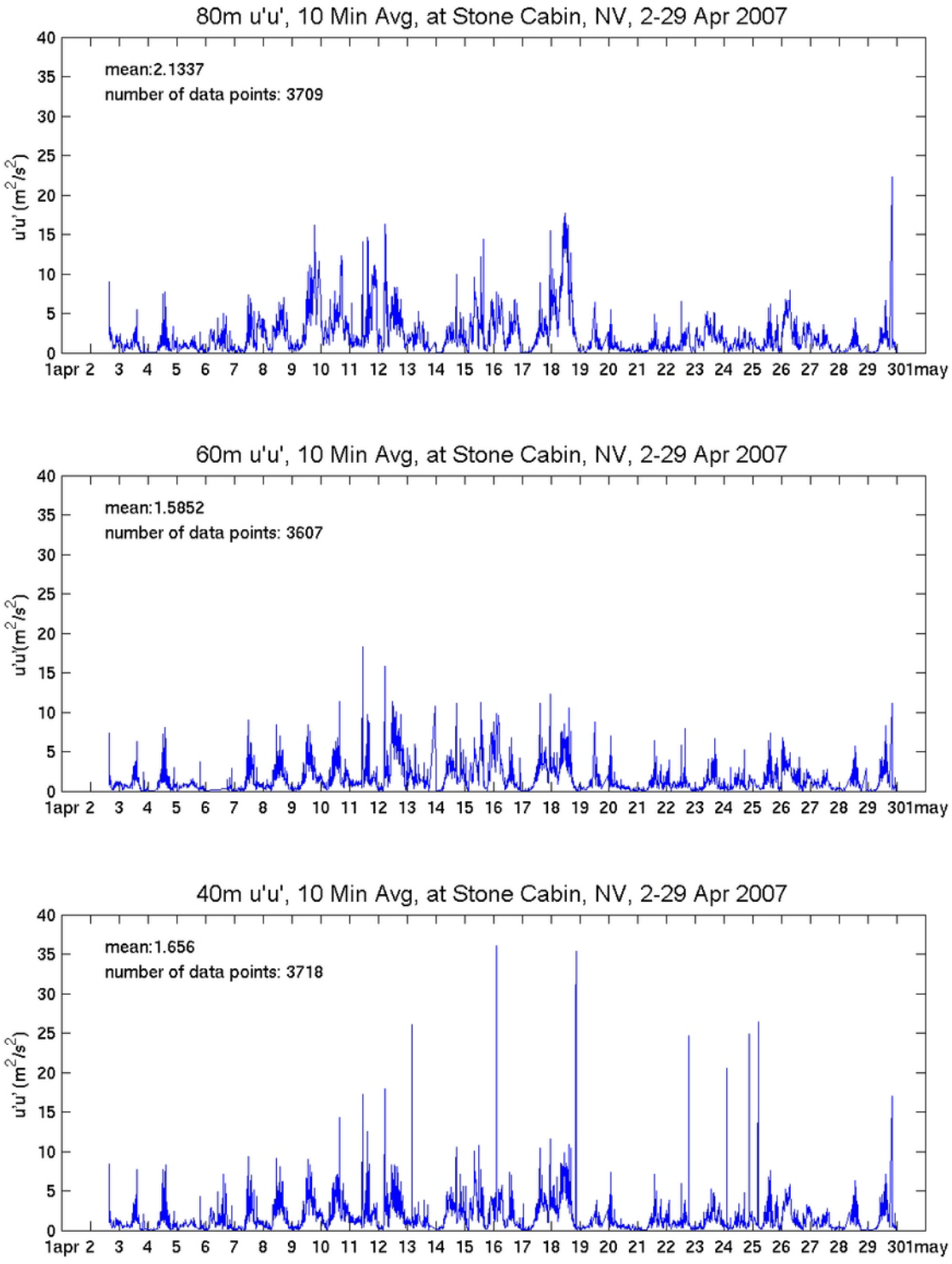

Figure 73. Same as Figure 71, but for a subset period 2-29 April 2007

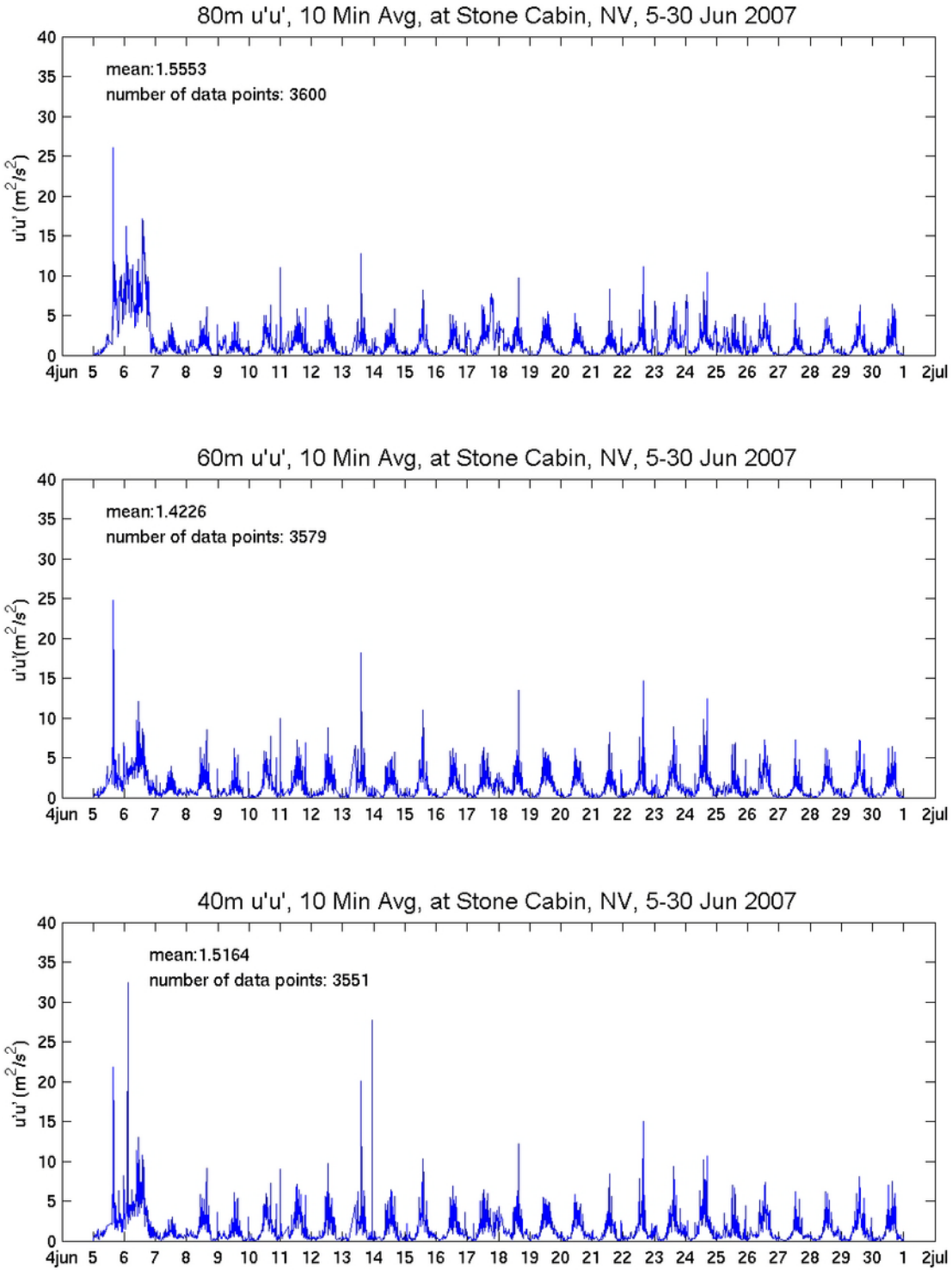

Figure 74. Same as Figure 71, but for a subset period 5-30 June 2007

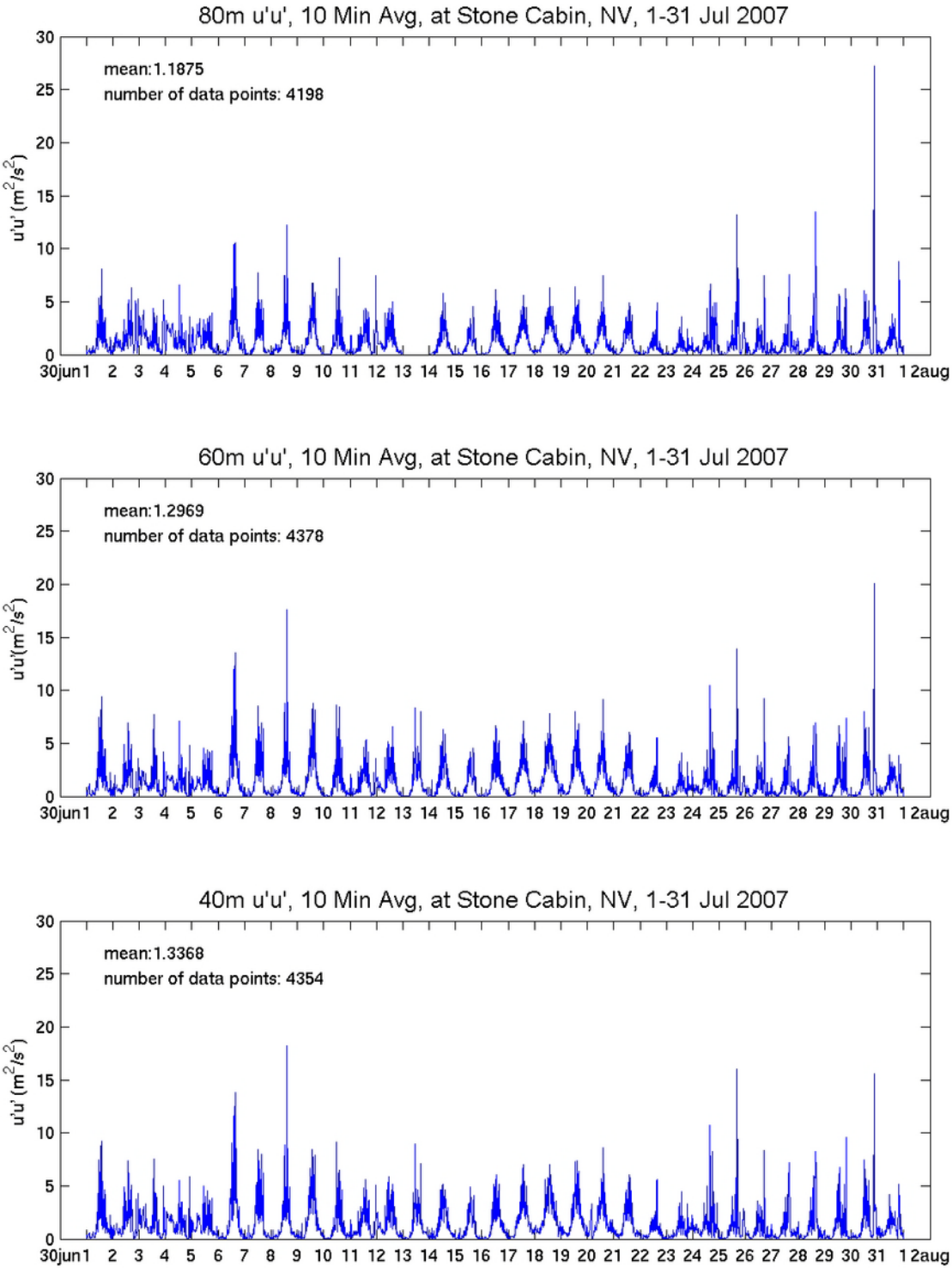

Figure 75. Same as Figure 71, but for a subset period 1-31 July 2007.

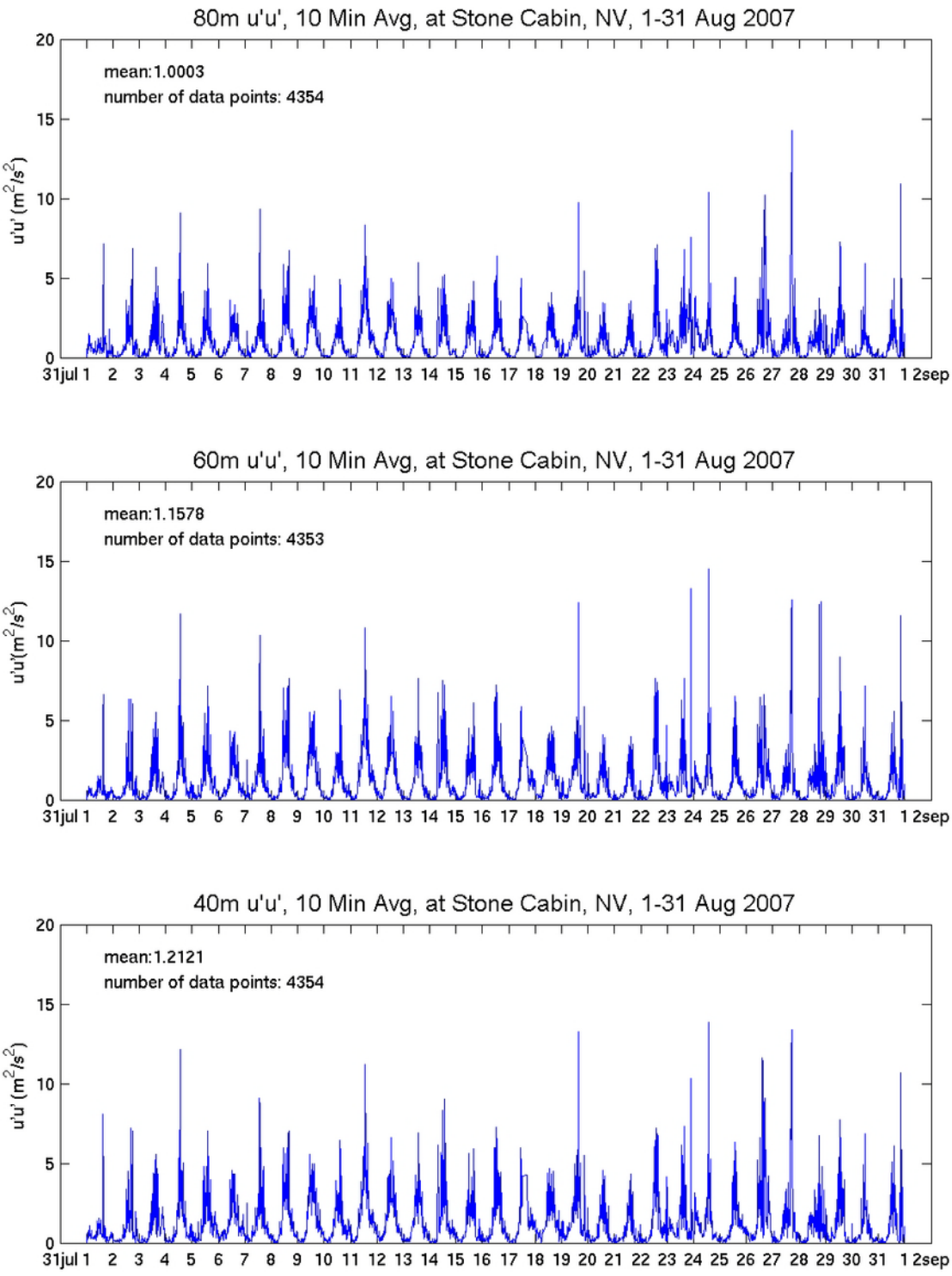

Figure 76. Same as Figure 71, but for a subset period 1-31 August 2007

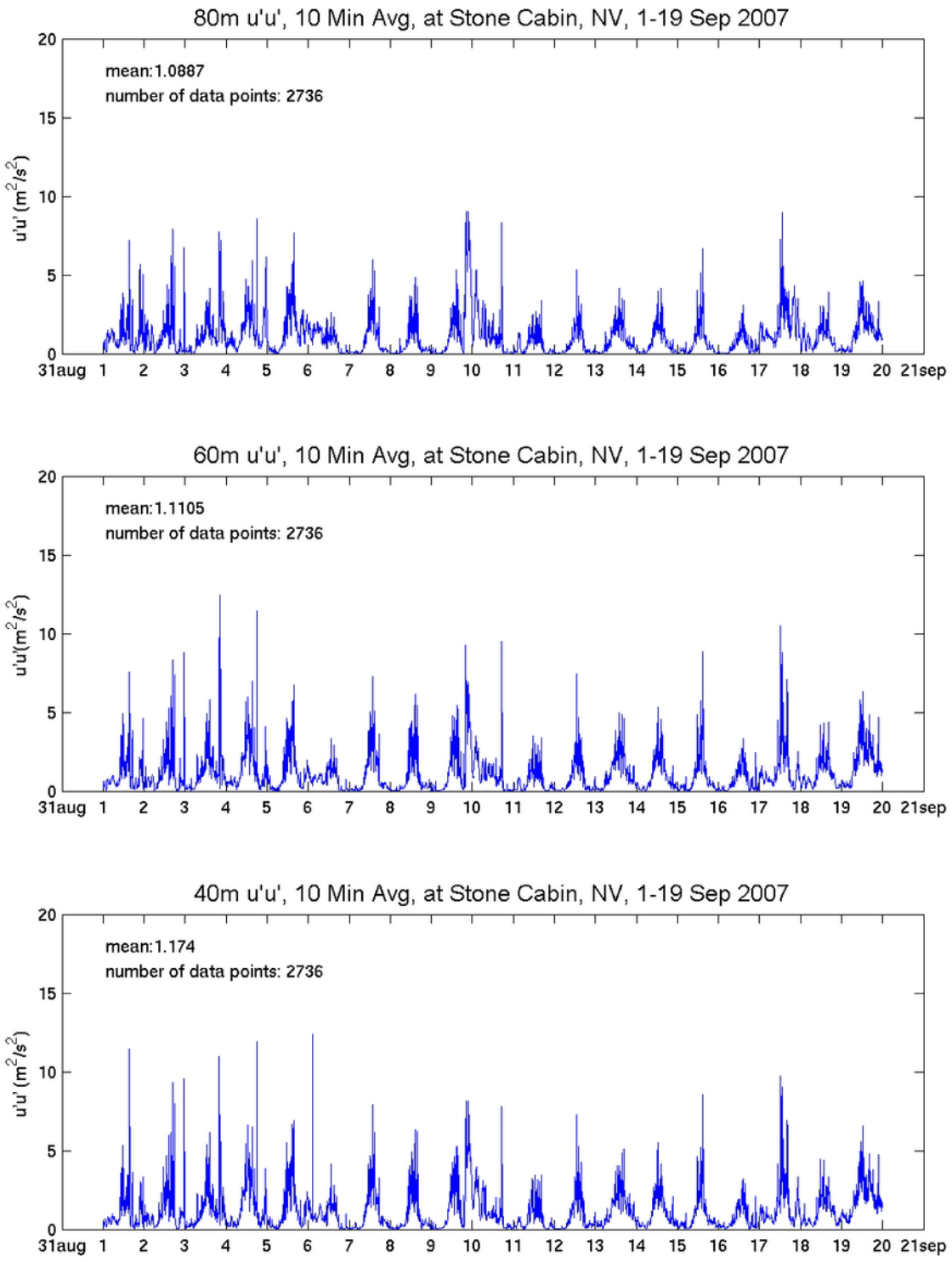

Figure 77. Same as Figure 71, but for a subset period 1-19 September 2007

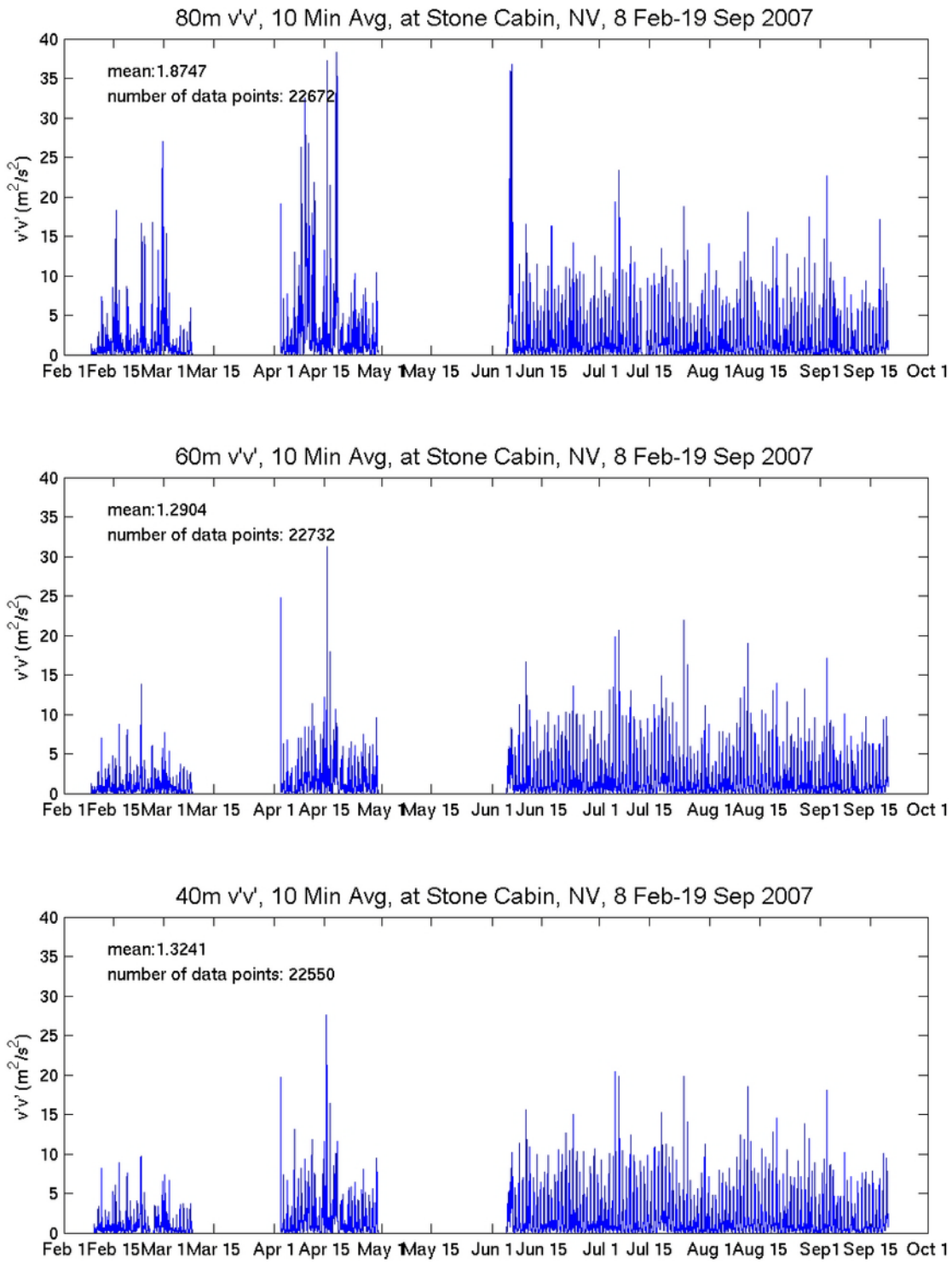

Figure 78. Sonic-measured turbulence momentum flux component v' v´ (units in m^2 s^{-2}) at different height levels (averaged over 10 minute period) at Stone Cabin for the period 8 Feb 2007-19 Sept 2007. The mean and population of the dataset are indicated (top) at 80 m, (center) at 60 m, and (bottom) at 40 m heights.

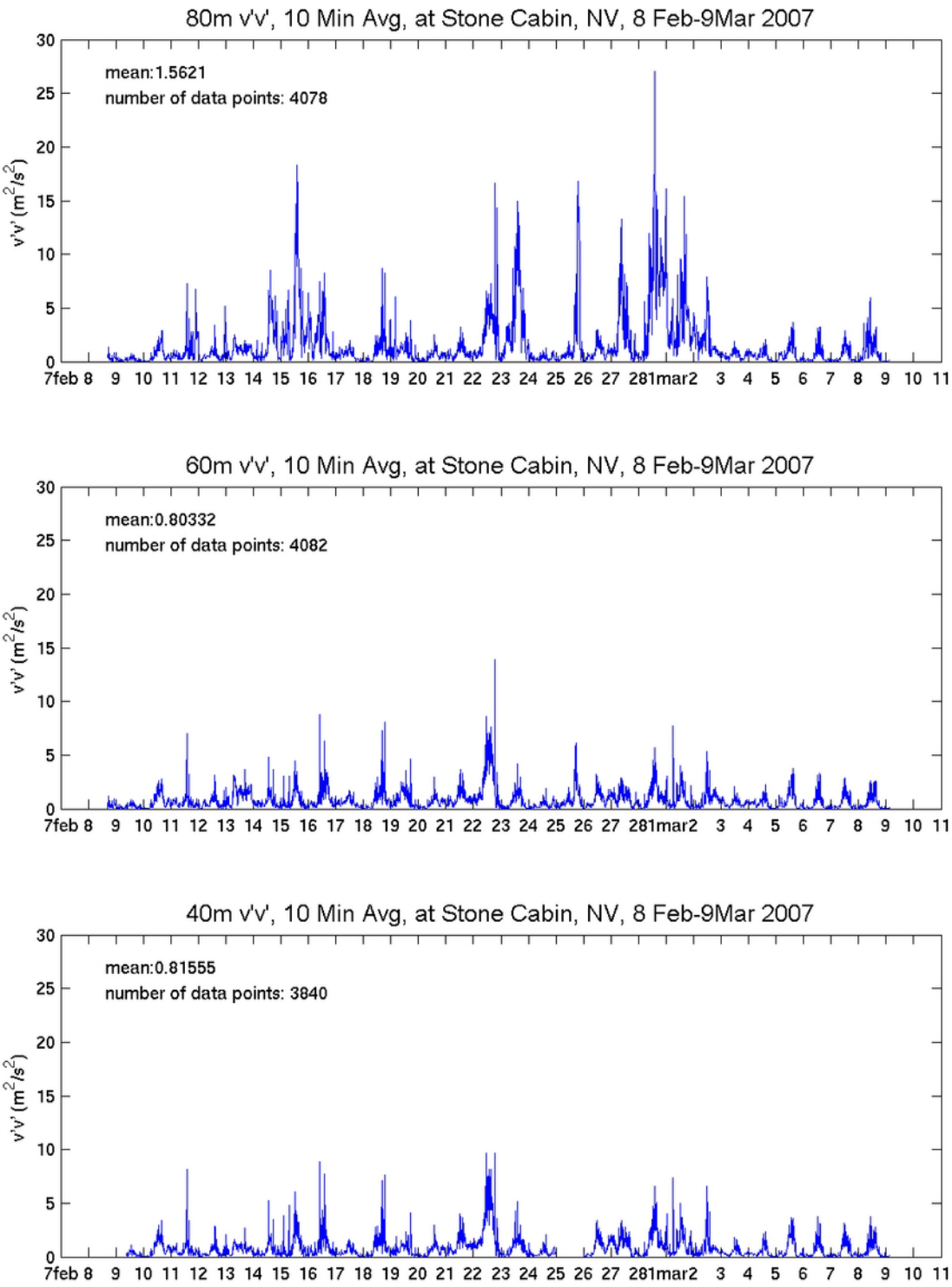

Figure 79. Same as Figure 78, but for a subset period 8 Feb-9 Mar 2007

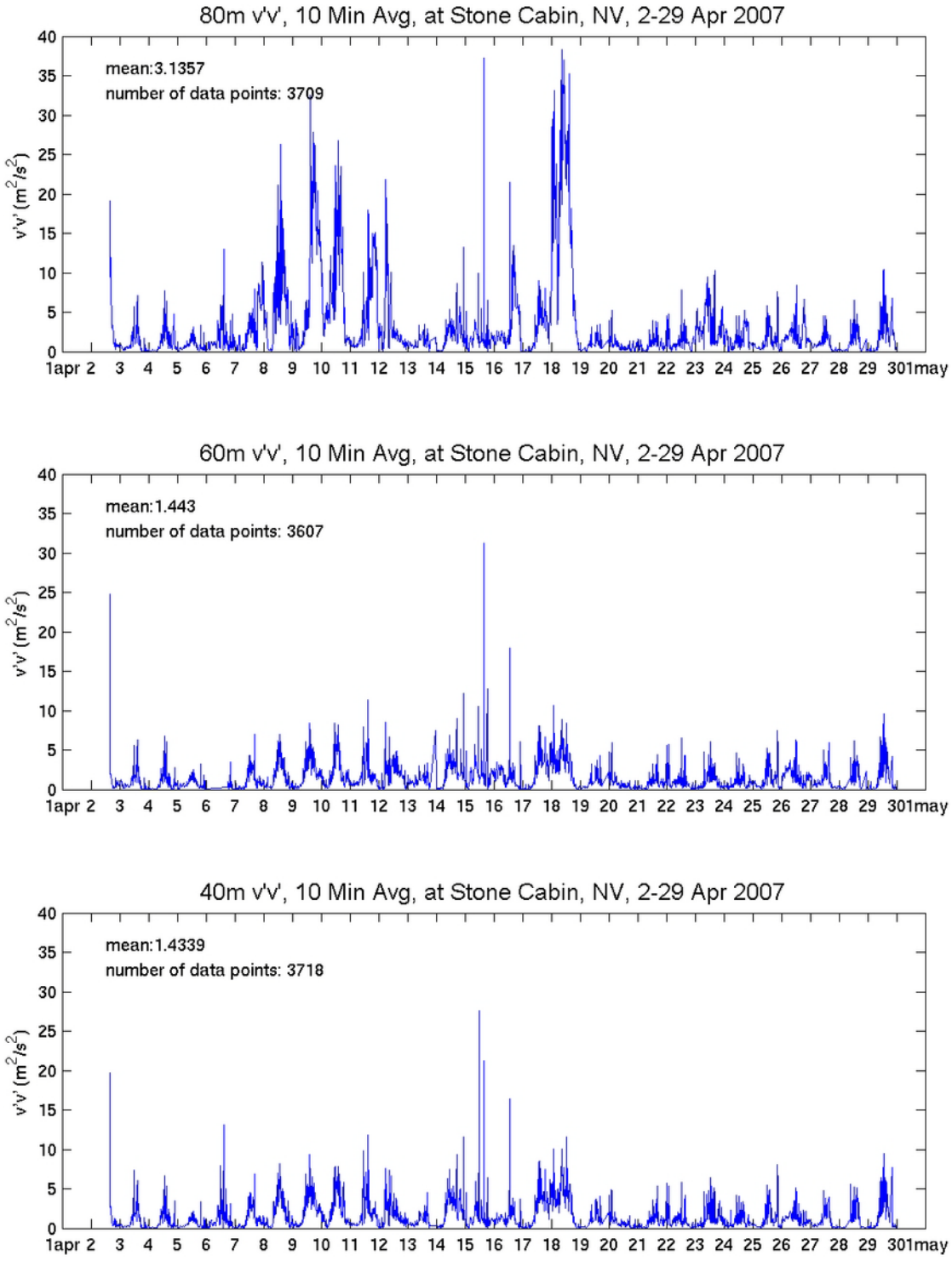

Figure 80. Same as Figure 78, but for a subset period 2-29 April 2007

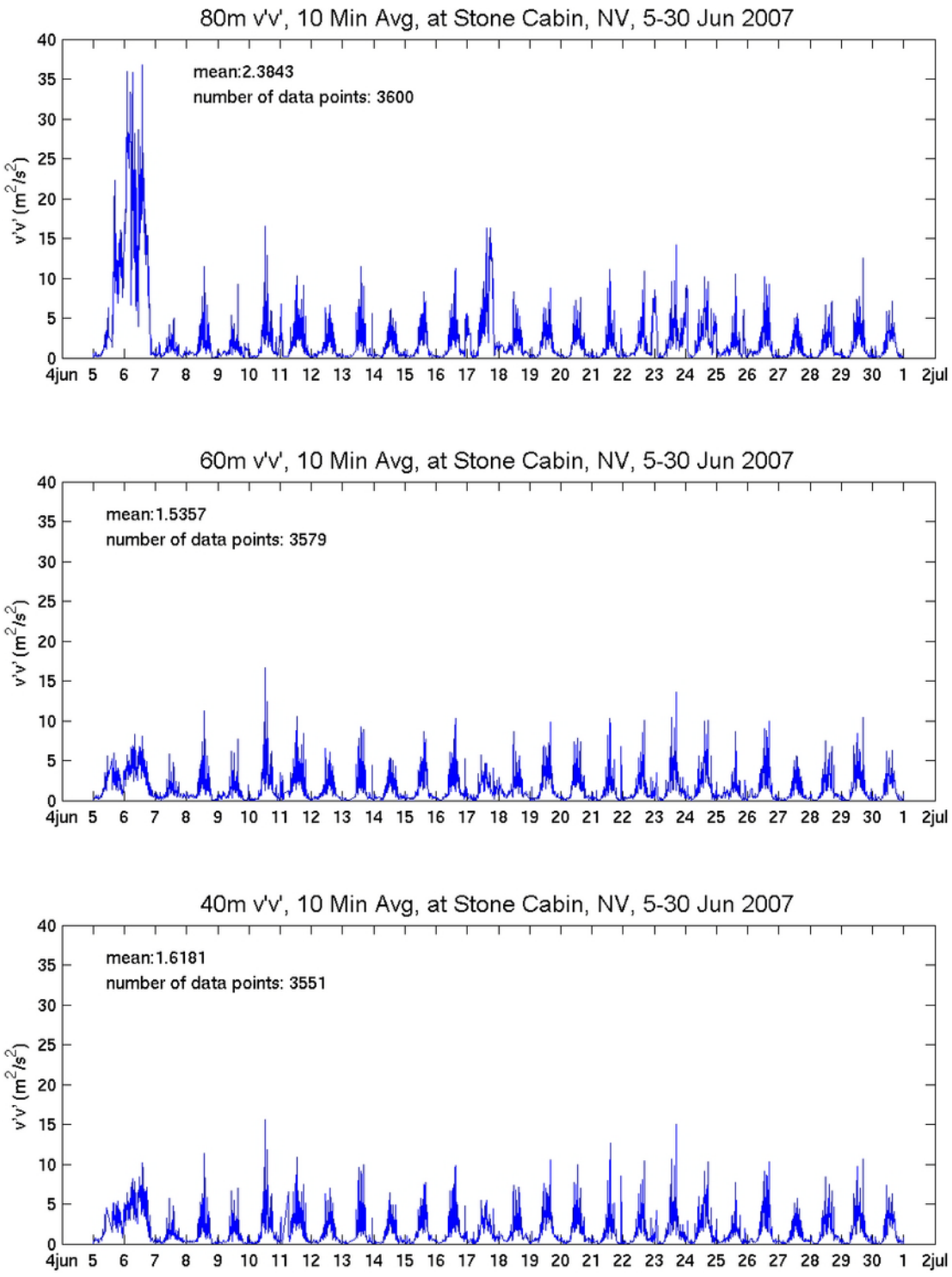

Figure 81. Same as Figure 78, but for a subset period 5-30 June 2007

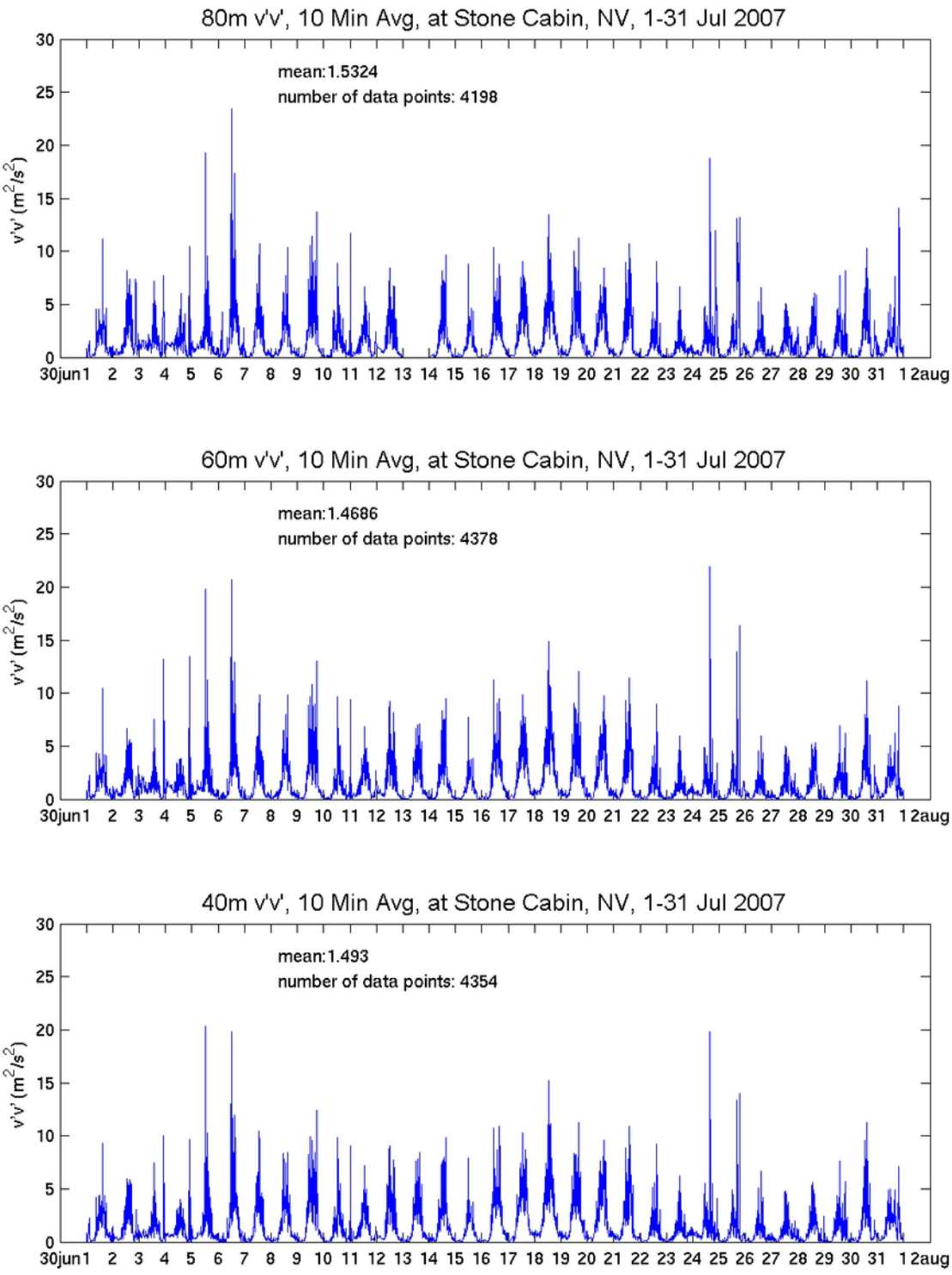

Figure 82. Same as Figure 78, but for a subset period 1-31 July 2007

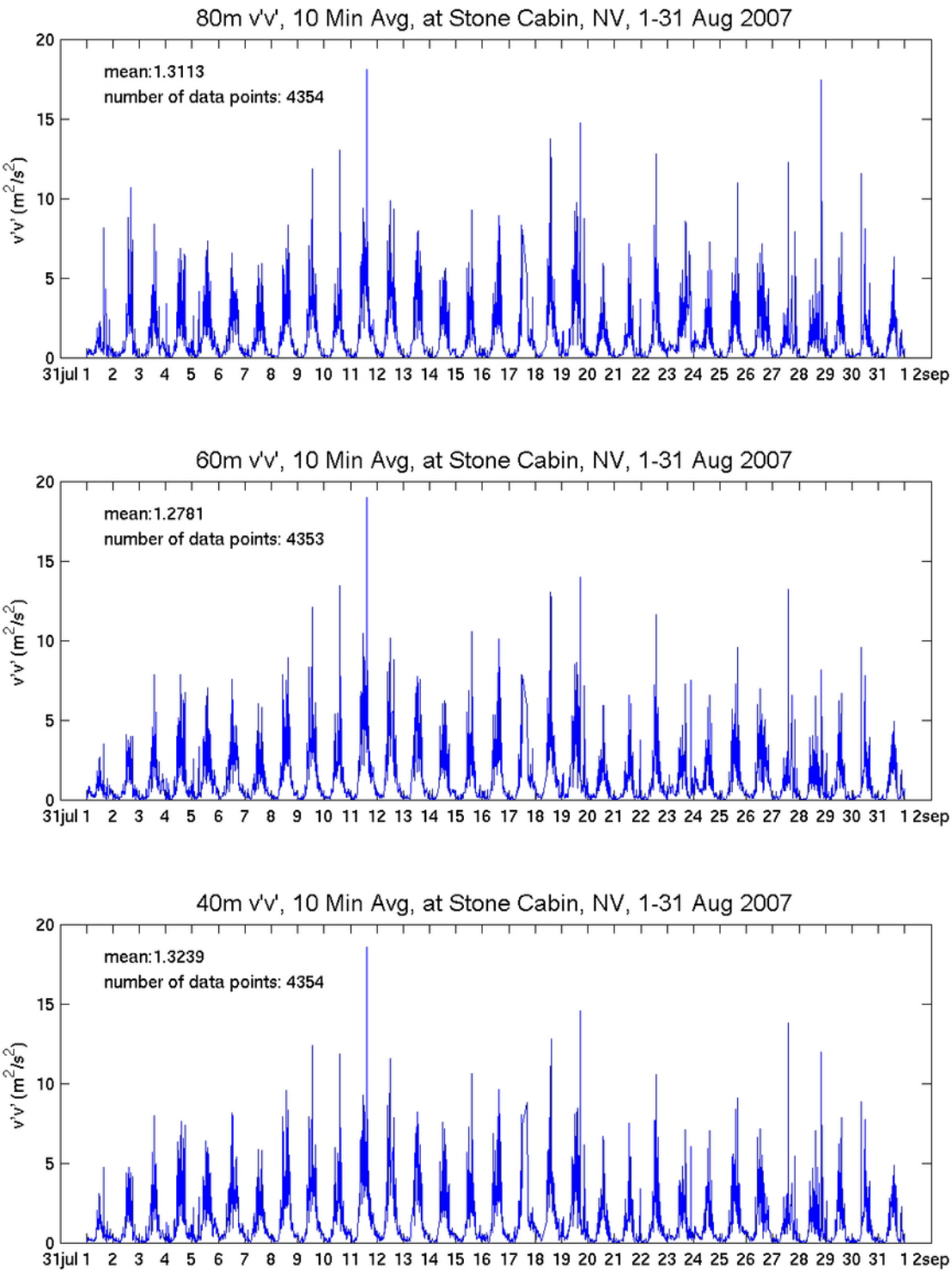

Figure 83. Same as Figure 78, but for a subset period 1-31 August 2007

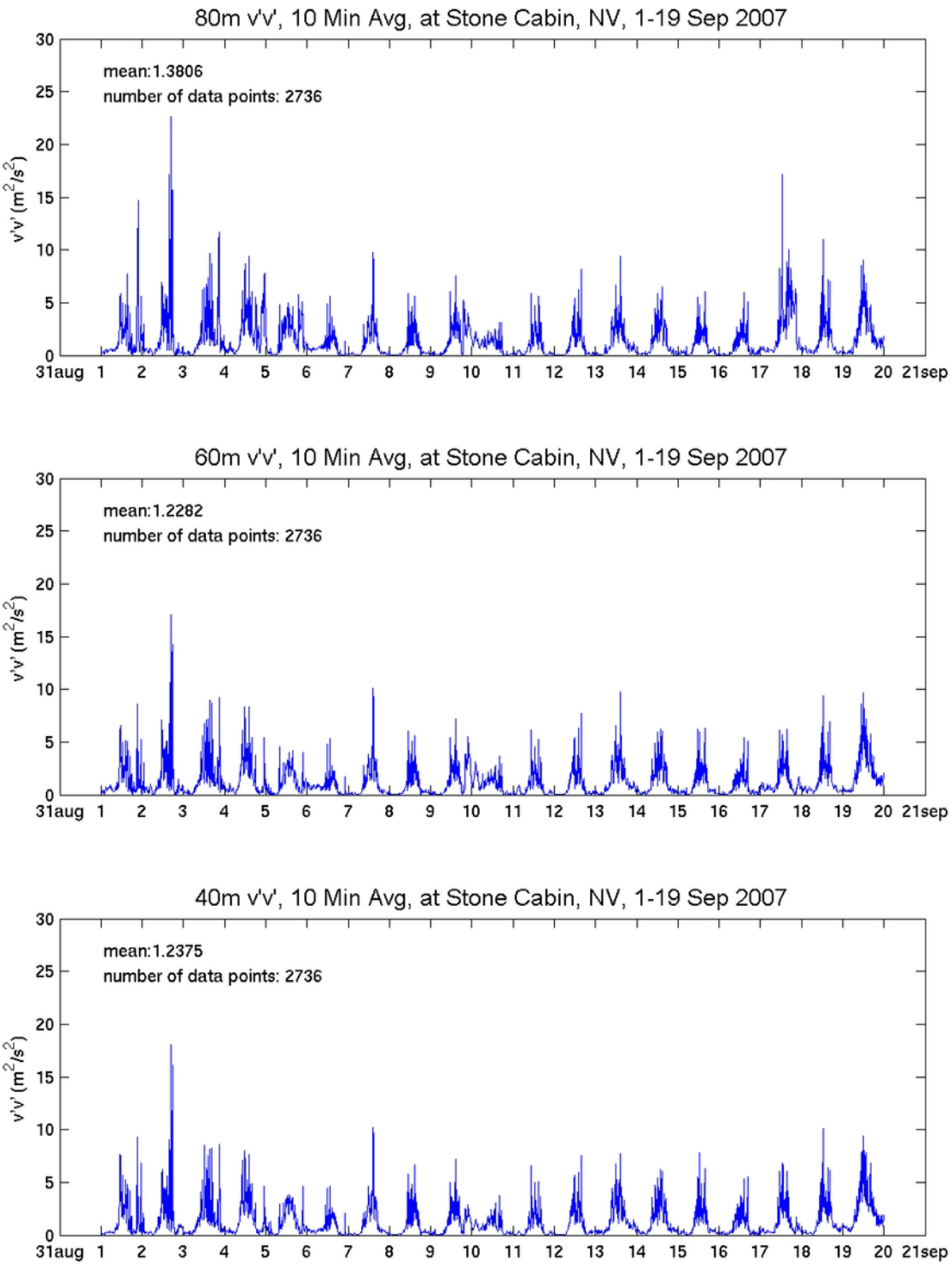

Figure 84. Same as Figure 78, but for a subset period 1-19 September 2007

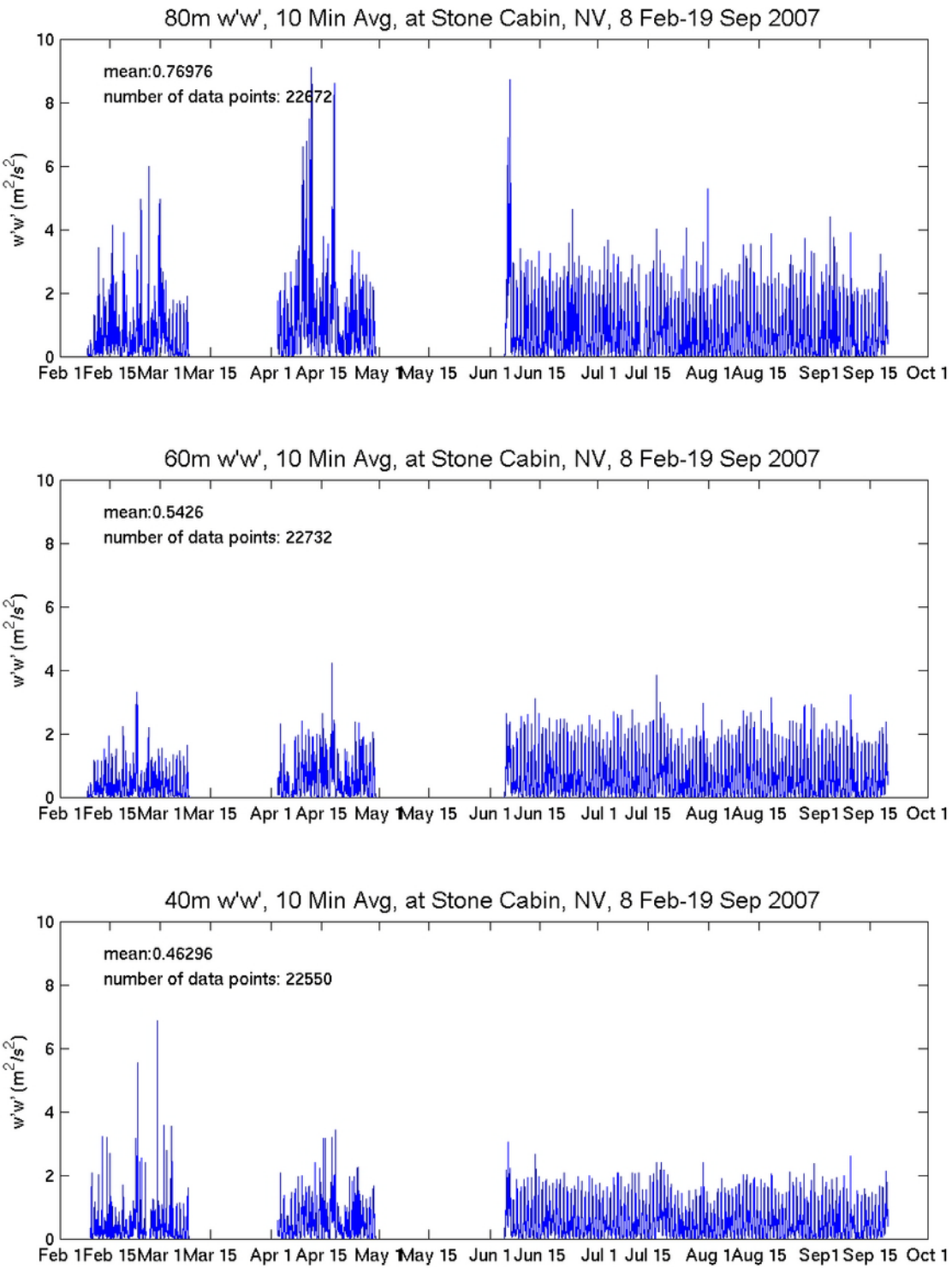

Figure 85. Sonic-measured turbulence momentum flux component w´ w´ (units in $m^2 s^{-2}$) at different height levels (averaged over 10 minute period) at Stone Cabin for the period 8 Feb 2007-19 Sept 2007. The mean and population of the dataset are indicated (top) at 80 m, (center) at 60 m, and (bottom) at 40 m heights.

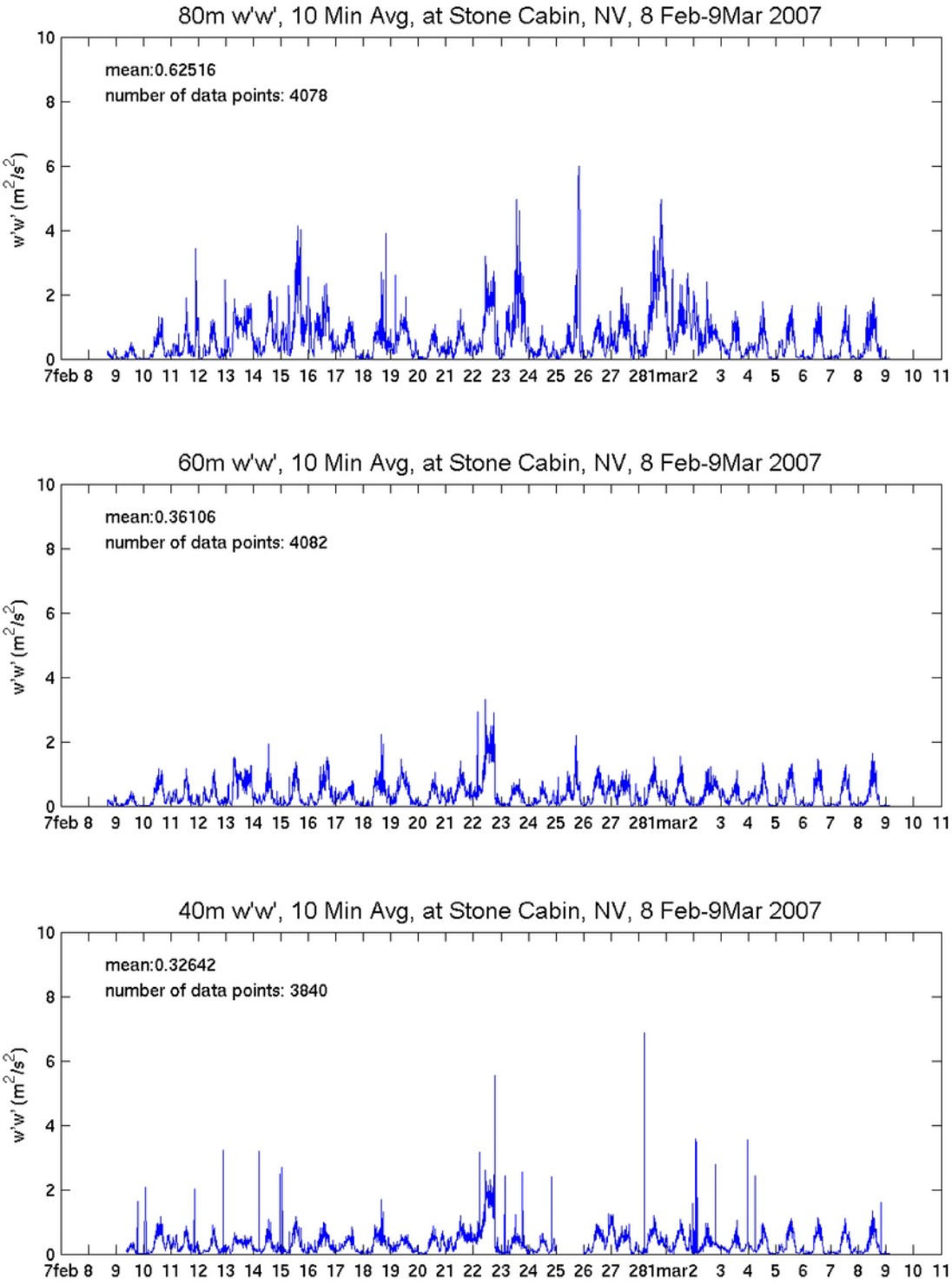

Figure 86. Same as Figure 85, but for a subset period 8 Feb-9 Mar 2007

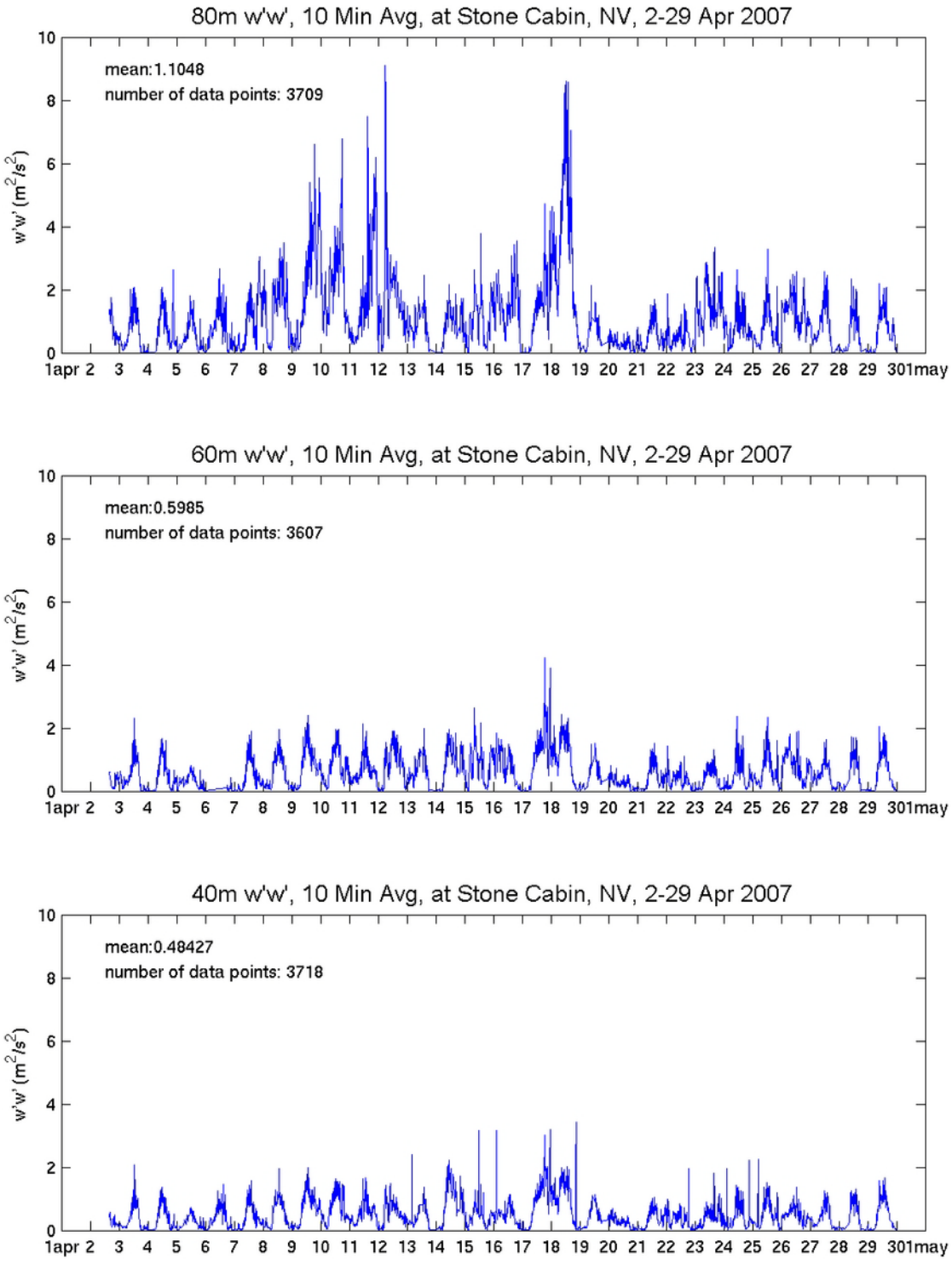

Figure 87. Same as Figure 85, but for a subset period 2-29 April 2007

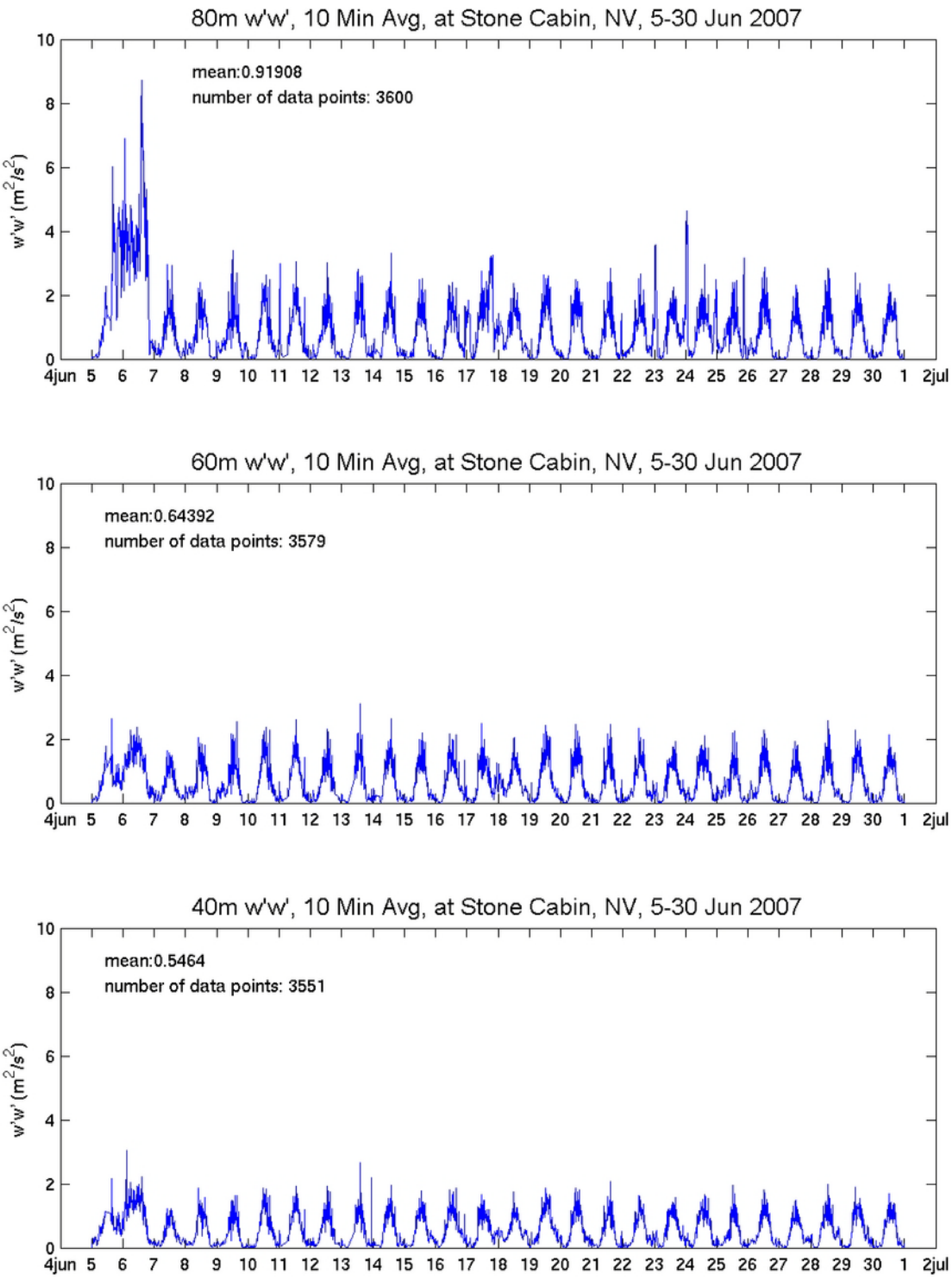

Figure 88. Same as Figure 85, but for a subset period 5-30 June 2007

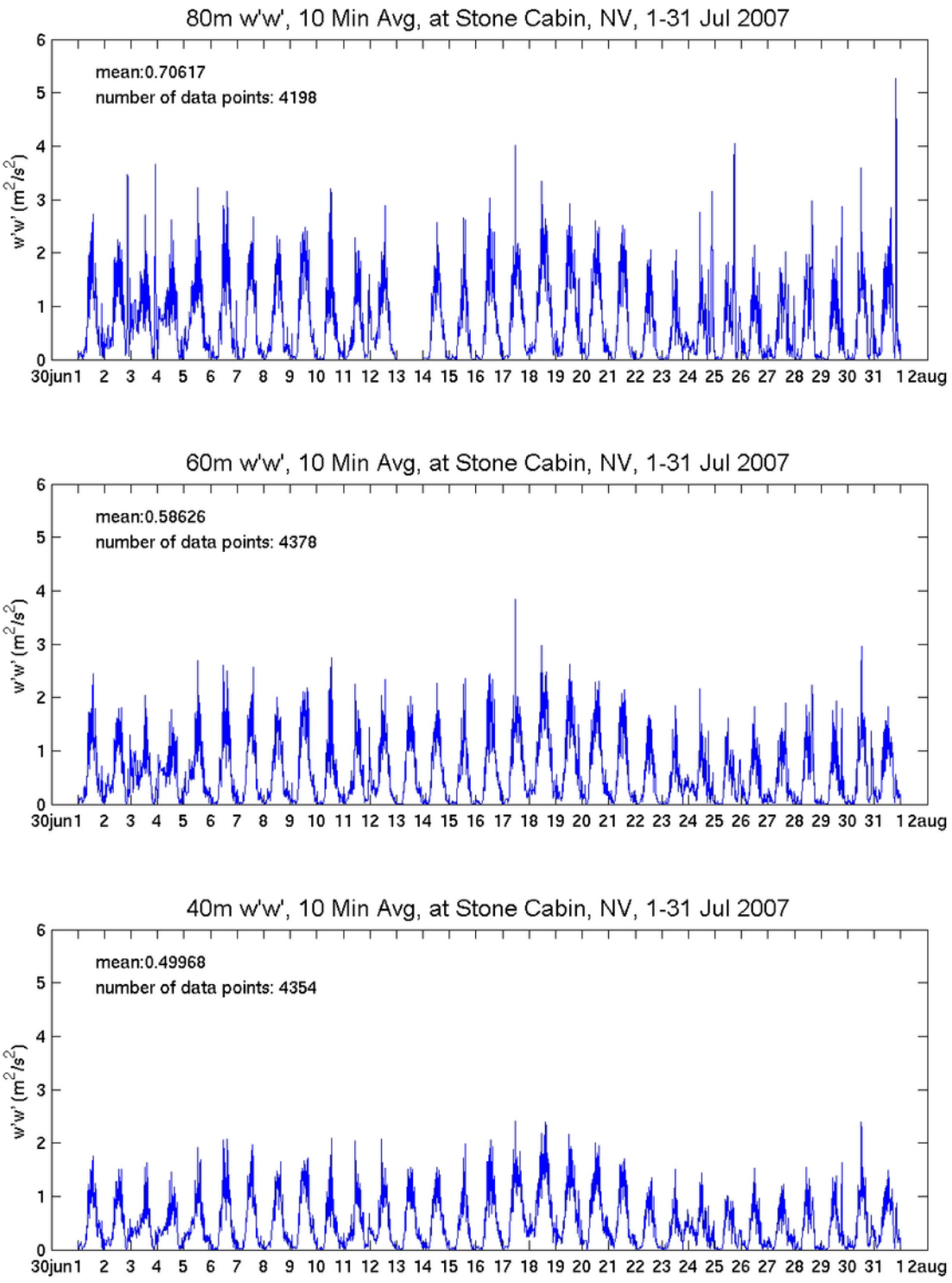

Figure 89. Same as Figure 85, but for a subset period 1-31 July 2007

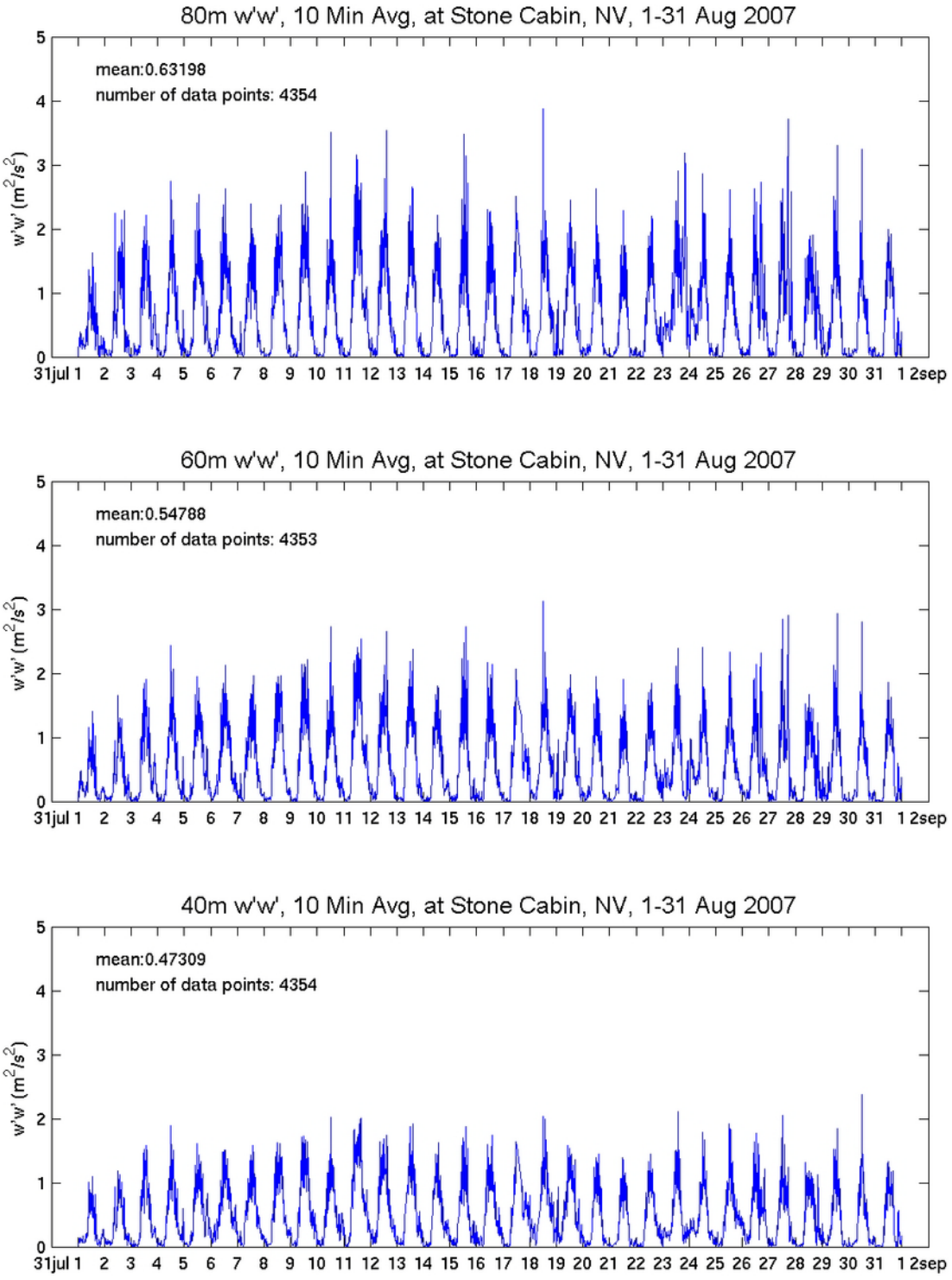

Figure 90. Same as Figure 85, but for a subset period 1-31 August 2007

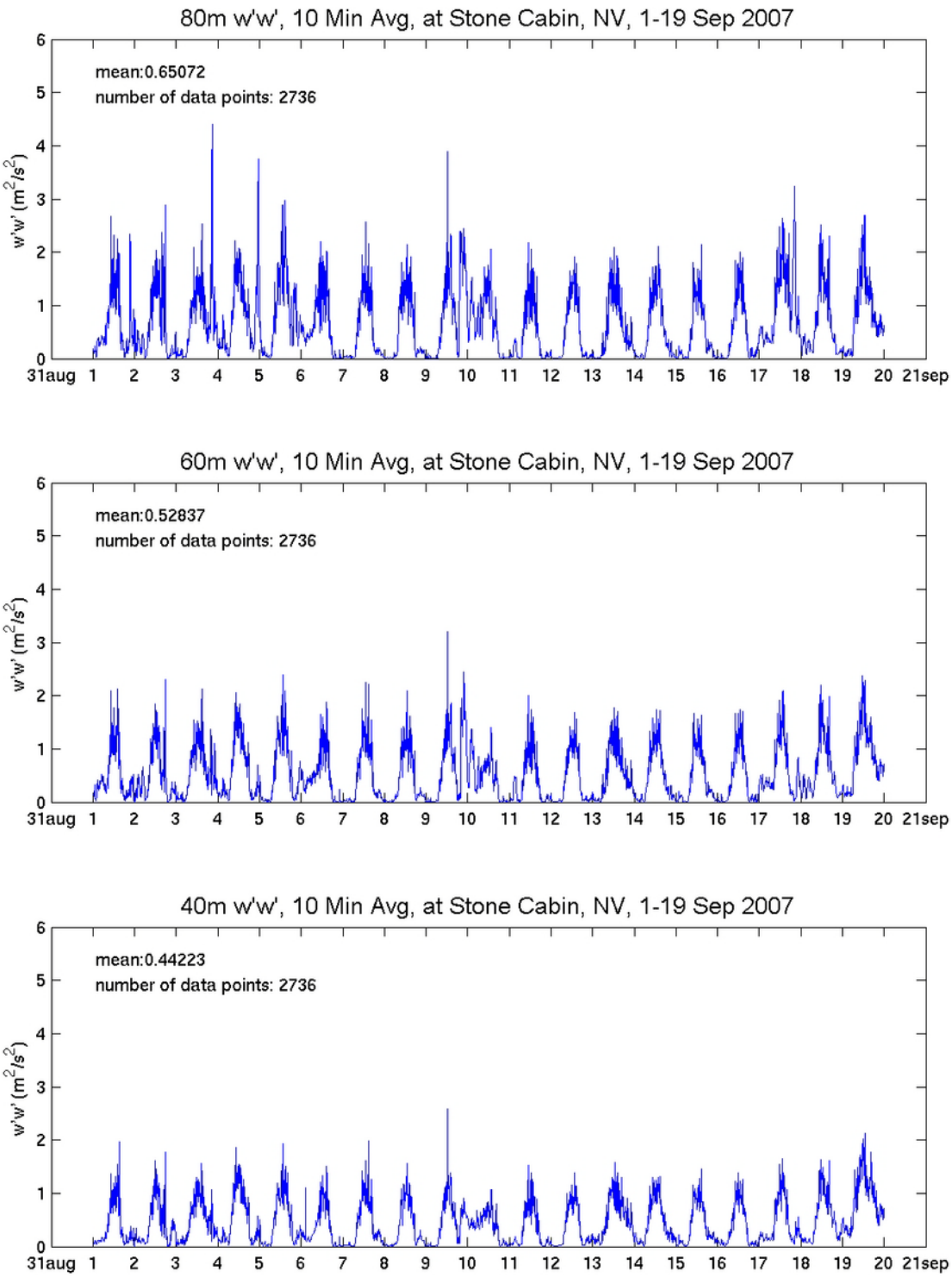

Figure 91. Same as Figure 85, but for a subset period 1-19 September 2007

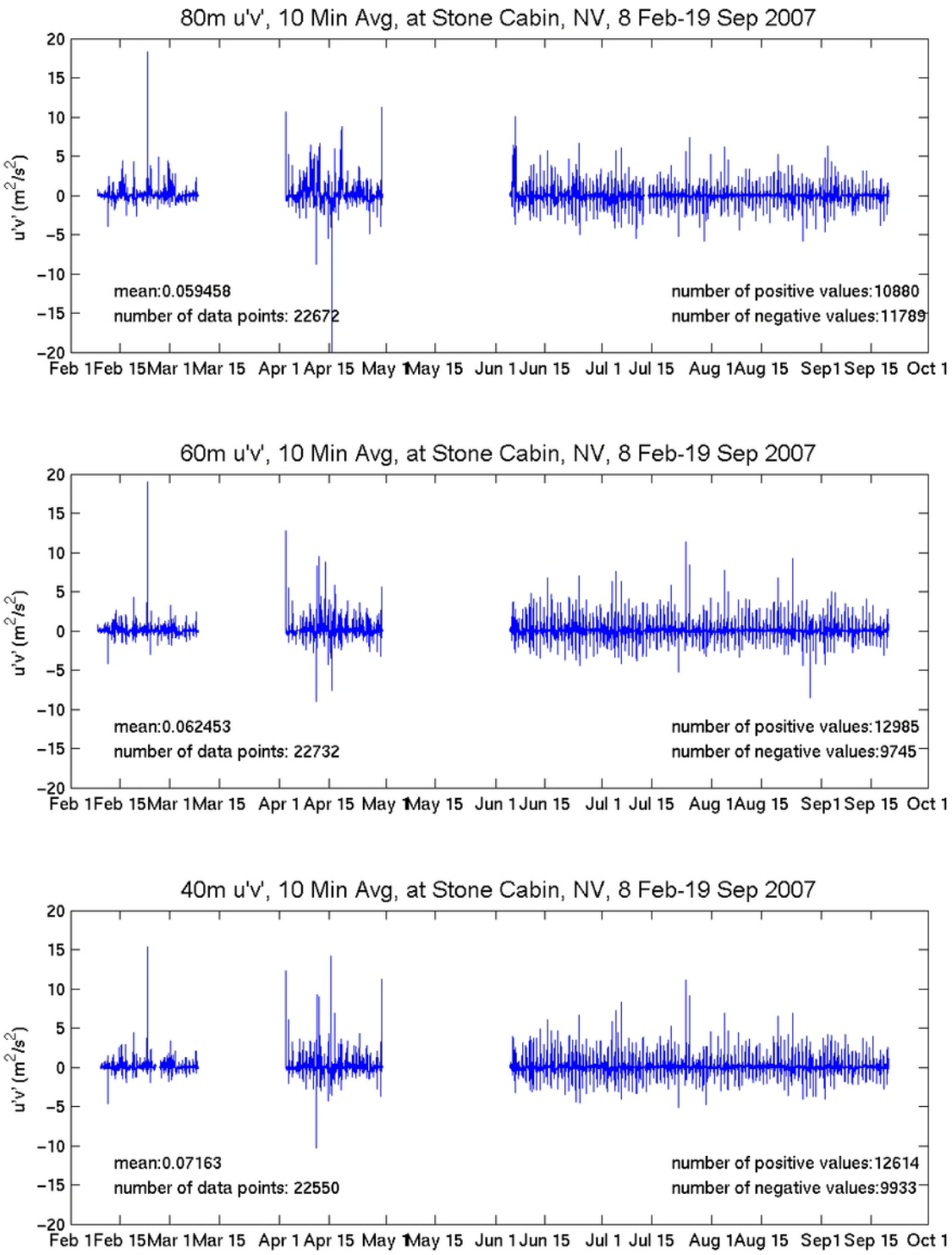

Figure 92. Sonic-measured turbulence momentum flux component u´ v´ (units in $m^2 s^{-2}$) at different height levels (averaged over 10-minute period) at Stone Cabin for the period 8 Feb 2007-19 Sept 2007. The mean and population of the dataset are indicated (top) at 80 m, (center) at 60 m, and (bottom) at 40 m heights.

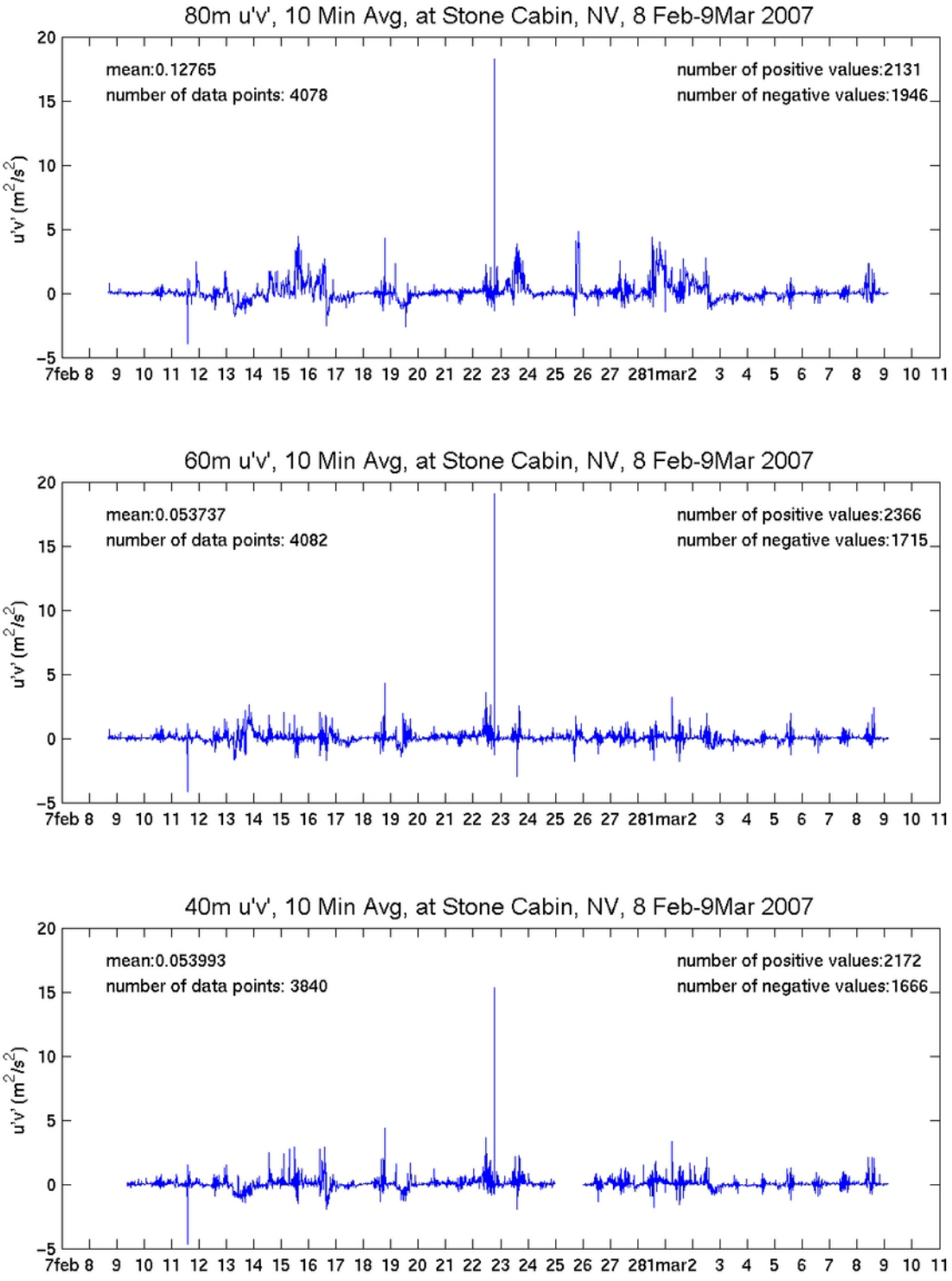

Figure 93. Same as Figure 92, but for a subset period 8 Feb-9 Mar 2007

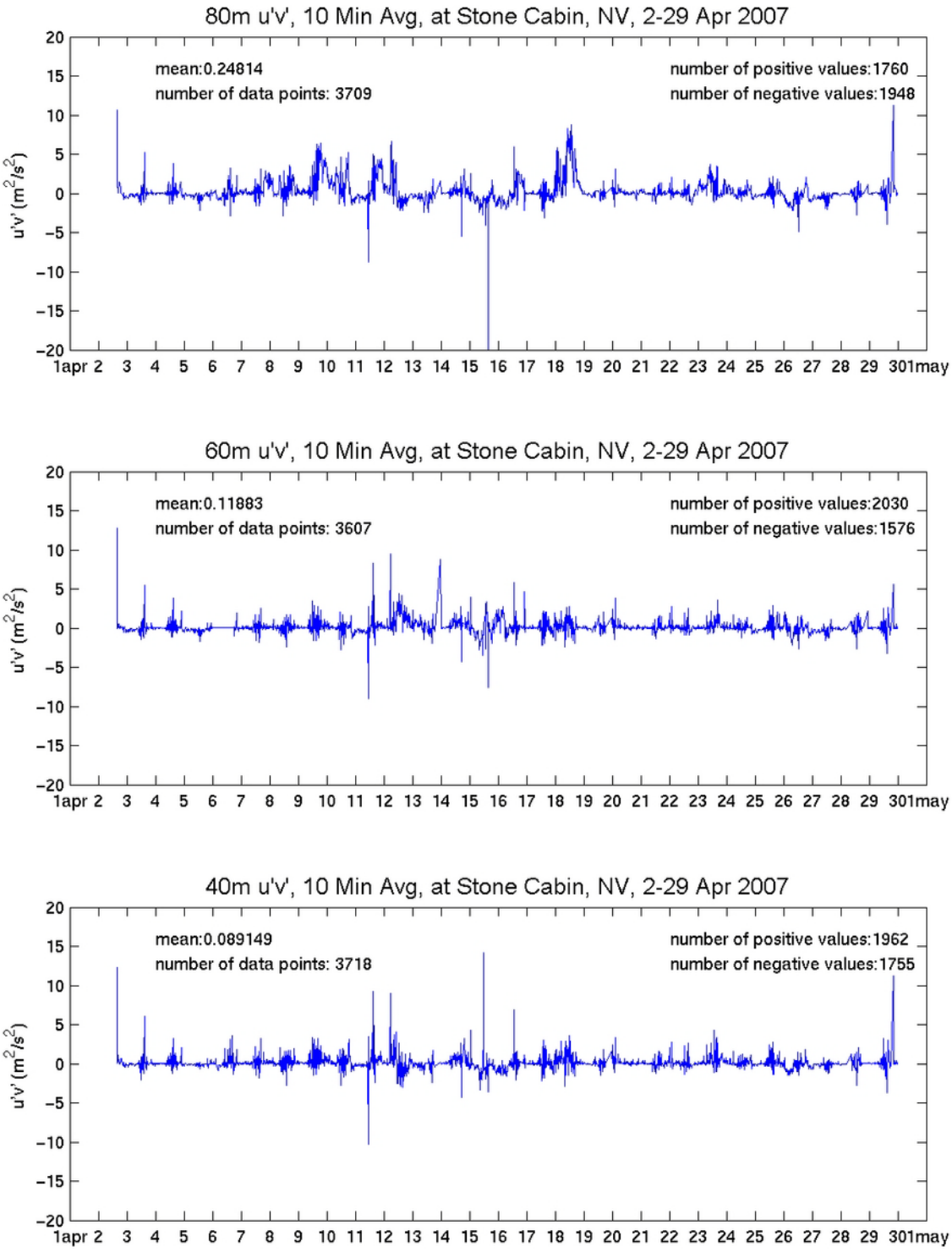

Figure 94. Same as Figure 92, but for a subset period 2-29 April 2007

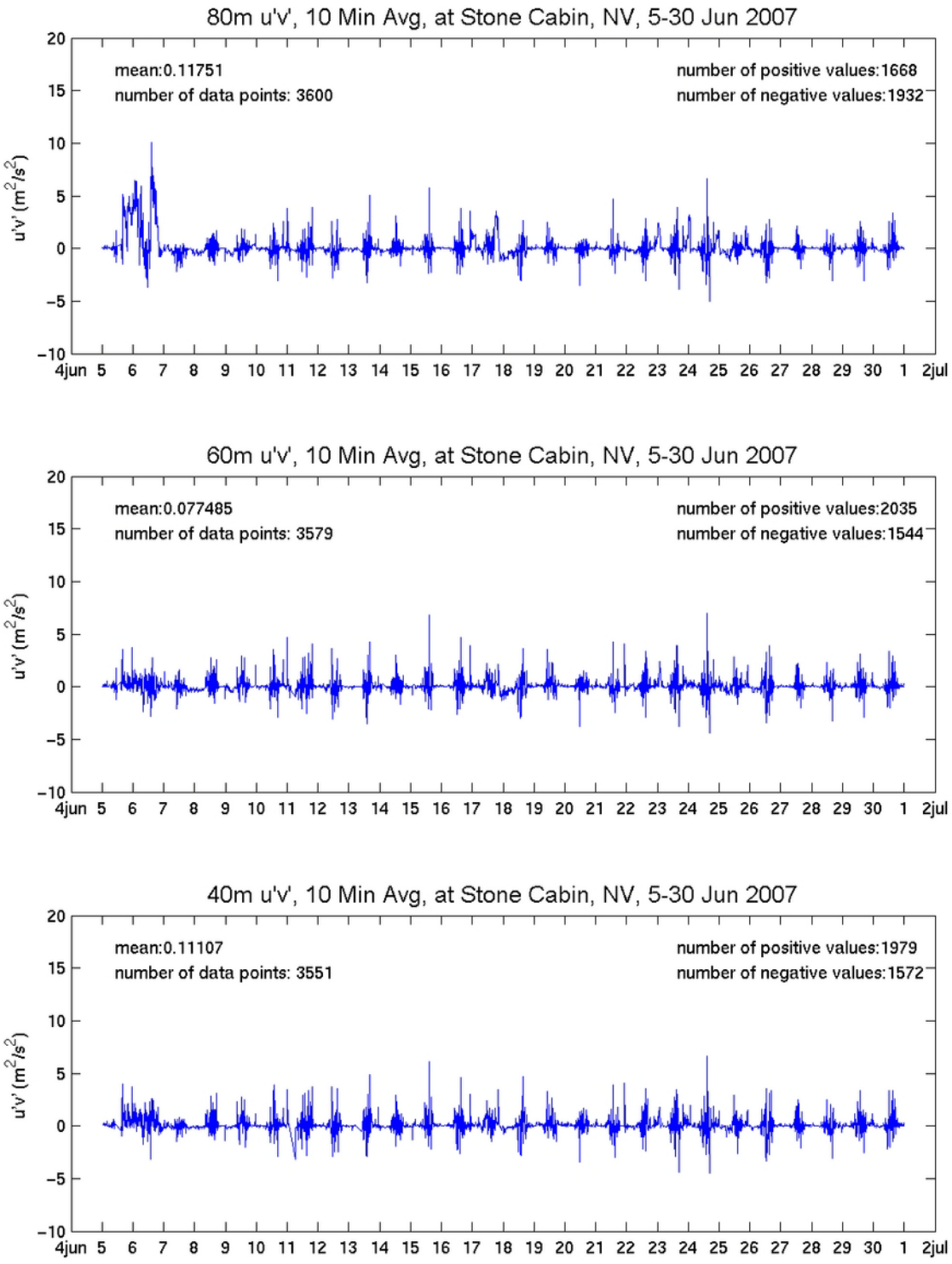

Figure 95. Same as Figure 92, but for a subset period 5-30 June 2007

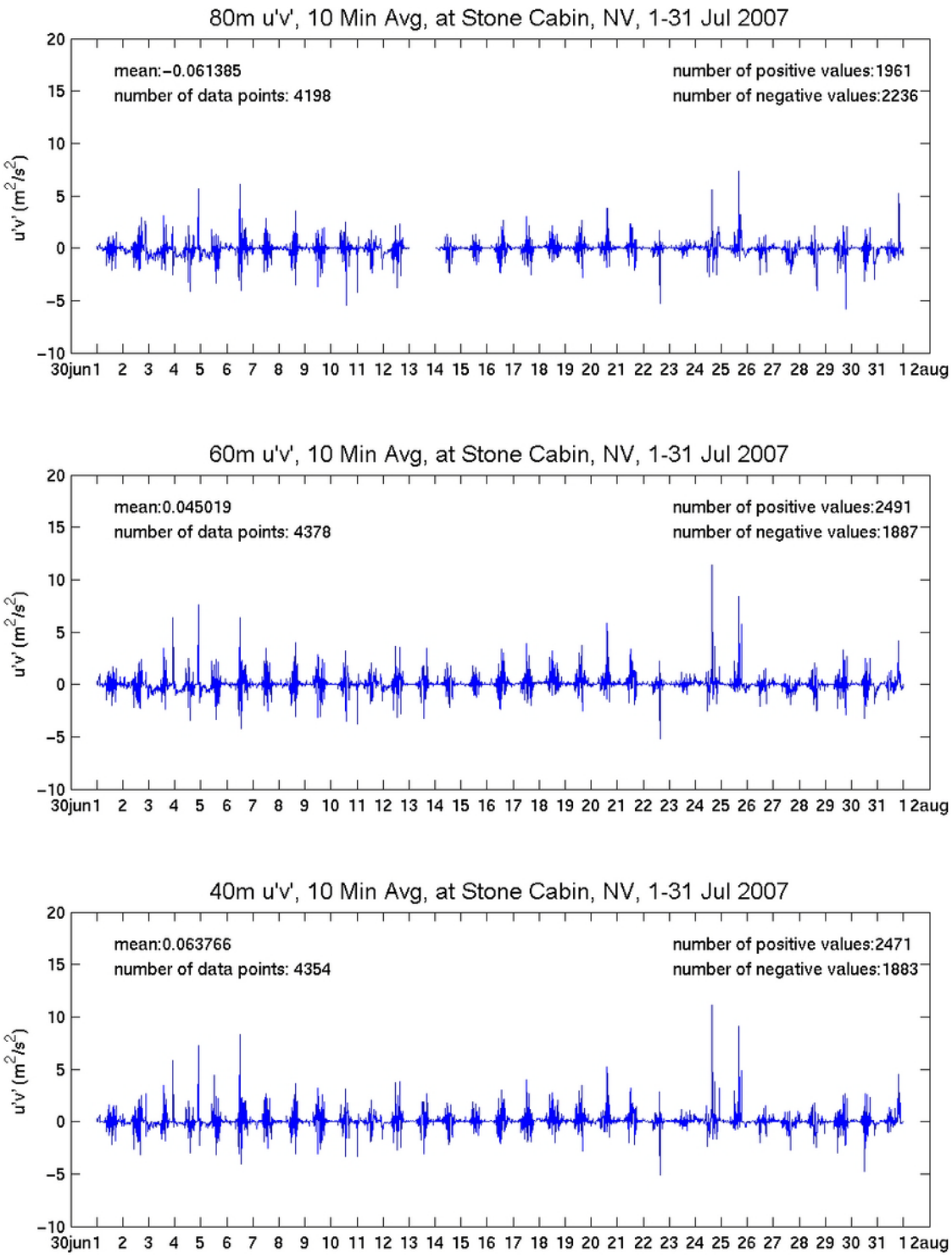

Figure 96. Same as Figure 92, but for a subset period 1-31 July 2007

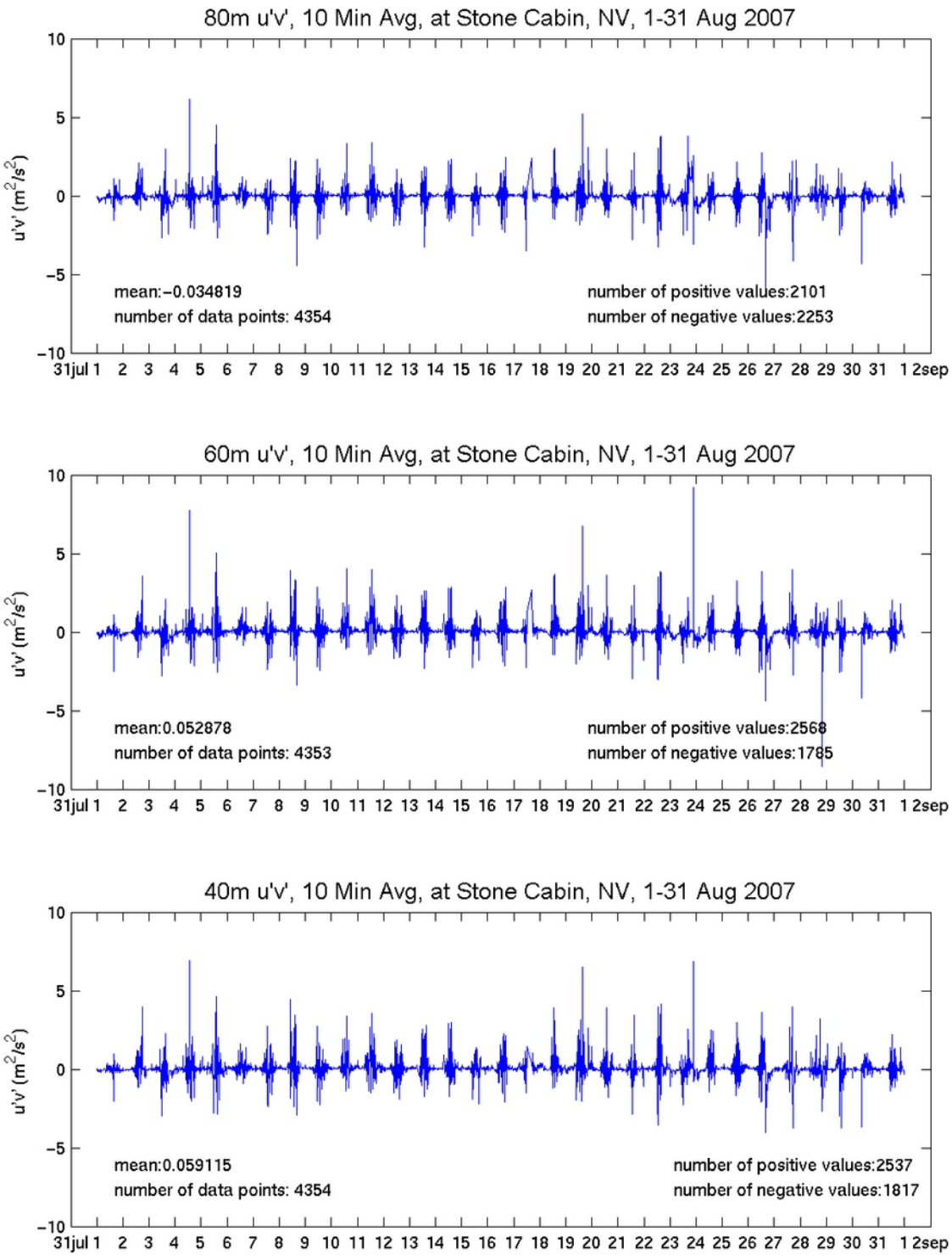

Figure 97. Same as Figure 92, but for a subset period 1-31 August 2007

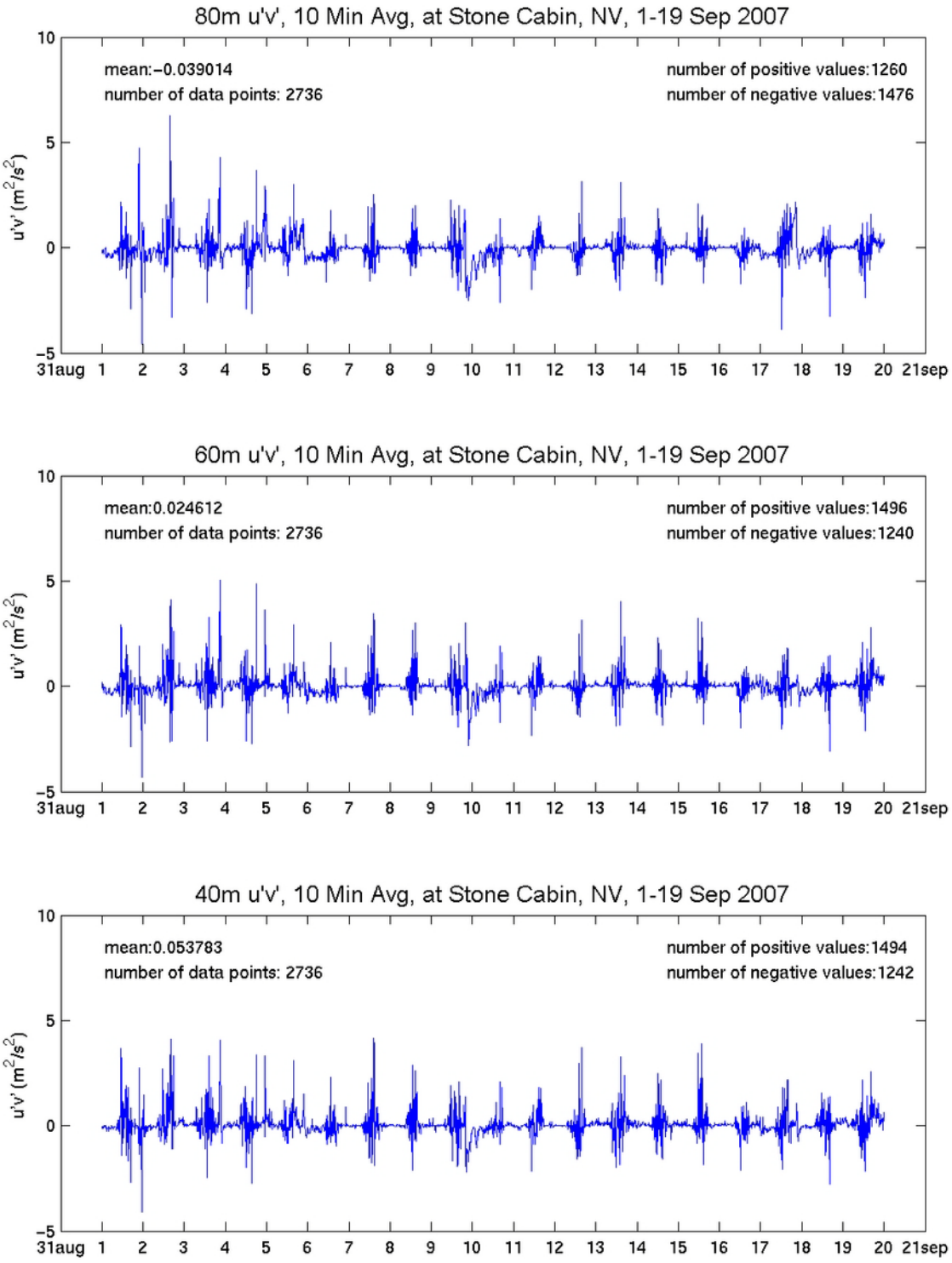

Figure 98. Same as Figure 92, but for a subset period 1-19 September 2007

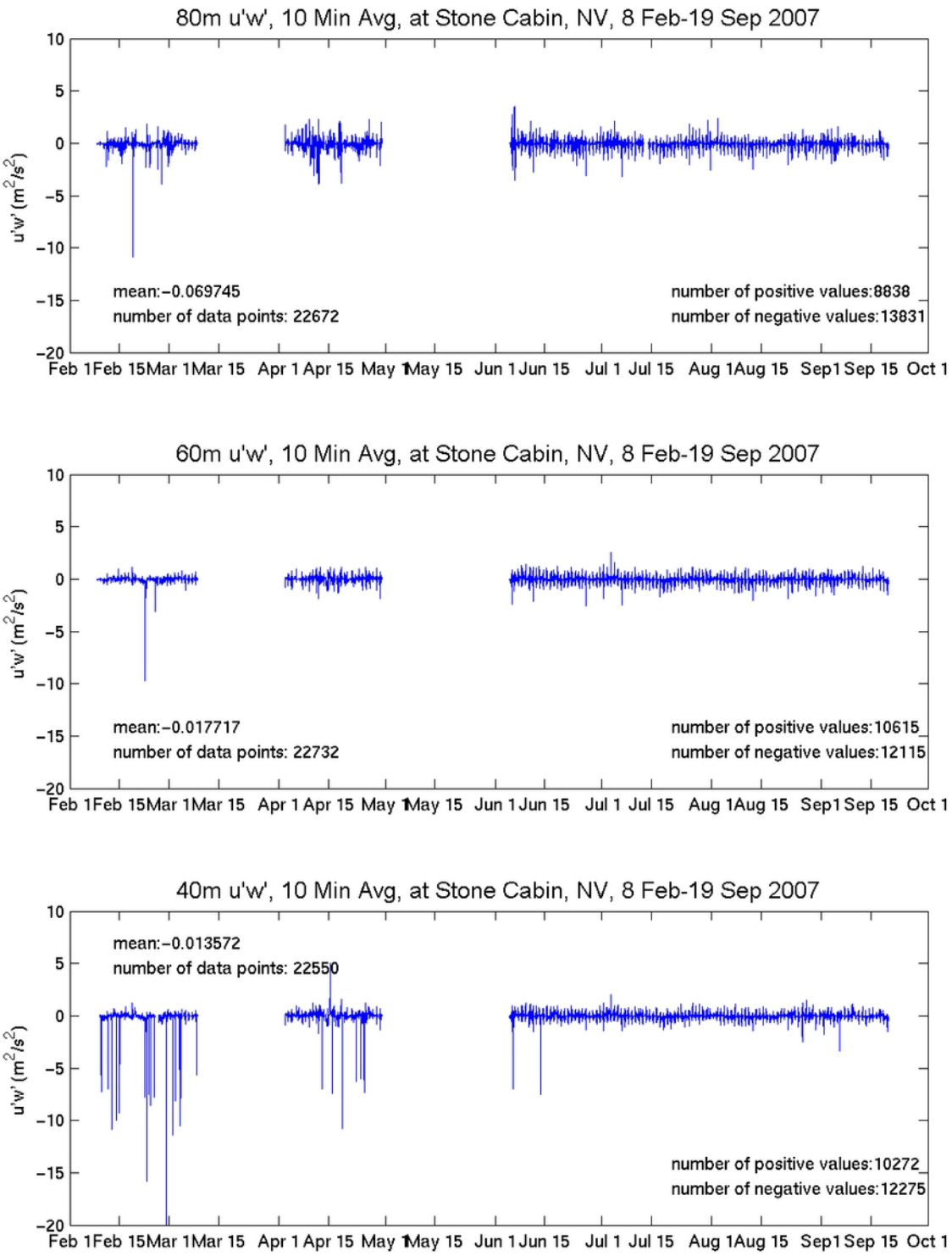

Figure 99. Sonic-measured turbulence momentum flux component u' w' (units in m^2 s^{-2}) at different height levels (averaged over 10-minute period) at Stone Cabin for the period 8 Feb 2007-19 Sept 2007. The mean and population of the dataset are indicated (top) at 80 m, (center) at 60 m, and (bottom) at 40 m heights.

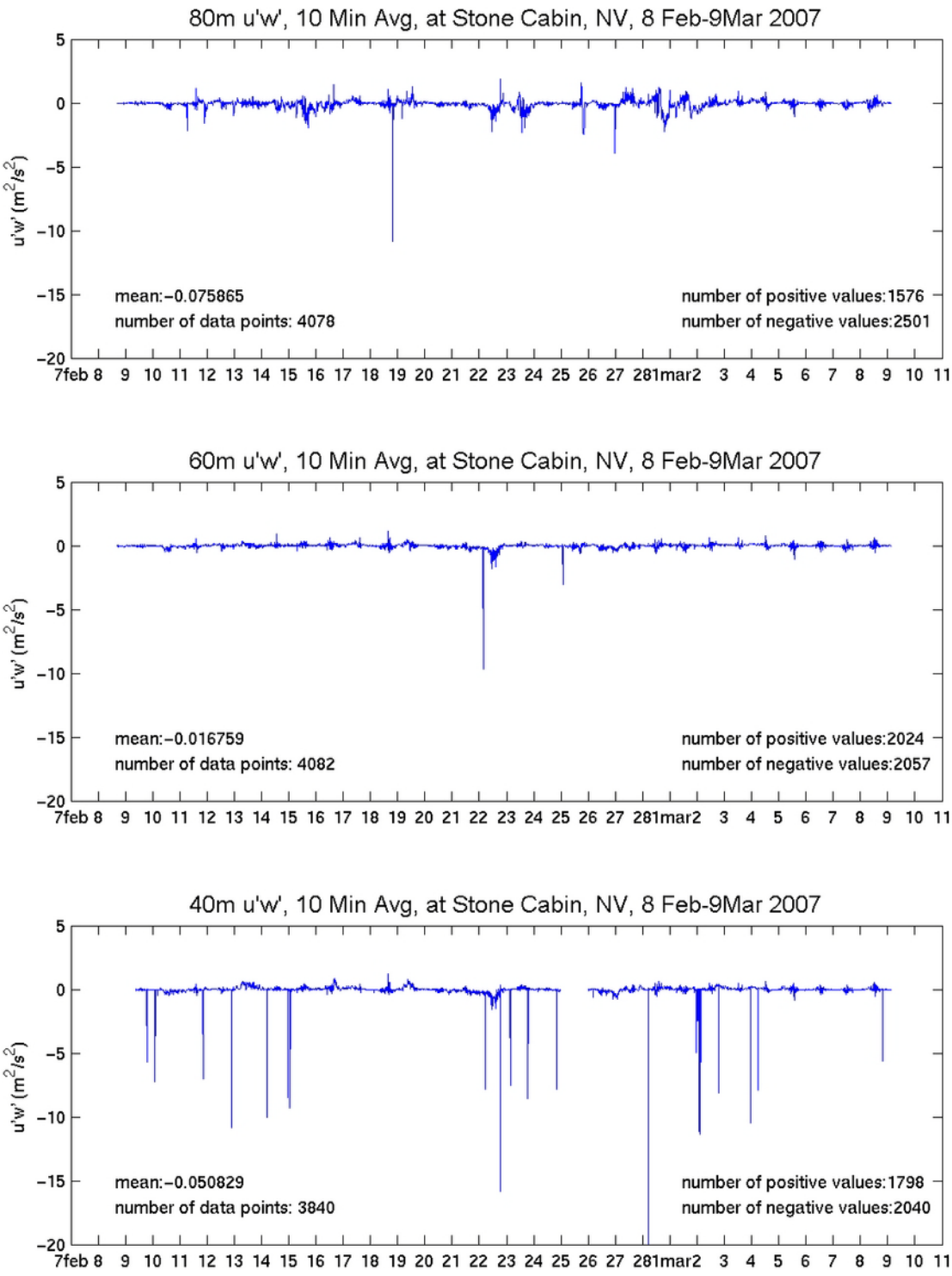

Figure 100. Same as Figure 9989, but for a subset period 8 Feb-9 Mar 2007

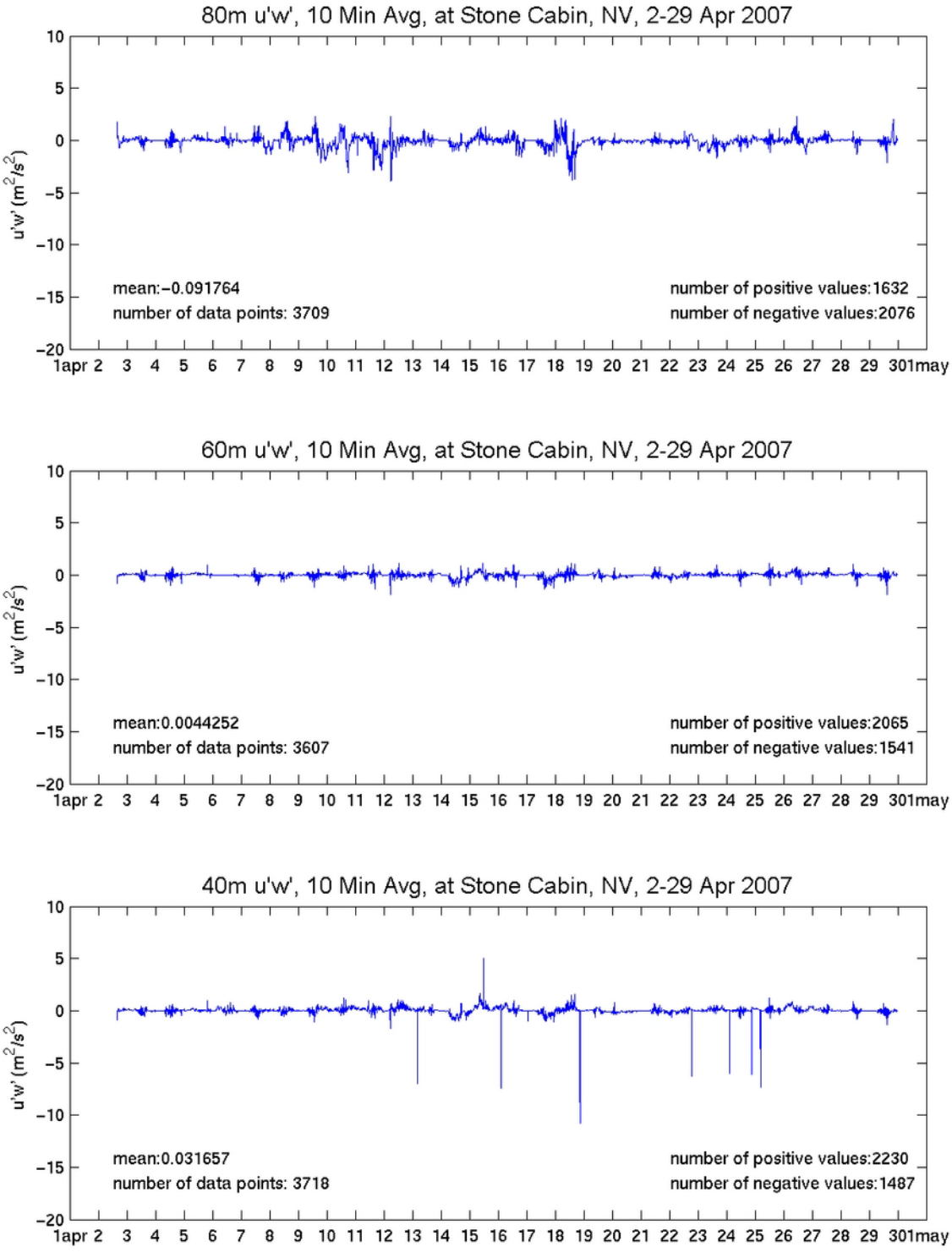

Figure 101. Same as Figure 99, but for a subset period 2-29 April 2007

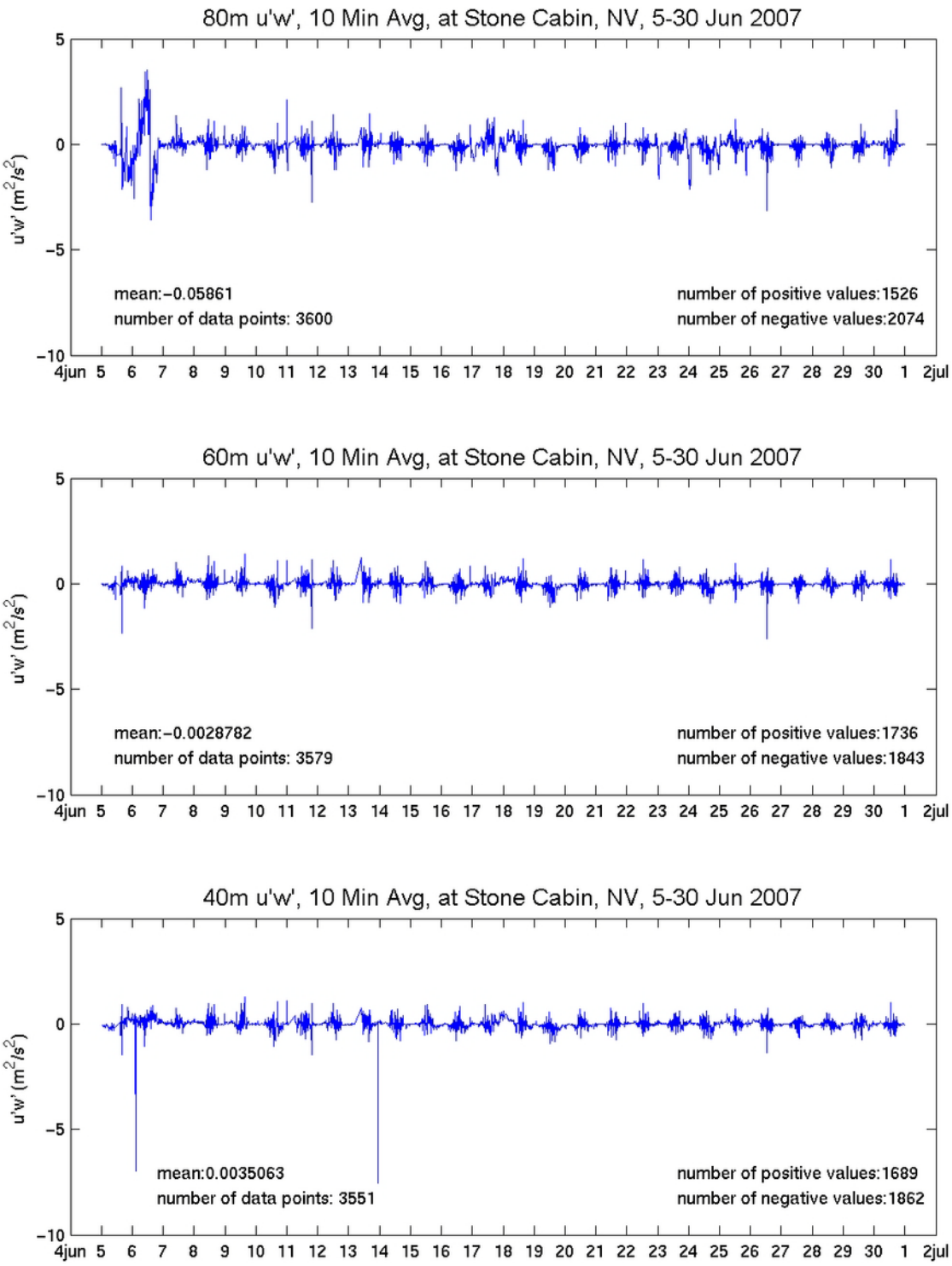

Figure 102. Same as Figure 99, but for a subset period 5-30 June 2007

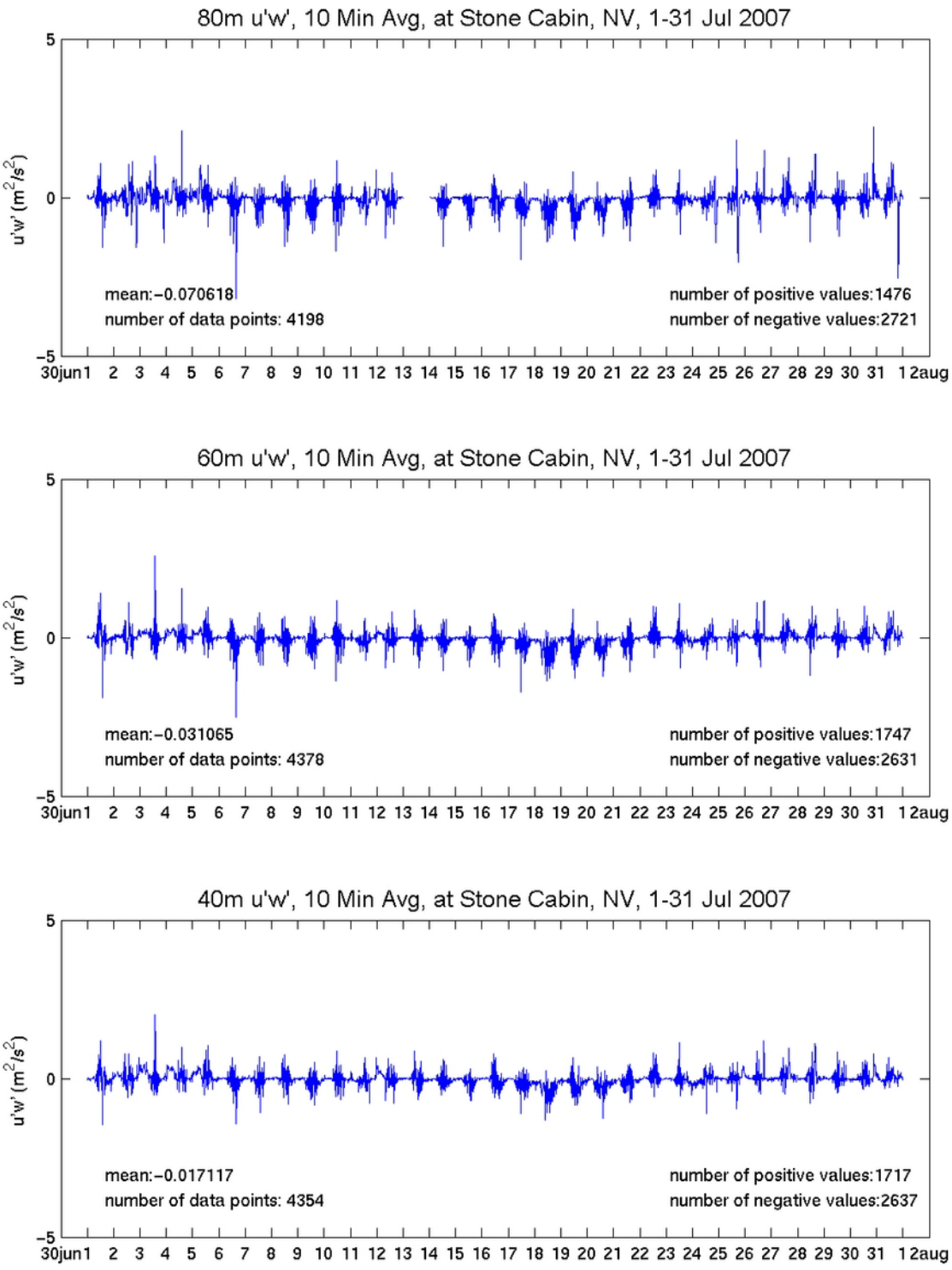

Figure 103. Same as Figure 99, but for a subset period 1-31 July 2007

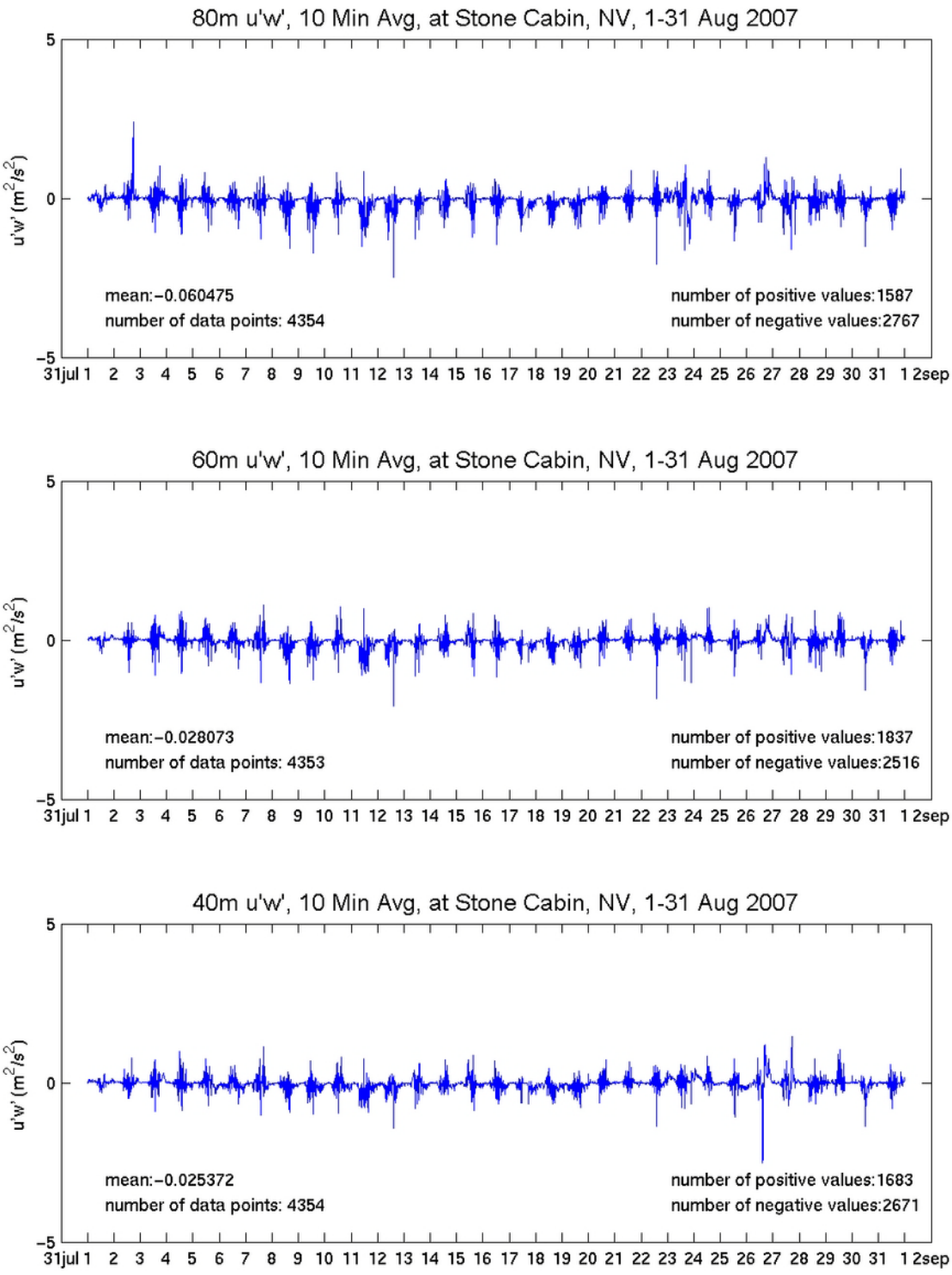

Figure 104. Same as Figure 99, but for a subset period 1-31 August 2007

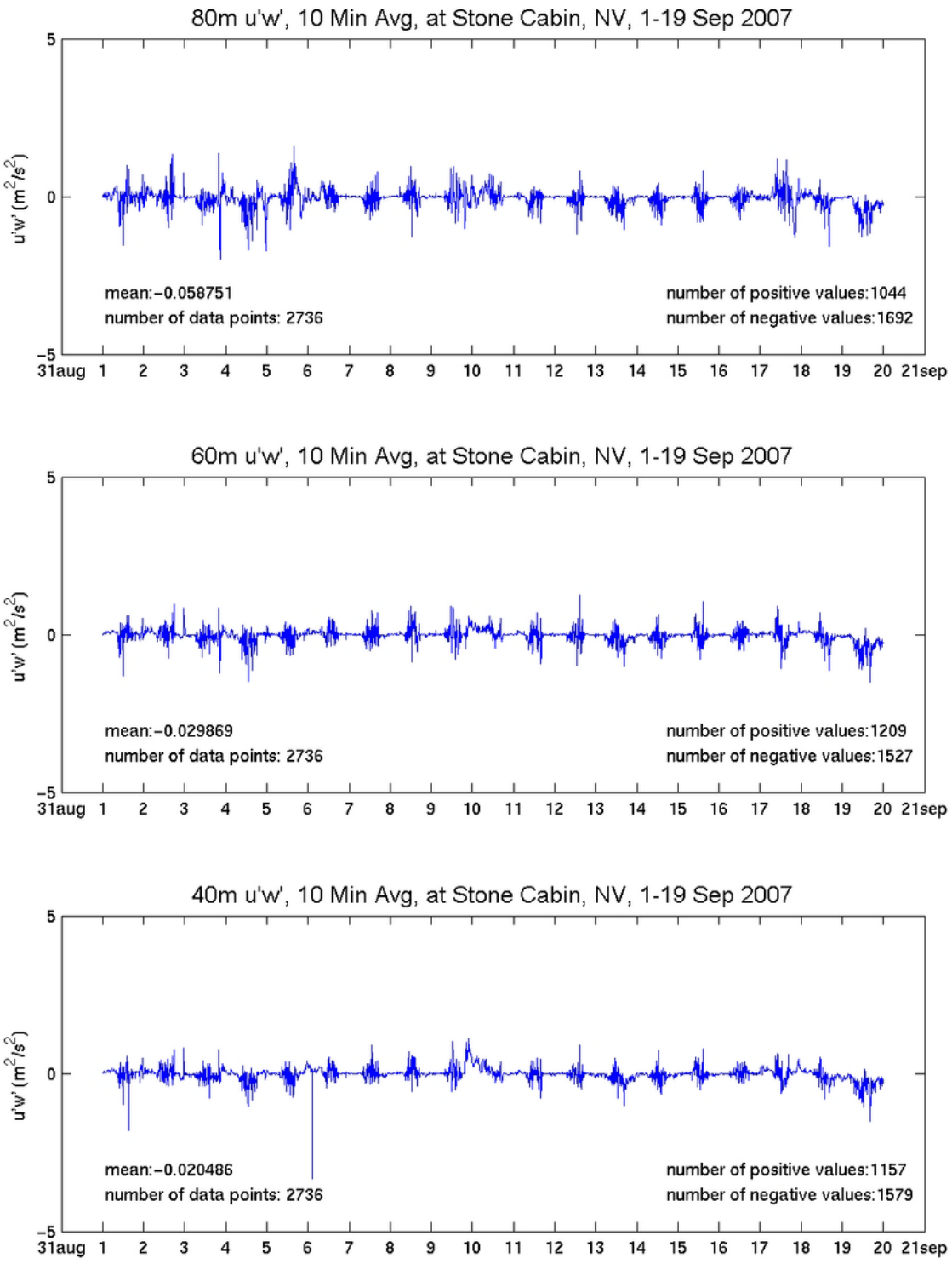

Figure 105. Same as Figure 99, but for a subset period 1-19 September 2007

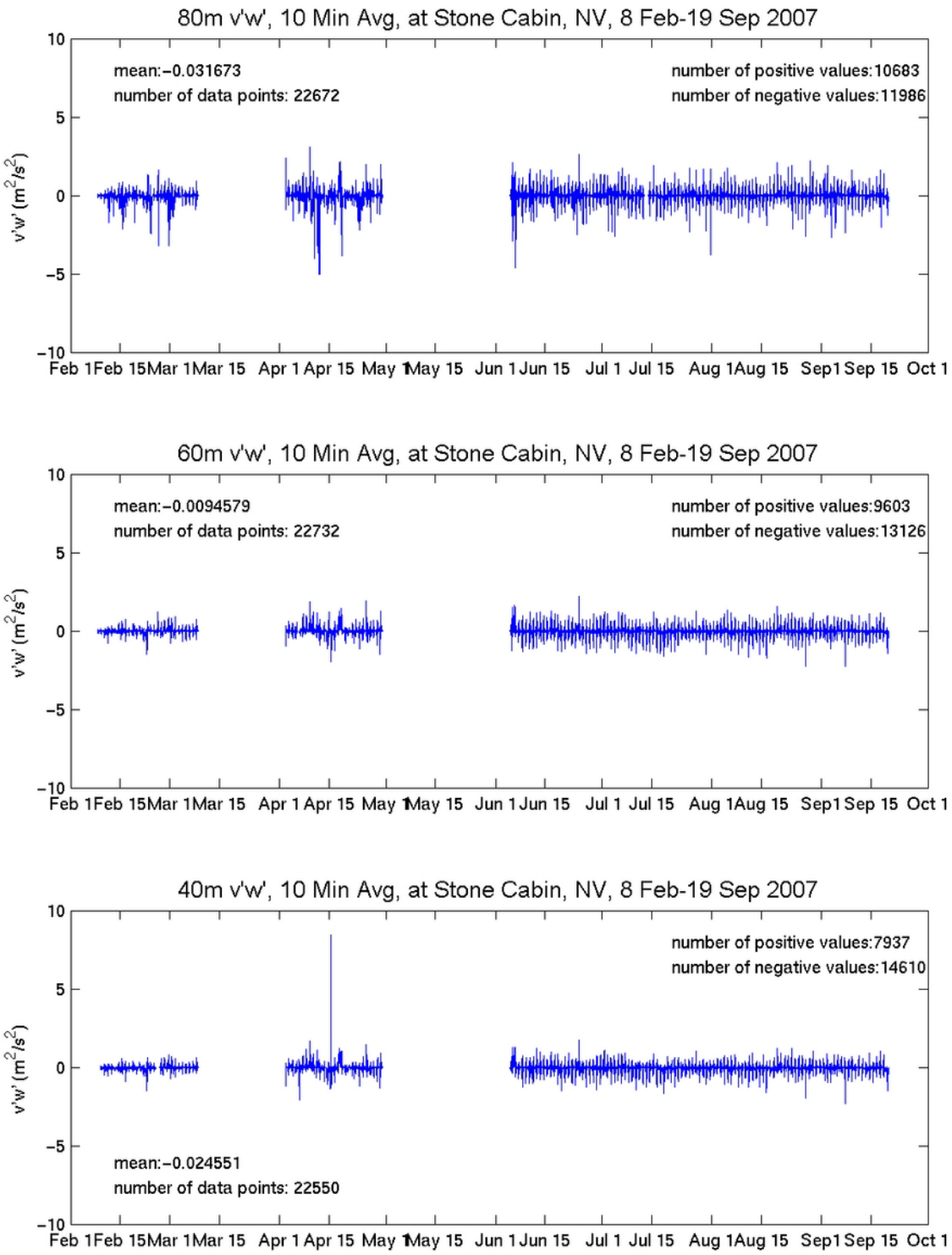

Figure 106. Sonic-measured turbulence momentum flux component v' w' (units in m^2 s^{-2}) at different height levels (averaged over 10-minute period) at Stone Cabin for the period 8 Feb 2007-19 Sept 2007. The mean and population of the dataset are indicated (top) at 80 m, (center) at 60 m, and (bottom) at 40 m heights.

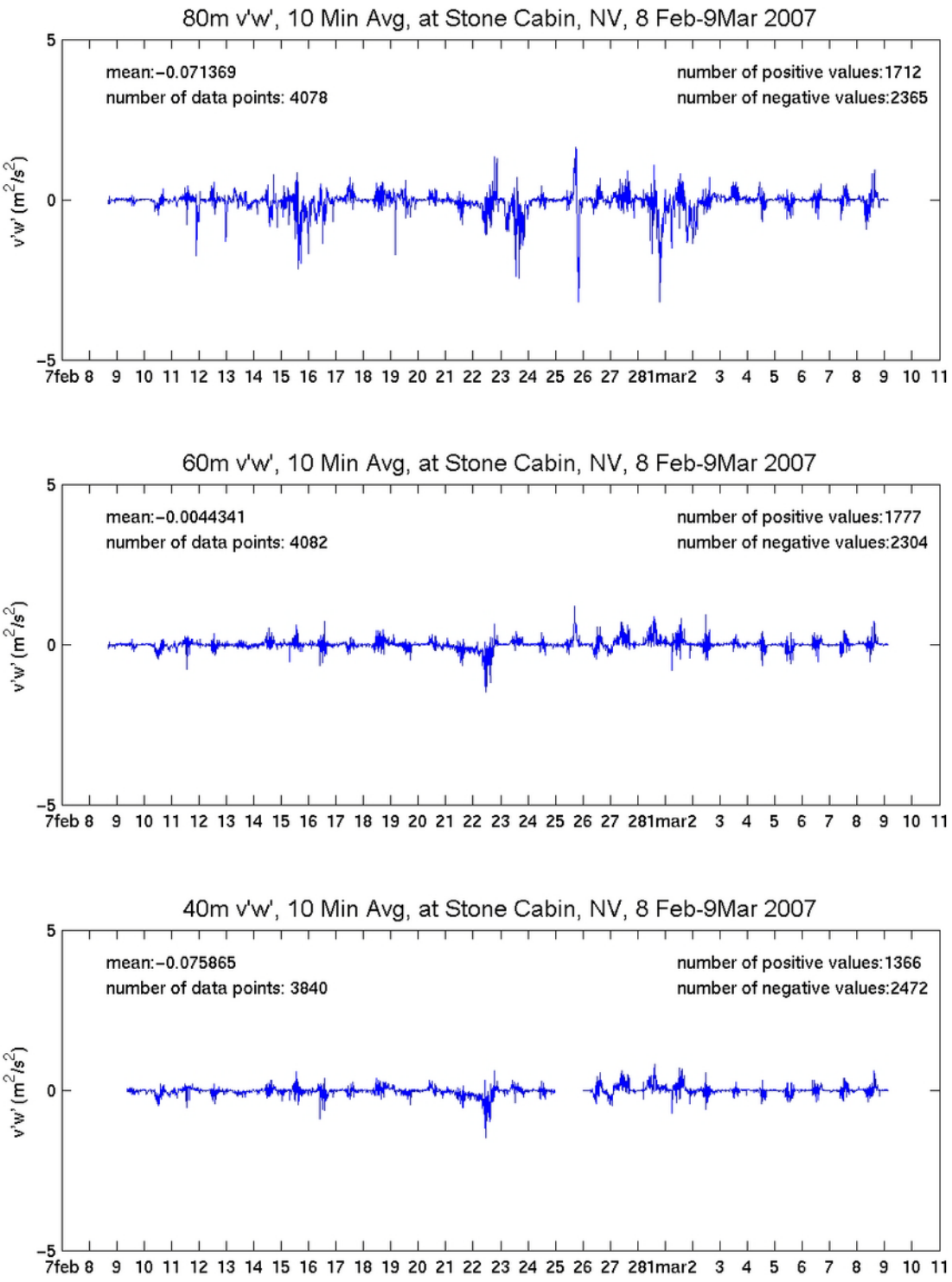

Figure 107. Same as Figure 106, but for a subset period 8 Feb-9 Mar 2007

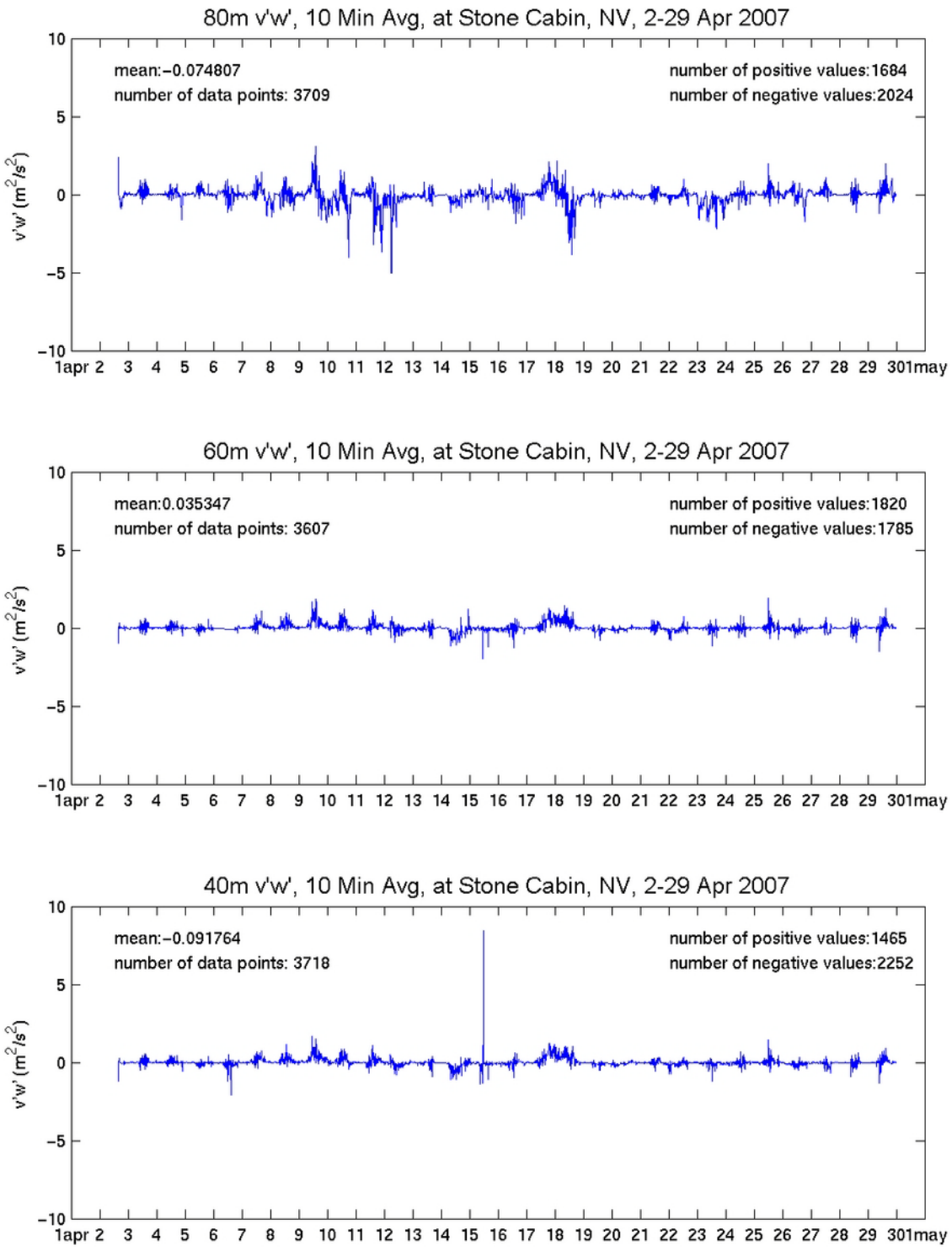

Figure 108. Same as Figure 106, but for a subset period 2-29 April 2007

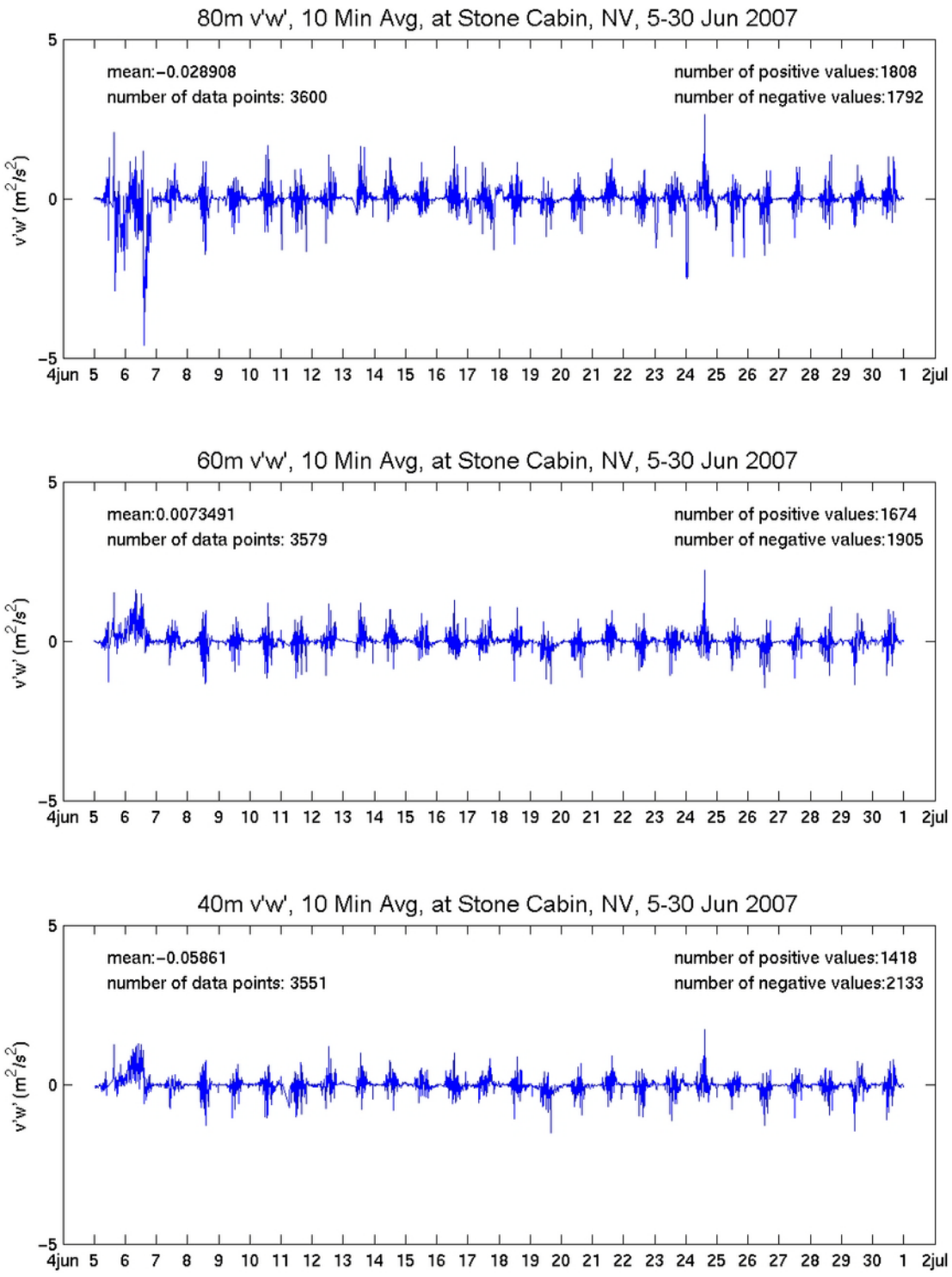

Figure 109. Same as Figure 106, but for a subset period 5-30 June 2007

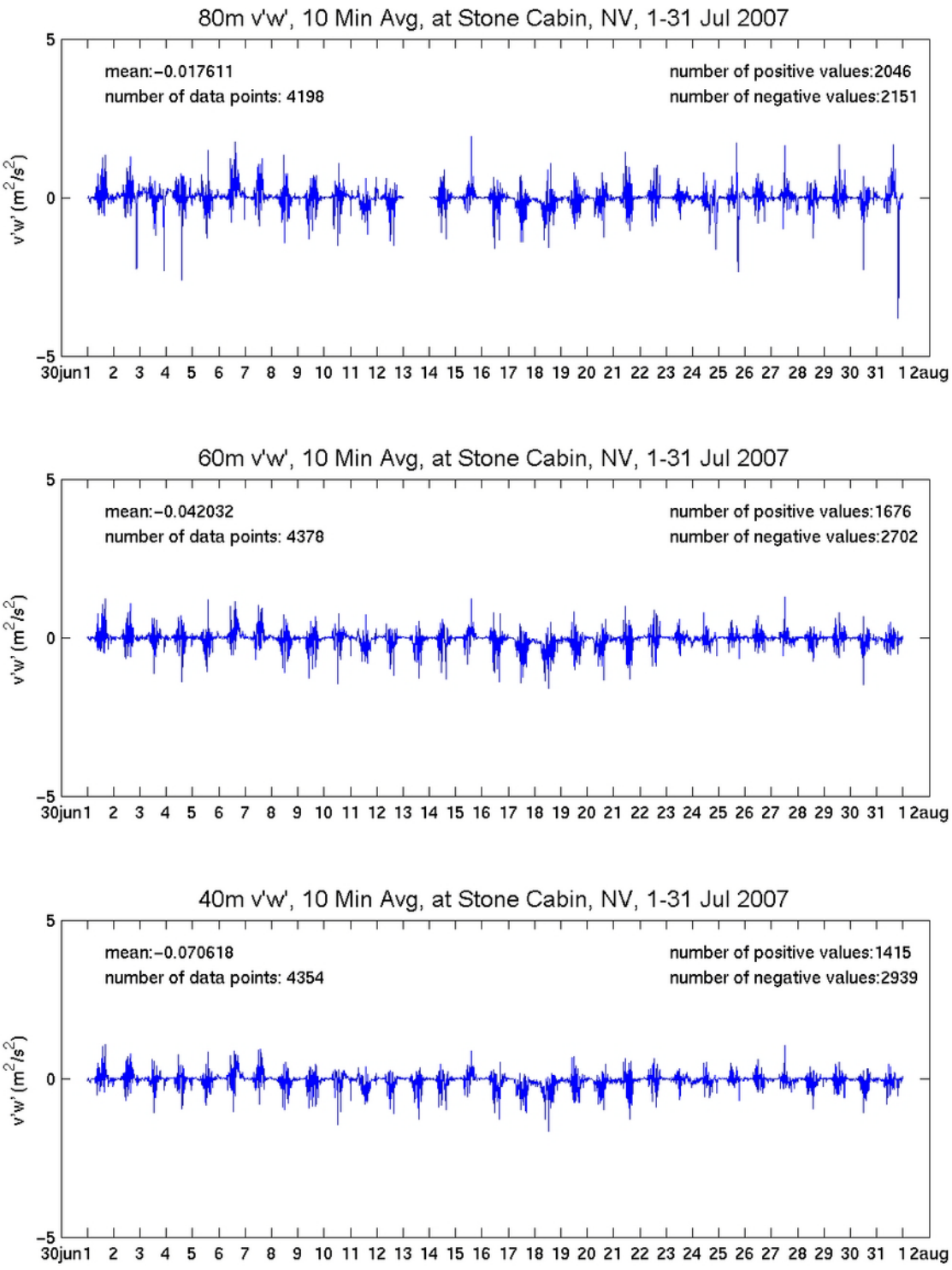

Figure 110. Same as Figure 106, but for a subset period 1-31 July 2007

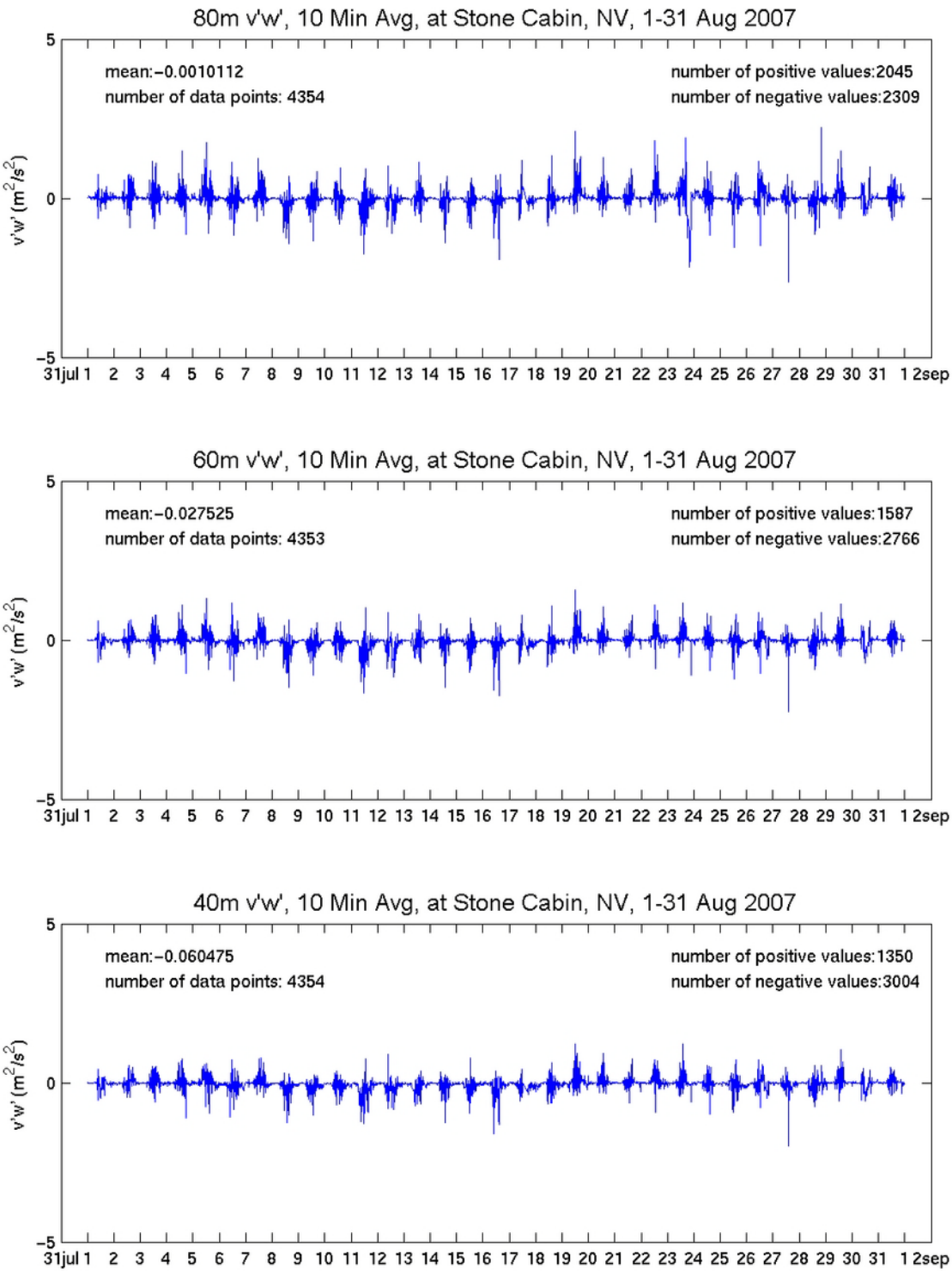

Figure 111. Same as Figure 106, but for a subset period 1-31 August 2007

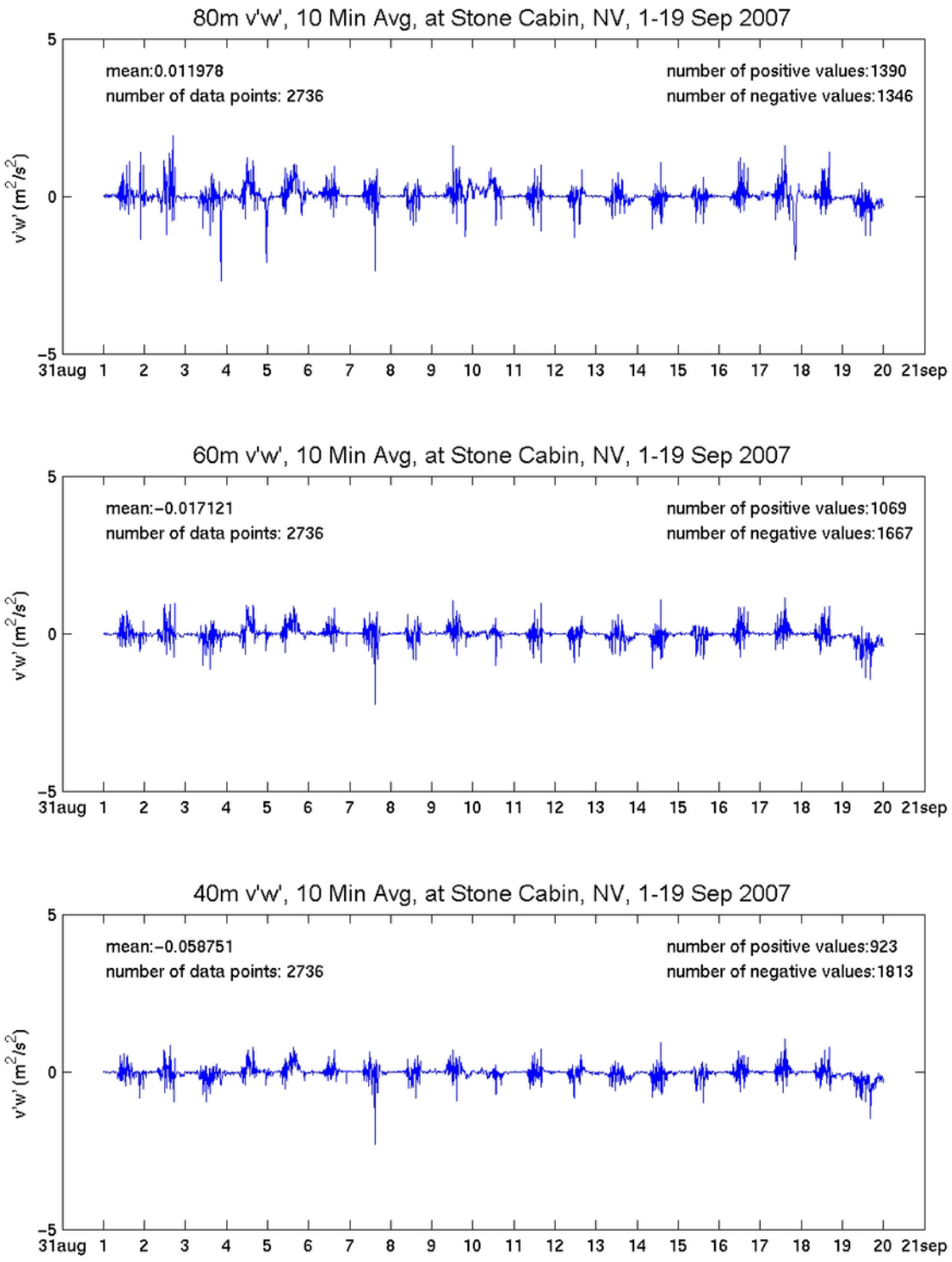

Figure 112. Same as Figure 106, but for a subset period 1-19 September 2007

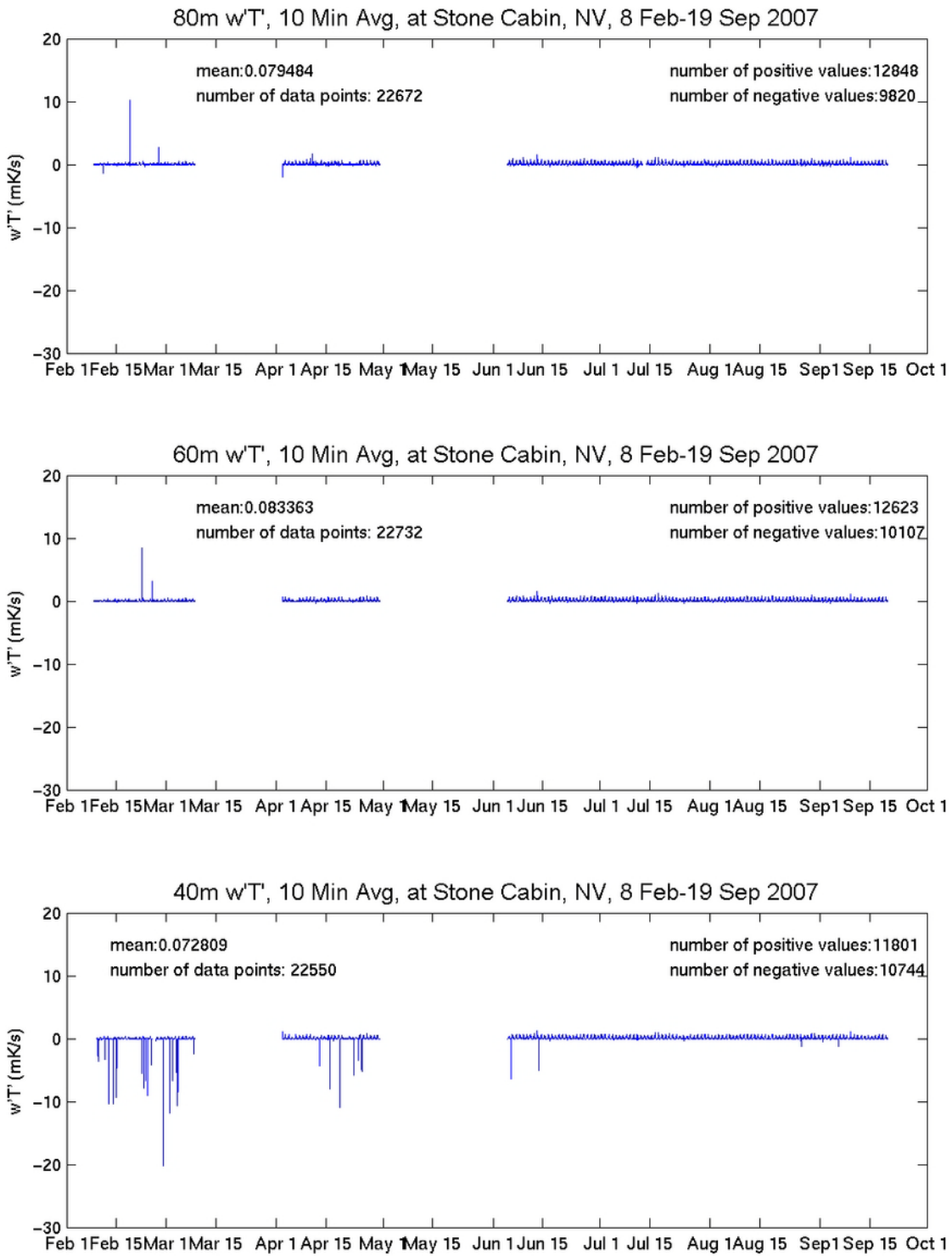

Figure 113. Sonic-measured kinematic heat flux w' T' (units in K m s^{-1}) at different height levels (averaged over 10-minute period) at Stone Cabin for the period 8 Feb 2007-19 Sept 2007. The mean and population of the dataset are indicated (top) at 80 m, (center) at 60 m, and (bottom) at 40 m heights.

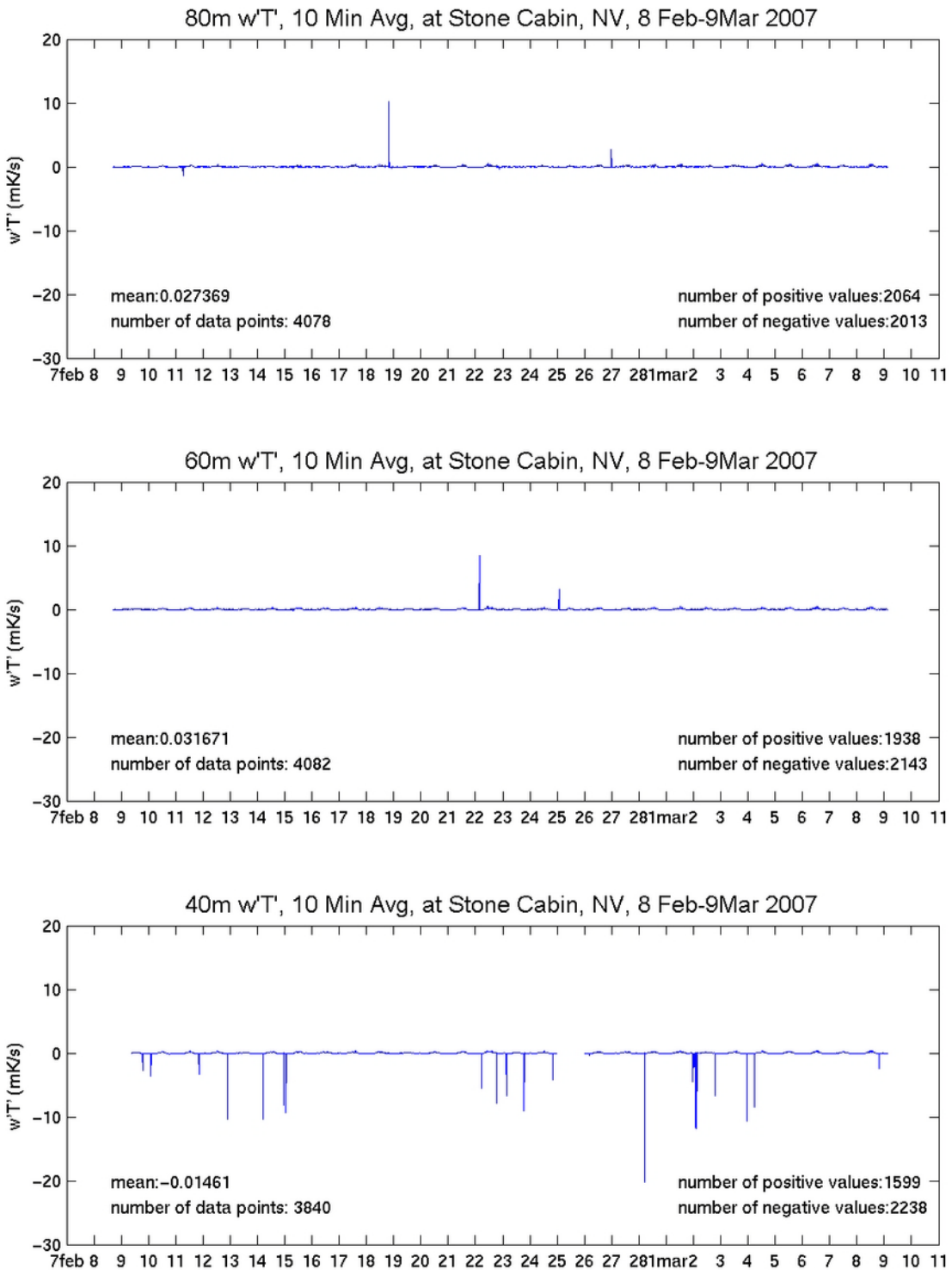

Figure 114. Same as Figure 113, but for a subset period 8 Feb-9 Mar 2007

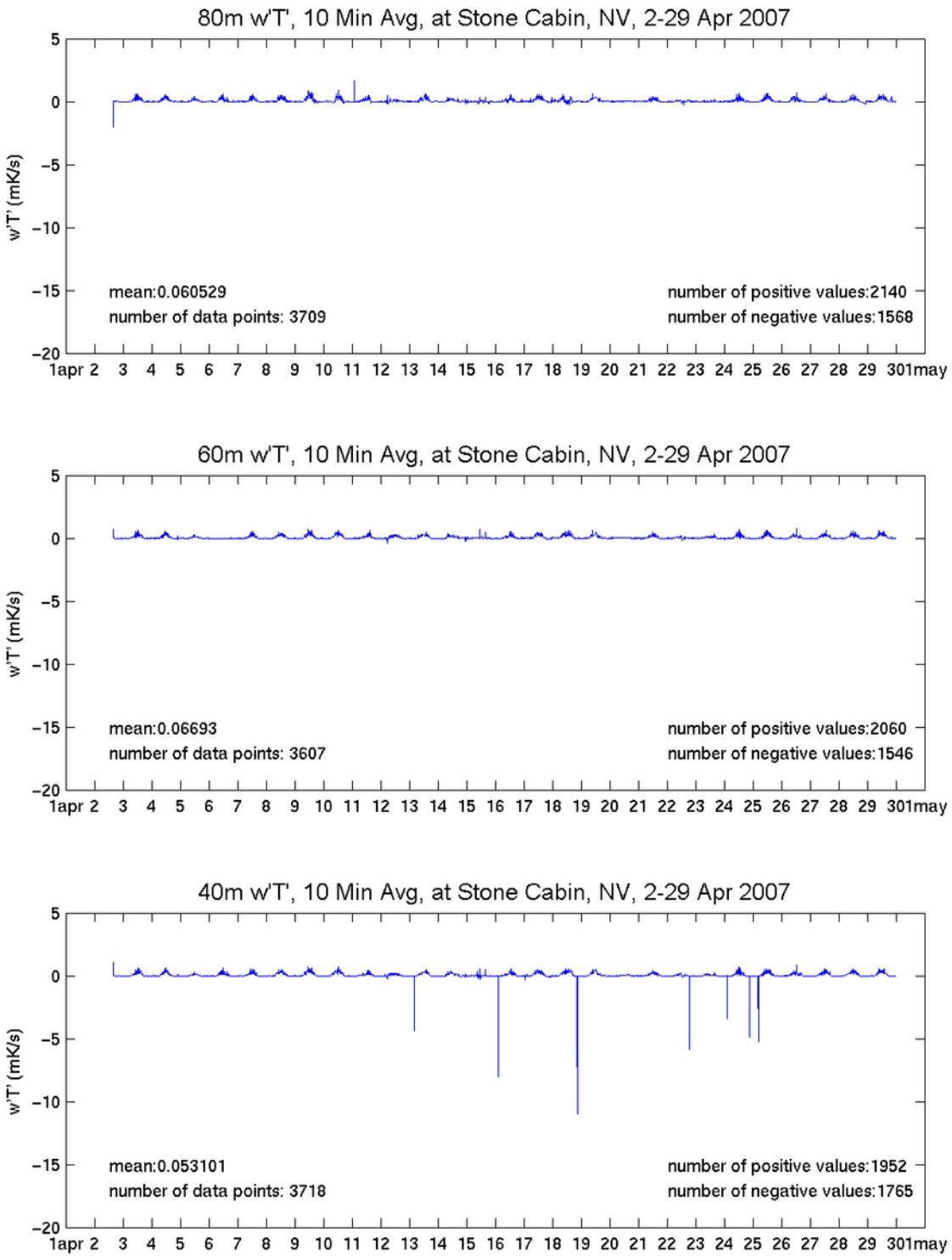

Figure 115. Same as Figure 113, but for a subset period 2-29 April 2007

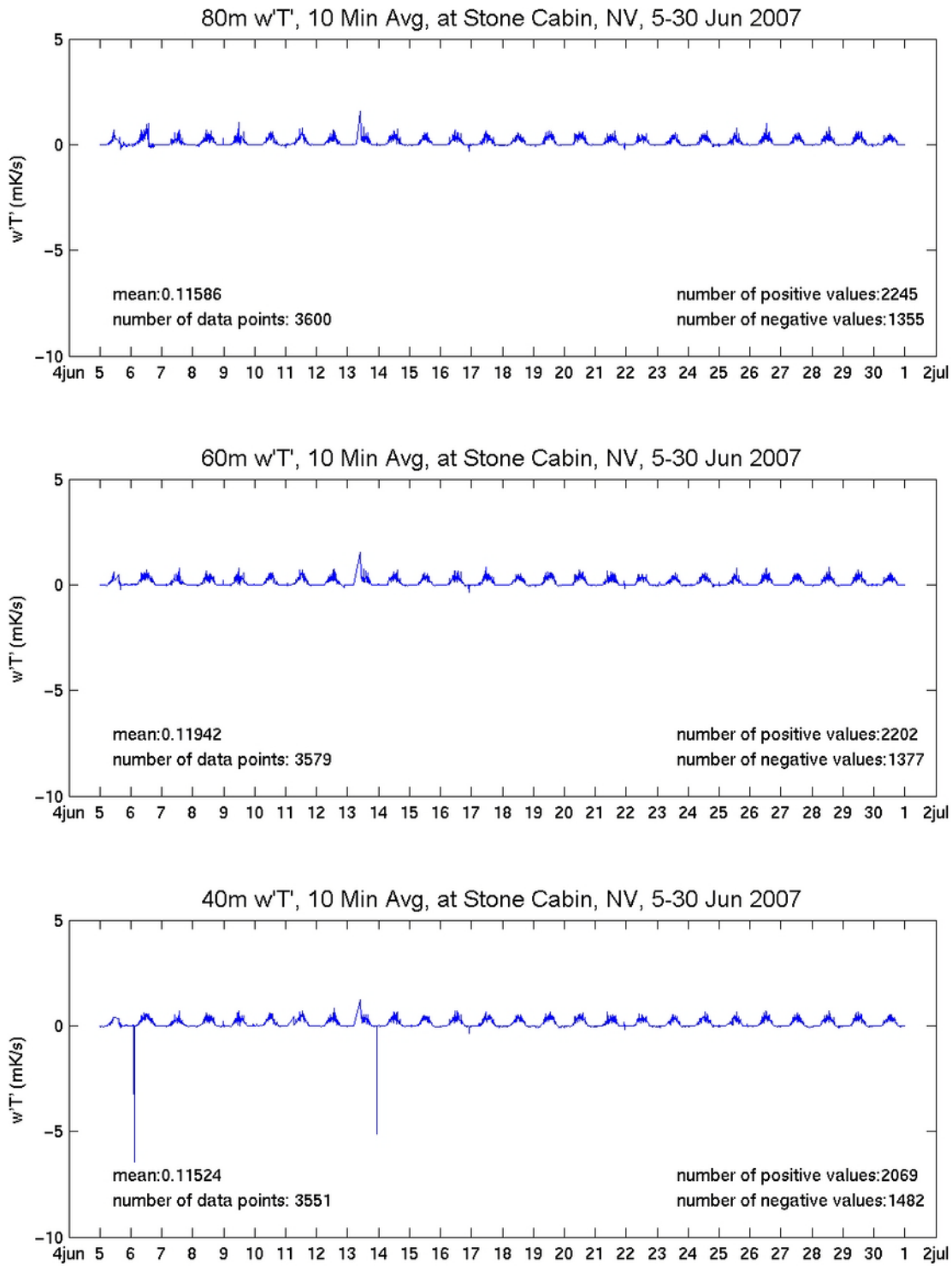

Figure 116. Same as Figure 113, but for a subset period 5-30 June 2007

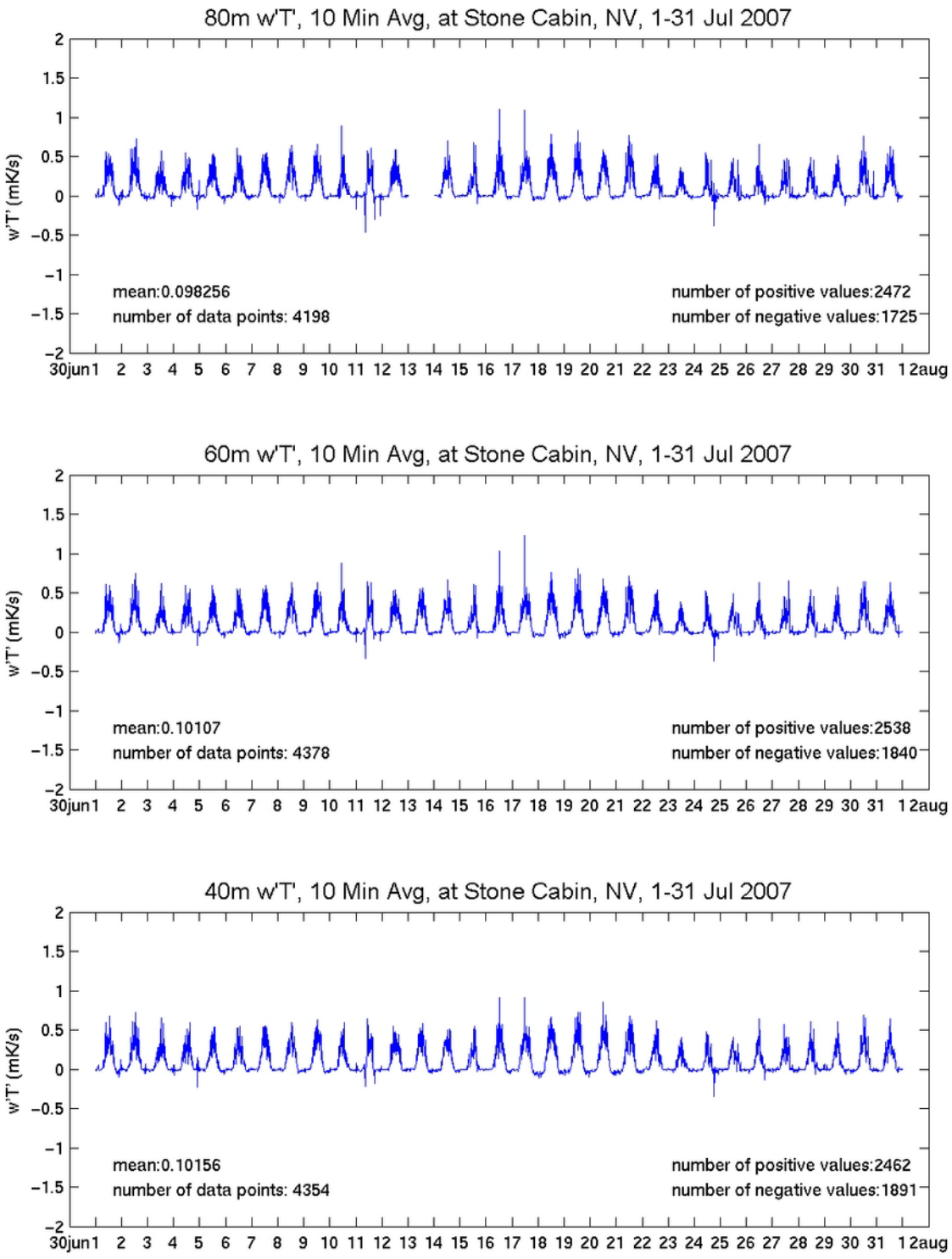

Figure 117. Same as Figure 113, but for a subset period 1-31 July 2007

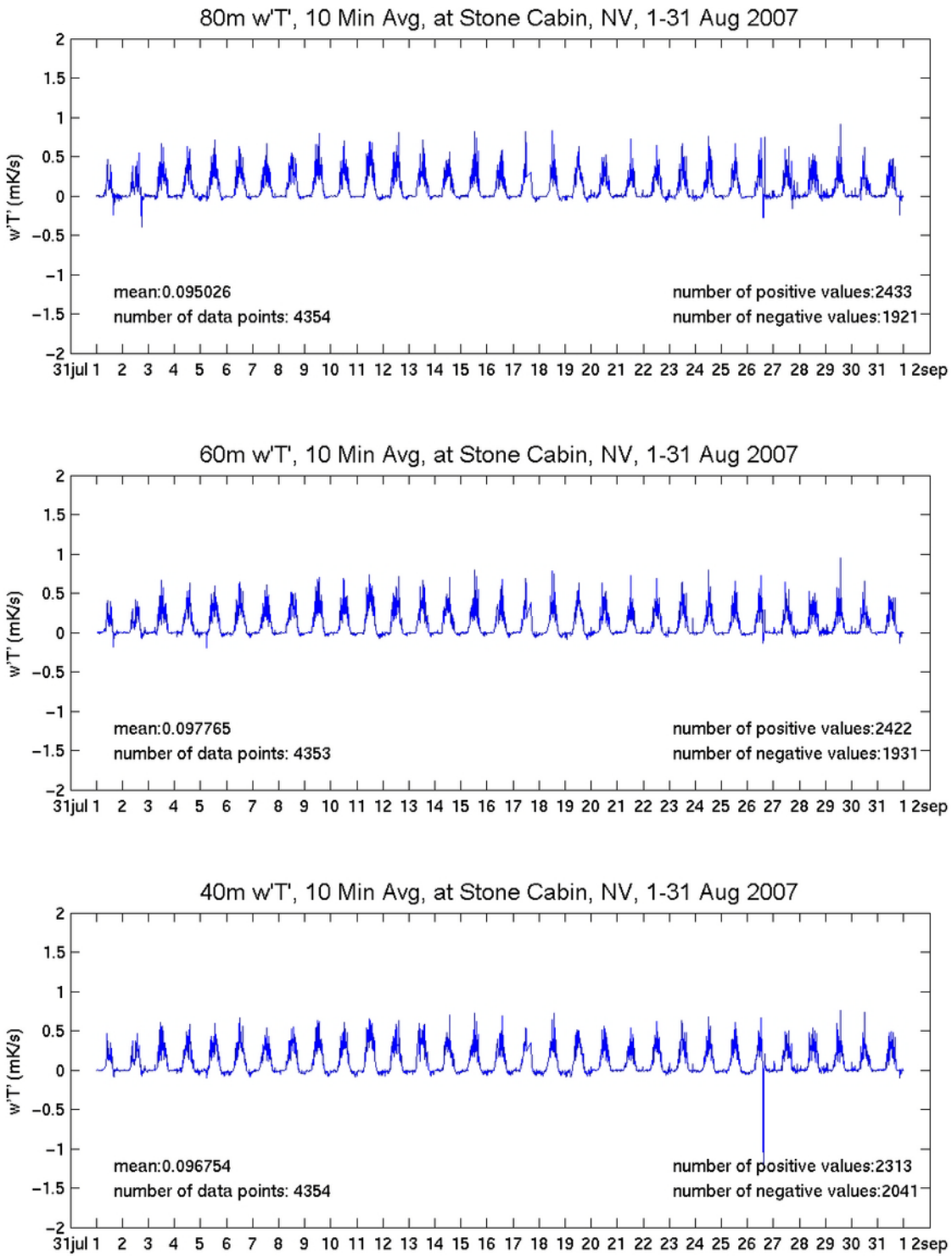

Figure 118. Same as Figure 113, but for a subset period 1-31 August 2007

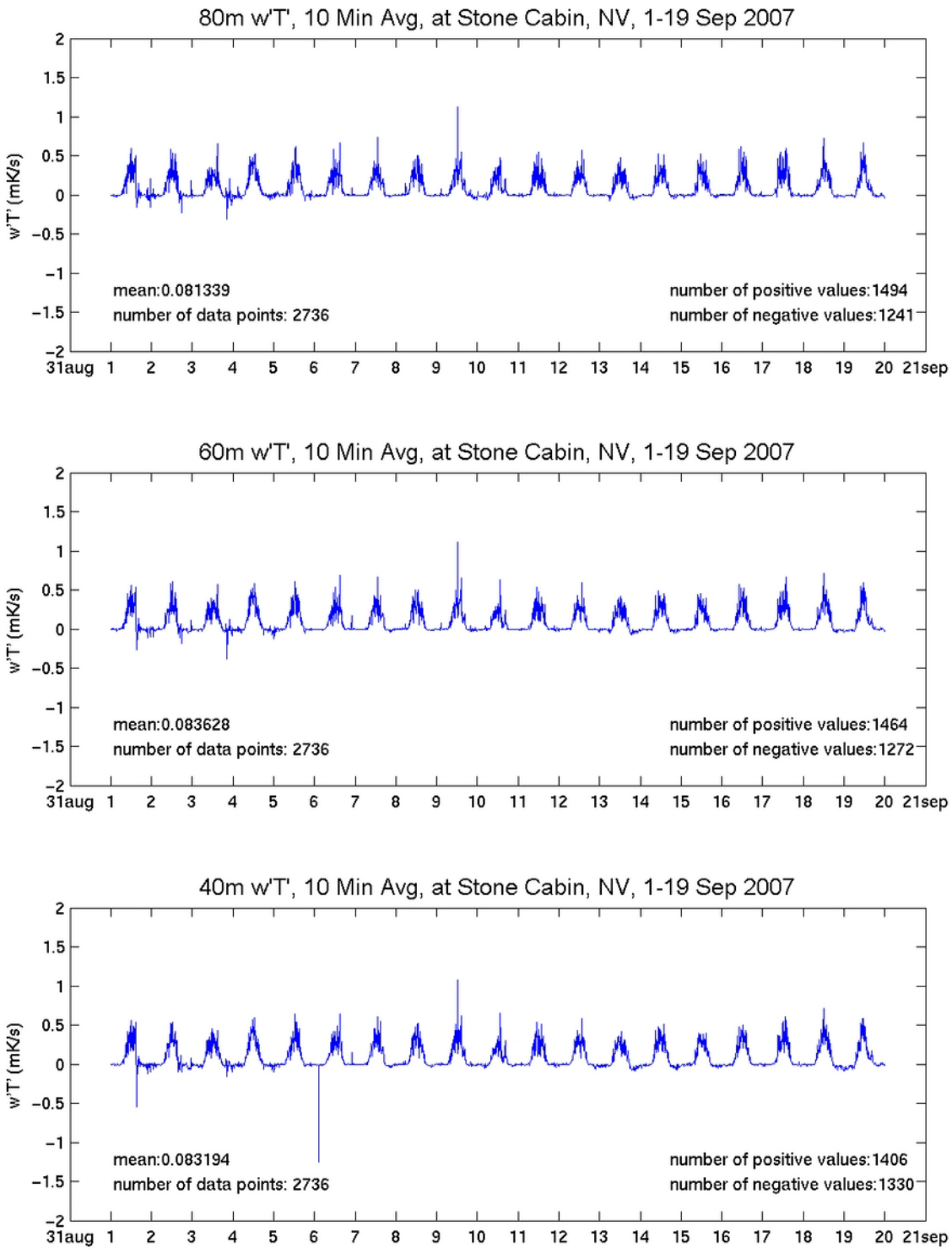

Figure 119. Same as Figure 113, but for a subset period 1-19 September 2007

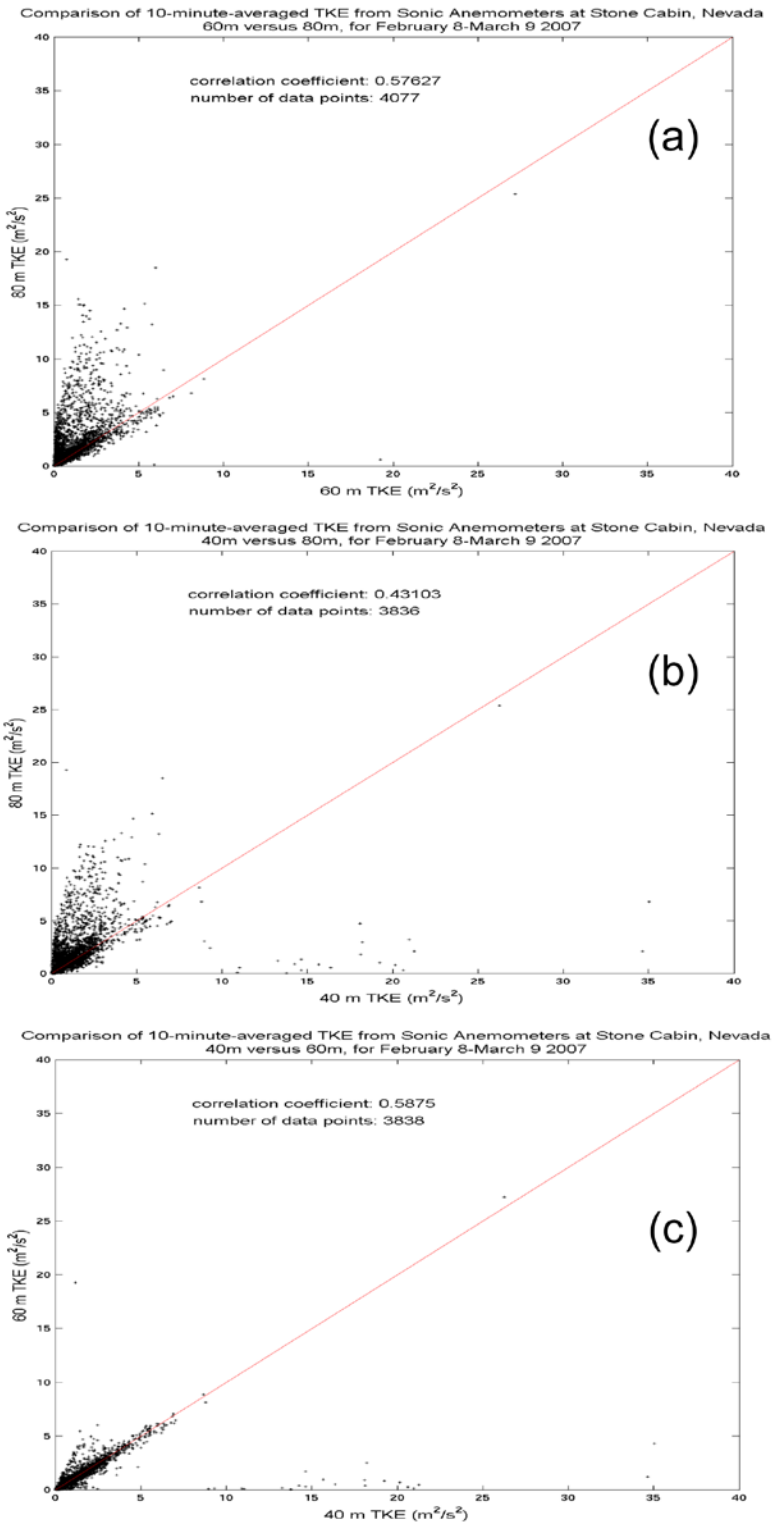

Figure 120. Scatterplots of sonic-measured 10-minute averaged turbulence kinetic energy for the period February 8-March 9, 2007. (a) 60 m vs. 80m, (b) 40 m vs. 80 m, and (c) 40 m vs. 60 m.

The sample density and correlation coefficients are indicated.

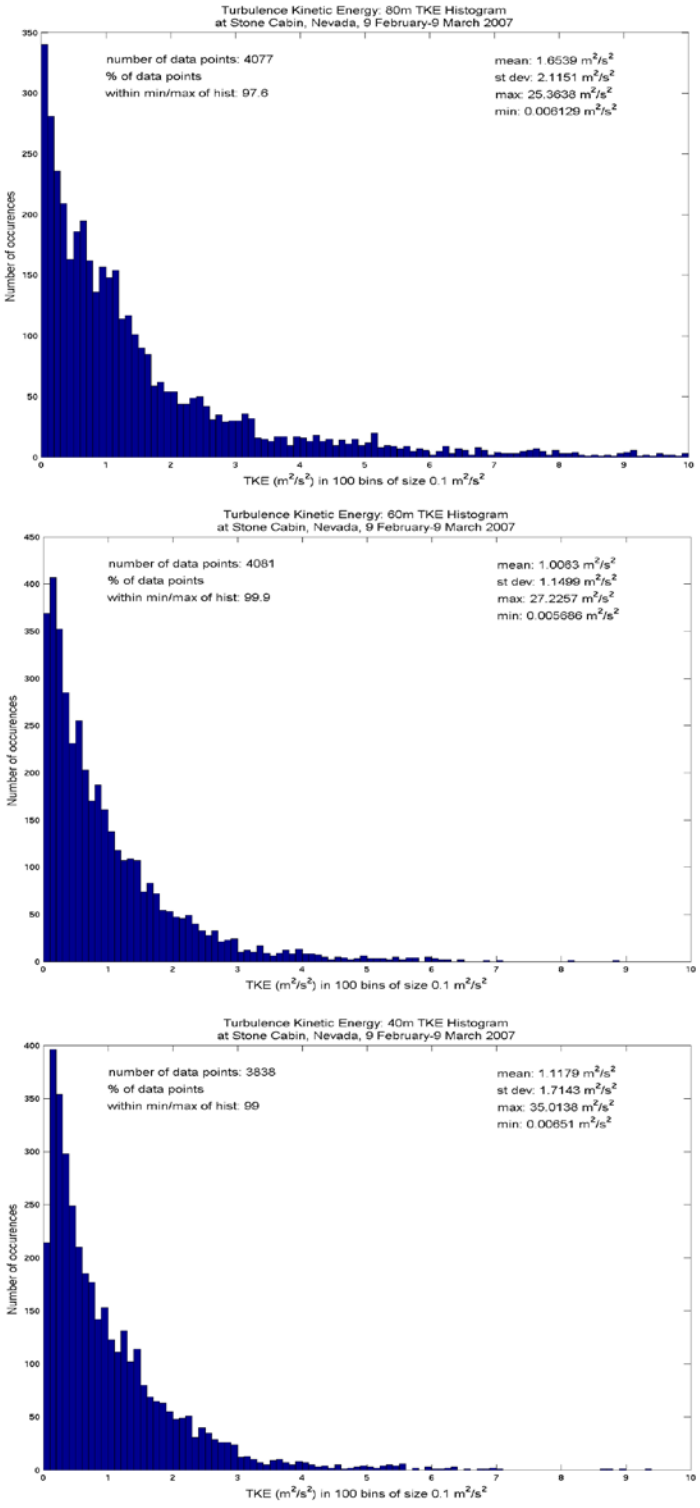

Figure 121. Histogram of sonic-measured turbulence kinetic energy for the period February 8-March 9, 2007 (top) 80 m, (center) 60 m, and (bottom) 40 m.

The statistics of the distribution are indicated.

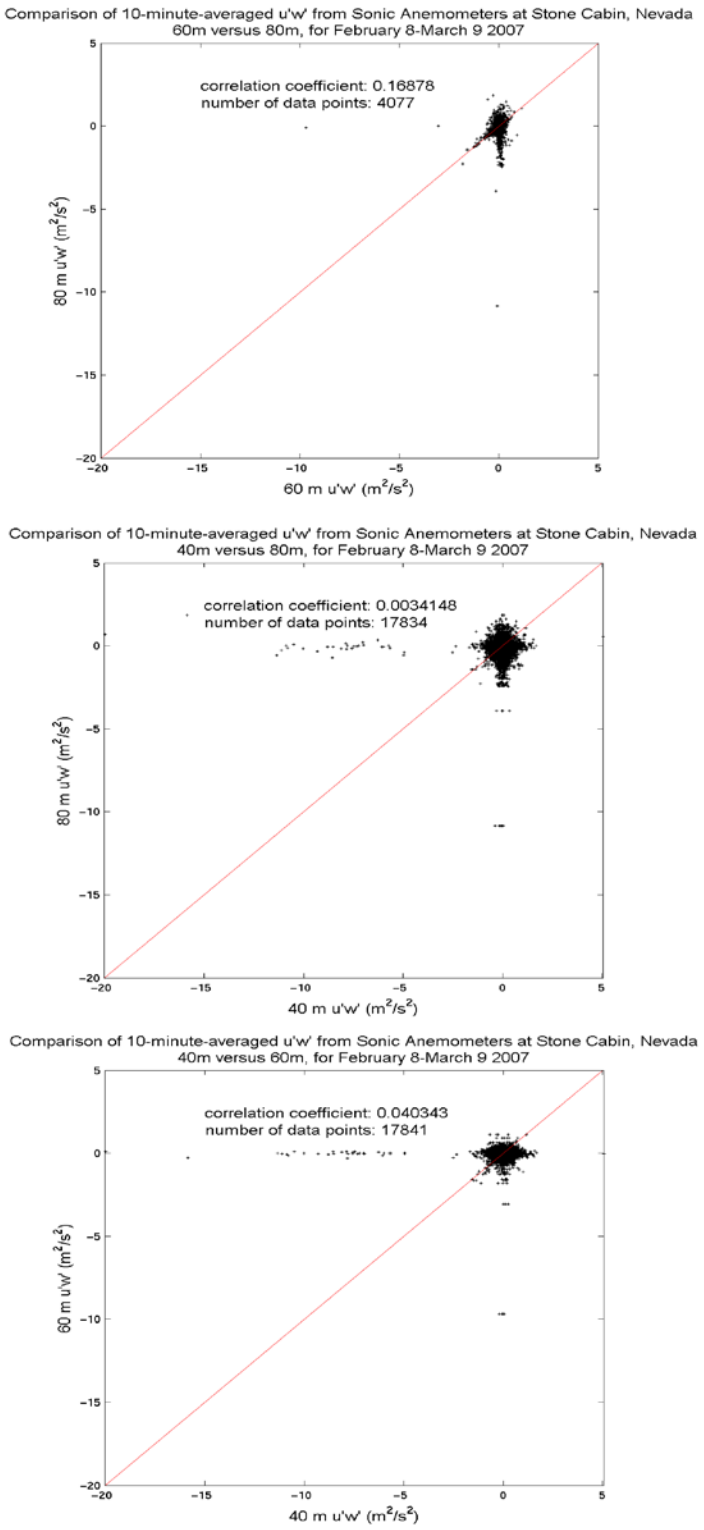

Figure 122. Scatterplots of sonic-measured 10-minute averaged kinematic momentum flux component u'w' for the period February 8-March 9, 2007 (top) 60 m vs. 80 m, (center) 40 m vs. 80 m, and (bottom) 40 m vs. 60 m.

The sample density and correlation coefficients are indicated.

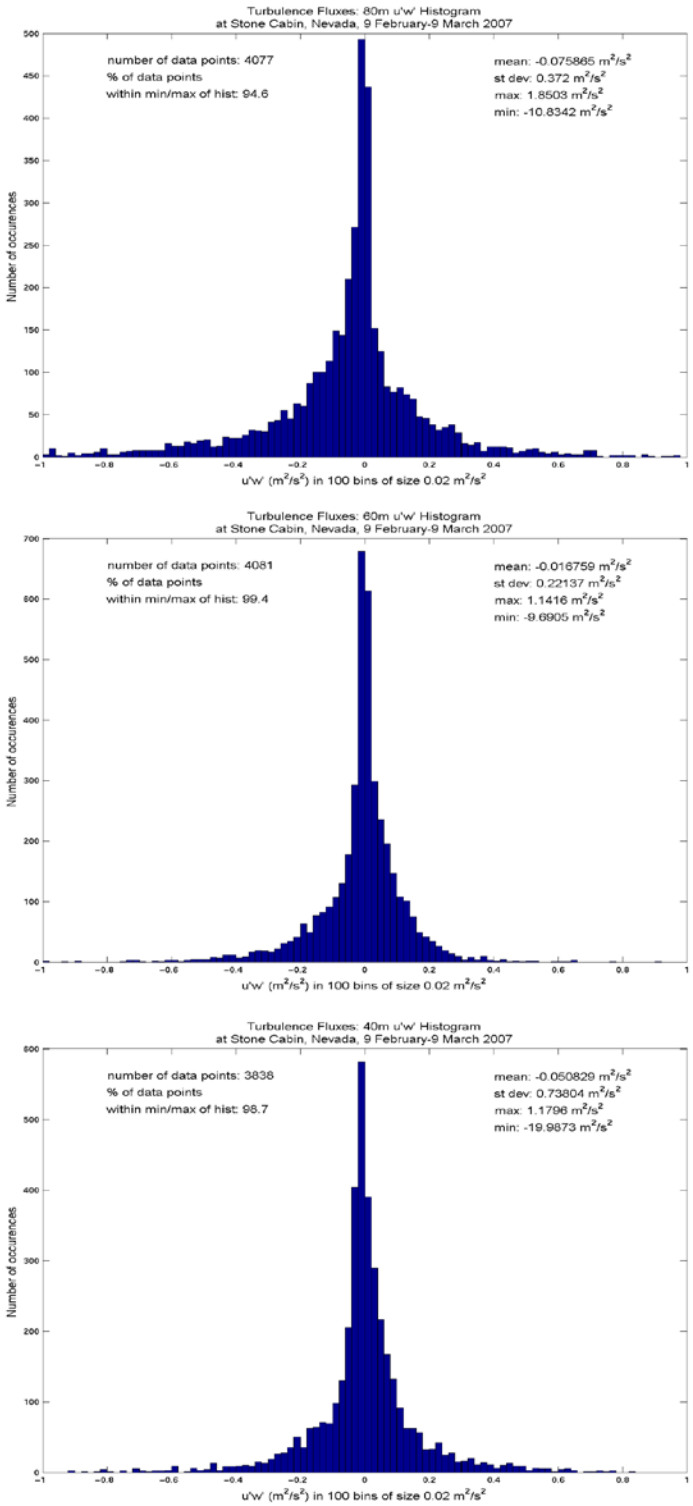

Figure 123. Histogram of sonic-measured kinematic momentum flux component u'w' for the period February 8-March 9, 2007 (top) 80 m, (center) 60 m, and (bottom) 40 m.

The statistics of the distribution are indicated.

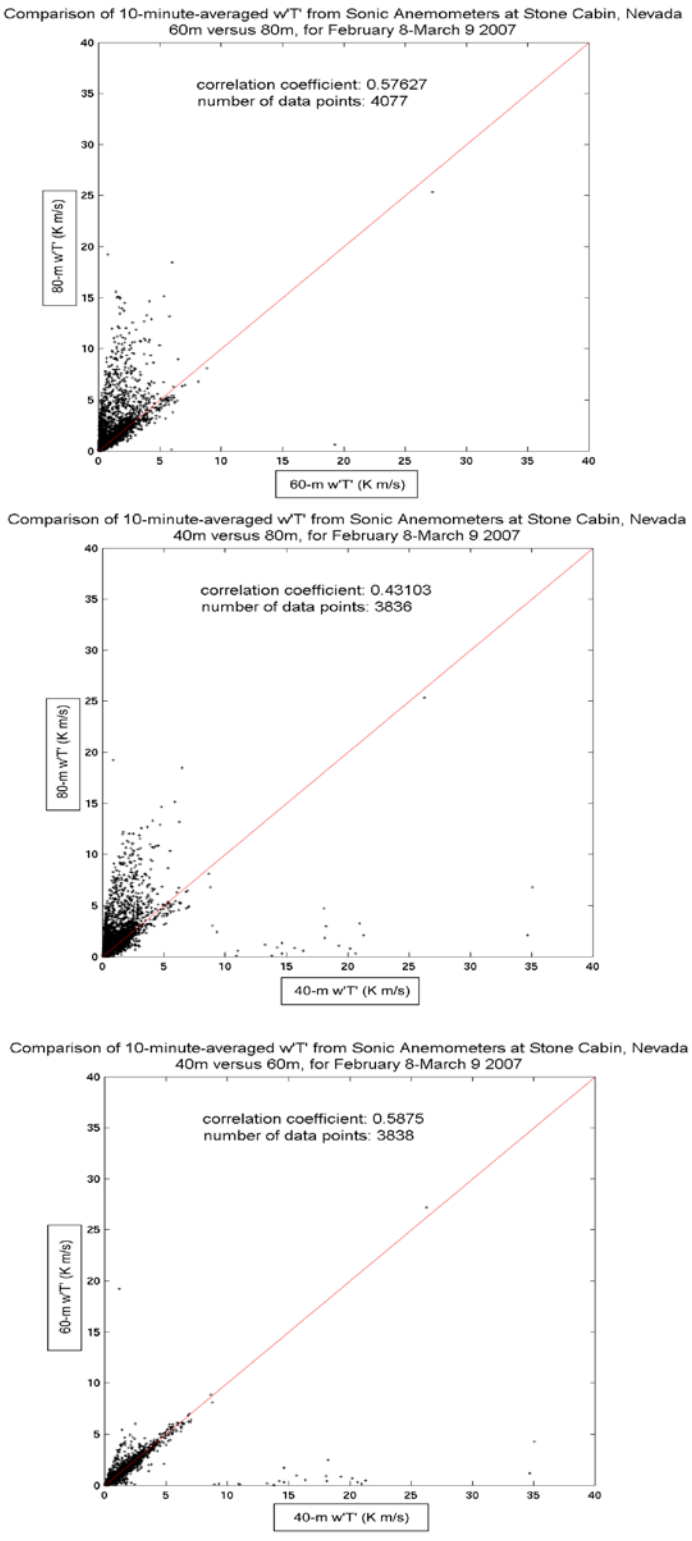

Figure 124. Scatterplots of sonic-measured 10-minute averaged kinematic heat flux for the period February 8-March 9, 2007 (top) 60 m vs. 80 m, (center) 40m vs. 80m, and (bottom) 40 m vs. 60 m.

The sample density and correlation coefficients are indicated.

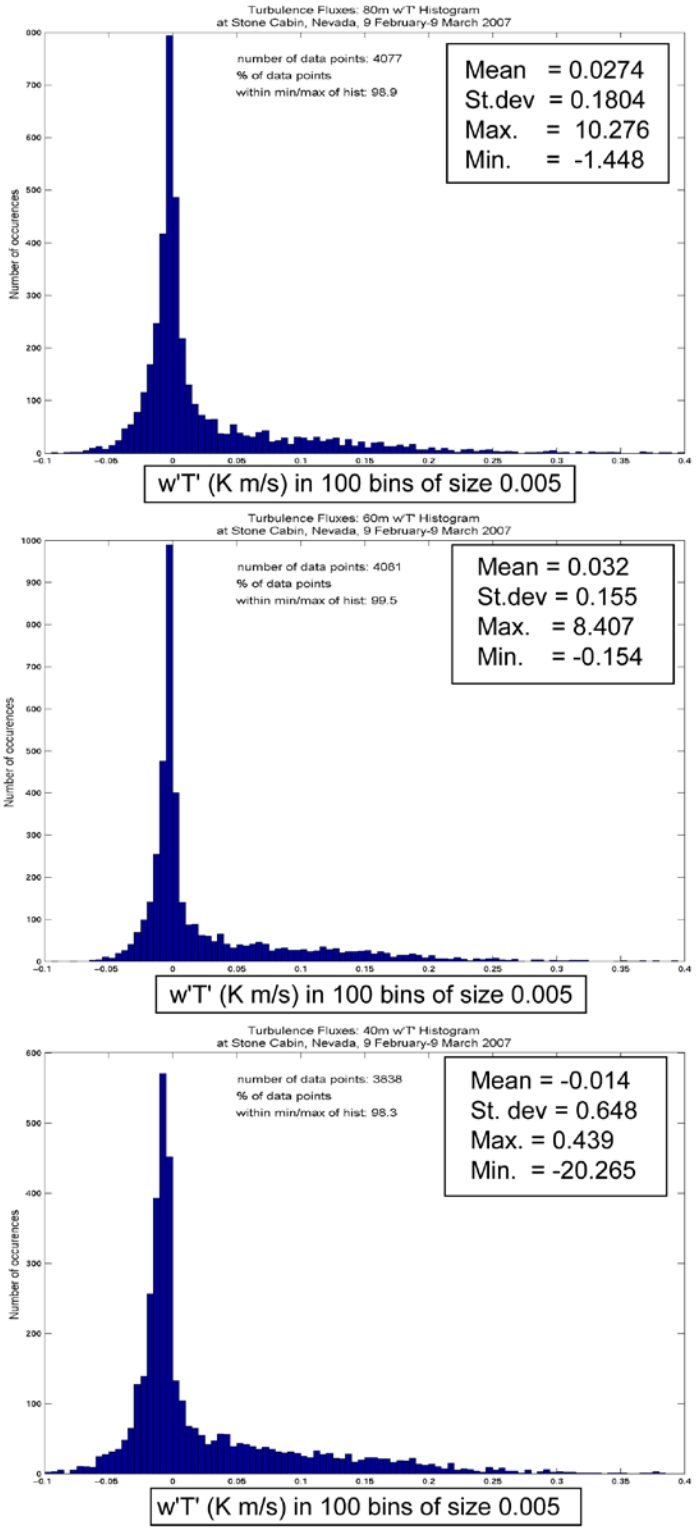

Figure 125. Histogram of sonic-measured kinematic heat flux for the period February 8-March 9, 2007 (top) 80 m, (center) 60 m, and (bottom) 40 m.

The statistics of the distribution are indicated.

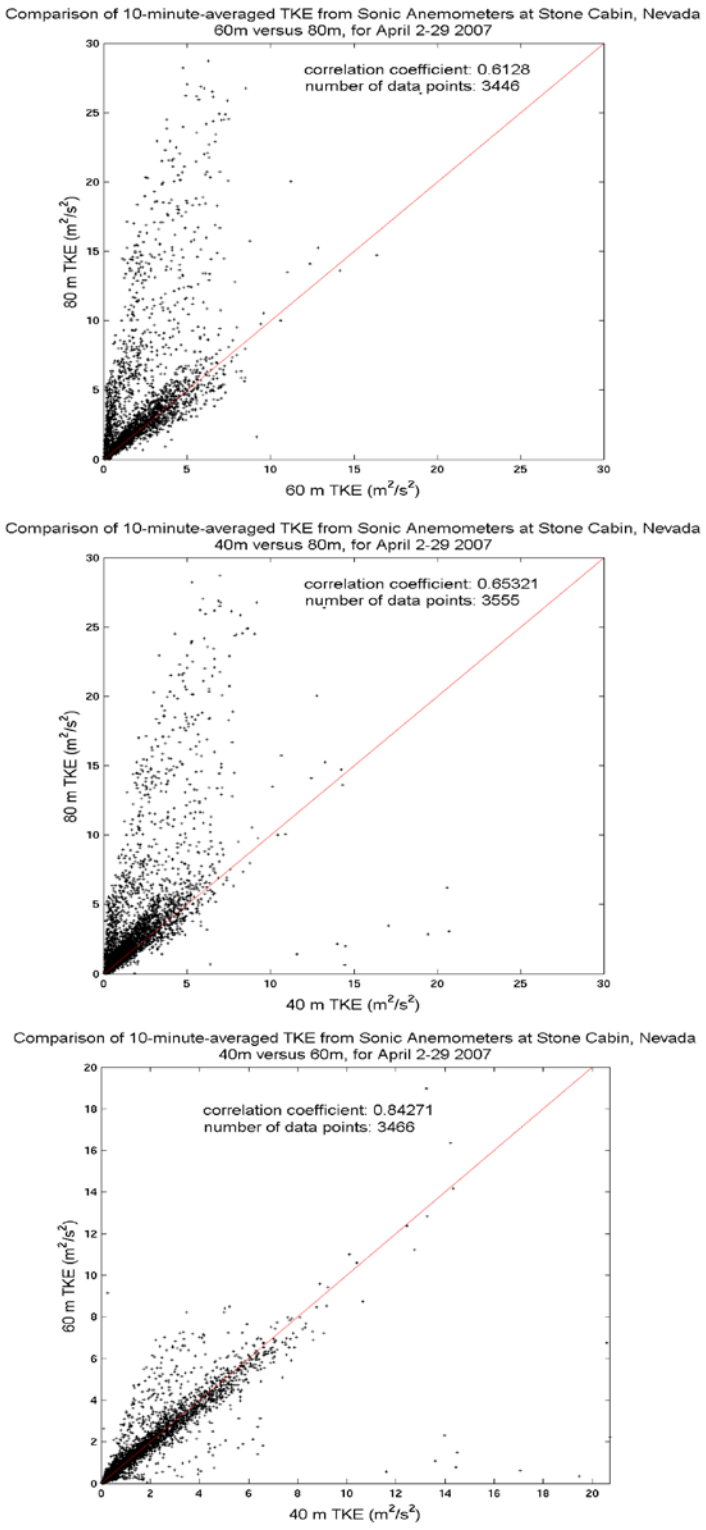

Figure 126. Scatterplots of sonic-measured 10-minute averaged turbulence kinetic energy for the period April 2-29, 2007 (top) 60 m vs. 80m, (center) 40 m vs. 80 m, and (bottom) 40 m vs. 60 m.

The sample density and correlation coefficients are indicated.

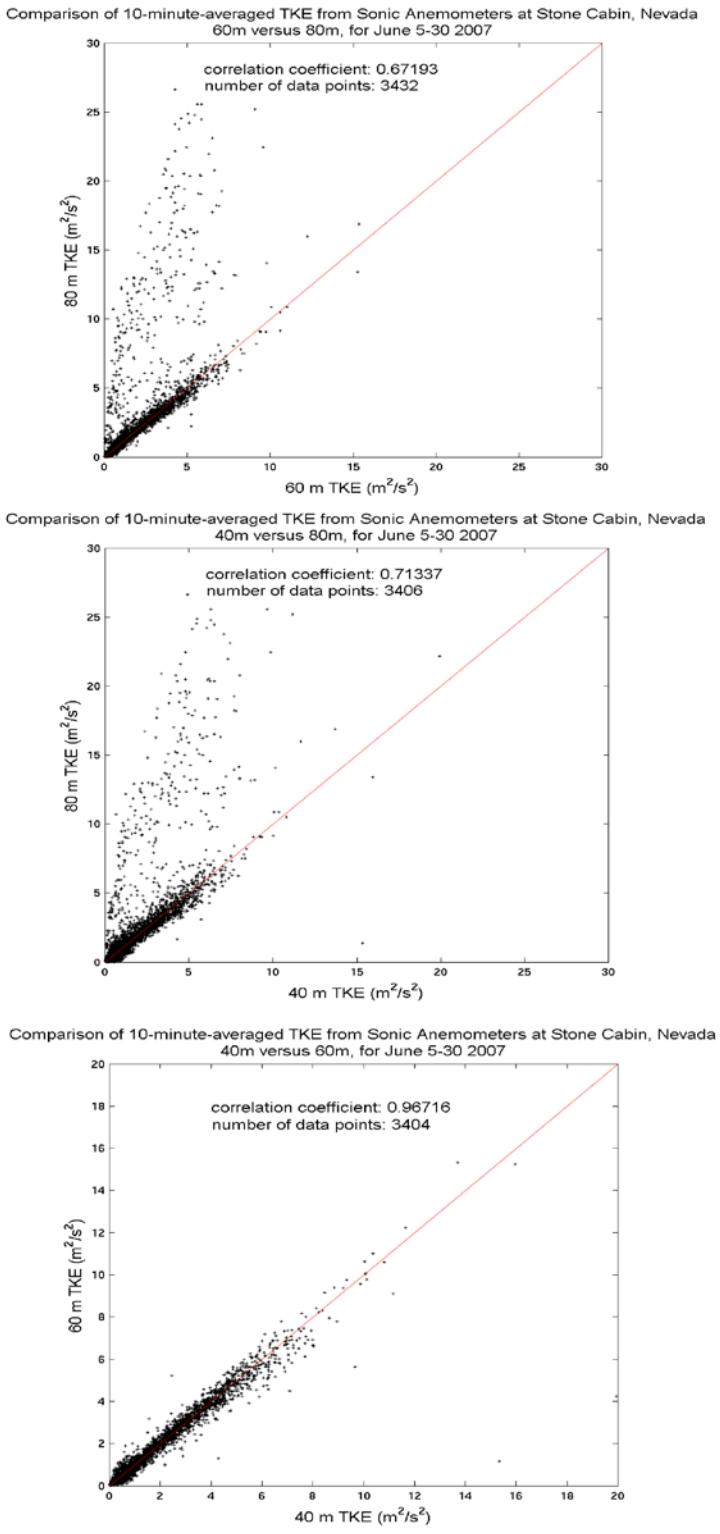

Figure 127. Scatterplots of sonic-measured 10-minute averaged turbulence kinetic energy for the period June 5-30, 2007 (top) 60 m vs. 80 m, (center) 40 m vs. 80 m, and (bottom) 40 m vs. 60 m.

The sample density and correlation coefficients are indicated.

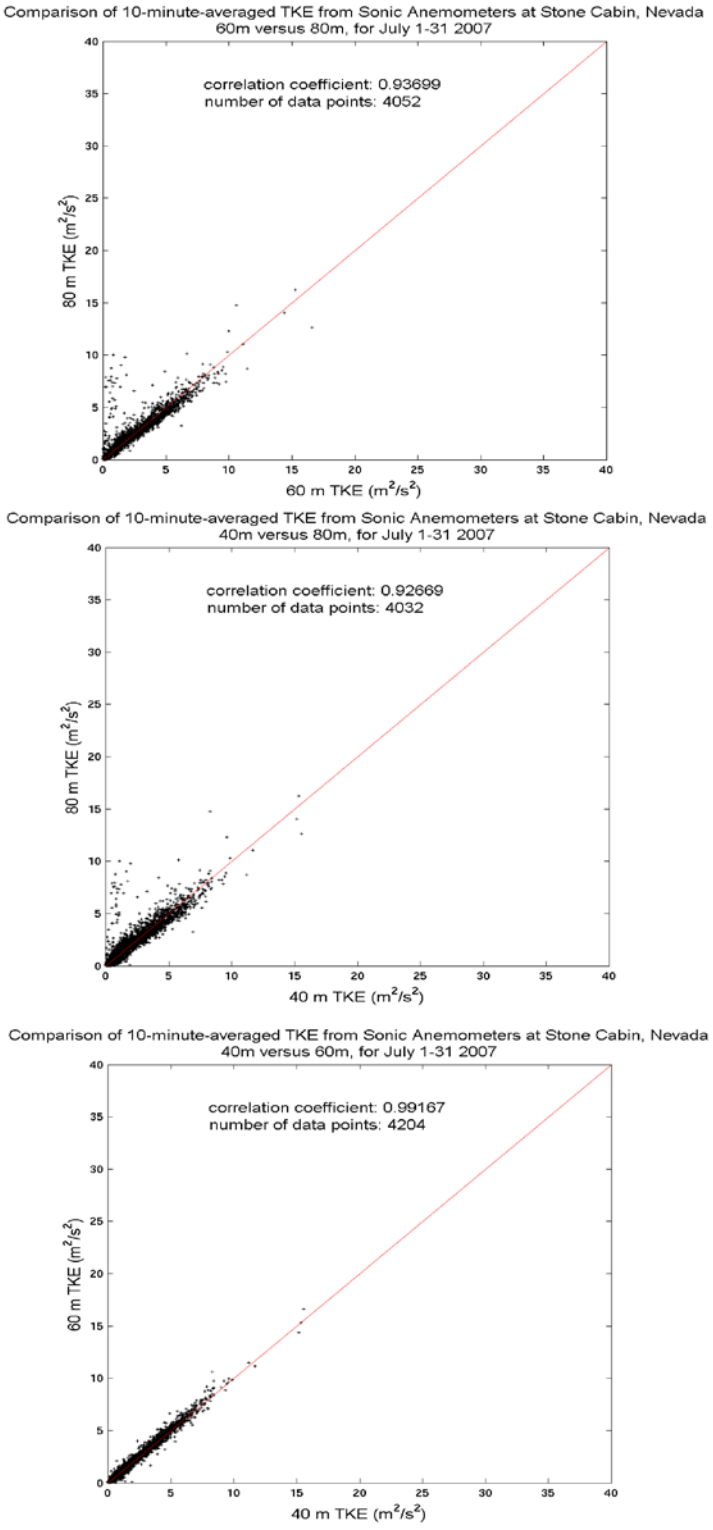

Figure 128. Scatterplots of sonic-measured 10-minute averaged turbulence kinetic energy for the period July 1-31, 2007 (top) 60 m vs. 80 m, (center) 40 m vs. 80 m, and (bottom) 40 m vs. 60 m.

The sample density and correlation coefficients are indicated.

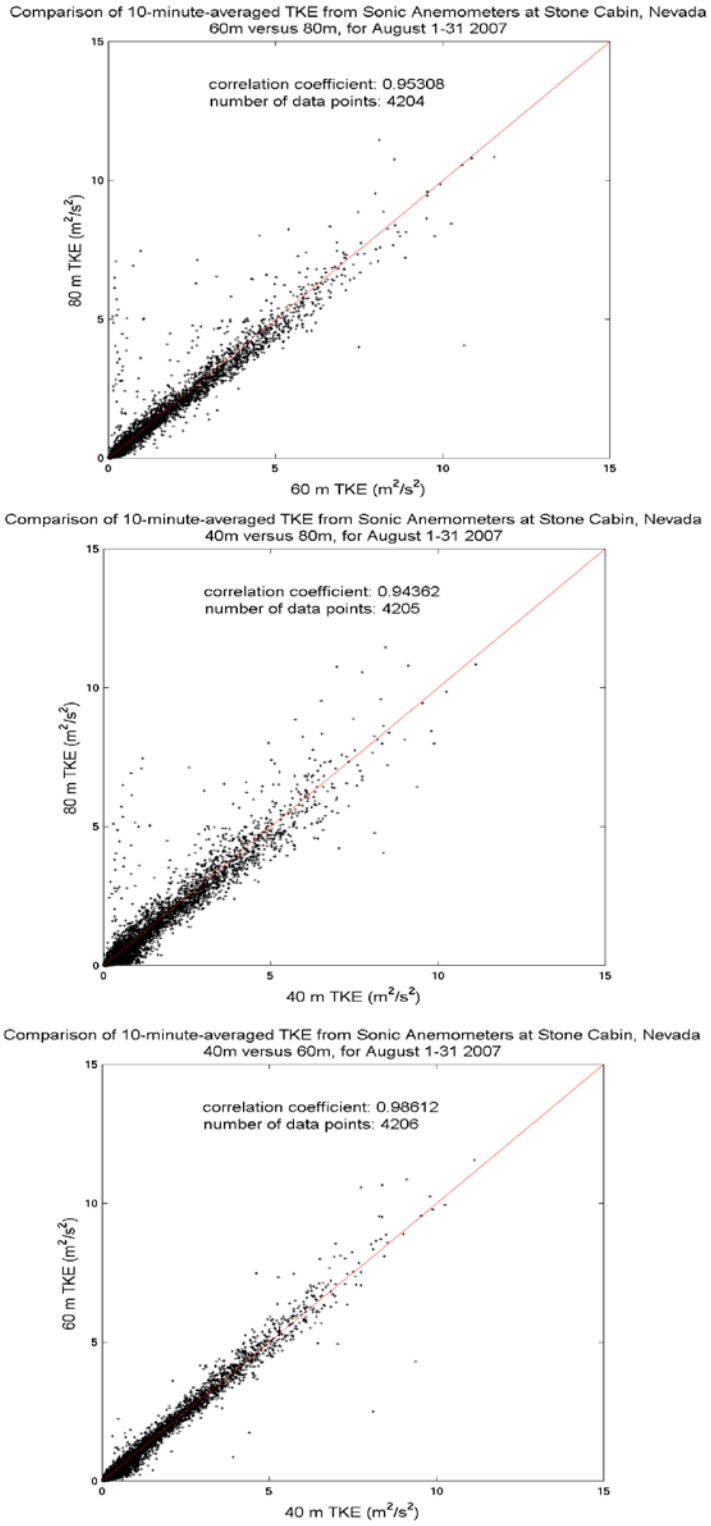

Figure 129. Scatterplots of sonic-measured 10-minute averaged turbulence kinetic energy for the period August 1-31, 2007 (top) 60 m vs. 80 m, (center) 40 m vs. 80 m, and (bottom) 40 m vs. 60 m.

The sample density and correlation coefficients are indicated.

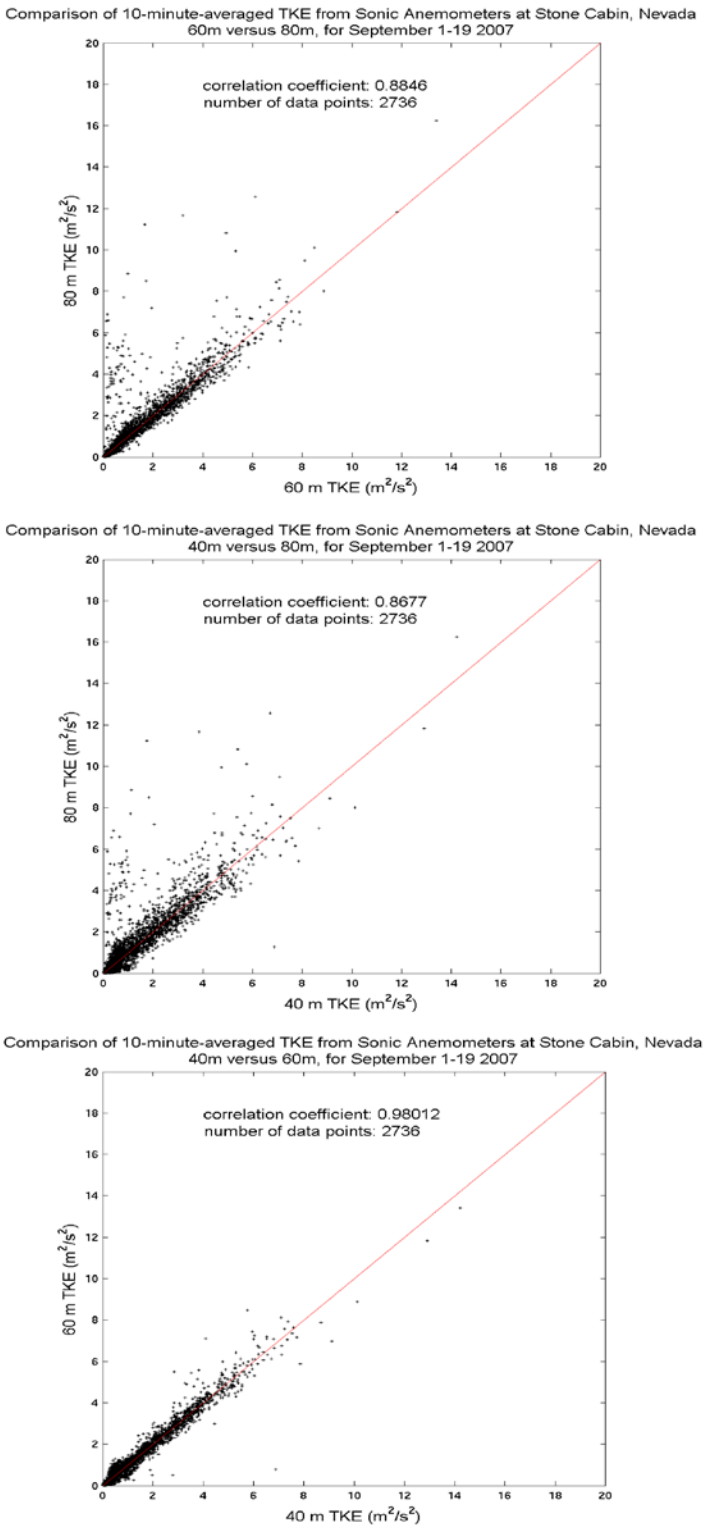

Figure 130. Scatterplots of sonic-measured 10-minute averaged turbulence kinetic energy for the period September 1-19, 2007 (top) 60 m vs. 80 m, (center) 40 m vs. 80 m, and (bottom) 40 m vs. 60 m.

The sample density and correlation coefficients are indicated.

7.2.1 Turbulence Kinetic Energy by Season

Most of the seasonal differences in the turbulence kinetic energy (TKE) are caused by convective activity in the spring and summer. While the results at 40 and 60 m are quite similar, the TKE at 80 m is noticeably greater where full-developed eddies could be expected. Notice a large "tail" (values greater than 5 m^2s^{-2}) in all seasons.

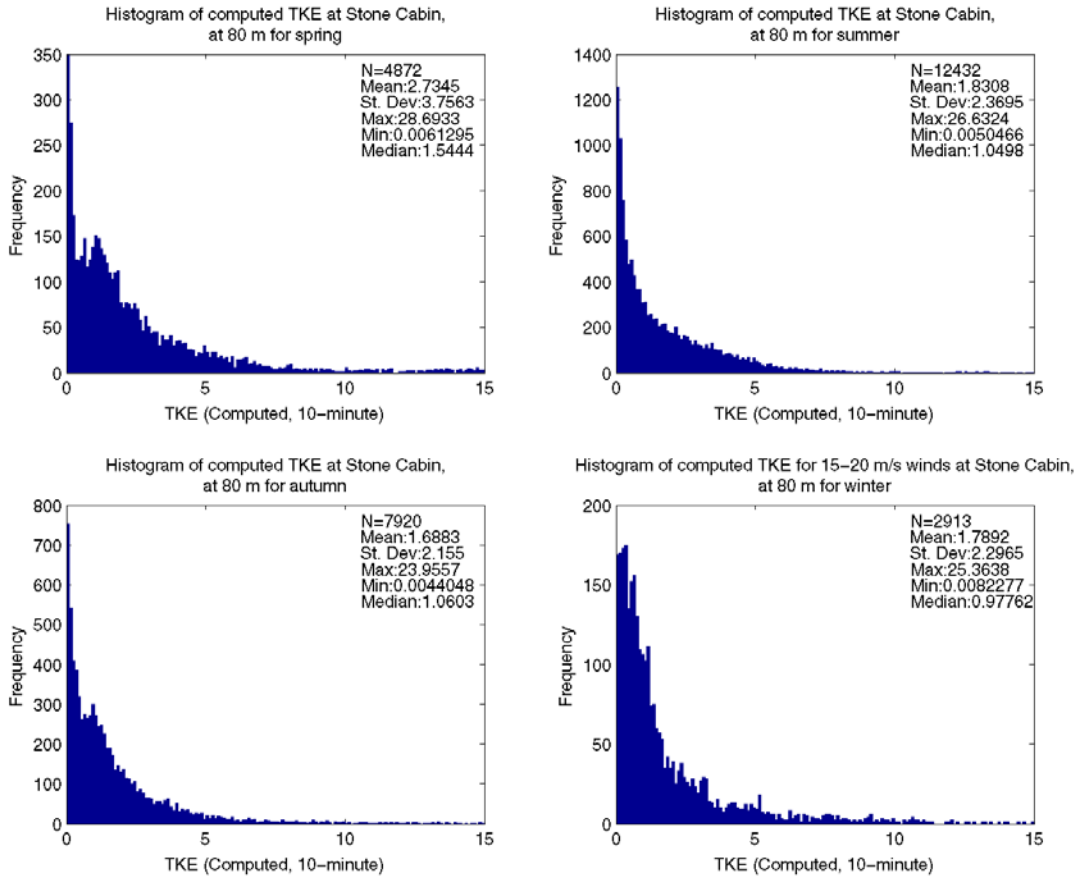

Figure 131. Histograms of the turbulence kinetic energy for calendar seasons computed from the sonic anemometer data for the period of 8 February to 20 September 2007 at 80 m.

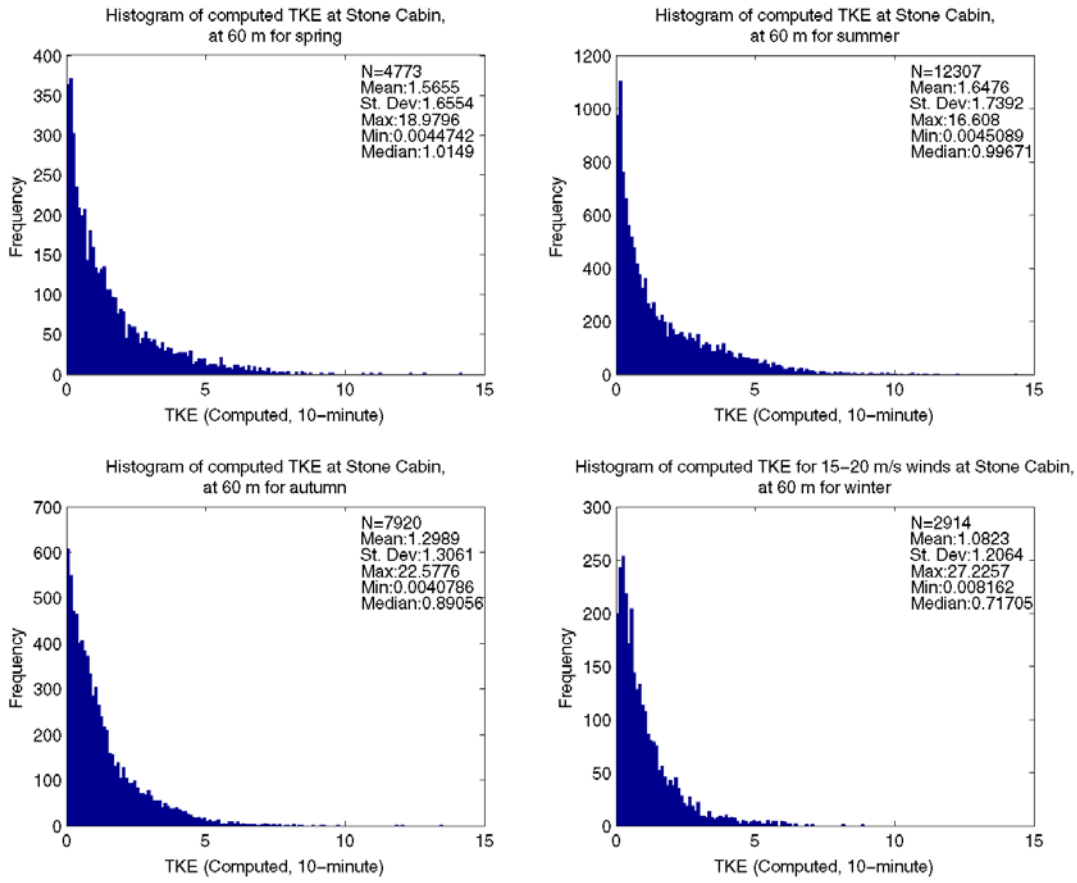

Figure 132. Histograms of the turbulence kinetic energy for calendar seasons computed from the sonic anemometer data for the period of 8 February to 20 September 2007 at 60 m.

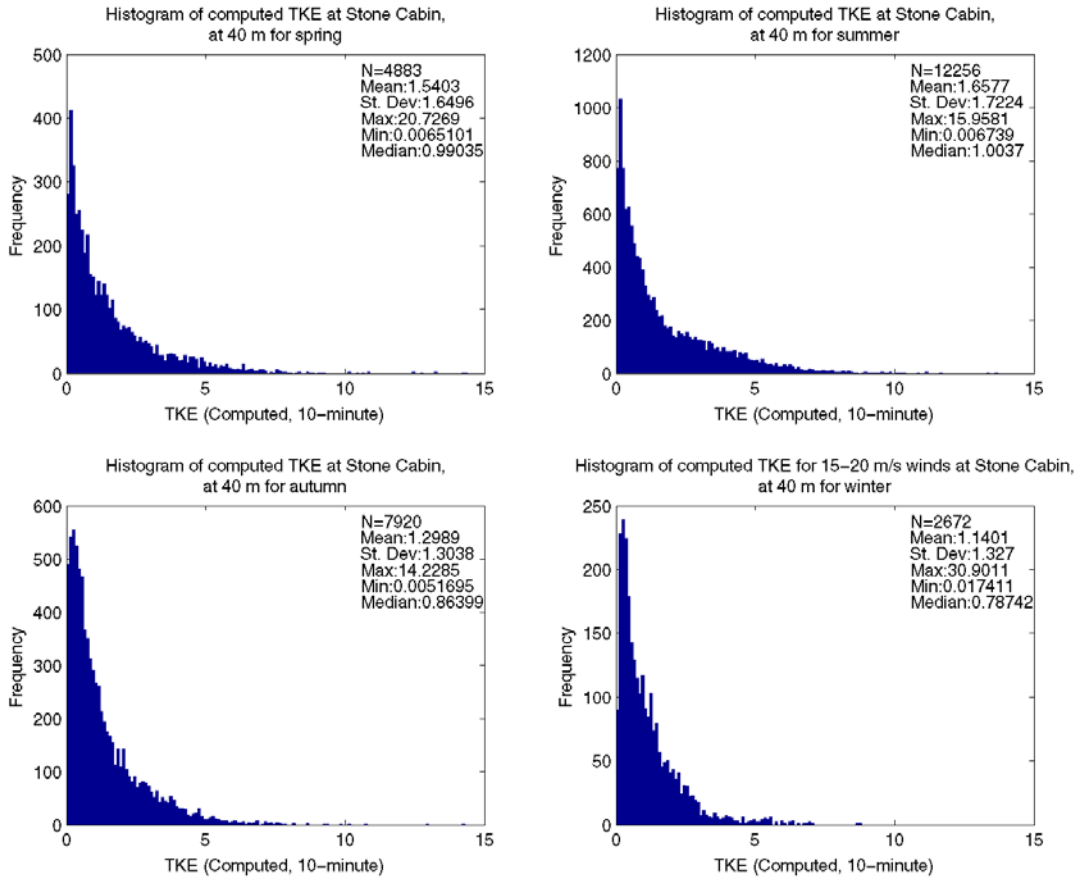

Figure 133. Histograms of the turbulence kinetic energy for calendar seasons computed from the sonic anemometer data for the period of 8 February to 20 September 2007 at 40 m.

8 Sub-km Evaluation

Task

In this section, we examine the effect of horizontal resolution on the accuracy of regional/mesoscale model predictions for the near surface (standard) height as well as hub heights. Data from tall towers will be used for the model evaluation.

Results and Status

Two mesoscale models, MM5 and WRF, were used for this task. The model setup consisted of 4 domains nested into a parent domain. The parent domain (Domain 1) consisted of 103×103 grid points in the horizontal with a grid resolution of 18 km. As for the nested domains, domain 2 consisted of 79×79 grid points in with a grid resolution of 6 km, domain 3 consisted of 121×112 grid points with a grid resolution of 2 km, domain 4 consisted of 148 ×100 grid points with a grid resolution of 666m, and domain 5 consisted of 34×34 grid points with a grid resolution of 222 m. Domains 1, 2, and 3 encompassed all of the meteorological tower locations listed in **Table 10;** domains 4 and 5 encompassed only the Tonopah and Stone Cabin wind towers,

respectively. The domain setup is shown in **Figure 134**. The atmosphere was divided into 40 unequally spaced layers. About half of them resolve the boundary layer processes in the lowest kilometer, of which the 10 layers from the ground were arranged at about 10 meter intervals in accordance with the meteorological tower measurements for verification.

Table 10. Meteorological Towers in Nevada[a].

Tower location	Coordinates Latitude; Longitude	Station Elevation (m)
Tonopah 24W [T]	38.3722º N; 117.4717º W	1535
Stone Cabin [SC]	38.1114º N; 116.7394º W	2004
Kingston 14 SE [K]	39.0455º N; 117.0008º W	1780
Luning 5 N [L5]	38.5725º N; 118.1755º W	1523
Luning 7W [L7]	38.54083º N; 118.2942º W	1354

[a] Winds are monitored at 10, 20, 30, 40, and 50 m at T, K, L5, L7 and at 40, 60, and 80 m at SC. SC has sonic anemometers installed.

For the initial and boundary conditions, which were composed of available synoptic observations ingested into the first-guess model fields archived, we used the Eta model outputs. The model physics were chosen accordingly to study the evolution of meteorological fields in the study region after a series of numerical experimentation. Similar physics options were chosen for MM5 and WRF. Briefly, the physics choices are: Gayno-Seaman scheme for boundary layer processes, Kain-Fritsch scheme and Reisner's scheme for convective and cloud microphysical processes, and Rapid Radiative Transfer Model calculations for radiative processes.

Model simulations with the same domain setup as shown in **Figure 134** have been carried out using MM5 and WRF for the period starting from 9 February 2007 at 1200 UTC to 11 March 2007 at 1200 UTC, and the modeled wind estimates and turbulence kinetic energy were compared against the meteorological tower observations at Stone Cabin. A preliminary sensitivity examination suggested that downscaling of meteorological variables from the parent domain into the nests at a later time (using an optional module known as 'NESTDOWN' in MM5) impacts the accuracy of the simulated winds over the complex terrain. In lieu of this, the simulations in all the domains have been started simultaneously. Also, a pre-forecast period of at least 12-24 hours was necessary for better accuracy in the high-resolution wind simulations.

The observed and MM5-simulated wind speed at 40, 60, and 80 m at the Stone Cabin tower location are shown in **Figures 135 and 136**. A first glance at the figures shows that there are significant differences in the results obtained on various grid resolutions. Moreover, there are also significant differences in the results using two mesoscale models. Notice that there are smaller differences among the various WRF grids compared to the MM5 grids. The significant high wind episodes were better simulated at sub-kilometer grids. Statistics derived using RMSE and index of agreement (IOA) (Willmott 1982; Wilks 1995) showed that, on average, the RMSE (**Table 11**) was about 4 m s^{-1}, and the skill of WRF simulated wind predictions is generally superior to MM5 by displaying a consistent trend of skill improvement and index of agreement as high as 0.65 (index of agreement 0 – worst and 1 is the best) at sub-kilometer grids. It is important to mention that the WRF results show improvement in the RMSE and IOA while using higher resolution (**Table 11**). The MM5 results do not show clearly this trend (**Table 11**).

Although the mesoscale models were not able to reproduce the high peaks of the TKE as computed from the sonic data (**Figures 138 and 139**), **Figure 137** indicates that the increased resolution had a tendency to generate few of the larger values compared to coarser grid resolution results.

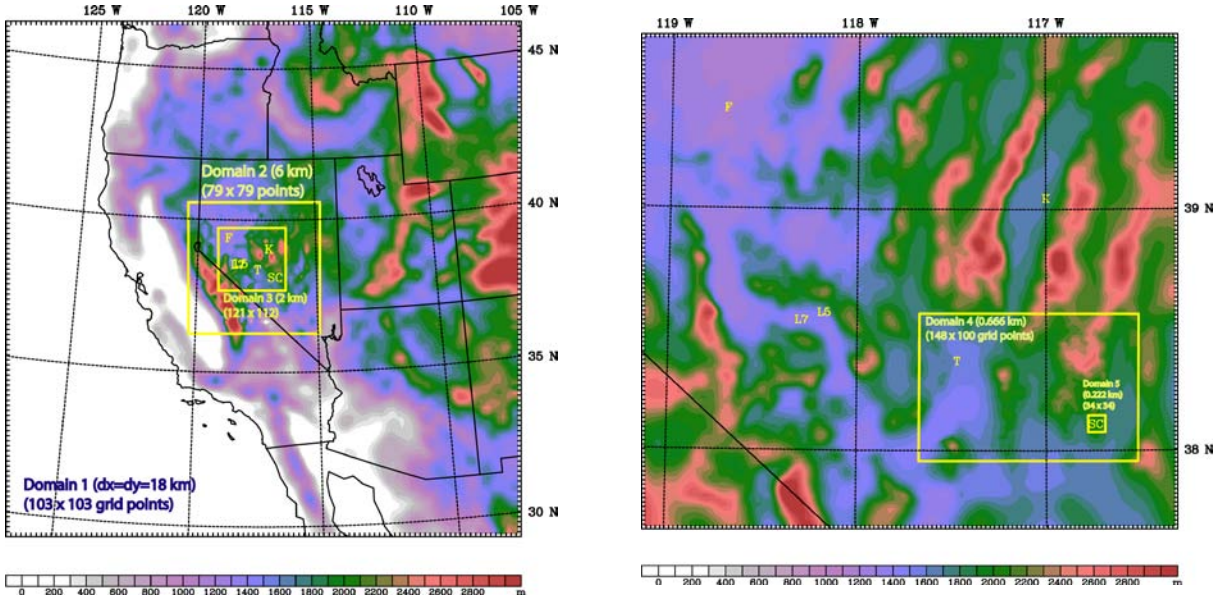

Figure 134. MM5 and WRF 5-domain setup. Meteorological towers located in the figure are: SC – Stone Cabin, T - Tonopah, K – Kingston, and L5, L7 – Luning (left) Domains 1, 2, and 3. (right) Domains 3, 4, and 5.

The frequency distribution simulated 40, 60, and 80-m wind speeds (**Figures 137 through 139**) is generally comparable with the observed distribution, following the generic Weibull distribution of scale and shape parameters (shown in **Table 12**) in the range 4.0-6.0 and about 1.7.

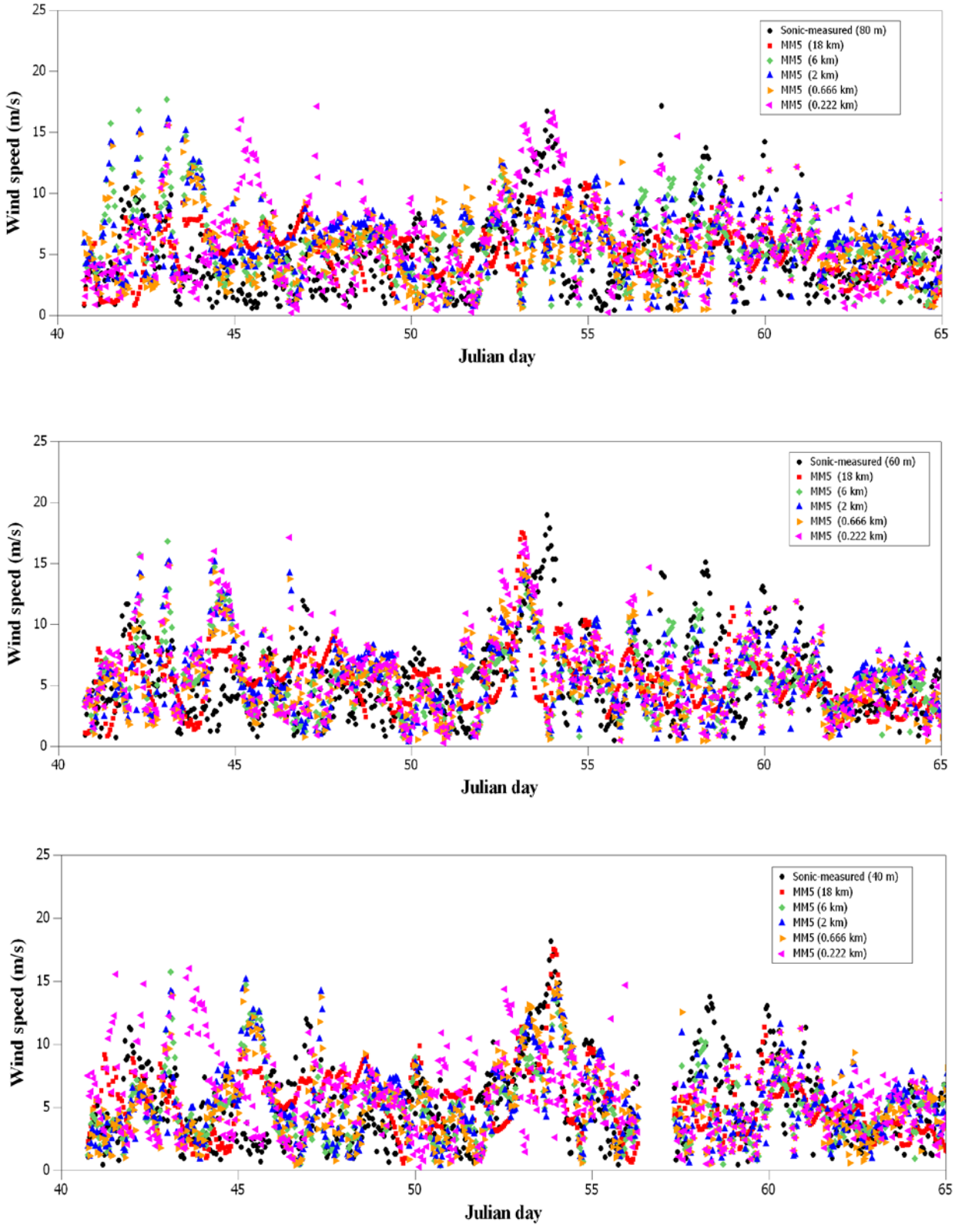

Figure 135. Observed (sonic anemometer wind measurements) and MM5-simulated wind speeds at Stone Cabin for the period of Julian days 40-65, (Julian day 40.5 = 9 Feb 2007 1200 UTC) (top) 80m, (center) 60 m, and (bottom) 40 m heights.

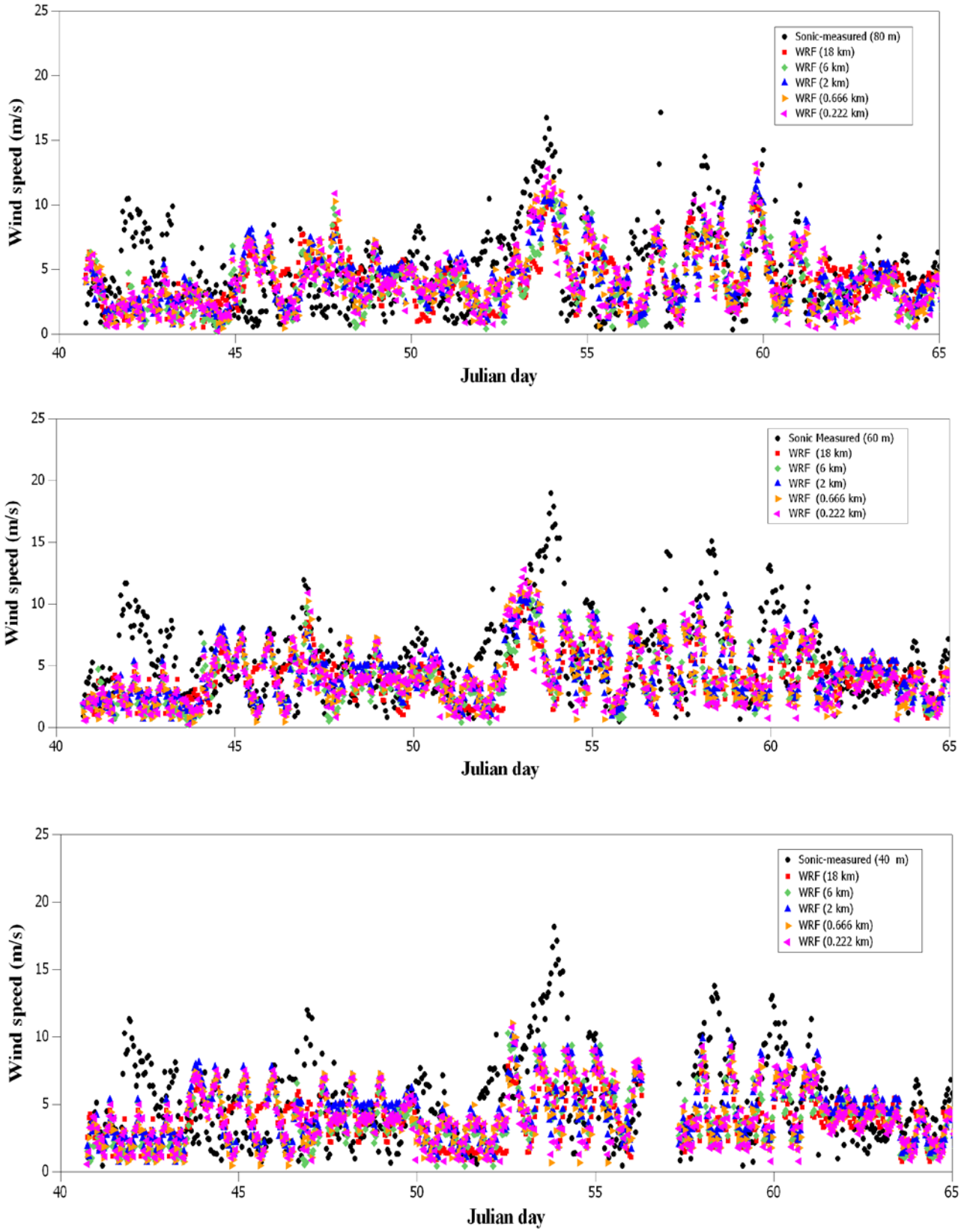

Figure 136. Same as Figure 135, but for WRF

Table 11. Wind Speed Statistics at Heights 40, 60, and 80 m Obtained from the Observed and MM5 and WRF Model Simulated Results at the Stone Cabin Tower Location for the Period 9 Feb 2007 12 UTC – 8 Mar 2007 12 UTC.[a]

Model grid resolution	MM5 (RMSE) Height=40 m	MM5 (Index of Agreement) Height = 40m	WRF (RMSE) Height = 40 m	WRF (Index of agreement) Height = 40m
18km	3.198	0.647	3.589	0.454
6 km	3.496	0.576	3.720	0.461
2 km	3.760	0.559	3.603	0.472
0.666 km	3.653	0.587	3.679	0.474
0.222 km	4.498	0.448	3.638	0.494

Model grid resolution	MM5 (RMSE) Height = 60m	MM5 (Index of Agreement) Height = 60m	WRF (RMSE) Height = 60m	WRF (Index of agreement) Height = 60m
18km	3.619	0.530	3.736	0.490
6 km	4.006	0.450	3.748	0.539
2 km	4.252	0.434	3.628	0.533
0.666 km	4.169	0.451	3.643	0.564
0.222 km	4.336	0.457	3.656	0.567

Model grid resolution	MM5 (RMSE) Height = 80m	MM5 (Index of Agreement) Height = 80m	WRF (RMSE) Height = 80m	WRF (Index of agreement) Height = 80m
18km	3.542	0.460	3.293	0.536
6 km	4.069	0.420	3.318	0.587
2 km	4.399	0.381	3.201	0.604
0.666 km	4.321	0.358	3.131	0.643
0.222 km	4.005	0.582	3.128	0.650

[a] The index of agreement indicates the quantitative measure of model performance (= 0, worst skill; = 1, best skill). RMSE = Root-mean square error.

8.1 Distribution Analysis for Sonic and Standard Anemometer Wind Speeds and Those Simulated by MM5 and WRF at Stone Cabin

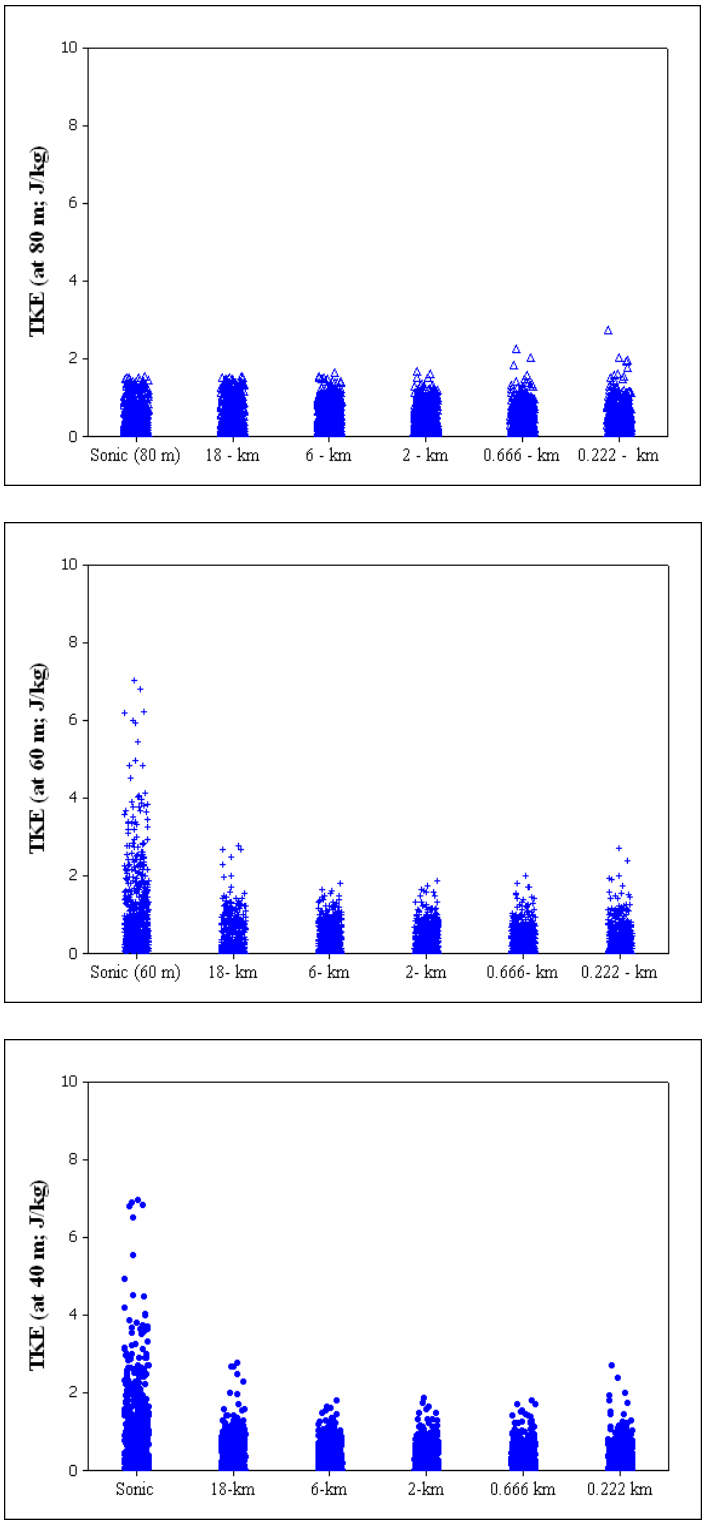

Figure 137. Individual value plots of sonic-measured 10-minute averaged turbulence kinetic energy and model simulated at various horizontal grid resolutions for the period Feb 9-Mar 8, 2007 (top) 80 m, (center) 60 m, and (bottom) 40 m.

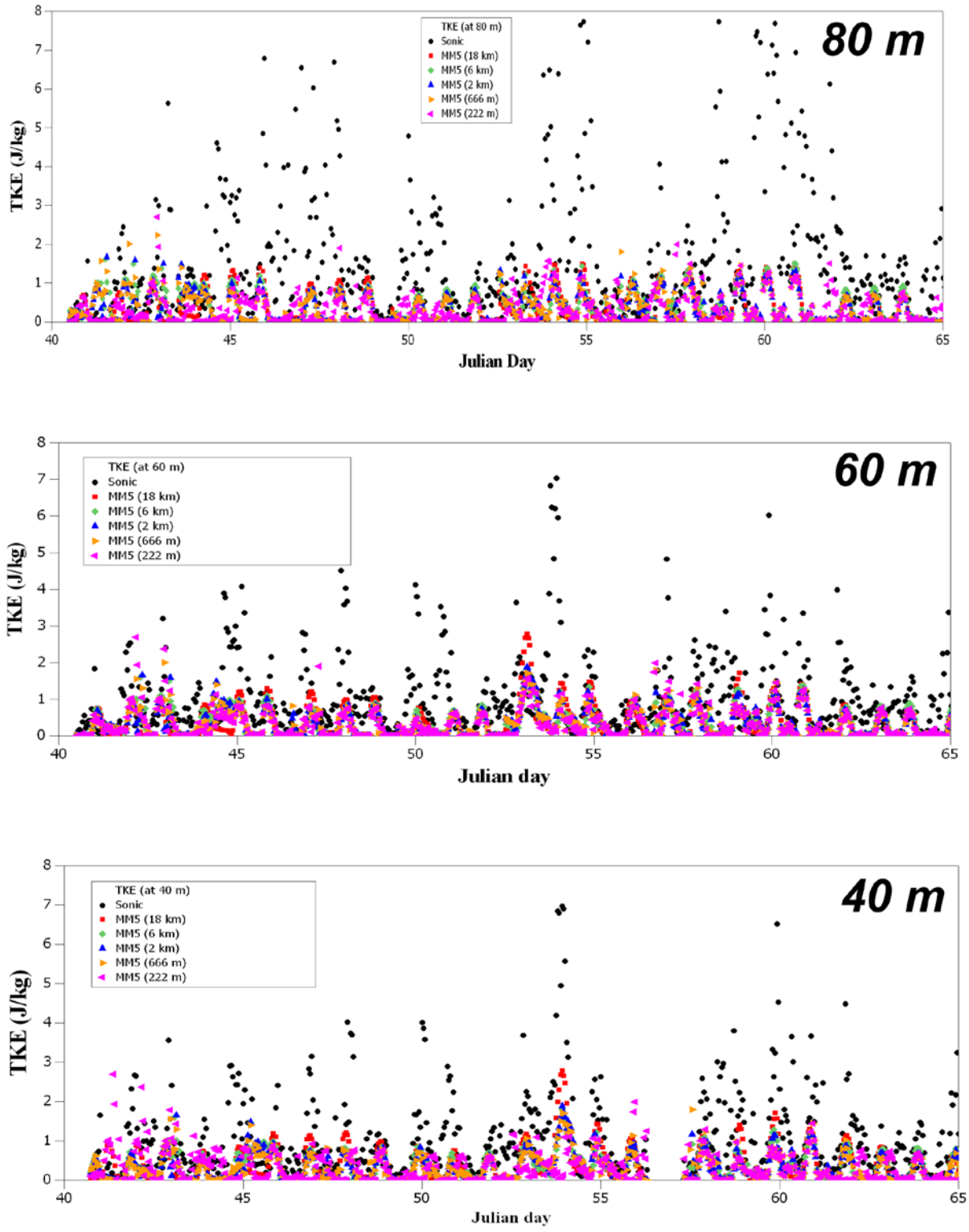

Figure 138. Observed (sonic anemometer) and MM5-simulated turbulence kinetic energy at Stone Cabin for the period of Julian days 40-65. (Julian day 40.5 = 9 Feb 2007 1200 UTC) (top) 80 m, (center) 60 m, and (bottom) 40 m heights.

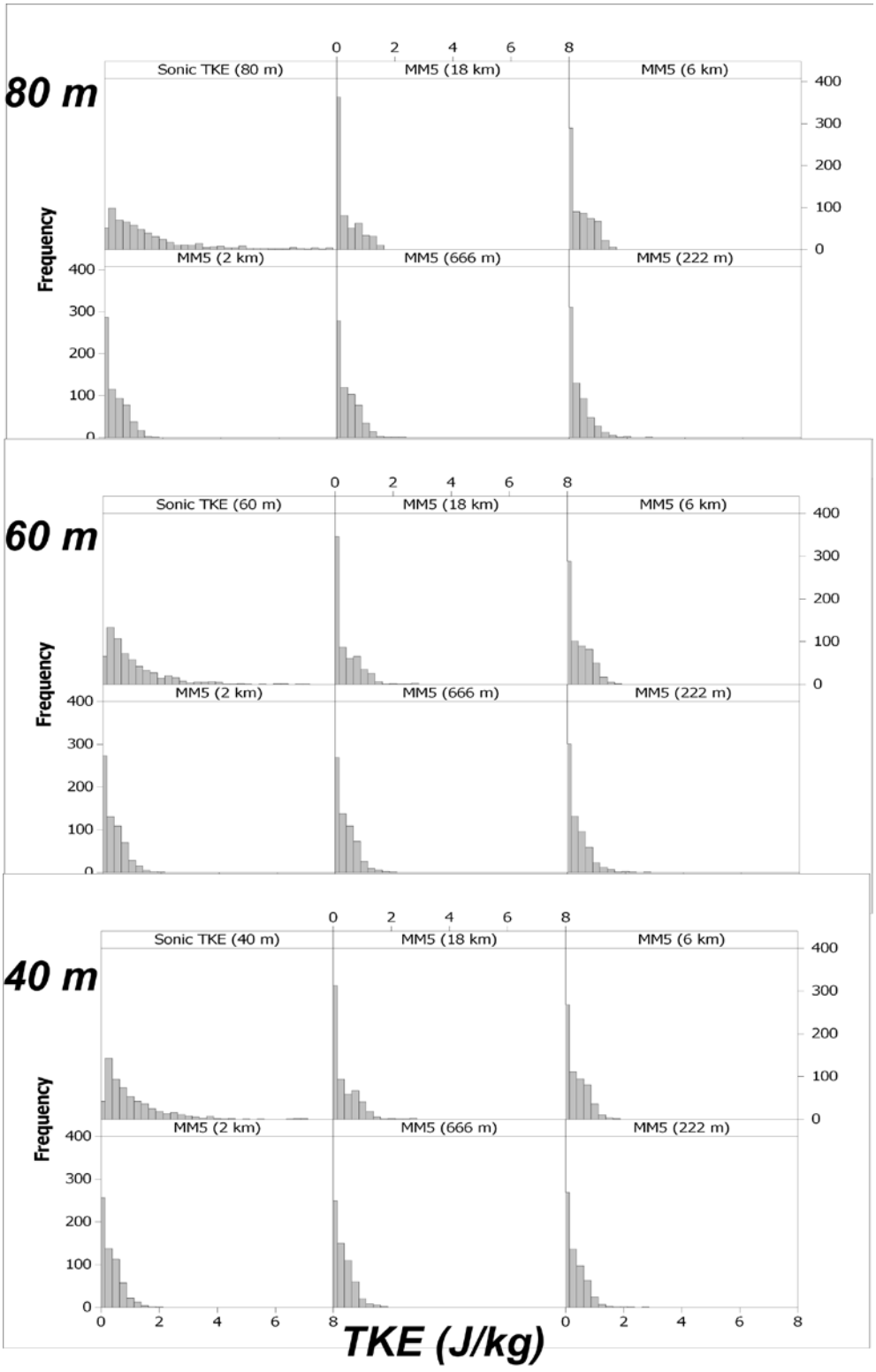

Figure 139. Frequency distribution of sonic-observed and MM5-simulated (at different horizontal grid resolutions 18 km, 6 km, 2 km, 0.666 km, and 0.222 km) turbulence kinetic energy at 80 m

8.1.1 Application of the Weibull Distribution

Weibull distributions often describe the distribution of instantaneous wind speed measurements over a period of time. The generic form of a Weibull distribution is a continuous probability distribution with probability density function *f*' as follows:

$$f(x;\alpha,\beta) = \frac{\beta}{\alpha^{\beta}} x^{\beta-1} exp\left[-\left(\frac{x}{\alpha}\right)^{\beta}\right]$$

where *x* greater than or equal to zero, and f (*x*; α, β) = 0 for *x* < 0. α is the scale parameter and β is the shape parameter of the distribution. β generally varies between 1 and 3 (mathematically, β could assume any value for describing wind speed distributions, however this narrow interval is of practical significance). Typically β indicates the dominance of the wind regimes, *i.e.*, β = 1 (β = 3) indicates a low (high) wind speed regime. For wind analysis, the Rayleigh distribution (a special case of Weibull distribution where β = 2) typically represents moderate wind regimes. The scale parameter α stretches or contracts the distribution along the x-axis in accordance with β. Higher values of α indicate that the wind speeds are less tightly clustered or well spread about the mean. Thus, the shape and scale parameters together give a statistical spectrum of wind speeds over a period of time.

Weibull curves were fit to hourly wind speed data sets simulated by MM5 and WRF, and measured by the sonic anemometers at Stone Cabin over for the time period of 9 February 2007 at 12 UTC to 8 March 2007 at 12 UTC. The model data sets were obtained from various horizontal grid resolutions (Δx = Δy =18 km, 6 km, 2 km, 0.666 km, and 0.222 km). **Figures 140 to 142** show the frequency distribution of the wind speed data with Weibull curves fit to them. The values of α and β obtained for the simulated time series of wind speeds correspond to the values obtained for sonic measurements. On average, the shape parameters of the observed and simulated wind regimes for the considered time period (**Table 12**) follow very close to the Rayleigh distribution. The scale parameters obtained from WRF simulated wind speeds were significantly smaller than the obtained from MM5; however, MM5 is closer to the sonic scale parameter than WRF. The higher wind regimes as seen in sonic measurements were mostly better captured by the model's finest grid resolution than from the coarse grid resolutions.

Two different metrics (at each of the three heights) have been devised to delve further into the differences between the MM5, WRF, and sonic wind speed data. The "relative difference product" (RDP) uses both shape and scale differences from the corresponding sonic shape and scale parameters to indicate a cumulative difference of model simulated and observed. The "squared difference" (SD) focuses on the difference in shape parameter of each model to a standard shape parameter. In **Figure 144**, the standard shape parameter is the corresponding sonic shape parameter; in **Figure 145** the standard shape parameter is the Rayleigh shape parameter (β = 2). Both sets of figures yield to a general finding that MM5 agrees with the sonic data better than the agreement of WRF with the sonic data at 40 m and 60 m, and also that the situation is reversed (the agreement of WRF is better) at 80 m. **Figure 143** illustrates that RDP shows substantial better overall (α and β) skill by MM5 at 40 and 60 m, and somewhat less skill at 80 m. **Figure 144**, which illustrates SD, mimics this finding, with not as big a gap in skill between the models. Comparison by SD with the Rayleigh shape parameter (**Figure 145**) show that, while the trends are very similar to the previous three figures, the differences are smaller, showing that both of the models' results tend towards the Rayleigh distribution more than the

sonic data does. There is a slight trend towards increased skill in these metrics at finer horizontal grid resolutions, which is also evidenced in other skill measure such as the index of agreement.

Figure 146 shows a comparison of data from the two anemometer types using Weibull fitting (for a more detailed comparison of sonic versus standard anemometers, please see Section 4). One item of interest stands out clearly. Because standard anemometers need to overcome their own inertia to start spinning, they register more zero ms^{-1} readings: they do not have the sensitivity to pick up very low wind speeds. This lack of low wind speed sensitivity is reflected in the differences between the shape parameters. The high number of zero wind speed readings of the standard anemometers moves the Weibull shape to the left—that is, towards lower values, or a lower wind speed regime. At each height, this same difference is illustrated. The sonic anemometers pick up the lowest wind speeds while the standard anemometer cannot. Hence in this case the Weibull curve generated by the sonic data gives a better description of the overall wind regime than that from the standard anemometer data.

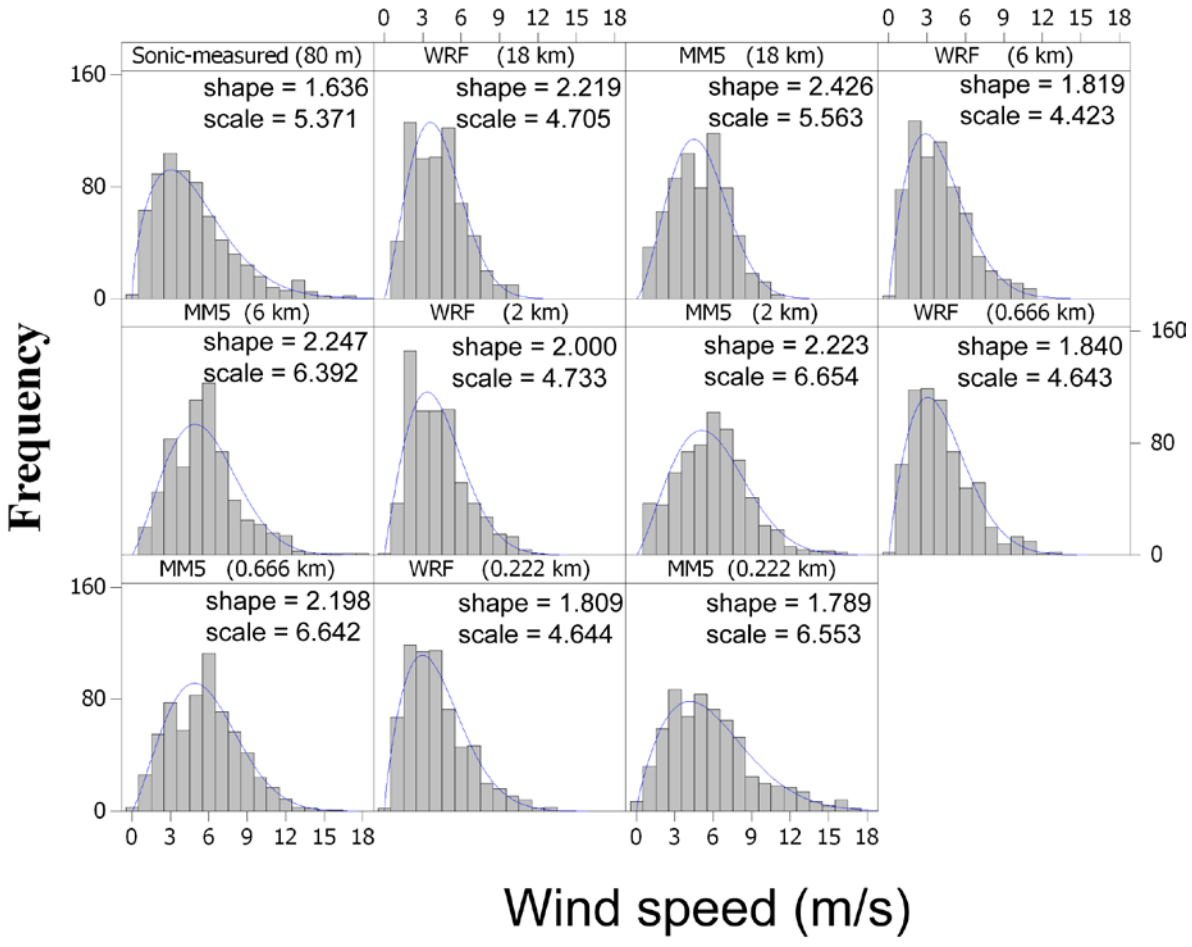

Figure 140. Frequency distribution of sonic-observed and MM5/WRF-simulated (at different horizontal grid resolutions 18 km, 6 km, 2 km, 0.666 km, and 0.222 km) wind speeds at 80 m. The Weibull curves are fit using Minitab 14. The shape and scale parameters are indicated.

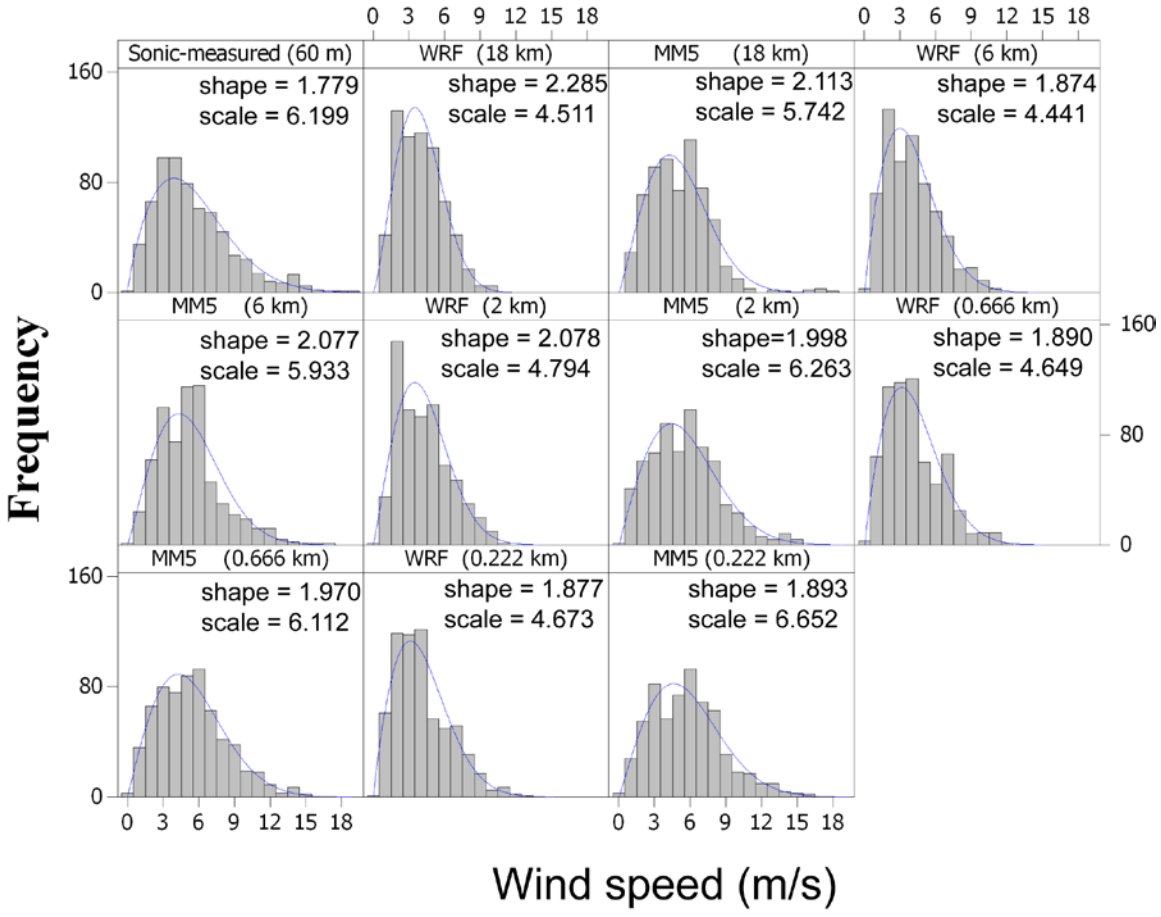

Figure 141. Frequency distribution of sonic-observed and MM5/WRF-simulated (at different horizontal grid resolutions 18 km, 6 km, 2 km, 0.666 km, and 0.222 km) wind speeds at 60 m. The Weibull curves are fit using Minitab 14. The shape and scale parameters are indicated.

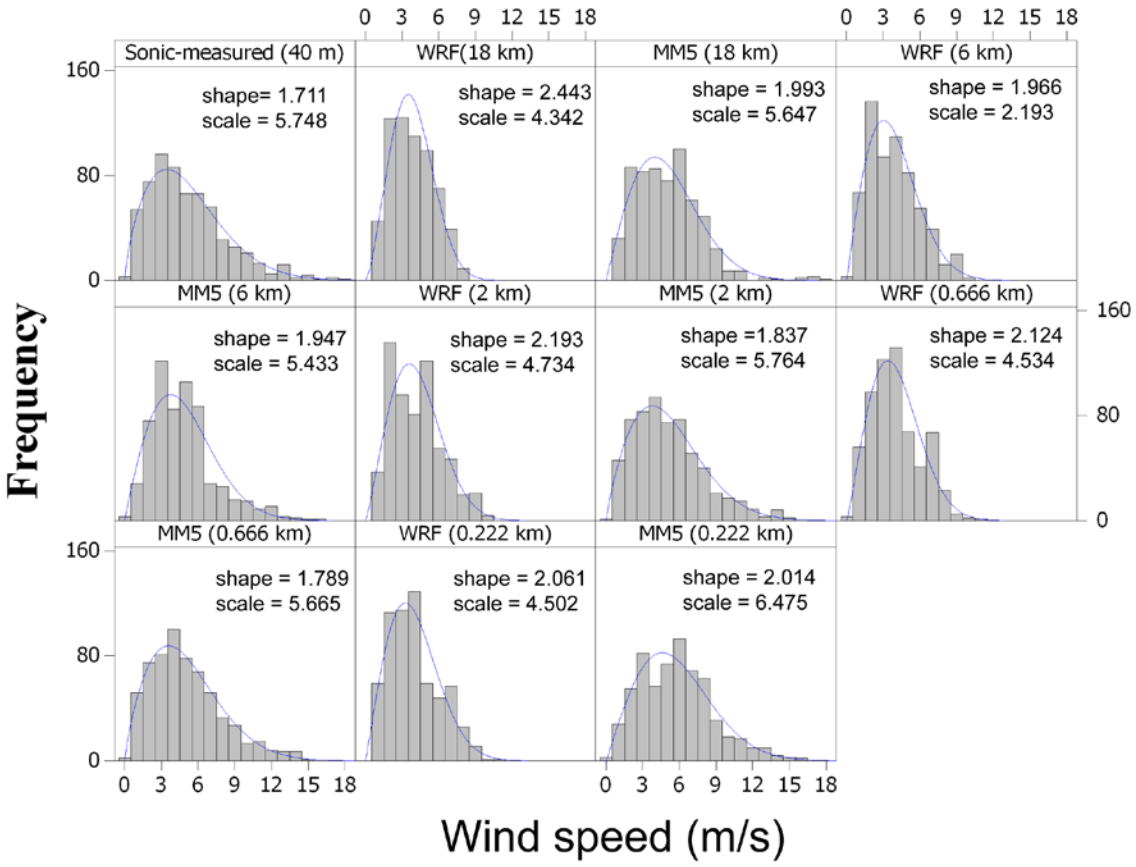

Figure 142. Frequency distribution of sonic-observed and MM5/WRF-simulated (at different horizontal grid resolutions 18 km, 6 km, 2 km, 0.666 km, and 0.222 km) wind speeds at 40 m.

The Weibull curves are fit using Minitab 14. The shape and scale parameters are indicated.

Table 12. Weibull Shape and Scale Parameters for MM5, WRF, and Sonic Anemometer Data

Weibull fitted Shape and Horizontal Scale Parameters For MM5, WRF, and sonic anemometer wind speed data (grid resolutions used in MM5/WRF = 18 km, 6 km, 2 km, 0.666 km, 0.222 km) at 40 m, Stone Cabin, NV, 9 Feb-8 Mar 2007					
	shape	scale		shape	scale
Sonic-40 m	1.711	5.748	Sonic-40 m	1.711	5.748
MM5 18 km	1.993	5.647	WRF 18 km	2.433	4.342
MM5 6 km	1.947	5.433	WRF 6 km	1.966	4.318
MM5 2 km	1.837	5.764	WRF 2 km	2.193	4.734
MM5 0.666 km	1.789	5.665	WRF 0.666 km	2.124	4.534
MM5 0.222 km	2.014	6.475	WRF 0.222 km	2.061	4.502
Mean (MM5)	1.916	5.797	Mean (WRF)	2.155	4.486
at 60 m					
	shape	scale		shape	scale
Sonic-60 m	1.779	6.199	Sonic-60 m	1.779	6.199
MM5 18 km	2.113	5.742	WRF 18 km	2.285	4.511
MM5 6 km	2.077	5.933	WRF 6 km	1.874	4.441
MM5 2 km	1.998	6.263	WRF 2 km	2.078	4.794
MM5 0.666 km	1.97	6.112	WRF 0.666 km	1.89	4.649
MM5 0.222 km	1.893	6.652	WRF 0.222 km	1.877	4.673
Mean (MM5)	2.010	6.140	Mean (WRF)	2.001	4.614
at 80 m					
	shape	scale		shape	scale
Sonic-80 m	1.636	5.371	Sonic-80 m	1.636	5.371
MM5 18 km	2.426	5.563	WRF 18 km	2.219	4.705
MM5 6 km	2.247	6.392	WRF 6 km	1.819	4.423
MM5 2 km	2.223	6.654	WRF 2 km	2	4.733
MM5 0.666 km	2.198	6.6424	WRF 0.666 km	1.84	4.643
MM5 0.222 km	1.789	6.553	WRF 0.222 km	1.809	4.644
Mean (MM5)	2.177	6.361	Mean (WRF)	1.937	4.630

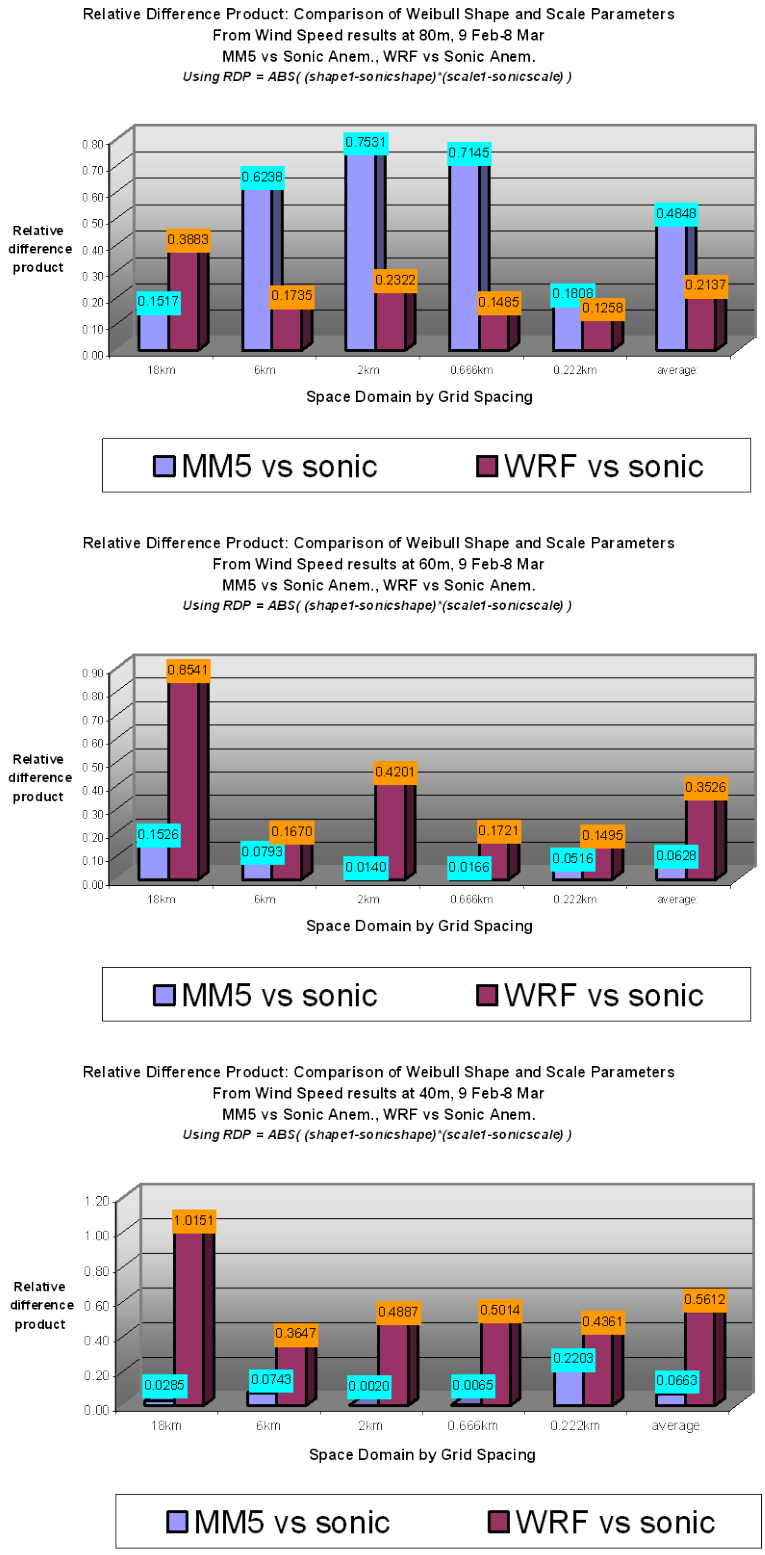

Figure 143. Relative Difference Product (RDP) comparison of shape and scale parameters at (top) 80m, (center) 60 m, and (bottom) 40 m

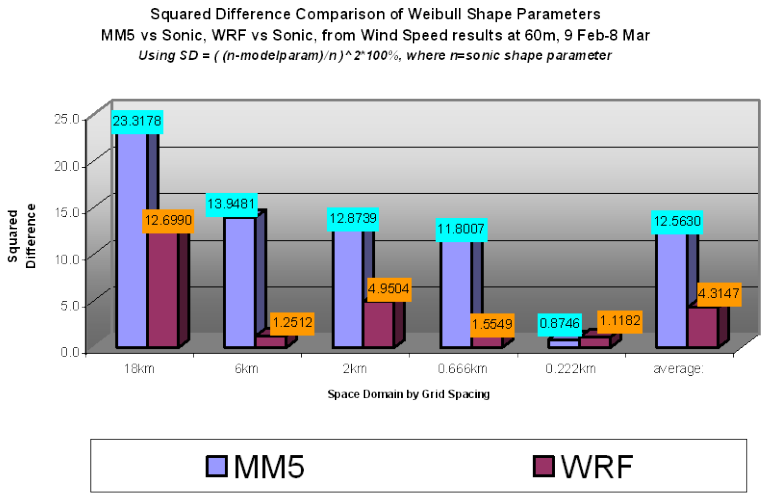

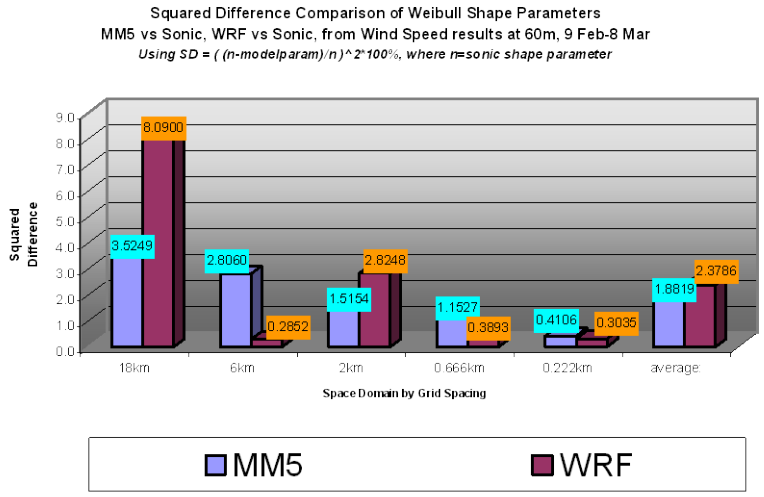

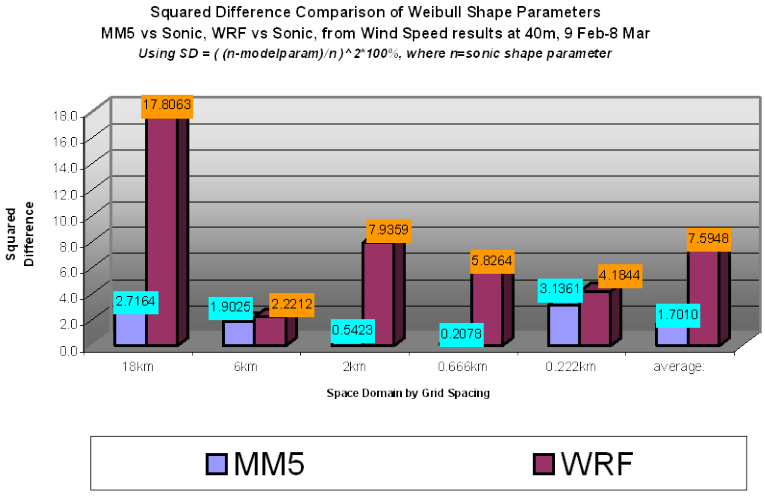

Figure 144. Same as Figure 143, but for SDs

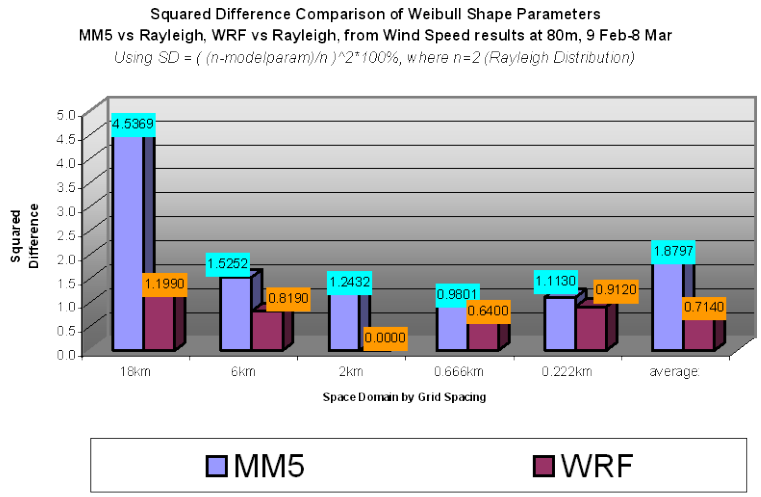

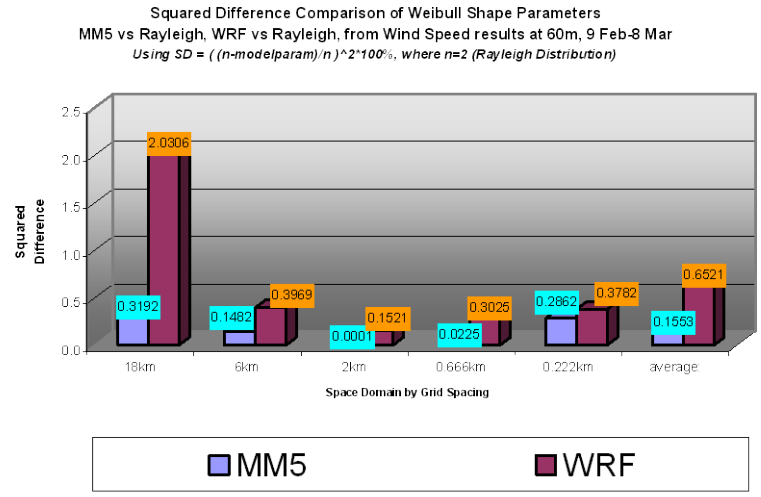

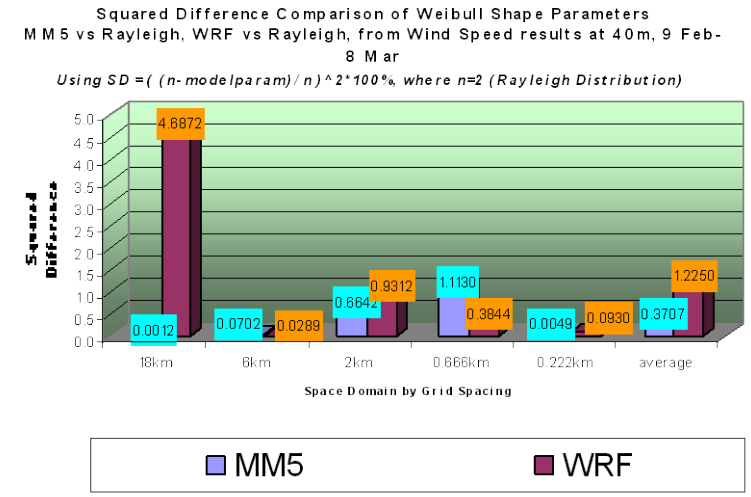

Figure 145. Same as Figure 143, but for the SD comparison using model results against the Rayleigh distribution shape parameter β=2

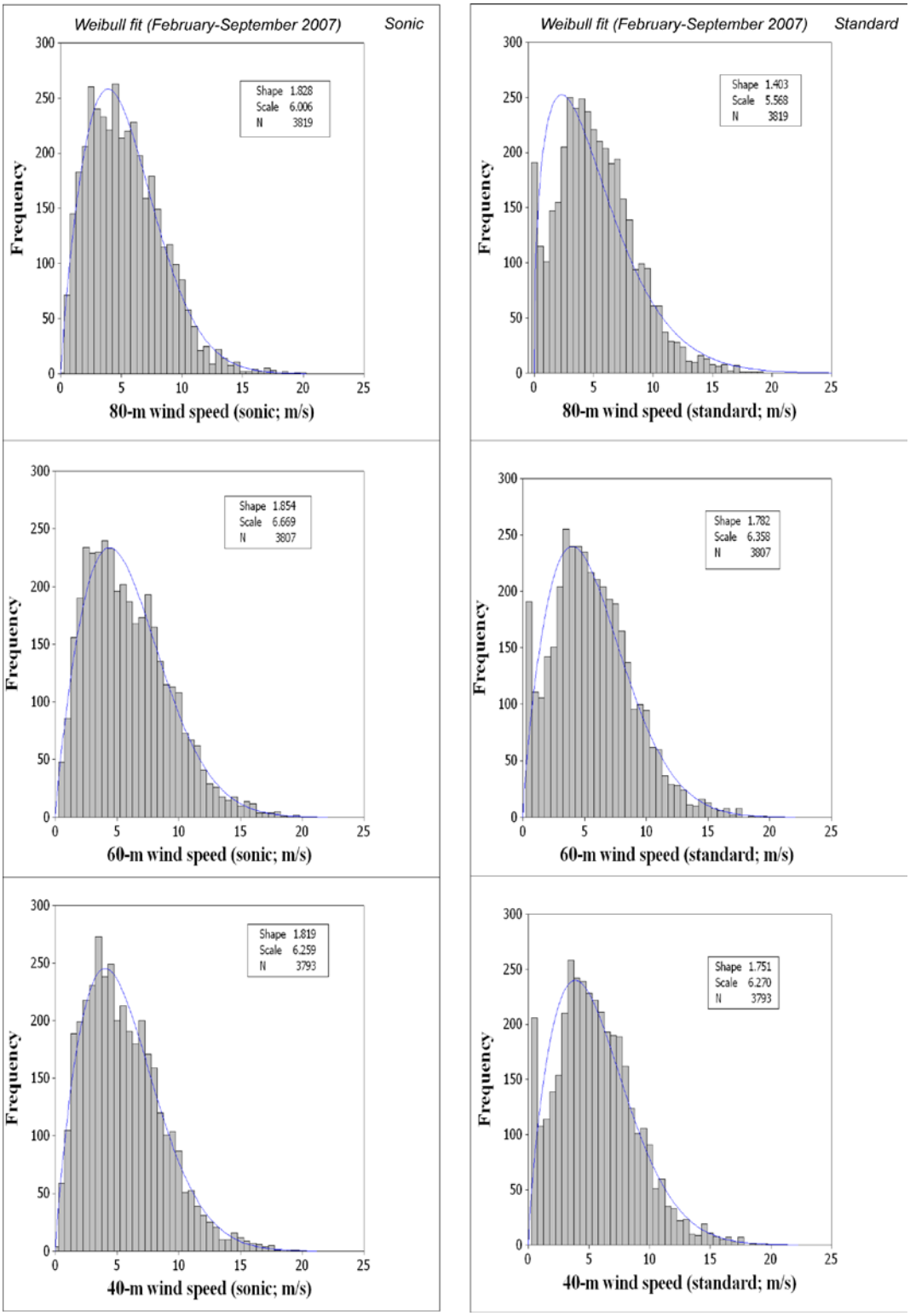

Figure 146. Weibull fit of 10-minute averaged sonic (left) and standard (right) anemometer measured wind speeds (m s^{-1}) at 40 m (bottom), 60 m (center), and 80 m (top) for the period February-September 2007.

N = number of samples used. The shape and scale parameters are indicated in each of the boxes.

8.2 Statistical Bootstrapping

The statistical bootstrap (also referred to as the resampling procedure) is one of the methods that can be used to calculate estimates of a certain number of unknown parameters of a random process or a signal observed in noise, based on a random sample. Such situations are common in signal processing and the bootstrap is especially useful when only a small sample is available or an analytical analysis is too cumbersome or even impossible. With the bootstrap, the random pairs of observations and model simulated results of the time series are reassigned, and estimates are recomputed. These are done thousands of times and treated as repeated experiments. The Bootstrap Toolbox is a set of Matlab functions consisting of procedures for resampling, hypothesis testing, and confidence interval estimation. In this study, the estimates are correlation coefficients and index of agreement were computed using random experiments for a sample pair size of 642. The repeated experiments were conducted for correlation coefficients for 20000 times, and for 1000 times for index of agreement.

Bootstrapped frequency distribution of correlation coefficients is plotted for sonic measurements against MM5 and WRF simulated wind speeds at various horizontal grid resolutions at heights 40, 60 and 80 m above ground level at the Stone cabin location. This is shown in **Figure 147**. The correlation coefficients show a consistent trend of improvement with height as well as for decreasing the grid resolutions for WRF simulated wind speeds as compared to MM5. Better correlation coefficients were in the range 0.3-0.4 at 80 m. Another random experiment was conducted using the estimator index of agreement at 80 m (**Figure 148**) showed significant improvement of skill by grid refinement at sub-kilometer grid resolutions. The skill of MM5 (WRF) is improved from 0.45 to 0.6 (0.5 to 0.65) by grid refinement from 18 km to 222 m.

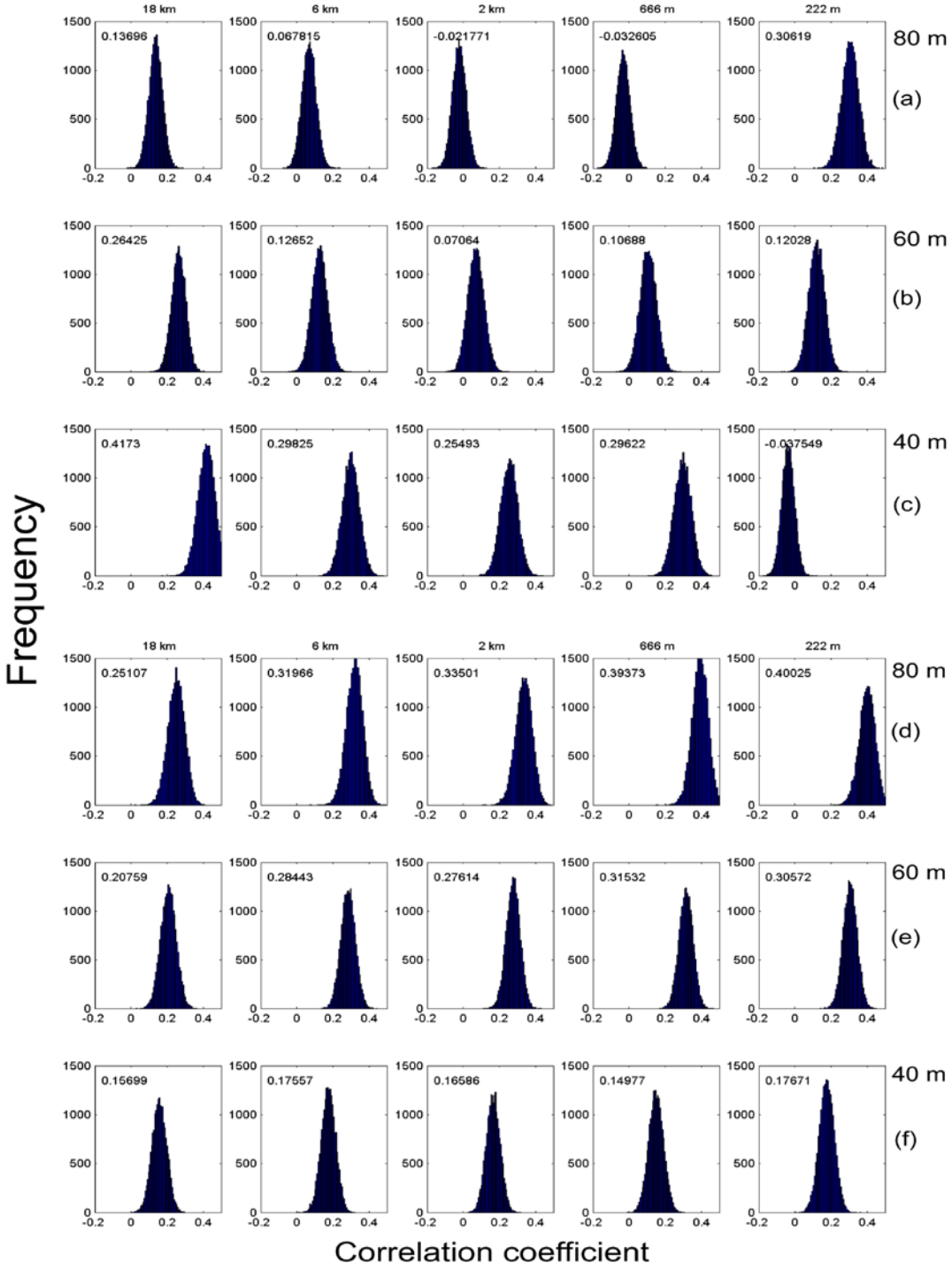

Figure 147. Resampled frequency distribution of correlation coefficients for the MM5/WRF-simulated wind speeds against sonic anemometer measurements.

MM5 (a: 80 m, b: 60 m, and c: 40 m) and WRF (d: 80 m, e: 60 m, and f: 40 m). The number of pairs at each of the heights is 642, and the resampling size is 20,000. The mean of the distribution is indicated in each of the boxes.

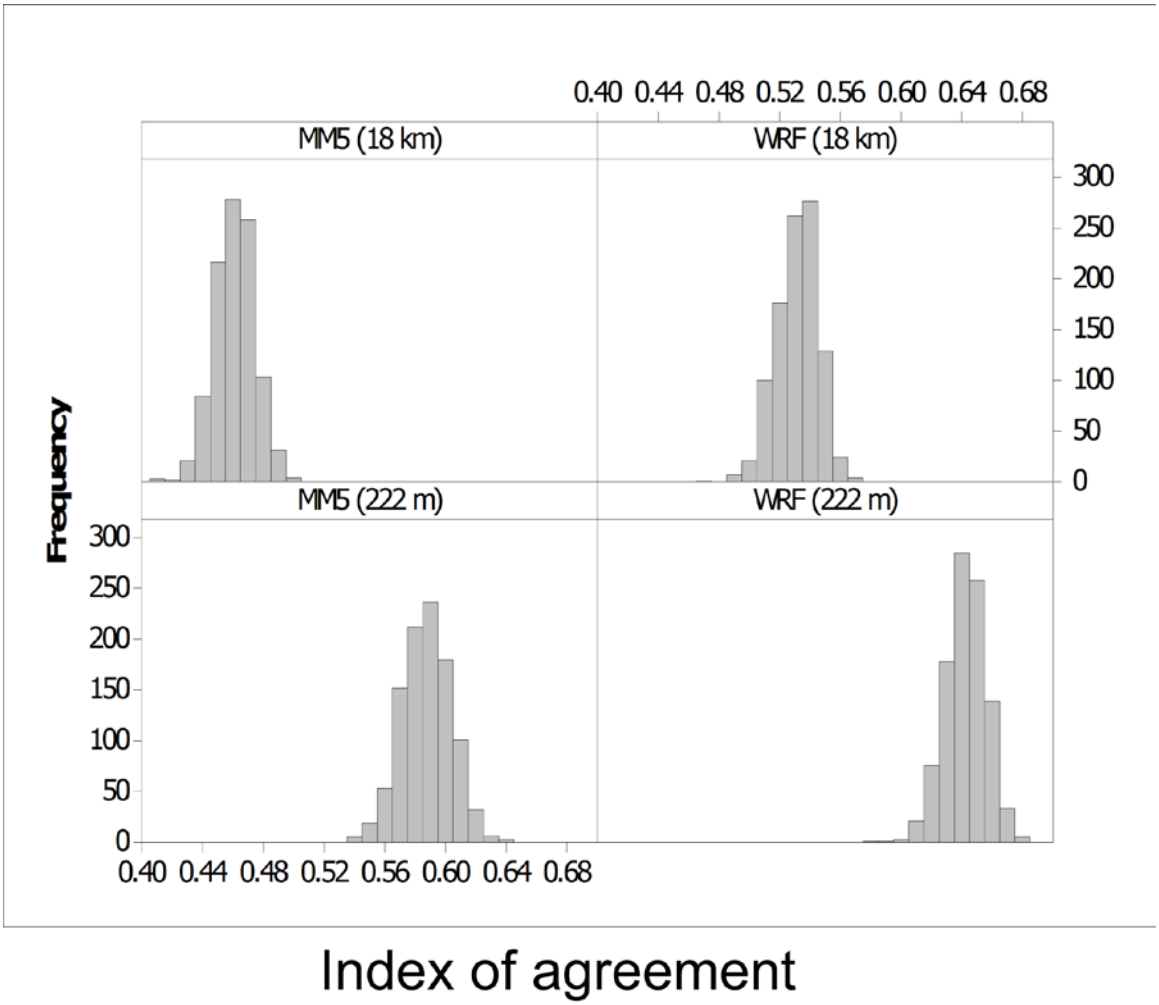

Figure 148. Resampled frequency distribution of index of agreements for the MM5/WRF-simulated 80m wind speeds at the coarsest (18 km) and the finest (222 m) horizontal grid resolutions against sonic anemometer measurements.

The size of the pairs is 642, and the resampling size is 1,000.

8.3 Spectral Analysis of Wind Speeds

A time series record often exhibits multiple periodic components. According to Parseval's Theorem, the total power computed for the time series in the time domain must be equal the total power computed in the frequency domain. The *power spectrum* gives the power in the signal at each frequency. The power of the time series is computed by simply applying the discrete Fourier transform to the given time series and, by convention, the transform has elements equally spaced in frequency, with the first element corresponding to zero frequency (theoretically infinite period), then up to the Nyquist frequency (the critical frequency; the frequency greater than half of the sampling frequency) at the middle of the record. Our interest is to see whether the observed and simulated time series of wind speeds at the height of the measurements exhibit periodicity for the diurnal cycle.

The power spectrum was computed for sonic observed and model simulated wind speeds at various horizontal grid resolutions, and is shown in **Figure 149**. The sampling period was during 9 February 2007-8 March 2007. The spectrum is normalized by the maximum value of the power spectrum so that the range lies between 0 and 1. The x-axis in Figure 6-16 represents the period in hours/cycles by inverting the frequency. The power spectrum shows a periodicity at 24 hours indicating that the observed and modeled time series exhibit a diurnal cycle distinctly. The WRF results on all grid resolutions better track periodicity computed from the measurements compared to the MM5 results. Notice that MM5 significantly overestimated mid-range values (between 15 and 24 hours), especially on high-resolution grids at 40 m.

Figure 150 shows a power spectrum of the turbulence kinetic energy (TKE) computed from the MM5 results and sonic data. Notice that this version of WRF did not provide direct output of the TKE. Although the model was able to reproduce daily TKE maximum, some of the results obtained on higher resolution grids overestimated sub-daily periodicity (15-24 hrs) and underestimated periodicity for larger periods.

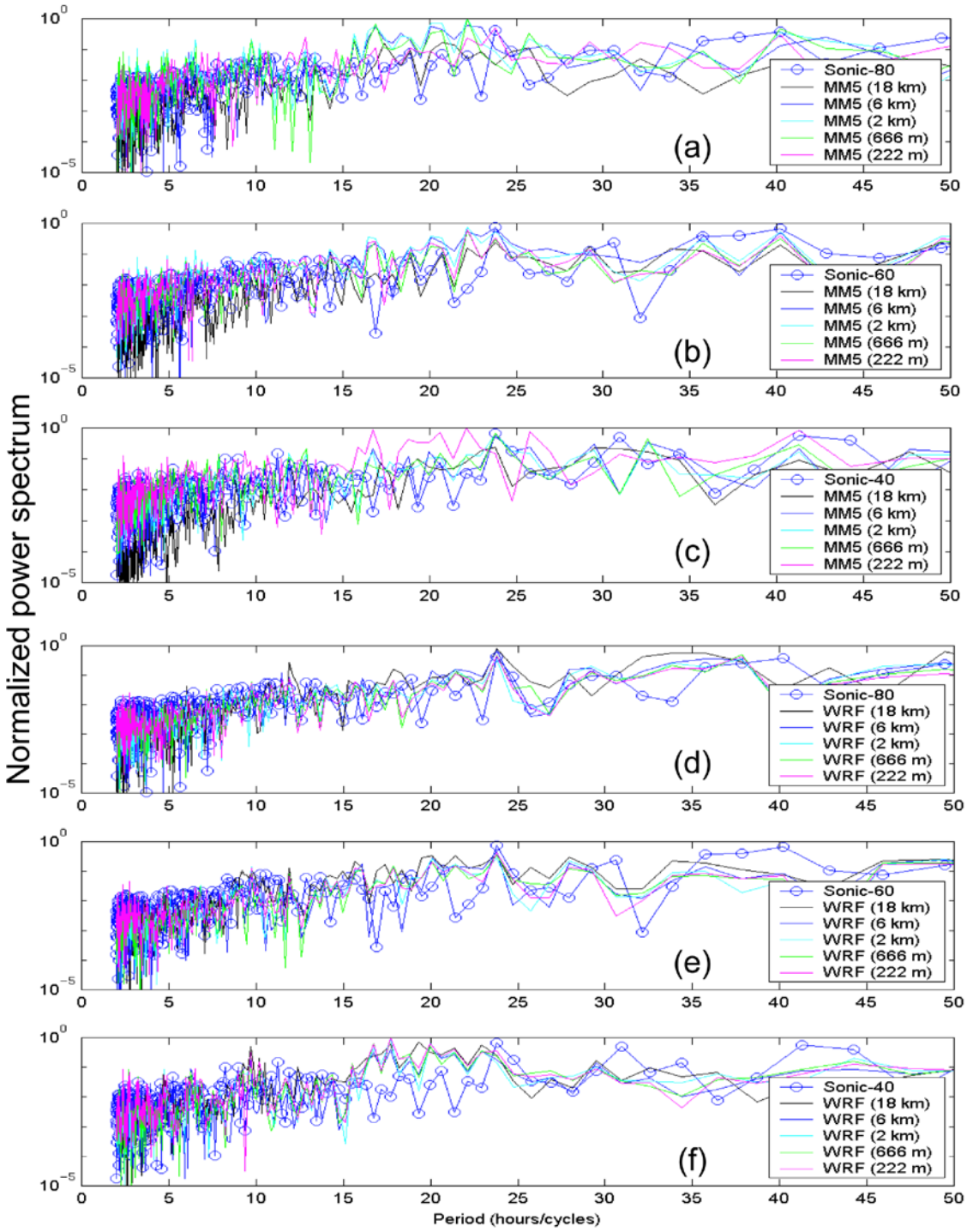

Figure 149. Power spectrum of sonic-measured (blue circle-dash) and MM5/WRF-simulated wind speeds at 40, 60, and 80 m obtained from different model horizontal grid resolutions.

MM5 (a: 80m, b: 60 m, and c: 40 m), and WRF (d: 80 m, e: 60 m, and f: 40 m). The power spectrum is normalized by the maximum value.

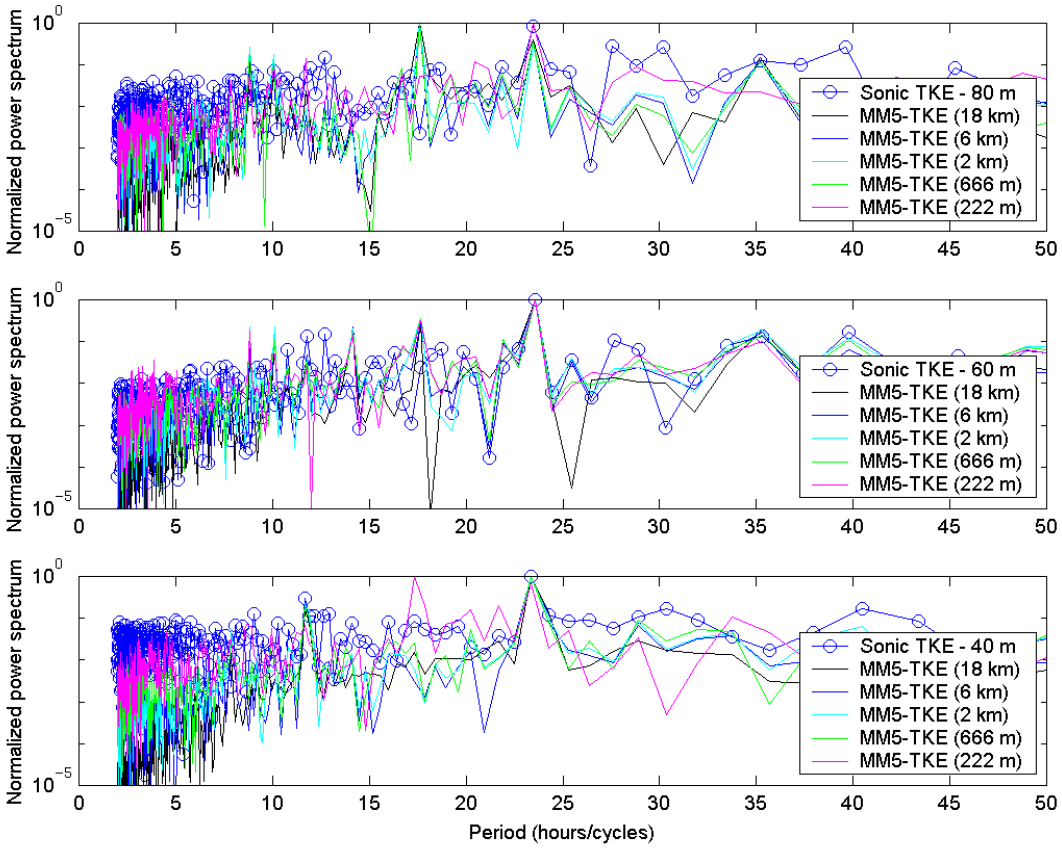

Figure 150. Power spectrum of sonic-measured (blue circle-dash) and MM5 turbulence kinetic energy at 40, 60, and 80 m obtained from different model horizontal grid resolutions.

MM5 (a: 80 m, b: 60 m, and c: 40 m). The power spectrum is normalized by the maximum value.

9 Results and Conclusion

The study results showed that both community models (MM5 and WRF) are capable of capturing basic flow properties. A spectrum of simultaneous horizontal model resolutions from 18km to 222m indicates that there is no firm conclusion that higher resolution automatically yields better results. This is mainly due to the model complexity in physical parameterizations, which might not be appropriate for very high model resolutions. Long-term (7 months) measurements by sonic anemometer showed much higher peaks in the turbulence kinetic energy (TKE) at all three levels than reported in the literature. Simulated TKE is noticeably underestimated compared to sonic measurements, which might have a significant impact for turbine deployment at these elevations. The empirical formulas to estimate winds at higher elevations based on the available standard heights (6 or 10 m) have large errors compared with actual tower measurements. The evaluated model results can provide guidance on possible errors and uncertainties while estimating wind maps in this and other areas.

10 Publications and Presentations

Belu, R., and Koracin, D. 2009: Wind characteristics and wind energy potential in western Nevada. *Renewable Energy*, 34, 2246-2251.

Koracin, D.; Reinhardt, R. "Wind energy assessment for Nevada: Observations and modeling." Presented at the 61st American Chemical Society Northwest Regional Meeting (invited talk), June 25-28, 2006, Reno, NV.

Koracin, D.; Reinhardt, R.L. Liddle, M.; McCord, T.; Podnar, D.; Minor, T. "Assessment of wind energy for Nevada using towers and mesoscale modeling." Energy Sustainability 2007, June 27-30, 2007, Long Beach, CA.

Koracin, D.; Reinhardt, R.L. Liddle, M.; McCord, T.; Podnar, D.; Minor, T. "Assessment of wind energy for Nevada using towers and mesoscale modeling." Presented at the 2007 Annual Energy Symposium (invited talk), August 15-16, 2007, UNLV, Las Vegas, NV.

Reinhardt, R.; Koracin, D.; Minor, T.; Pepper, D.; Hess, R.; Osborn, D. "Wind energy assessment for Nevada and the Southwest: Observations and modeling." Wind Power Conference and Exhibition 2006, June 4-7, 2006, Pittsburg, PA.

REPORT DOCUMENTATION PAGE

Form Approved
OMB No. 0704-0188

PLEASE DO NOT RETURN YOUR FORM TO THE ABOVE ORGANIZATION.

1. REPORT DATE *(DD-MM-YYYY)*	2. REPORT TYPE	3. DATES COVERED *(From - To)*
December 2009	Subcontract Report	26 June 2005 – 31 December 2007

4. TITLE AND SUBTITLE
Wind Energy Assessment Study for Nevada – Tall Tower Deployment (Stone Cabin): 26 June 2005 – 31 December 2007

5a. CONTRACT NUMBER
DE-AC36-08-GO28308

5b. GRANT NUMBER

5c. PROGRAM ELEMENT NUMBER

6. AUTHOR(S)
D. Koracin, R. Reinhardt, G. McCurdy, M. Liddle, T. McCord, R. Vellore, T. Minor, B. Lyles, D. Miller, and L. Ronchetti

5d. PROJECT NUMBER
NREL/SR-550-47085

5e. TASK NUMBER
DPN6.6002

5f. WORK UNIT NUMBER

7. PERFORMING ORGANIZATION NAME(S) AND ADDRESS(ES)
Desert Research Institute
2215 Raggio Parkway
Reno, NV 89512

8. PERFORMING ORGANIZATION REPORT NUMBER
NDO-5-44431-01

9. SPONSORING/MONITORING AGENCY NAME(S) AND ADDRESS(ES)
National Renewable Energy Laboratory
1617 Cole Blvd.
Golden, CO 80401-3393

10. SPONSOR/MONITOR'S ACRONYM(S)
NREL

11. SPONSORING/MONITORING AGENCY REPORT NUMBER
NREL/SR-550-47085

12. DISTRIBUTION AVAILABILITY STATEMENT
National Technical Information Service
U.S. Department of Commerce
5285 Port Royal Road
Springfield, VA 22161

13. SUPPLEMENTARY NOTES
NREL Technical Monitor: M. Schwartz and H. Thomas

14. ABSTRACT *(Maximum 200 Words)*
The objective of this work effort was to characterize wind shear and turbulence for representative wind-developable areas in Nevada.

15. SUBJECT TERMS
Tonopah (Stone Cabin); wind shear; turbulence; tall towers; Desert Research Institute; National Renewable Energy Laboratory; NREL; DRI

16. SECURITY CLASSIFICATION OF:			17. LIMITATION OF ABSTRACT	18. NUMBER OF PAGES	19a. NAME OF RESPONSIBLE PERSON
a. REPORT	b. ABSTRACT	c. THIS PAGE			
Unclassified	Unclassified	Unclassified	UL		19b. TELEPHONE NUMBER (*Include area code)*

Standard Form 298 (Rev. 8/98)
Prescribed by ANSI Std. Z39.18